

CRANFIELD UNIVERSITY

L. MORTARA

**ANALYSIS AND DEVELOPMENT OF AN AQUEOUS TAPE CASTING
CERAMIC PROCESS**

School of Industrial and Manufacturing Science

PhD THESIS

CRANFIELD UNIVERSITY
School of Industrial and Manufacturing Science
Department of Advanced Materials

PhD THESIS

Academic years 2001-2004

L. MORTARA

**Analysis and Development of an Aqueous Tape Casting Ceramic
Process**

Supervisor: Dr. J. R. Alcock

November 2005

**This thesis is submitted in partial fulfilment of the requirements for
the degree of Doctorate of Philosophy**

**© Cranfield University, 2005. All rights reserved. No part of this publication may
be reproduced without the written permission of the copyright holder**

To Lisa

Abstract

The laboratory scale process developed by Navarro [Navarro, 2001] for the production of pyroelectric ceramics was used as a case study for the design of a high-level methodology for the scale-up of ceramic processes.

A twofold approach was adopted as the basis of the methodology to perform the process scale-up. A “process focussed” approach was used that considered the sequence of processing operations, their feasibility on a larger scale and the potential problems foreseeable for a scaled-up process. Secondly, a “product focussed” approach analysed the quality of the product in respect to the customer requirements (the specifications). This approach also concerned the analysis of the process potential to perform within an essential tolerance interval. This aim was pursued through the use of a statistical technique, the Statistical Process Control.

With the product focussed approach, the mechanical and electrical characteristics of the wafers obtained with the laboratory scale process were compared with the industrial requirements. The ceramic wafers possessed satisfactory characteristics except for their strength. The processing parameters were investigated in order to optimise the sintered ceramic microstructure and to understand their relative influence on the achievement of adequate characteristics for allowing handling and machining. Sintered density and grain size were studied as functions of green density and firing temperature. Increasing the green density from the original 37% to approximately 65% of the theoretical density by means of warm pressing allowed the wafers to achieve a more homogeneous microstructure and a higher sintered density up to approximately 97% of the theoretical. Thanks to the increase in green density, the sintering temperature could be reduced by 100°C and the total sintering time was shortened by 190 minutes. The samples produced with warm pressing were more resistant as 75% of them survived during the poling and machining test, in contrast with the 5% of the original samples.

The suitability of the warm pressing technique to increase the green density up to 5 g.cm⁻³ (61% of the theoretical density) was investigated by means of the statistical process control tool. A correct design of the press equipment was judged the most relevant factor for determining the control and the capability of the process.

A rheological study was directed to understand how the slurry ingredients influenced the ceramic suspension, the green tape density and morphology. Two preparation routes were compared in order to discriminate among the effects induced by the electrosteric dispersant and the polyvinyl alcohol binder on the PZT particles suspension. It was shown how the dispersant influenced both the suspension characteristics and the comminution efficiency of the milling. The binder was shown to adsorb onto the ceramic particles. A model was proposed describing the interaction among ingredients which suggested that the adsorbing polymer induced particles flocculation by bridging mechanism, especially when added to stabilised slurries. As a result, PVA was judged inappropriate for tape casting of this PZT powder as it yielded low green density tapes.

Acknowledgements

To the people who have been close to me during this adventure.

Immensely grateful thanks to my family. To my Mum, my Dad and my Brother, who have supported me all my life, and who, I know, I can count on in any circumstance. Thanks for the joy that they always transmit to me. Through them I feel at home now, as I always did, in spite of the physical distance that now exists.

Thanks to Spa, with whom I started this great adventure. For sharing with me the joys and sorrows of life.

Thanks to my Aunt Elda, for gifting me the ‘unique’ car that gave me freedom. Thanks to my Grandmother Anna who couldn’t see the end of this journey. And to Sandra and Paolo, to Silvana, and to all the dearest friends that continuously spoil me with their nice thoughts from Italy.

Thanks to my supervisor, for his calmness and advice, and for supporting me thoroughly in every step of the PhD, even when I didn’t know I wanted a PhD.

Thanks to Paul, for transmitting me his experience, for his patience and practical help.

Thank you to Prof. Whatmore and Mr. Clayson, for their continuous trust and support. Thanks to the company which has supported my research practically and financially, and to KTP and EPSRC for the opportunities that they provided to me. Thanks to Cranfield University and its competent, helpful and friendly staff. In particular to Enza, Sharon, Colin, Andy and Jim.

Thanks to Cranfield campus with its peaceful green, for the extraordinary people that I met there.

Thanks to Heather for her remarkable friendship and help. Thanks to all my dear, special friends: to Valentino, for his wittiness, to Silvia and Alessio and their warm hugs. To beautiful Anna, for her work, help and nice smile, to Spyros and the office time spent together. To Mauro and his instinctive character, to Mimmo, Antonietta and to their sweet daughter Cecilia. To Chris, and his ‘puns’.

Thanks to my Italian friends: Dando, my friend of a lifetime, to Lina and Marcello, perennially separated by thousands of miles, to Roberto, and our philosophical chats.

Thanks to my boss David, for allowing me the privilege of time to work at my thesis. To my colleagues Clare and James for their precious suggestions. To Lewis and Giles without whom I probably would not have been able to recover my ‘lost thesis’.

To Italy and England.

TABLE OF CONTENTS

Abstract	iii
Acknowledgements	iv
TABLE OF CONTENTS	v
List of figures	ix
Abbreviations and Constants	xvi
1 INTRODUCTION	1
1.1 Background	1
1.1.1 The outputs of the original process as by Navarro	1
1.2 Scale- up specifications	2
1.2.1 Mechanical requirements	2
1.2.2 Electrical specifications	3
1.2.3 Process Yield	3
1.3 Research aims	3
1.4 Outline of the development of the research	4
1.5 Thesis outline	5
2 LITERATURE REVIEW	6
2.1 Brief Introduction on Process Planning and Scaling Up	6
2.1.1 Key concepts in process design	7
2.1.2 The problem solving methodology	14
2.2 The Six Sigma concept	15
2.2.1 Some statistical basic concepts for Six Sigma	17
2.2.2 Process variation and process capability	19
2.2.3 Statistical Process Control (SPC)	21
2.3 Brief introduction to ceramic processing by tape casting	24
2.3.1 The slurry preparation: ingredients	24
2.3.2 Ingredients interactions	31
2.4 The slurry preparation: processing	33
2.4.1 Dispersion milling	33
2.4.2 Slurry Conditioning and Characterisation	34

Table of contents

2.4.3	General overview on Tape Casting	36
2.4.4	Tape drying	39
2.4.5	Tape cast shaping	41
2.4.6	Organics Burnout	41
2.5	Brief overview on the densification of ceramics (sintering).....	42
2.5.1	Solid state sintering	43
2.5.2	Liquid phase sintering	44
2.5.3	Factors influencing the sintered microstructure	45
2.6	Stabilisation of particles suspensions.....	49
2.6.1	Electrostatic stabilisation	49
2.6.2	Steric Stabilisation	53
2.6.3	Electrosteric stabilisation	54
2.6.4	Characterisation of particles suspensions: optimisation of the dispersing agent amount	56
3	METHODOLOGY	66
3.1	The twofold approach towards the scale-up	68
3.2	Methodology of the scale-up development	69
3.3	Description of the research.....	74
3.3.1	The focus on the product characteristics	74
3.3.2	The focus on process efficiency	75
4	EXPERIMENTAL METHOD	78
4.1	The original process	78
4.1.1	The materials	79
4.1.2	The procedure	80
4.2	General characterisation techniques	86
4.2.1	Green density	86
4.2.2	Sintered density	86
4.2.3	Microstructure and Morphology	87
4.2.4	Flatness and roughness measurements	88
4.2.5	Electrical characteristics	88
4.2.6	Rheological characterisation of ceramic suspensions	89
4.2.7	Assessment of the PVA adsorption onto the particles' surface	90
4.2.8	The assessment of the tapes glass transition temperature (Tg)	90

5	RESULTS AND DISCUSSION OF THE PROCESS FOCUSED APPROACH	91
5.1	Process charts	91
5.1.1	Process layout	91
5.1.2	Process flow chart	93
5.2	Process Analysis	97
5.2.1	The process yields, times and wastes	97
5.2.2	Analysis of the potential causes of low yield	98
5.2.3	The problem solving: an example	98
5.2.4	The newly designed process	106
5.3	Considerations about the process scale-up	108
5.3.1	The evaluation of the process yield	108
5.3.2	The estimated yearly throughput	110
6	RESULTS OF THE PRODUCT FOCUSED APPROACH	112
6.1	Microstructure characterisation of the ceramic achieved by the original process.....	112
6.1.1	Sintered density	112
6.1.2	Ceramic surface microstructure	112
6.1.3	Ceramic cross-sectional microstructure	113
6.1.4	Samples Flatness and roughness (Ra)	115
6.1.5	Resistance to stresses	116
6.1.6	Crack morphology	116
6.2	Electrical characteristics of the tape cast material	116
6.3	Conceptual Design Phase I: Study on the factors influencing the ceramic microstructure	118
6.3.1	Study of the effects of the sintering temperature and dwell time on the ceramic characteristics	119
6.3.2	Study of the effects of the green density and the sintering temperature on the ceramic characteristics	128
6.3.3	Study of the effects of the sintering heating rate on the ceramic characteristics	144
6.3.4	Results of the studies on the factors influencing the sintered microstructure	146
6.4	Definitive Design Phase I: The Statistical Process Control to assess the sources of variation in the warm pressing stage	150
6.4.1	Method	150
6.4.2	Results	151

Table of contents

6.4.3	Capability Indexes	153
6.5	Conceptual Design Phase II: the influence of the ingredients and the drying conditions on the green tape	156
6.5.1	Method	156
6.5.2	Results	162
7	DISCUSSION OF THE PRODUCT FOCUSED APPROACH	197
7.1	The Conceptual Design Phase I: study of the factors which influence the sintered ceramic microstructure	197
7.1.1	The sintered material characterisation	198
7.1.2	Study on the factors influencing the ceramic microstructure	199
7.1.3	Conclusions of the sintering studies	211
7.1.4	Characteristics of the pressed wafers	212
7.2	The Definitive Design Phase I: the Statistical Process Control technique to assess the causes of variation	214
7.2.1	Conclusions of the statistical process control experiment	220
7.3	The Conceptual Design Phase II: The influence of the ingredients and the drying conditions on the green tape	221
7.3.1	The effects of the ingredients on the green tapes	221
7.3.2	The effects of the drying conditions	235
8	CONCLUSIONS AND FURTHER WORK	236
8.1	Future work	237
9	REFERENCES	197
APPENDIX A: NEW PROCESS FLOW CHART STEPS DESCRIPTION		246
APPENDIX B: PAPERS		249

List of figures

Fig. 1: Infrared image taken with an imaging radiometer which used	2
Fig. 2: Example of a manufacturing system (process)	6
Fig. 3: The stages in the manufacturing process design	8
Fig. 4 : Iterative development of design stages modified from Wu [1994]	9
Fig. 5: Production routing sheet example	10
Fig. 6: Layout chart example	12
Fig. 7: Example of flow chart based on material flowing, taken from the current study	13
Fig. 8: Standard Symbols published by ANSI	13
Fig. 9: An empty house of quality diagram	16
Fig. 10: Stages in SPC application	17
Fig. 11: Example of histogram: the variable was measured A (3 times), B (4 times), C, (1 time), D (3 times) and E (2 times)	17
Fig. 12: Normal or Gauss distribution	19
Fig. 13: Comparison of specification and tolerance interval with the data population	20
Fig. 14: Example of not in control Mean and Range charts	22
Fig. 15: A typical layout of ceramic processing	24
Fig. 16: Schematic illustration of the working principles of the most common dispersants: a) electrostatic, b) steric, c) electrosteric	26
Fig. 17: Chemical structure of a Polyacrylic acid segment.	27
Fig. 18: Polyvinyl alcohol hydrolysis and molecular weight effects (reported from producer (Celanese Chemicals) brochure of Celvol TM Polyvinyl Alcohol)	29
Fig. 19: Strain-stress diagrams for differently plasticized materials. a) Not plasticized, b) type 1 plasticizer, c) type 2 plasticizer	31
Fig. 20: Schematic representation of the cross section of a ball mill with an enlargement of the impact of two milling media.	33
Fig. 21: Schematic representation of the ‘Zipper bag theory’	34
Fig. 22: Sketch of the mechanism at the basis of the tape casting equipment	36
Fig. 23: Forces involved in the tape casting process	38
Fig. 24: Buffer reservoir scheme	38

List of figures

Fig. 25: Stages of drying and trend of the evaporation rate: A) The constant rate period; B) The first falling rate period, C) The second falling rate period.	40
Fig. 26: Thickness comb gauge	41
Fig. 27: Essential stages in the solid state sintering of particles, adapted from Rahaman [1995]	44
Fig. 28: The grain growth: A) normal grain growth, B) abnormal grain growth	46
Fig. 29: Sintering mechanism of coarsely packed particles according to Greskovich and Lay	47
Fig. 30: Pores coordinated by grains-particles in a two-dimensional plane	48
Fig. 31: Hydration of metal oxides and Zeta-potential variation with pH	50
Fig. 32: Schematic representation of the diffuse double layer and potential profile according to the Gouy-Chapmann and the Stern models	51
Fig. 33: Effect on the electric potential: two particles approach each other and the double layers overlap.	52
Fig. 34: Potential Energy curves against particle distance, showing different total interactions [Pugh and Bergström, 1994]	53
Fig. 35: Schematic representation of Polymers action on particles suspensions: A) Bridging flocculation; B) Steric stabilisation; C) Depletion flocculation; D) Depletion stabilisation	54
Fig. 36: A) Adsorption of a cationic copolymer on a negative particle surface; B) adsorption of an anionic copolymer on a negative particle surface	55
Fig. 37: Classification of rheological behaviour for any material	57
Fig. 38: A) Cup and bob, B) cone and plate configurations	57
Fig. 39: Scheme showing the shearing of a prismatic portion of liquid and its effect on the shape of the prism (dashed figure)	58
Fig. 40: Interaction of particles in a suspension and their contributions to the overall slurry rheological behaviours	60
Fig. 41: Typical viscosity profile of ceramic slurries while sweeping the dispersant level. Example from current work.	61
Fig. 42: A) Sweep of shear rates in loops; B) Step shear rate test; 1 = not thixotropic slurry; 2 = thixotropic slurry. Examples from current work.	63
Fig. 43: The schematic response strain (γ) to an oscillating stress (s) applied to a material	64
Fig. 44: Outline of the methodology towards the scale-up. The coloured boxes represent the specific steps taken in the case study at the basis of this work.	67
Fig. 45: Process development stages: specific progression of the research reported in this work and techniques employed (adapted from Rosenthal, S. [1992]).	70
Fig. 46: The Conceptual Design phase: creative design of solutions which approximate the performances to the required value; the best one (e.g. Sol 5) is selected, according to criteria of feasibility and risk	71

List of figures

Fig. 47: The Definitive Design stage: attunes the performances to the required specifications so that the process becomes precise and accurate	72
Fig. 48: Development of the Definitive Design stage	73
Fig. 49: Research development in detail. The bullet point items represent the experiments performed. In the grey boxes is a description of the experiment purpose. Future work is shown in dotted boxes	77
Fig. 50: Process steps for tape casting preparation	78
Fig. 51: Laboratory scale de-airing equipment	81
Fig. 52: Schematic representation of the doctor blade: A) top view and B) cross section with view of the blades positions	82
Fig. 53: Schematic outline of the green tape thickness measurements	83
Fig. 54: Standard configuration for the casting and sintering of the samples	84
Fig. 55: Schematic representation of a top view for the placement of an individual sample on the sintering support	85
Fig. 56: Schematic diagram for wafer's flatness measurements	88
Fig. 57: Layout of the process (focusing on time flow)	92
Fig. 58: Original Process Flow Charts	96
Fig. 59: A) The buffer configuration as suggested by Feng; B) the stack configuration proposed	102
Fig. 60: Sintering configuration of multiple samples	103
Fig. 61: The proposed new process	105
Fig. 62: Process as designed through the Conceptual Design Phase I	107
Fig. 63: The evaluation of the process yields. The ceramic process studied in this research is evidenced by the shadowed area. Its yield was 35%.	109
Fig. 64: Optical microscope images of the surfaces of a sintered ($T = 1270^{\circ}\text{C}$) tape-cast sample obtained with the original process. (Side A in contact with the support during sintering and side B free to air)	113
Fig. 65: SEM images of the surfaces of a sintered ($T = 1270^{\circ}\text{C}$) tape-cast sample obtained with the original process. (Side A in contact with the support during sintering and side B free to air)	113
Fig. 66: Typical sample cross section with description.	114
Fig. 67: A crack developing through the ceramic microstructure	116
Fig. 68: Ishikawa (cause-effect) diagram for the characteristics of the sintered ceramic	118
Fig. 69: Methodology for determining the effects of sintering temperature and dwell time. The rectangles represent the two experiments	119

List of figures

Fig. 70: Microstructure of central areas of samples cross sections, obtained at decreasing sintering temperature and dwell time	122
Fig. 71: Trend of the calculated grain size and of sintered density with temperature	123
Fig. 72: Microstructure of central areas of samples obtained at decreasing sintering temperature. In the pictures the distinctive characteristics are highlighted with circles and lines	127
Fig. 73: SEM pictures of 1) carrier side and 2) upper side of the cast tape.	129
Fig. 74: SEM picture of the ceramic powder after a complete milling cycle. The particles look equiaxed with diameter smaller than 1 μ m.	129
Fig. 75: SEM picture with details of the cross section of a green tape along its fracture surface: A) close to the carrier surface, B) close to the free surface, C) in a central area	130
Fig. 76: Methodology for determining the effects of sintering temperature and Green density.	131
Fig. 77: Pressing configuration of green samples	132
Fig. 78: Samples configuration under the press. 1) Side by side; 2) stack	133
Fig. 79: Fracture surfaces of sintered microstructures	135
Fig. 80: Graph of the variation of the calculated average grain size against the variation of the green density	137
Fig. 81: Graph of the variation of the sintered density, expressed as a percentage of the theoretical, against the variation of the green density	137
Fig. 82: Increasing of the green density by warm pressing with rising pressures at room temperature	139
Fig. 83: Increasing of the green density by warm pressing with 65 MPa pressure at rising temperature	140
Fig. 84: Increasing of the green density with increasing pressing time at 65 MPa and 50°C	141
Fig. 85: 1) Fracture surface of not pressed tape cast thick film with green density of 3.0 g.cm ⁻³ ; 2) fracture surface of warm pressed tape cast thick film with green density of 5.1 g.cm ⁻³	143
Fig. 86: Microstructure of central areas of samples sintered with an increasing heating rate	145
Fig. 87: 1) Original microstructure as obtained before the sintering studies; 2) microstructure achieved after the modification of the sintering conditions	146
Fig. 88: Wafers profile, after sintering	148
Fig. 89: Direct comparison between a reference material (a different pyroelectric ceramic) and the tape cast material performances in application	149
Fig. 90: Thermal image acquired with device mounting the tape cast material, resulted from the modified process	149
Fig. 91: Samples stacked in the pressing configuration	150

List of figures

Fig. 92: Individual observation chart: upper and lower control limits (UCL, LCL) lines, mean line \bar{X}	152
Fig. 93: Mean (1) and Range (2) charts	155
Fig. 94: Process flow sheet for the slurry preparation and the tape casting [Route 1]	158
Fig. 95: Route 2: procedure	160
Fig. 96: Viscosity profiles of slurries prepared with different dispersant amounts containing the binder system	162
Fig. 97: Trends of the parameters obtained by fitting the viscosity profiles with the Bingham and the Casson Model: Yield (s_0), Plastic viscosity (κ)	164
Fig. 98: Plasticity calculated for the Bingham and Casson coefficients	164
Fig. 99: Viscosity trends (at 20 s^{-1}) for slurries prepared according to Route 1 with and without binder, associated with green density figures	165
Fig. 100: Comparison of rheological figures of slurries containing the binder system (Samples B) prepared following Route 1	167
Fig. 101: Time-dependent behaviour for the slurries prepared with Route 1, tested at 2 and 50 s^{-1} shear rates	169
Fig. 102: Trends of thixotropy. Comparison of recovery time and thixotropy coefficient	169
Fig. 103: Variation of the microstructure of the burnt out tapes produced with different amount of dispersant	171
Fig. 104: Variation of the microstructure of the green tapes produced with different amount of dispersant.	173
Fig. 105: High magnification micrographs of the particle surfaces after the organic burnout. 1) Tape 1 milled with 0.0046 dispersant ratio. 2) Tape 3 milled with 0.0238 dispersant ratio	174
Fig. 106: Plot of PVA adsorbed and particle size versus dispersant concentration	175
Fig. 107: Viscosity profiles of slurries without binder (samples NB). The dispersant was varied between 0.4% and 5.5%	176
Fig. 108: Parameters obtained by fitting the viscosity profiles with the Casson Model: 1) Yield (s_0), 2) Plastic viscosity (κ)	178
Fig. 109: Variation of plasticity with dispersant amount for samples NB	179
Fig. 110: Variation of plasticity with dispersant amount for samples B	179
Fig. 111: Viscosity trends (at 20 s^{-1}) for slurries prepared according to Route 2 at the lowest powder content, associated with green density figures	182
Fig. 112: Viscosity trends (at 20 s^{-1}) for slurries prepared according to Route 2 at the highest powder content, associated with green density figures	182

List of figures

Fig. 113: Comparative graph reporting the trends for binderless samples (blue) and samples with binder (red) of the three experiments performed at the lowest powder content (final amount = $62 \pm 3\%$).	183
Fig. 114: Comparison of rheological figures of slurries containing the binder system (Samples B) prepared following Route 2 at 15% volume of powder	185
Fig. 115: Comparison of rheological figures of slurries containing the binder system (Samples B) prepared following Route 2 at 21% volume of powder	185
Fig. 116: Comparative graph reporting the trends for Elastic modulus (G') (red) and Max Elastic modulus ($G' \text{ max}$) (blue) of the three experiments performed at powder content $62 \pm 3\%$.	186
Fig. 117: Time-dependent behaviour for the slurries at 21% vol. powder content, tested at 2 and 50 s^{-1} shear rates	188
Fig. 118: Recovery time and thixotropy coefficient trends for the slurries at 21% volume of powder	189
Fig. 119: SEM pictures of the green bodies as cast into plastic moulds. Side B was the lower side of the green body, in contact with the mould. Side A was the free to air surface	191
Fig. 120: Microstructure of green tapes produced varying the powder and the plasticizer content	193
Fig. 121: Microstructure of green tapes produced varying the powder and the plasticizer content, after the organic burnout	194
Fig. 122: Green densities achieved with different drying conditions. A) Green density plotted against drying temperature. B) Green density plotted against drying time.	196
Fig. 123: Visualization of sintering profile variation with the reduction on the dwell time in experiment 1	202
Fig. 124: Visualization of sintering profile variation with the reduction on the sintering temperature and the total sintering time in experiment 2	204
Fig. 125: Proposed mechanism: 1) low green density; 2) porous; 3) less porous.	207
Fig. 126: Representation of pressing of unevenly thickened samples. The pressing results in a gradient of density. Thicker areas would be more influenced by the pressure.	210
Fig. 127: Comparison of original sintering profile with the newly designed one.	212
Fig. 128: Representation of the SPC study results.	215
Fig. 129: Fishbone analysis: contribution factors to pressed green density	217
Fig. 130: Mean and range charts reproduced with the day-by-day upper and lower control limit lines.	219
Fig. 131: Summary of the trends for Route 1 and Route 2 (with 68% in weight of powder) as in the results section 6.5.2	225
Fig. 132: Comparison of viscosity trends for Route 1 and Route 2 (at 68% in weight of powder)	227

List of figures

Fig. 133: A model for the effects of the dispersant amount in absence of binder (Samples NB) 229

Fig. 134: A model for the effects of the dispersant on the suspension, when the binder system was added 232

Abbreviations and Constants

DFSS – Design for Six Sigma
DFMA – Design for Manufacture and Assembly
QFD – Quality Function Deployment
MSA – Measurement System Analysis
SPC – Statistical Process Control
TQM – Total Quality Management
 \bar{X} - Arithmetic mean
 σ – Standard deviation
n – Number of values
 x_i – Individual values
USL – Upper specification limit
LSL – Lower specification limit
R – Range
 \bar{R} - Average range
UCL – Upper control limit
LCL – Lower control limit
Cpk_u - Cpk_l – Cp – Capability indexes
PZT – Lead zirconate titanate
PAA – Polyacrylic acid
PVA – Polyvinyl alcohol
T_g – Glass transition temperature
 $\dot{\gamma}$ - Shear rate
v - Speed of the carrier
 h_0 – Gap height under the doctor blade
P – Pressure on the casting head
 Q_r – Mass of slurry
g – Gravity acceleration
l_r – reservoir length
CRP – Constant rate period
FRP – Falling rate period
TGA – Thermogravimetric analysis
N – Coordination number
 ξ - Zeta-potential
 ψ_0 - Surface potential
A – Coefficient specific of medium
1/k – Thickness of double layer
r – Distance from the particle surface
V_T – Total electric potential
DLVO - Derjaguin, Landau, Verwey and Overbeek theory
V_A – Sum of attractive forces
V_R – Sum of repulsive forces
V_{max} – Maximum potential
V_{min} – Minimum potential
 γ - Strain
s – Stress

τ - Relaxation time
 t_0 – Experiment time
De – Deborah number
T – Area
F – Shearing force applied
 α - Shift angle of the prismatic portion of liquid under shearing force
 s_{xy} – Shear stress on the plane xy
 η - Viscosity
 κ – Plastic viscosity
 s_0 – Yield stress
 η_0 – Viscosity of a suspension extrapolated at zero particles concentration
 ϕ – Particles volume fraction
 ϕ_{eff} – Effective volume occupied by the particles, including the steric hindrance of any grafted polymer
 Δ - Steric hindrance of a polymer attached to the particles
 ϕ_m – Maximum packing fraction
 δ – Delay time
LVR – Linear viscoelastic region
Tc – Critical shear stress
G' – Elastic modulus or Storage modulus
G* - Complex dynamic modulus
 s_I - The peak value of the stress
 γ_I - The strain associated to the peak value of the stress
G'' - Loss modulus
 ρ - Resistivity
p – Average pyroelectric coefficient
 ϵ_r – Relative permittivity
 ϵ - Electric permittivity
Tan δ - Loss
 F_v – Figure of merit
 F_D – Figure of merit
Ra – Average roughness of the samples
GD – Green density
SD – Sintered density
TD – Theoretical density
w – Sample 's Weight
V – Sample 's Volume
h - Sample 's Thickness
l – Length of a drawn line
d – Calculated average grain size
m – Number of grains intercepting a drawn line
RPM – Revolutions per minute
SEM – Scanning Electron Microscope
DSC – Differential Scanning Calorimetry
 R^2 – Correlation coefficient

1 Introduction

1.1 Background

Pyroelectric ceramics are commonly used as IR sensors for applications such as door openers, security systems, thermal imagers and people counters. To produce pyroelectric ceramic materials for these applications the conventional technique is to cut, lap and polish a hot-pressed monolithic ceramic block into discs of a predetermined thickness. This process is time consuming and expensive. It is also a limiting process for increasing the production outcomes and for the planning and management of resources.

Tape casting is a forming technique used commonly in industry to produce thin, flat ceramics for many purposes. The use of tape casting as an industrial forming method goes back to the nineteen fifties, but only in recent years the employment of water as a solvent has been studied and considered for processing.

A potential solution to improve yield and reduce the costs of produced pyroelectric arrays is to use the tape casting technique as a ceramic forming methodology. Navarro [2001] developed an aqueous laboratory scale tape casting process using PZT ceramic, obtaining promising results.

The scale-up of such a process to industrial production volumes was desirable as it presented multiple advantages. Firstly, the tape casting route was potentially cheaper, more flexible and able to satisfy an increasing demand. Secondly, Navarro's process was designed considering environmental, health and safety concerns, as water was used as the main component in slip preparation as a substitute of organic solvents.

The research presented here is an analysis of the initial stages of scaling up such a laboratory scale process. Whilst the general process was specifically developed for thick film PZT production, the sub-processes within it are commonly used in ceramic manufacture. Therefore, many of the process scale-up issues and methodologies discussed here are of general applicability in ceramic manufacture.

1.1.1 The outputs of the original process as by Navarro

Navarro [2001] demonstrated the potential of the tape casting technique to achieve pyroelectric ceramic wafers ready for industrial application. In Fig. 1, an image is reported, taken with a thermal imager which used Navarro's tape-cast material.

In Table 1 the electrical characteristics of the material are reported.

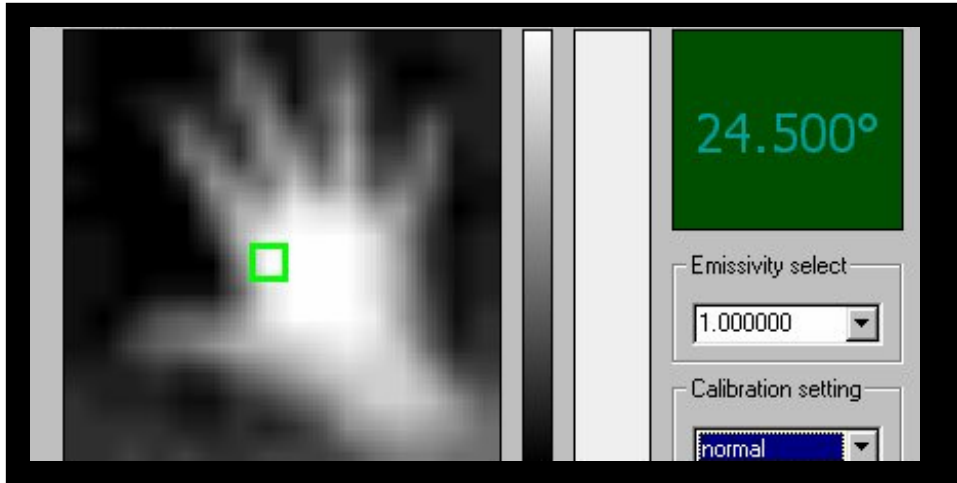


Fig. 1: Infrared image taken with a thermal imaging radiometer which used Navarro's tape cast material [Navarro, 2001]

Before poling			After poling					
ϵ_r (30 Hz)	Tan δ (30 Hz)	ρ	ϵ_r (30 Hz)	Tan δ (30 Hz)	p	p/ϵ	F_v	F_D
	%	$\Omega m \times 10^{-9}$		%	$Cm^{-2} K^{-1}$ $\times 10^{-4}$	$Vm^{-2} K^{-1}$ $\times 10^{-5}$	$m^2 C^{-1}$	$Pa^{-1/2}$ $\times 10^{-5}$
277	1.7	3.1	220	1.6	2.5	1.3	0.051	1.8

Table 1: Electrical characteristics of the tape cast material achieved by Navarro [2001]

The flatness of Navarro's wafers, i.e. the peak to valley distance over 40 mm diameter averaged between 2 perpendicular directions, as explained later in the experimental section, was $\pm 85 \mu m$. Their roughness (R_a) at the top surface was $0.55 \mu m$ and $0.46 \mu m$ at the bottom surface.

1.2 Scale- up specifications

The following values listed were the industrial (product and process) targets ideally required for the scale-up of Navarro's process. These values will be referred as 'specifications' later in this thesis.

1.2.1 Mechanical requirements

- Wafers thickness $200 \pm 20 \mu m$
- Orientation and alignment flats in accordance with manufacturer documentation
- Ideal flatness to be $\leq \pm 6 \mu m$ across 10 mm. This value represents an ideal target as it reflects the characteristics of lapped and polished wafers, produced with the traditional sintering/hotpressing-pressing technique. However, Navarro's study showed that the material could be processed

successfully although the taper of the samples were 10 times greater (80 μm).

1.2.2 Electrical specifications

- Acceptable poling process to be defined and demonstrated.
- Electrical characteristics to fulfil requirements listed in Table 2, as derived from Navarro's product characteristic.

Before poling			After poling			
ϵ_r (30 Hz)	Tan δ (30 Hz)	ρ	ϵ_r (30 Hz)	Tan δ (30 Hz)	p	p/ϵ
	%	$\Omega\text{m} \times 10^{-9}$		%	$\text{Cm}^{-2} \text{K}^{-1} \times 10^{-4}$	$\text{Vm}^{-2}\text{K}^{-1} \times 10^5$
250 ± 50	< 2.0	2.0 ± 0.5	250 ± 50	< 2.0	2.5 ± 0.3	> 1.1

Table 2: Electrical specifications obtained from Navarro's results

1.2.3 Process Yield

- Target yield, acceptable for submitting into wafer processing was greater than 50% for at least 12 poled and characterised wafers.

Parameter	Short-Term Target (Batch Process)	Longer-Term Target (Continuous Process)	Notes
<u>Wafers</u> per Annum	500 –1000	70 000	To demonstrate the capability of the process, <u>not</u> to actually produce this quantity

Table 3: Process scale-up targets

Other internal specifications, i.e. the outputs of the sub-processes that build the total process, were determined during the study (e.g. green tape density). Those will be reported in the text, when appropriate.

1.3 Research aims

The aims of this study were to:

- formulate a methodology for performing a scale-up for a ceramic process by investigating a suitable design approach.

- develop an understanding of the effects of the processing parameters upon the final ceramic microstructure.
- investigate the interactions among the slurry ingredients of the process under investigation, relating the material parameters (ingredients concentrations) to the intermediate (green tape) and final (sintered ceramic) product.

1.4 Outline of the development of the research

In order to fulfil the aims of this study, experimental work has been carried out in the context of the scale-up of the laboratory process. The scale-up was approached with a two-fold perspective which provided the context for the in-depth investigation of several distinct issues.

Firstly, the process was analysed considering the sequence of processing operations, their feasibility on a larger scale and the potential problems foreseeable for a scaled-up process. This perspective will be referred as the “process focused approach”.

Secondly, the investigation considered the product, i.e. the ceramic wafer, characteristics. In this perspective, the product features were assessed against the requirements set by the industrial application, i.e. the “product specifications”. It was also a primary objective to understand and evaluate the capability of the process to produce ceramic in a reliable and consistent way. This perspective will be referred as the “product focused approach”.

Both these approaches will be explained in more detail in the Methodology section. For both approaches, potential threats (problems) for industrial scale-up were highlighted. The most significant of these were systematically analysed, using design tools and techniques in a series of improvement cycles, to provide alternatives to the original prescribed set-up. A detailed description of how this was conducted can be found in the Methodology section.

During the “product focused” investigation, the lack of resistance to mechanical stresses of the ceramic material represented the greatest concern with regards to the potential of the process to be of industrial use. The development of potential solutions to correct the low resistance to mechanical stress problem provided case studies to supply answers to the research aims. In this specific context, the green density was recognised as the most influential parameter on the ceramic microstructure. The warm pressing technique was considered as a viable solution to increase the green density of the tape cast material.

Studies to assess its capabilities were conducted involving the use of a statistical tool, Statistical Process Control. In addition, further investigations were directed towards finding an alternative solution to the warm pressing technique that could reduce the costs of a scaled-up process. In this light, the influence of the slurry ingredients and their proportions on the ceramic suspension and the tape cast material was evaluated.

The “process focused” approach aimed to obtain a high level of understanding of the major processing threats to the scale-up.

The combination of the two approaches provided an example for the formulation of a methodology to develop the scale-up of ceramic processes.

1.5 Thesis outline

Chapter 1 introduces the background and the aims of the study.

In Chapter 2, the relevant principles of process design and ceramic manufacturing are described in order to provide the basis for the interpretation of the research results, illustrated by this thesis.

Chapter 3 summarises the methodology followed in the development of the thesis. This chapter contains a detailed description of the principles and the techniques used to approach the process scale-up, which provided the structure of the research. This chapter was designed to help to put the experimental work carried out in context within the wider scale-up development.

Chapter 4 describes the original laboratory process at the start of the investigation. The chapter also details the experimental techniques used in the research.

In Chapter 5, the results of the investigation of the process focused approach are reported and discussed. The process characteristics and the potential problems in the development of a scaled-up process were assessed. A series of examples illustrating individually treated problems are provided.

Chapter 6 summarises the detailed results obtained during the investigation with the product focused approach.

The following Chapter 7 discusses the results presented in Chapter 6. In this section, the reasons lying behind the lack of resistance to stress of the ceramic were investigated. The influence of several processing parameters on the ceramic microstructure was explored.

Finally, Chapter 8 summarises the research findings, foreseeing the opportunities for future studies.

2 Literature review

This chapter reviews relevant bodies of knowledge to establish a theoretical foundation for the research. It begins by providing an overview of the core literature, covering the topic of process planning, design for manufacturing and Six Sigma.

Other areas specific to the tape cast processing and ceramic manufacturing, are then reviewed to better understand their implications for the research. This broad literature review approach was necessary to overcome disciplinary boundaries and provide a complete overview of the generic issues related to scale-up, and to put in context the specific topics treated during the research.

2.1 Brief Introduction on Process Planning and Scaling Up

Manufacturing is the activity dedicated to transforming raw materials (inputs) into economic goods (outputs). A system is commonly thought of as a transformation process that converts a set of inputs into a set of outputs. Usually a manufacturing system makes use of a series of sub manufacturing processes to obtain the final product. Often the output of one sub-process is utilised as input of another one as schematised in Fig. 2.

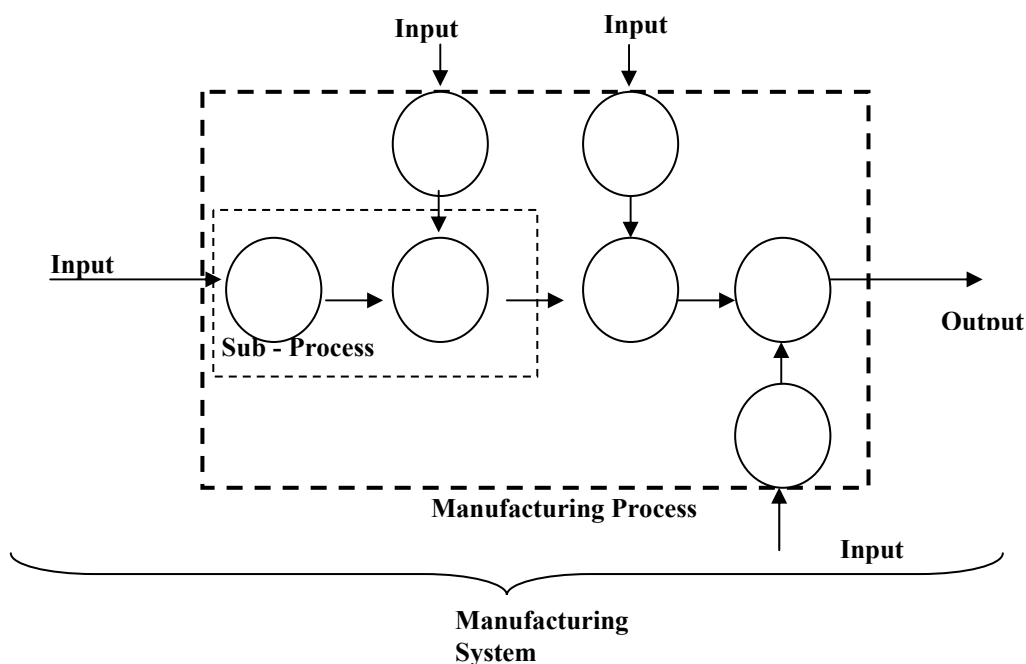


Fig. 2: Example of a manufacturing system (process)

The design of a manufacturing system is a highly complex operation involving the knowledge of many disciplines having as the primary aim the successful creation

of a compact and efficient process. Moreover, the design is of primary importance as corrections after implementation are extremely expensive and not always successful.

2.1.1 Key concepts in process design

2.1.1.1 *Process planning*

The objective of process planning is to transform a laboratory scale process to industrial scale process which delivers saleable products. Process planning determines how a product is to be manufactured: costs, production preparation, production efficiency and product quality are decided in this phase. In other words, process planning defines in detail the progression that transforms raw materials into the desired form. During process planning, dimensions, tolerances, sequences of operations, tools, machinery, times, quality statements and other important issues have to be determined.

2.1.1.2 *Specifications*

Rigorous specifications are the important basis for any manufacturing system: they are the foundation keys for the manufacturing design project. The specifications are a detailed description of the scope of the work (i.e. a summary of deliverables and process requirements to fulfil the customer needs and expectations). During the design stages the results of the tested production solutions (products) are compared with the customer based specifications to measure the appropriateness of the method employed. It is of utmost importance that the specifications are rigorously and unmistakably defined.

2.1.1.3 *Design strategies and ‘philosophical’ approaches*

The successful realisation of the process design is reliant on a sensible management: a manufacturing strategy, (i.e. a philosophical approach) is needed in order to achieve the objectives.

The classical way to approach problems has its roots in the philosophy of René Descartes’ *Discourse on Method* (1637), basis on the western science for more than 350 years. This is the “reductionist” approach where each problem is divided into a more complex structure of sub problems and the solution of a single sub-problem is pursued.

Another example of a systematic approach to the design process is defined as “concurrent engineering” approach. Recently it has been demonstrated as effective in improving reliability and quality of the design by reducing cost and time, in contrast with the traditional hierarchical design method [Edwards, 2002, Herder and Weijnen, 2000]. In the concurrent engineering system all life cycle phases of the product and all the external factors of possible relevance are considered simultaneously, approaching the product as a totality, in a holistic way.

Most recently, the Six Sigma approach has been considered of increasing importance in the manufacturing sector. Six Sigma is both a philosophy and a methodology that improves quality by analyzing data using statistics. Six Sigma is used to find the root cause of quality problems and to put controls in practice. Six Sigma is a statistical concept which measures a process in terms of its defects. Achieving a 'Six Sigma' accreditation for a process is another way of saying that the process is delivering just 3.4 defects per million of opportunities or that it works nearly perfectly..

Although Six Sigma was designed originally to improve manufacturing, the method can also be used in other business processes, such as product design and supply chain management [Brue, 2002, Koch et al., 2004, Markarian, 2004]. The Six Sigma concept methodology and tools is discussed in a further section of this thesis (section 2.2).

2.1.1.4 Process design of a manufacturing system stages

The design of a manufacturing system is of particular importance as corrections after process implementation are extremely expensive and not always successful. Fig. 3 explains how a new product introduction could be mapped [Rosenthal, 1992]. After the product idea has been generated and its feasibility has been demonstrated, an implementation project starts for the passage from the laboratory to the industrial dimension. Its output is a prototype ready for further scale up.

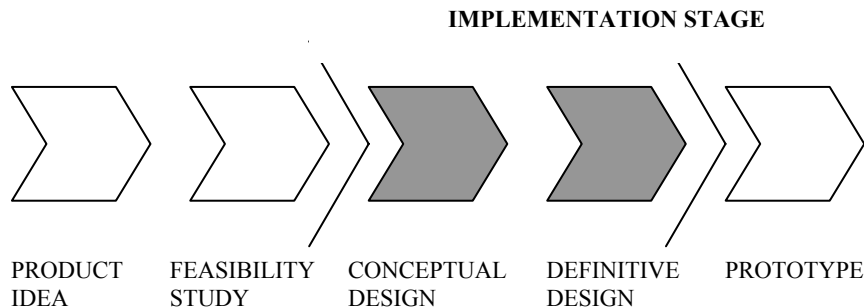


Fig. 3: The stages in the manufacturing process design

The feasibility study produces a process that demonstrates potential but is not sufficiently refined and adjusted in order to allow an easy scale up. During the subsequent phases of conceptual design and definitive design the most compact, efficient and economical process is created in order to permit higher product output, attuned to the customer requirements. The general rule is that manufacturing systems must be kept as simple as possible. In the conceptual design phase existing technological options to develop a product are evaluated and applied together with issues regarding suitable manufacturing facilities. Thus the original process layout, derived from the feasibility study stage, is changed to originate a streamlined sequence of operations reducing risks, eliminating bottlenecks and facilitating the following work.

The core stages in the manufacturing process design are the conceptual and definitive design stages. They are belonging to a broader stage commonly denominated implementation stage.

Although Fig 2 shows the stages in succession the phases are not strictly linear. Common practice sees the development of a manufacturing process following an iterative progression that leads from the idea generation to the prototype and the scale-up, as schematically illustrated in Fig. 4.

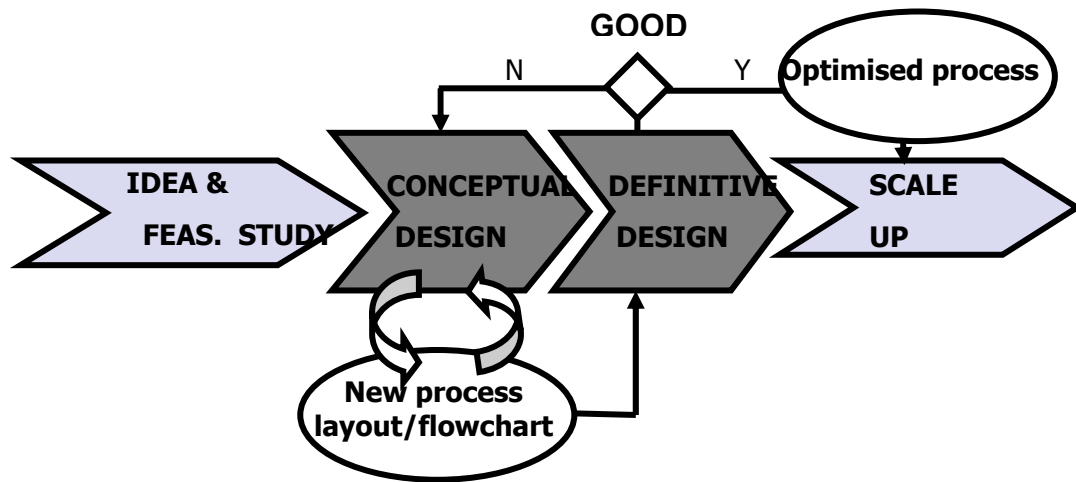


Fig. 4 : Iterative development of design stages modified from Wu [1994]

2.1.1.5 Implementation Process

The implementation stage encompasses the conceptual and definitive design stages. It develops through the following phases:

Phase 1: Laboratory knowledge achievement. (See section 2.1.1.7)

Phase 2: Conceptual design. This is the most crucial phase where the greater part of the costs are determined. It is the phase when each step is reviewed, in order to make the production route easier, cheaper, quicker and safer. Therefore the whole process must be questioned from the practical point of view and, if necessary, modified to reflect the emerging reality. This leads to a new material flow. Some tools and techniques are commonly used at this stage. A very important one is the problem solving technique (See section 2.1.2).

Phase 3: Detailed design and manufacturing. This step refines the parameters and tests the entire process on a larger scale. Previously unsolved problems are addressed.

Management tools and techniques can be used to help in optimising the process into the desired specifications and tolerances. This phase is crucial in terms of achieving a Six Sigma status.

Phase 4: Commissioning or quality planning. This tests sub-assemblies and their combination into the total system in order to satisfy the specification. Procedures and manuals are elaborated. It is important to think of a process in terms of quality: creating a Total Quality Management (TQM) model is relevant to obtaining continuous quality improvement and cost reduction. It is easier to implement TQM before all production systems are in place and proper planning enables this. [Fox, 1993, Kehoe, 1996, Oakland, 1989]

Quality control leads to the definition of operational standard specifications, tolerances of the fundamental parameters, acceptability criteria and procedures to keep process at the predetermined standard and, when necessary, to correct errors. In this context it is necessary to speak about the concept of the “internal customer”: the idea is to refer to the next person in the manufacturing process who uses the feature created by an operation as if he were a customer.

Routing sheets have to be created in order to provide all people involved in the production with a description, which is as clear as possible, of each operation. Routing sheets can contain a huge amount of information, such as the name of the product, date of processing, tools to be used, order and code of operations and ingredients to be added, customer requirements, revisions dates, controls to be used and any additional information useful for the process routing. Fig. 5 reproduces an example of process sheet.

The final process routing sheets may be developed in multiple stages since the pilot plant material may be produced in development facilities rather than in longer term equipment.

♣	PRODUCT NAME						Date
					Production n°		
	Revisions		Production instruction: a) Weight 1. Add 2. b) Mill for LLLL hours. c) Heat for 10 min at 350° C d)				
		Quantity					
1. Raw material 01		10.3					
2. Raw material 02		20.3					
3. Raw material 03		26.2					
4. Raw material 04		45.6					
		102.4					
Filter	A5			Notes		Quality controls	
Mill	S3						

Fig. 5: Production routing sheet example

Based on the process sheet, the control plan has to be designed.

The control plan tells production staff, how to monitor the process and what to do in case non-conformance is detected.

Rules have to be written to cover “when, how many, how, which, etc.” controls.

Control sheets have to be designed and filled for each step of the monitoring.

2.1.1.6 Scale-Up

The scale-up is the redesigning of a process from a laboratory scale to accommodate higher production output. A successful scale up is the determination of the most compact, economical and efficient process design that satisfies industry requirements.

Traditionally industrial scale has connotations of processing tonnes of material per day, but in some cases a few kilograms of material could be enough to satisfy the monthly requirements; this is the case for example of speciality chemicals, where valuable pharmaceutical products are processed. Another example could be semiconductor industry.

Even in these situations the extension from a laboratory scale to a larger one can be complex needing process planning.

The key to the successful delivery of any innovative product is through a comprehensive practical understanding of the design to realisation process. This understanding leads to the development of the best approach to the management and the control of the process in order to deliver the right solution in the most efficient way. Process planning determines how a product is to be manufactured: costs, production preparation, production efficiency and product quality are arranged in that phase. In other words, process planning defines in detail the progression that transforms raw materials into the desired form.

During process planning, dimensions, tolerances, sequences of operations, tools, machinery, times, quality statements and other important issues have to be resolved.

Once the knowledge of the laboratory scale process is satisfactory and it is clearly reproducible, it is the time to review each step, in order to make the production route easier, cheaper, quicker and safer. Therefore the whole process must be questioned from the practical point of view and, if necessary, changed. This leads to a new material flow. Tentative parameters are then specified to construct a pilot run under production conditions.

2.1.1.7 Achieving knowledge on the laboratory scale process

The knowledge on a laboratory process, resulting from the feasibility study, can be achieved by the analysis of its structure and purposes. A checklist of questions can be developed in order to implement the investigation: it is possible to summarise the knowledge by using wide categories; an example of checklist is outline below.

Nature of the item to be produced: What are the basic characteristics (chemical mechanical, physical)? Which are its properties (i.e. how does it work)? What are the best conditions to produce it and to store it? What are the actions/conditions that can affect the product/process? How the maximum yield could be achieved?

Prescriptions to produce it: Which are the components? In what proportion are they added? What are the tolerances?

Process in laboratory scale: Is the process reproducible? What equipment has been used? What are the reasons that subtend this choice? How long does it take to

produce the item? What are the main variables that can not be changed? Which ones are instead changeable without compromising the final product? Does the order of the actions compromise the final product? How it is possible to map the process (layout and flow charts)?

Process tools available on the market: What machines are available on the market for the required task? What equipment does the company already own? Which one is most economical?

The above categories have to be investigated as much as possible, this phase is fundamental to the understanding and the developing of the future Conceptual design.

2.1.1.8 Charts of the Process

Flow-charting an entire process is the basis for analysing and improving it [Bicheno, 2002]. There are different classes of charts that could describe a process: as a result it is necessary to choose a sort depending on what is wanted to be highlighted (time, flowing of materials, etc.). Two main categories of charts are commonly exploited: process layouts and flowcharts.

Fig. 6 shows an example process layout. It provides a quick overview of process and which shows the succession of the operation and times in producing the item: rectangles and lines with arrows are the major symbols in the flow diagram. The rectangles represent activities and the arrows indicate the direction of the information flowing and the interaction among activities. It is useful to show also the time of each operation.



Fig. 6: Layout chart example

In addition, the material flow chart indicates more details than the layout charts, like, for example, processed quantity, quality controls and times. An example is made in Fig. 7.

This chart represents of what happens to the product during manufacturing. Standard symbols, shown in Fig. 8, are published by ANSI [2005], the American National Standard Institute.

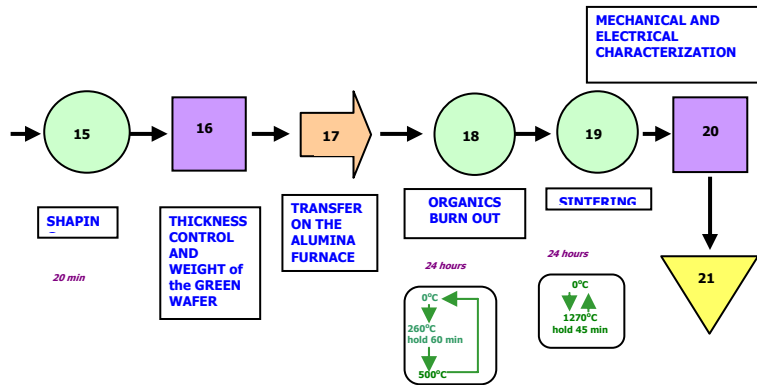


Fig. 7: Example of flow chart based on material flowing, taken from the current study

A common methodology is to divide the industrial process into several activities arranged serially. Usually each activity handles a different stage of the process; the input of each step represents the output of the previous one. Flow charting is both important for the laboratory scale process and the plant scale process; in particular, the laboratory scale charts could help in achieving knowledge of the original versions and of the developed ones.

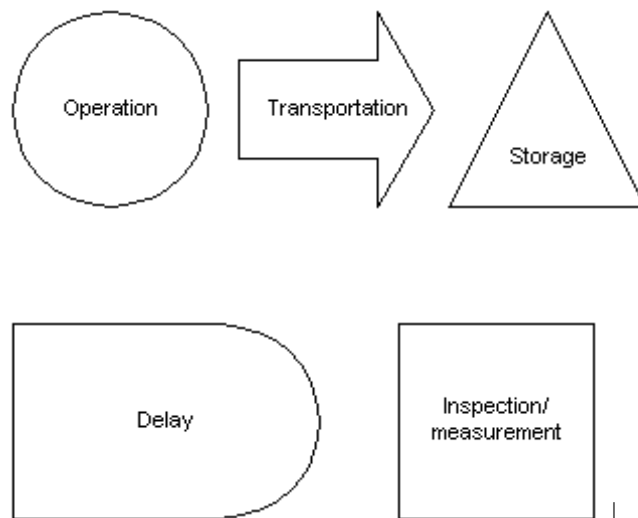


Fig. 8: Standard Symbols published by ANSI

2.1.2 The problem solving methodology

Two problem solving methodologies [Wu, 1994], can be adopted to facilitate conceptual design. Hard problem solving methodology can be used for structured problems where a quantitative aspect can be highlighted. The soft problem solving approach is used when ill-structured difficulties need to be considered.

Both approaches consist of a series of stages to guide the analyst to face a wide variety of complications; they lead to the answers in an iterative manner. Soft and hard systems are to be considered complementary rather than exclusive.

A soft problem solution is developed as follows: as neutral as possible a collection of information is obtained (Unstructured Problem), a summary of the problem is given (Problem Expression) to obtain a so-called rich picture of the situation. Then a precise verbal description of the nature of the variables that affect the problem is given (Root Definition). Hence, a picture of a system developed through deductive logic is created (Conceptual Modelling) which indicates possible solution paths to the problem. These paths are finally compared with the original problem and the actual reality (Comparison), and discussed (Debating) to select the best one, which is put into action (Action to improve situation).

2.2 The Six Sigma concept

Six Sigma is a statistical concept which measures a process in terms of its defects. Achieving a 'Six Sigma' in a process is another way of saying that the process is delivering just 3.4 defects per million of opportunities or that it works nearly perfectly.

With the use of statistical tools, Six Sigma method identifies the vital factors for improving the quality of a process and, better, it defines, measures, analyses, improves and controls the vital aspects of the process.

The methodology of Six Sigma is not rigid as the approaches can vary significantly. However, the Six Sigma procedure requires a well-defined (measurable) problem and breakthrough (measurable) goals.

The Six Sigma approach involves the entire organisation, it is customer focused and mostly it consists of five main phases:

- Definition of the goals and the deliverables to customer (internal and external)
- Measure of the process performances
- Analysis of the data and to determine the causes of the defects
- Improvement of the process to eliminate the defects
- Control of the process performances

The Six Sigma methodology uses statistical tools in order to achieve an improved quality within the Six Sigma interval. The basic statistical figures described above (Mean, Standard Deviation) and other simple ones such as the Mode or the Median are commonly used to understand patterns and correlation in occurrence of defective events.

The Six Sigma philosophy is important in particular during the design of a new process. Design for Six Sigma (DFSS) [Creveling et al., 2003] and Design for Manufacture and Assembly (DFMA) techniques are complementary approaches: the former applies a statistical approach to achieving a nearly defects free product, while the latter considers 10 fundamental rules to minimise the design complexity [Revelle, 2002].

The use of flowcharts helps in understanding each step of a process which can be very complicated. By dividing the system into sub-systems, the process is broken up into more controllable units (see section 2.1.1.8).

Several design tools and techniques are employed to develop a Six Sigma process. For example, the Quality Function Deployment (QFD) implies filling in a large matrix, known as 'The House of Quality' (in view of its shape), a complete set of customer needs (the 'voice of the customer', which become the names of the rows), and system design metrics (which become the names of the columns). When completed, the matrix is used to reorder and prioritize the design specifications, directing the development team to concentrate its efforts on those specifications that really matter in satisfying customer needs. An important side

benefit of the QFD process is that it forces to think creatively about how to solve various system design problems and which metrics to put in place to be sure that they are evaluating their progress correctly. [Bicheno, 2002, Revelle, 2002]

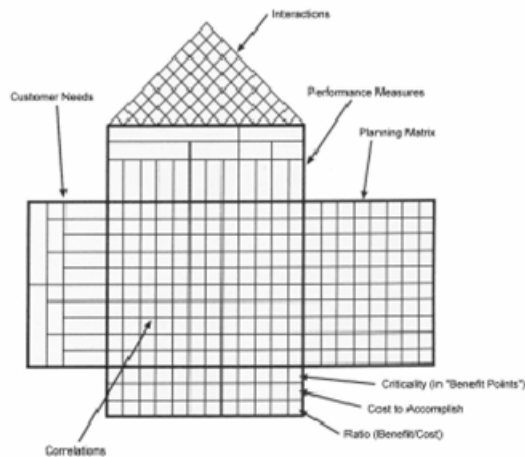


Fig. 9: An empty house of quality diagram

Another tool, the measurement system analysis (MSA) [Revelle, 2002] is an experimental and mathematical method for determining how much the variation within the measurement process contributes to overall process variability.

The statistical process control technique (SPC) [Bicheno, 2002, Oakland, 1999, Revelle, 2002] is an analytical tool that plotting the data provides predictions of the future behaviour using the past behaviour of the process as a model.

To assess a process one should:

- recognise if variation is present
- associate the variation with the causes (special or random)
- develop a strategy to eliminate the causes if they are assignable.

The methodology to improve the design is based on the use of statistical methods for decision making. The Statistical Process Control (SPC) technique has become a standard tool in many manufacturing sectors to implement, analyse, assess and control process variation, since its application has been proved to enhance problems and reduce costs.

SPC is mainly used to control industrial process variation in production. However, the application of control charts provides a simple yet powerful tool for presenting and studying results in many circumstances.

This technique can be applied either to entire processes or to parts of them. Fig. 10 shows the stages of SPC. The stages are:

- The identification of process variables, the process parameters that should be monitored,
- The collection and analysis of the process data and capabilities
- The control of the process through charts.

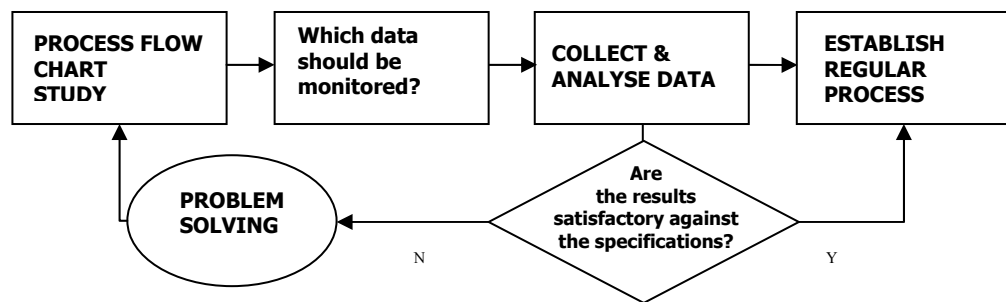


Fig. 10: Stages in SPC application

SPC is used to assess if the process is in control (i.e. if its values are found within the statistically calculated upper and lower control limits) and if it is capable (i.e. if the process can meet the specification requirements, since its response population is centred on the specification value). A more detailed explanation on how the indexes are calculated is reported following (section 2.2.3).

2.2.1 Some statistical basic concepts for Six Sigma

In order to understand the Six Sigma idea, some basic statistical concepts are needed. They are listed following.

A variable is what is measured, controlled, collected or manipulate. By plotting the value of the variable in the x axis and the number of data points got for each value of the variable in the y axis, one can plot the distribution of the population of that variable. A common way to plot the data acquired from a variable measurement is the histogram as shown in Fig. 11, which gives the perception of the occurrence of the variable values (Distribution).

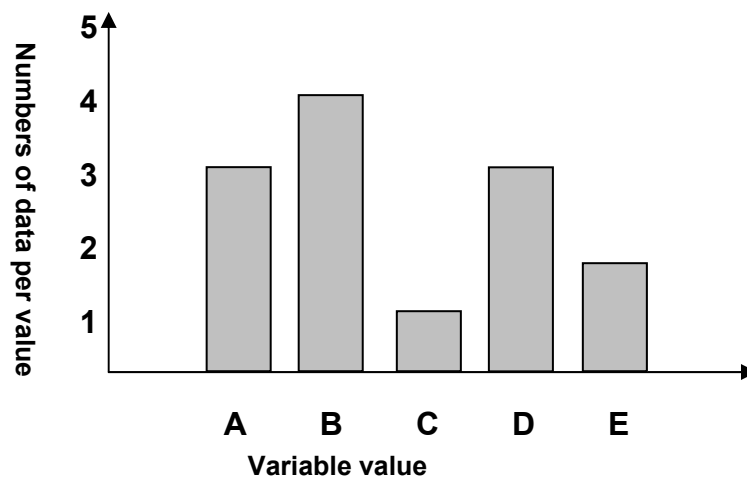


Fig. 11: Example of histogram: the variable was measured A (3 times), B (4 times), C, (1 time), D (3 times) and E (2 times)

When the variable measurements increase considerably in number, the distribution will be continuous and likely of forming a shape similar to a bell.

The "Normal distribution" or Gauss distribution (Gaussian) is the most commonly achieved and used distribution of variables in statistics. The exact shape of the normal distribution (the characteristic "bell curve" shown in Fig. 12) is defined by a symmetrical function which has only two parameters: the mean (\bar{X}) and the standard deviation (σ). The Normal distribution represents most typical distribution, but other distribution could be found. Statistical tests exist in order to assess the normality of a population.

The arithmetic mean is the medium value of a population of n values and it is calculated as in Equation 1 where x_i is representing the individual values.

$$\bar{X} = \frac{\sum x_i}{n}$$

Equation 1

$$\sigma = \sqrt{\frac{\sum (x_i - \bar{X})^2}{n - 1}}$$

Equation 2

Equation 2 describes the Standard Deviation Sigma (σ) which is a term in statistics that can be associated with the dispersion among the measures in a given population. In other words, in a normal distribution, σ is a measure of the amplitude of the Gauss curve.

A characteristic property of the Normal distribution is that 68% of all of its observations fall within a range of ± 1 standard deviation from the mean, and a range of ± 2 standard deviations (2σ) includes 95.46% of the scores. Ultimately, the interval ± 6 standard deviation (6σ) contains 99.99966% of the values, practically all the distribution. The values left outside the 6σ interval are 3.4 per million. This explains the meaning of the achieving of a six sigma status: just 3.4 products on a million opportunities have characteristics outside the 6σ interval, i.e. are defective.

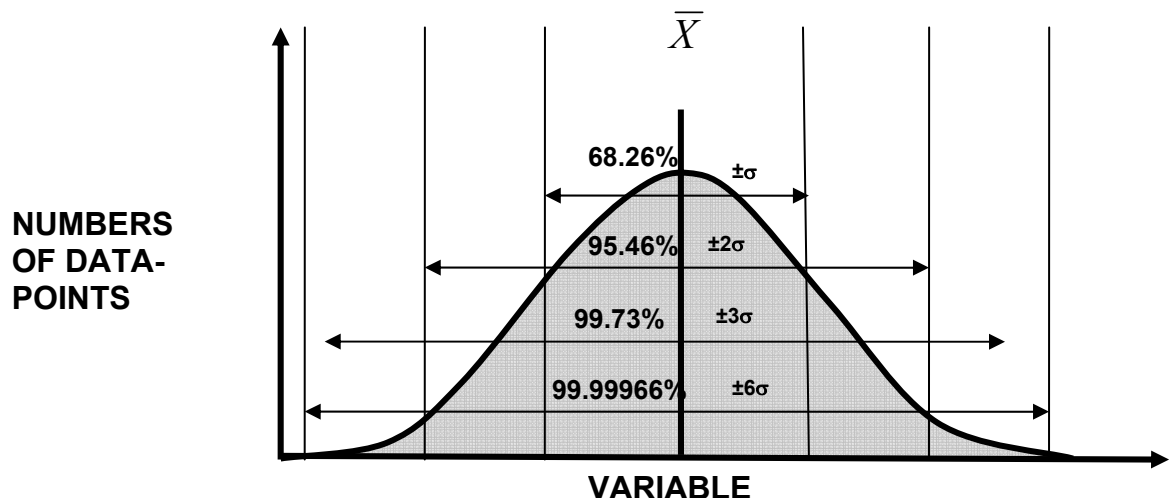


Fig. 12: Normal or Gauss distribution

2.2.2 Process variation and process capability

A process is any repetitive action whether in a transactional, manufacturing or services environment. Any process has inputs (what goes through the process) and outputs (the outcomes of the process).

The outputs, as well as the inputs, have characteristics which can be defined just if they could be measured. The output(s) characteristics have to meet the customer requirements which must be quantifiable and hence described by the process specifications (the wanted value for an output characteristic) and tolerances (the acceptable interval of error for the specification).

In other words, the specifications and the tolerances set a target values for the product characteristics and an upper and a lower specification limits (USL and LSL respectively).

When the production yields with characteristics which are outside these acceptable customer limits it is said it produces defects.

A variation is any quantifiable difference between individual measurements; any process output is naturally subjected to a variation of its outputs which can not be completely eliminated; nevertheless, it can be reduced and controlled.

Variation is due to two main categories of causes:

- random or common causes. They are due to uncontrollable events.
- special or assignable causes. They can be associated with a special reason.

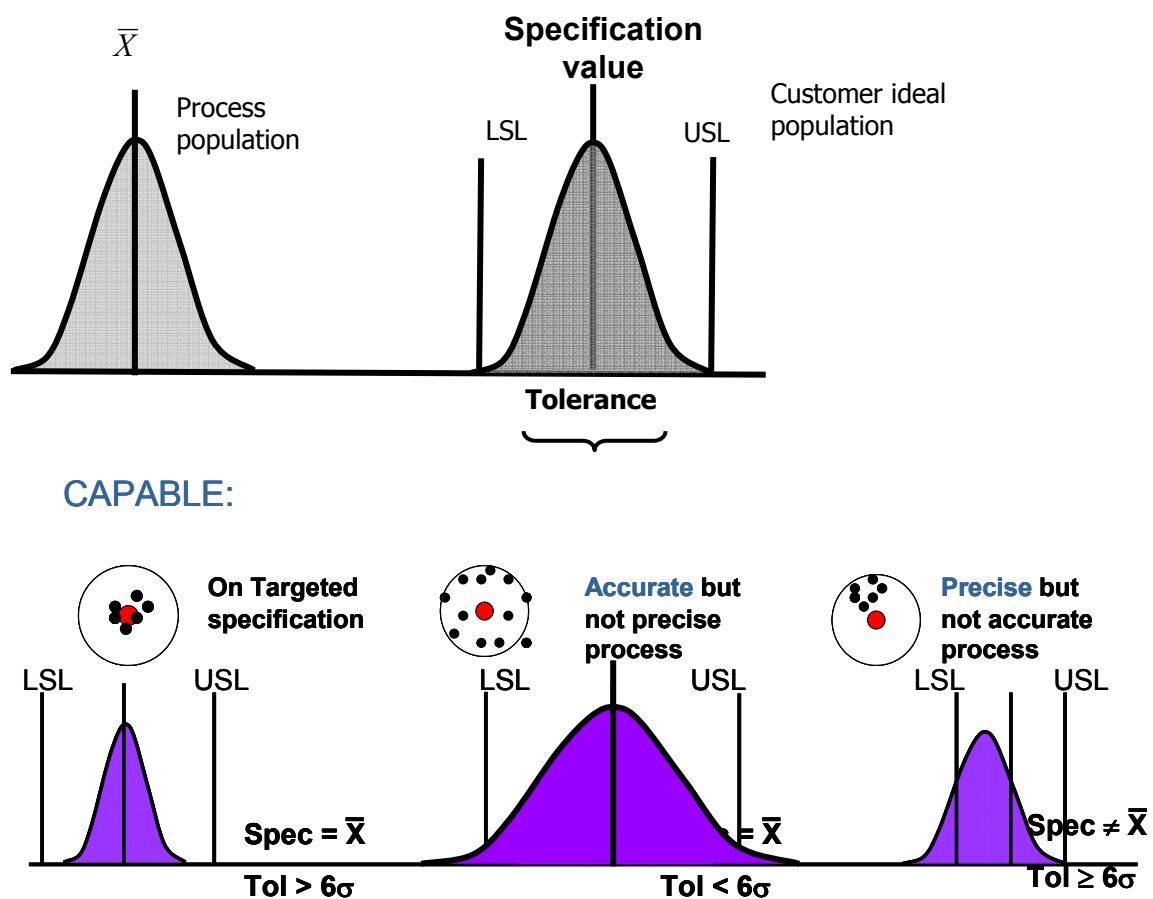
When only random causes of variation are present, the process is said to be stable or in 'statistical control'. Special causes lead instead to a 'out of statistical control' process.

The variation of the process has to be compared with the specifications and tolerance interval.

Consequently, as shown in the following scheme, a process ideally should be:

- in control: i.e. precise (meaning that the process varies less than the tolerance interval)
- capable: i.e. accurate (meaning that the process can meet the specification requirements, since its response population is centred on the specification value).

Fig. 13 shows the comparison of the population of the data with the tolerances and specifications.



2.2.3 Statistical Process Control (SPC)

SPC technique makes use of several tools to monitor the process variation: mainly the control charts and the capability indexes.

2.2.3.1 Control charts

SPC uses control charts to plot the data which can have many forms according to the necessity; the data on the x axis are sequential, usually denoting the evolution of time, while on the y axis is the statistic (the value of the variable or the average, the range, or any other figure of group of them):

Typically SPC uses:

- individual control charts where single values are plotted
- mean charts where mean values (\bar{X}) of data subgroups are plotted
- range charts (R), where the difference between higher and lower value of data subgroups are plotted.

In the Individual Control Cart, two lines corresponding to the Upper and Lower Control limits (UCL and LCL respectively) are drawn, in addition to the line representing the specification target. One way to calculate these lines is described in Table 4.

Whether continuous variables can not be normally distributed, their mean is always a normal population (Central Limit Theorem). For this reason, Mean and Range charts are the main tools for the interpretation of the process control state. These graphs are obtained by appropriately grouping the variables according to the necessity. The mean and range of each group is calculated and these values are plotted as pictured in Fig. 14. Then the average of the averages ($\bar{\bar{X}}$) and the range average (\bar{R}) are calculated. Similarly to the individual charts, Upper and Lower Control and Warning limits are calculated for the mean and range charts as following, where σ is the standard deviation of the group and n the number of data for each group.

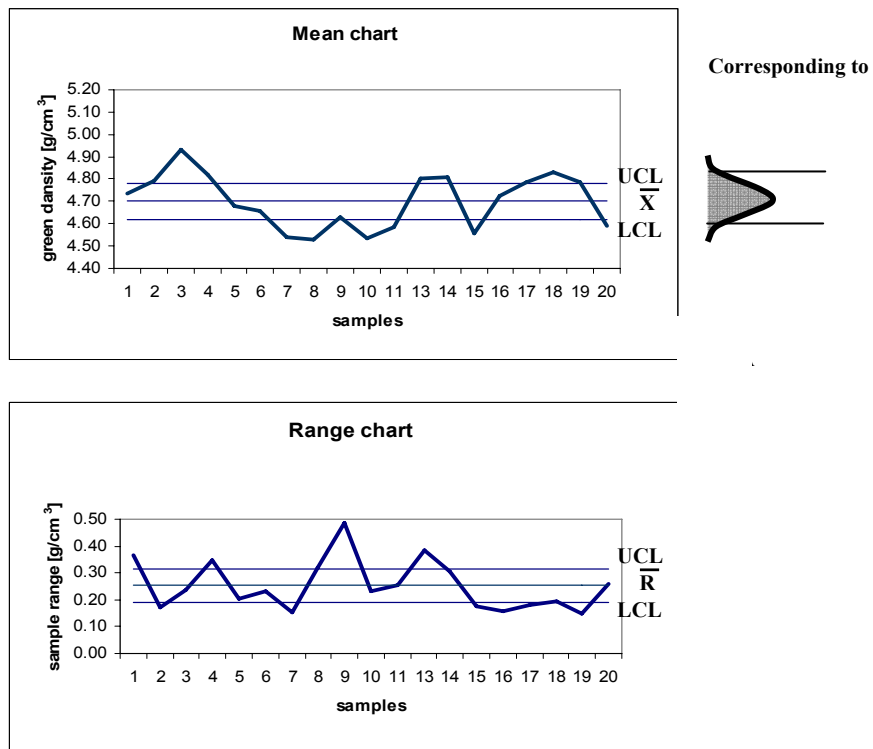


Fig. 14: Example of not in control Mean and Range charts

The interpretation of the control charts follows simple rules. The main indications of out of control state arise if any point is found out of the control limit, and if there are identifiable ascendant or descendant trends in the charts.

The region between the UCL and the LCL defines the variation which is expected from the process statistic and which is imputable to common causes. If the chart points exceed this region limits, then this is imputable to a special cause.

	Individual charts	Mean and Range charts
Upper action (or control) limit	$\bar{X} + 3\sigma$	$\bar{\bar{X}}$ or $\bar{R} + 3\sigma/\sqrt{n}$
Lower action (or control) limit	$\bar{X} - 3\sigma$	$\bar{\bar{X}}$ or $\bar{R} - 3\sigma/\sqrt{n}$
Upper warning limit	$\bar{X} + 2\sigma$	$\bar{\bar{X}}$ or $\bar{R} + 2\sigma/\sqrt{n}$
Lower warning limit	$\bar{X} - 2\sigma$	$\bar{\bar{X}}$ or $\bar{R} - 2\sigma/\sqrt{n}$

Table 4: Relevant formulas in SPC

2.2.3.2 The capability indexes

Through the use of capability indexes [Roth, 2005], SPC also assesses if the process can meet the required specifications and tolerances.

The capability indexes compare the spread of the variation and the position of the central value with the specifications and tolerance.

Equation 3 describes how to calculate the capability indexes:

- | | |
|--------------------------------------|----------------------|
| A) $Cpk_u = (USL - \bar{X})/3\sigma$ | Measure of accuracy |
| B) $Cpk_l = (\bar{X} - LSL)/3\sigma$ | Measure of accuracy |
| C) $Cp = (USL - LSL)/6\sigma$ | Measure of precision |

Equation 3

The minimum value for a process to be considered capable is 1 (where the variation coincides with the tolerance interval). Anyway, it is desirable for the indexes to be much greater than 1.

2.3 Brief introduction to ceramic processing by tape casting

In the following sections an overview of the principles of ceramic processing is given, mostly focussing on the issues relative to the particular tape casting process discussed in this work.

The general route to produce ceramic objects is shown in Fig. 15.

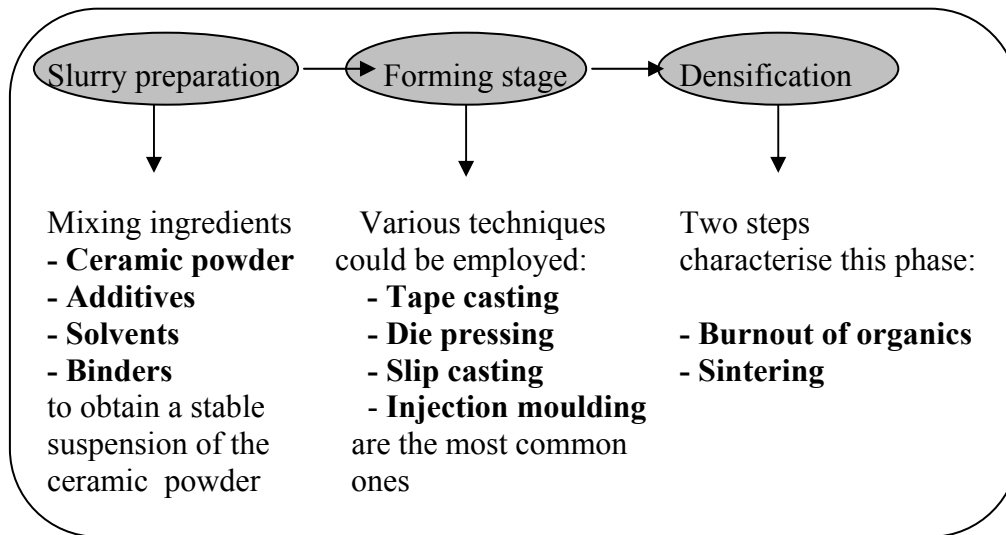


Fig. 15: A typical layout of ceramic processing

During the first step of the process, the ceramic powder is comminuted and mixed with the other organic ingredients to form a stable suspension. Subsequently, the liquid slurry is cast and the solvent is evaporated so that the material acquires a shape (green ceramic body). Finally, the green ceramic is heated in order to burn the organic phase which has been added in the slurry and in order to promote the consolidation of the powder (sintering).

A key factor for the achievement of a ceramic body with the desired satisfactory requirements is related to the packing density and the packing homogeneity in the green body. These factors are dependant on a number of variables among which the most important are intrinsic of the powder characteristics, of the ingredient chosen and their relative dosages and of the forming technique employed.

2.3.1 The slurry preparation: ingredients

The accurate choice of the ingredients (their nature and relative amount) is fundamental for the achievement of a satisfactory result.

The system is multiphase and therefore it is extremely complicated and sensitive to variations. Often a relatively minor change in the slurry composition could lead to a great variation in the cast results.

The general rule for formulating slurries is to keep the amount of solvent and organic ingredients the lowest possible.

The variety of the ingredients is huge but some generalisation on the requirements for tape casting can be done.

2.3.1.1 The powder

After binder removal the only material left is the powder, which obviously determines the characteristics of the final material.

Consequently, it is of utmost importance to preserve the nature of the powder during processing by avoiding contamination.

Many kinds of ceramic powders (metal oxides) have been processed by tape casting both in aqueous and solvent environment such as Al_2O_3 , [Doreau et al., 1998, Kristoffersson et al., 1998a], Si_3Na_4 [Bitterlich and Heinrich, 2002, Gutierrez and Moreno, 2000], Yttria Stabilised Zirconia [Maiti and Rajender, 2002, Snijkers et al., 2004] or PZT [Jantunen et al., 2004, Navarro et al., 2004a, Roncari et al., 2001].

In the dry state the particles clump together: firstly as they are subjected to the Van der Waals forces, they create soft (low energy) agglomerates which can be broken by simple stirring; secondly, they can be strongly agglomerated (hard agglomerates) needing a severe and energetic method to be dispersed.

The powder has to be able to closely and homogeneously pack in the green body. This is a necessary requirement for improving the sintered microstructure, reducing the firing shrinkage, the defects and warpage. It also allows better dimension control in the formed material.

Generally, better results are achieved for strongly de-agglomerated powders with a fine (in the range 0.1-1 μm) and narrow particle size distribution and a regular, equiaxed shape. [Roosen and Bowen, 1988b]

The most common way to achieve de-agglomerated powders is by wet milling processing. The powders are rolled in sealed jars for several hours (usually more than 10) with hard media and solvent(s). Additives (dispersants) are usually added in order to improve the comminution efficiency and to provide the suspension a better stabilisation. [Herbst and Fuerstenau, 1972]

2.3.1.2 Solvents

The solvent dissolves the organic materials and distributes them uniformly in the slurry. Although historically the slurries for tape casting were prepared in a non aqueous environment (typically alcohols, ketones or hydrocarbons), in more recent times techniques to cast water based slurries have been developed as an alternative [Hozta and Greil, 1995, Mistler and Twiname, 2000]. This happened especially because of the environmental and health related aspects, but also because of the reduced costs and of the easy attainment of water.

In this section only the issues related to the use of water as a solvent will be covered.

Although water has certain advantages from the health perspective, the achievement of good tapes and the reproducibility of the results are more difficult to obtain [Harper, 1990, Nahass et al., 1990]

This is because aqueous slurries in fact have a smaller tolerance to minor changes in processing conditions and slurry composition. In addition, the selection of the organic ingredients is harder as the variety of soluble binders, plasticizers and dispersants is restricted to few systems. Moreover, the use of the water, because of its high surface tension, implies the use of ulterior additives such as wetting agents [Navarro, 2001] to promote the adhesion of the slip to the carrier support.

2.3.1.3 Dispersants

When the powders are comminuted, they reach a particle size in the range of hundreds of nanometres to few microns. In this range, when they are placed in a liquid medium, the colloidal forces are often more relevant than the gravity force. Consequently, the ceramic primary particles tend to spontaneously form agglomerates (soft) which can be broken by stirring; in order for the particles soft agglomerates not to be reformed after being destroyed when the agitation is removed, the primary particles have to be stabilised by adding dispersing agents. These agents, commonly called dispersants or deflocculants, act by increasing the repulsive forces among the particles to counterbalance the Van der Waals attractive forces. Their action could be of different nature such as electrostatic (the charging of the particles surfaces in order to keep them apart by electrostatic repulsion, as shown in Fig. 16a), or steric (the hindrance of molecules adsorbed on the particles surfaces prohibits the particles to come in contact, as illustrated by Fig. 16b), or their combination (electrosteric Fig. 16c) (see section 2.6 in the Literature Review, Page 49) [Pugh and Bergström, 1994, Tadros, 1996].

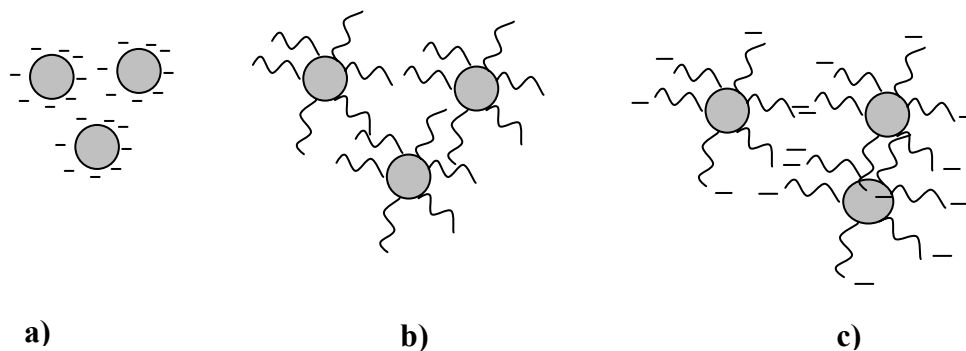


Fig. 16: Schematic illustration of the working principles of the most common dispersants: a) electrostatic, b) steric, c) electrosteric

The good dispersion of the slip is required for many ceramic forming techniques, but it is of utmost importance in the tape casting process. This is for several reasons: first, the soft agglomerates can trap air which could create problematic and unsuccessful de-airing, ending in unwanted porosities in the tape. Second, if

the agglomerates are present, the binder will envelop the agglomerated particles ending in a defective packing in the green body (Zipper- bag theory) [Mistler and Twina, 2000]. Thirdly, a well deflocculated slip will pack to a higher density than a flocculated slurry [Reed, 1988, Sumita et al., 1991, Ueyama and Kaneko, 1987]. Fourthly, flocs in the slip cause lack of homogeneity in the green tape, introducing highly localised porosity, which represents a major threat for the reproducibility of the final product.

In addition, although this is debated [Kapur et al., 1996], the dispersant is believed to act also as a comminution aid, promoting the breakage of the hard agglomerates as it affects the rheology of the slurry [Frances and Laguerie, 1998, Funk and Dinger, 1994, Shi and Napier-Munn, 2002].

In summary, as a result of the dispersant addition it is possible to:

- decrease the amount of solvent needed and hence increase the solid loading,
- achieve a stable suspension of the primary particles preventing the re-creation of the soft agglomerations,
- improve the packing in the green tape,
- reduce the particle size of the powder.

The adsorption of polyelectrolytes (dispersants which act both on the sterical and electrostatical principles) on the ceramic surface is probably the most commonly used method for dispersing oxide powders in water. Among those available for water processing, one of the most used is the polyacrylic acid (PAA) [Cesarano Iii and Aksay, 1988]. In Fig. 17 the structure of a typical PAA is reported.

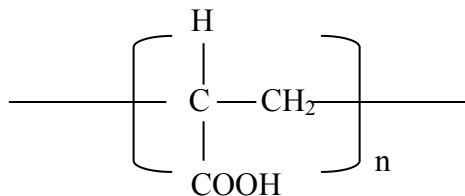
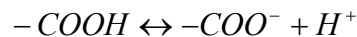


Fig. 17: Chemical structure of a Polyacrylic acid segment.

The PAA functional group is a ---COOH (carbossilic group) which is subjected to the equilibrium reported in Equation 4. It is therefore clear that its action is strictly related to the environment's pH.



Equation 4

Normally, the PAA is added as a salt whose counterion, typically NH_4^+ , is totally eliminable by burn out in order not to contaminate the ceramic.

2.3.1.4 Binders (water-compatible)

The binder(s) is added to the slurry in order to provide the cast tapes with strength. In the dried green tape, the binder holds the ceramic particles together by bridging among them. In this way, the tape can keep its shape and can be easily manipulated (cut, punched, stacked and laminated) before being sintered.

A reduced range of water-compatible binders is known compared to the solvent ones. The general configuration of the organic polymer is made by a backbone of covalently bonded atoms of carbon, oxygen and hydrogen to which side groups are attached at intervals along its length. It is the nature of these side branches, highly polar, to give the polymer a certain compatibility with the water solvent.

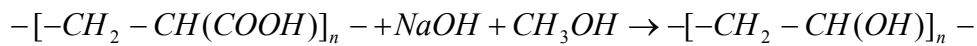
The length of the molecule can vary and depends on the degree of polymerisation of the originating monomers. Normally, it is expressed in average molecular weight. This characteristic gives to polymers of the same nature different macroscopic properties: in general, the higher the molecular weight, the more viscous and the more resistant to mechanical stresses is the polymer. The organics binders are either dissolvable in water or dispersed in water as emulsions.

The most used binders for aqueous tape casting are polyvinyl alcohol (PVA), cellulose ethers and latexes. The first two belong to the group of the water soluble polymers, while latex is supplied as water emulsion. Kristoffersson et al. compared the properties of these binders for tape casting use [Kristoffersson et al., 1998b].

In this section only polyvinyl alcohol as a binder will be described.

2.3.1.4.1 Polyvinyl alcohol (PVA)

Commercial PVA is usually a mixture of polyvinyl alcohol and polyvinyl acetate since the acetate is left from its processing production as shown in Equation 5. If the acetate is present in a percentage between 11 and 17 %, then the PVA is denominated as partially hydrolysed PVA. When the amount falls to 1 or 2%, then it is called fully hydrolysed.



Equation 5

The sketch in Fig. 18 portrays the change in properties of the PVA with the degree of hydrolysis and the molecular weight. The solubility of the PVA increases with the increase of the acetate groups, while its glass transition temperature (T_g) and tensile strength are lowered with a lower degree of hydrolysis. Both the viscosity and the surface tension are lower for higher degree of hydrolysis.

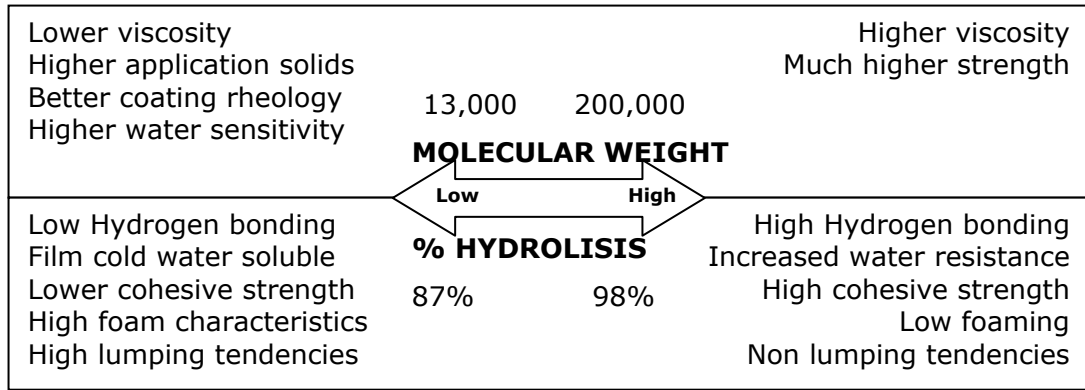


Fig. 18: Polyvinyl alcohol hydrolysis and molecular weight effects (reported from producer (Celanese Chemicals) brochure of Celvol™ Polyvinyl Alcohol)

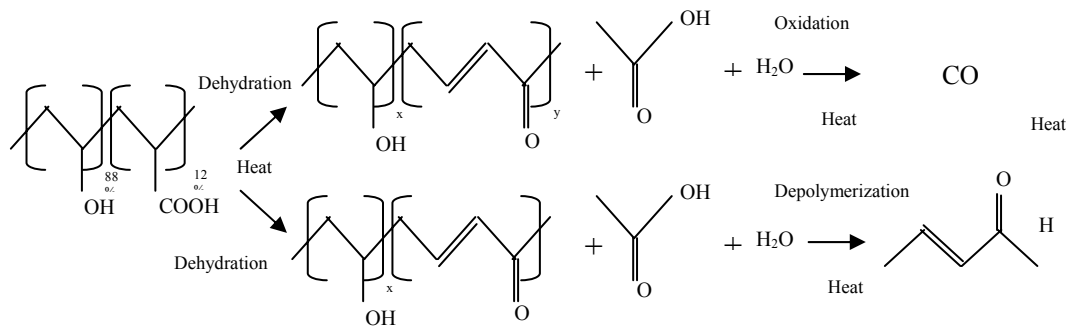
The high strength of the PVA combined with its very controlled and clean burnout in a variety of atmospheres, makes it a suitable ingredient for the manufacturing of ceramics.

The PVA for tape casting use needs to be plasticized in order to modify its flexibility; commonly, the plasticizers used belong to the glycols category, typically Glycerol, Polyethylene or Polypropylene Glycols.

Water also acts as a plasticizer for PVA, hence its amount has to be carefully maintained under control.

The PVA is usually supplied in powders or small granules to be dissolved in water. Due to its solubility characteristics, the processing of the PVA is sensitive to the water temperature: the most critical step in dissolving the polymer is to completely disperse the particles in water. Since the surface of the particles will swell very quickly and clump the particles together, it is important to disperse the powder accurately and slowly in cold (<38°C) water. When good particle dispersion is achieved, the polymer solution can be heated above 85 °C for a minimum of 30 minutes to allow a complete dissolution. Adequate agitation is required for both these dissolving steps.

The PVA thermally degrades in a controlled way both in a rich and in a poor oxygen atmosphere. However, the burnout path for the two conditions is different, as described by Equation 6.



Equation 6

The partially hydrolysed PVA is known to behave differently in suspensions, depending on the nature of the particles surfaces. It contains 4-12% of acetate groups which promote the grafting onto hydrophobic surfaces such as polystyrene. The hydrophilic vinyl alcohol segments are instead more affine to polarised surfaces [Tadros, 2003a]. All types of adsorbing behaviour are known in literature; for example while the PVA is almost non adsorbent onto alumina particles [Khan et al., 2000], it is known in literature for promoting flocculation, when absorbed onto the particle surface as in Silica [Kahdilkar and Sacks, 1988].

2.3.1.5 Plasticizers

An ingredient commonly defined as plasticizer is often added to most of the tape casting compositions, depending on the binder variety used.

The purpose of a plasticizer is to enable the green tape to be easily bent without cracking. This because most of the polymeric binders (PVA belongs to them) typically used would form a relatively strong tape but stiff and brittle, if no plasticizer is used.

Instead, the tape cast material has to be extremely versatile and malleable as often it has to be punched, cut, rolled and laminated.

As its name suggests, the plasticizer modifies the mechanical properties of the ceramic sheets by increasing their plasticity, i.e. their ability to permanently deform. The increased plasticity of the green body results in the tape augmented flexibility.

Two different plasticizing principles are used:

- Type I plasticizers which are used to soften the binder polymer chains, allowing them to stretch and bend easier. They modify (lower) the glass transition temperature (T_g) of the binder by either solvating the binder or shortening its polymer chains [Song et al., 2000]. In fact most of these plasticizers are polymeric solvents and their only difference from the slurry solvent is their far lower evaporation rate which allows them to remain in the green body after all the slurry solvent has been evaporated. The most common plasticizers belonging to this category are phthalates and glycols.

The main drawback of this plasticizer variety is that an excess would increase the stickiness of the tapes both to the carrier (complicating the tape release) and to other ceramic material, dust and handling tools (requiring protection and care in the material storage and the handling).

- Type II plasticizers act as lubricants in the tape matrix, working among the binder polymer chains, facilitating their relative motion and preventing their cross linking. The lubrication results in a larger strain to failure, but contemporarily decreases the yield stress.

A lowered yield is beneficial both for non planar applications such as wrappings and coatings and for multilayer lamination improving the tape adaptability to various shapes. Also, the employment of this variety of plasticizer can reduce the stresses caused by the drying of the tapes, decreasing the risks of tape cracking. More, by limiting the binder's binding quality, it can aid the tape release from the carrier.

Oils and stearates are used typically as Type 2 plasticizers.

The drawbacks of an excessive employment of the Type 2 plasticizer are the reduced yield stress and tape strength on one side and the possibility of phase separation and plasticizer migration which causes lack of homogeneity on the other side.

Fig. 19 shows the different effects of Type 1 and 2 plasticizers on the mechanical characteristics of the ceramic tapes.

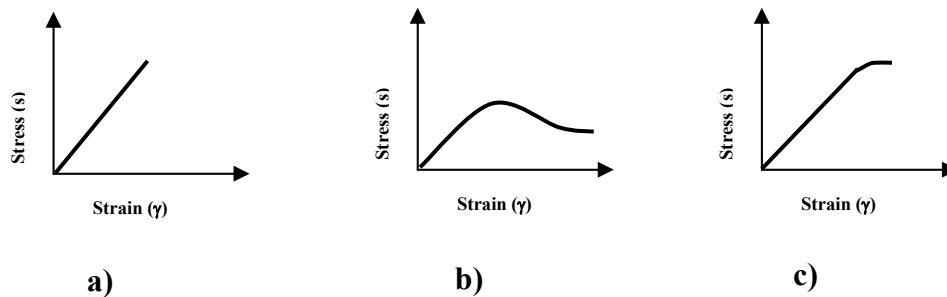


Fig. 19: Strain-stress diagrams for differently plasticized materials. a) Not plasticized, b) type 1 plasticizer, c) type 2 plasticizer

2.3.2 Ingredients interactions

The number of interactions possible in slurries designed for tape casting is very high, due to their complexity and multiphase nature. The interactions are very specific to the systems used and it is quite difficult to generalise. Some examples of interactions among the ingredients are:

Binder/dispersant interactions:

- as the stabilisation of the particle can occur in many ways and the categories describing the organic ingredients is purely determined empirically according to their activity, it can happen that a polymer added

to act as binder behaves as a dispersant too. In this case its effect will shadow the dispersant effect and the system viscosity will be dropped at the addition of the 'binder'. On the contrary, the binder added, can mask the effect of the dispersant and induce flocculation.

- The dispersant and the binder can react chemically. The reactions can take a long time to occur, varying the characteristics of the slurry with time.
- Some binders can displace the dispersant from the particle surface, or vice-versa [Rachas et al., 2000]. The order of the ingredients addition is therefore extremely important in order to achieve a good reproducibility of the slip characteristics [Rachas et al., 2000]. When the dispersant and binder are added at the same time for example, there is competition for adsorption on the particles' surface. This can result not just in less binder being available to network the particles and to give strength to the material, but also in some free dispersant which reduces its effectiveness resulting in flocculated or partially flocculated slurries.

Binder/plasticizer interactions:

- These are normally very desirable interactions which have been explained in the previous section (2.3.1.5).

Dispersant/plasticizer interactions:

- Usually these two genders of molecules do not interact. However, it is logical to assume that in some cases, the polymeric dispersant can act as plasticizer.

2.4 The slurry preparation: processing

2.4.1 Dispersion milling

As seen in Fig. 15, the first step in the preparation of any ceramic is the slurry preparation. This happens by mixing the ingredients chosen, normally by using high energy techniques such as wet ball milling or planetary milling.

The purposes of this dispersing procedure are: first, to break apart the particles agglomerates (soft and hard) by the pounding and grinding of the media; second, to distribute the organics evenly on the particles surface and third, to create a stable suspension.

A ball mill, the most commonly used technique, consists of a rolling reservoir containing the slurry and half of the volume of milling media (normally spherical or cylindrical). By rolling, the media crush the powder and the energy of the impact breaks the powder's hard agglomerates and reduces the particle size. (This is illustrated in Fig. 20).

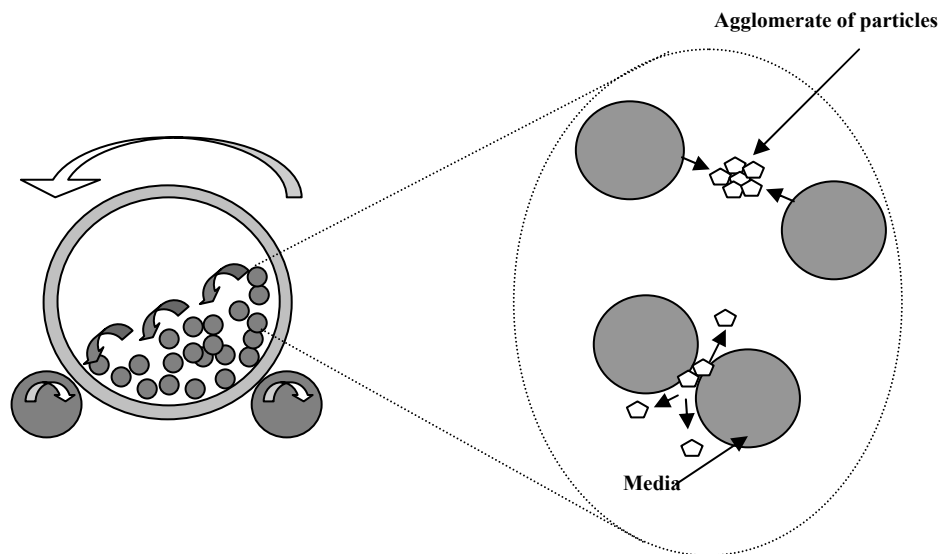


Fig. 20: Schematic representation of the cross section of a ball mill with an enlargement of the impact of two milling media.

The size and the type of the mill have to be chosen according to the amounts to be prepared and the characteristics of the powder and the slurries:

- the batch size can vary from 0.3 litres up to over 3000 litres;
- the material of the ball mill and the milling must be adequate in order not to contaminate the slurry with debris: high alumina and zirconia are typically employed especially for the milling media, but in some cases a plastic (such as polyethylene) container is preferred as its debris can be eliminated in the de-binding stage.

- The milling media have to be of an adequate density, higher than the slip's specific gravity.
- The mill rotation speed should be a fraction (typically 35-90%) of the critical speed (at which the media don't tumble any more, but follow the motion of the pot).

In the preparation of a tape casting slip, the procedure requires that the ball milling is performed in two stages:

- 1) 1st ball milling: dispersant, solvent and powder are added in the ball mill. This is a very critical stage when a good stable suspension should be achieved. The milling time can vary between 4 and 48 hours. During this time, not just the agglomerates are destroyed, but also the dispersant is adsorbed onto the newly formed particle surfaces, providing a good stabilisation against flocculation and settling.
- 2) 2nd ball milling: where the plasticizer and the binder are added (in this order). This milling, lasting usually more than 12 hours, provides that the plasticized binder is distributed uniformly across the particles. If the binder is added to imperfectly dispersed slurry, it will envelop clusters of particles trapping portions of solvent and resulting in a non homogeneous slip. (Zipper-bag theory [Mistler and Twinaime, 2000] Fig. 21)

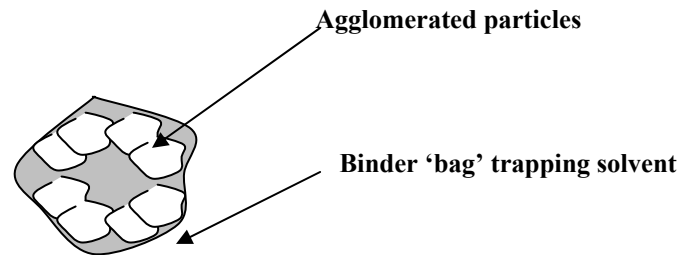


Fig. 21: Schematic representation of the 'Zipper bag theory'

2.4.2 Slurry Conditioning and Characterisation

The next step, so that the slip is ready to be cast, is the removal of the air trapped in the slip during the millings. Air bubbles cause defects in the tape such as pinholes (rounded craters) or 'crow foot' defects (cracks radially extending from the pinholes). The equipment for the de-airing is normally a vacuum container where the slip can be maintained under constant agitation. The agitation helps the de-airing by lowering the viscosity of the (pseudoplastic) slurry. Along with the

air, some solvent can be extracted by the vacuum, so the depression shouldn't be kept for too long. However, the de-airing conditions strongly depend on the slurry characteristics and the equipment employed. For example, very slow rotation in a sealed container for long periods of time (24 hours or more) can be an alternative to the vacuum, since the bubbles tend to be eliminated from the surfaces of the slip. This technique is suggested when the solvent is particularly volatile or in case of very viscous slips.

The elimination of unwanted residues (e.g. undissolved binder, big agglomerates of particles not successfully destroyed by milling, debris coming from the milling media or container) is achieved by sieving the slurry through a fine mesh filter. This is usually done also to separate the media from the slurry.

2.4.3 General overview on Tape Casting

The tape casting technique is of the most commonly used forming methods for producing thin and flat ceramics, mainly for the electronic industry.

Typical application examples for tape cast material are multilayer capacitors and actuators. However, the range of the applications has been expanded to ceramic laminates, ceramic membranes, fuel cells for power generation, separators for batteries and heat exchangers [Mistler and Twiname, 2000].

The thickness of the layers produced can vary from few microns up to 1 mm. The technique can be used in continuous (mainly in industrial plants) or in batch (typically laboratory scale) production.

Slurries especially formulated can be cast by a blade into a flat layer, then dried into a flexible solid tape which is further cut into the desired shape and subsequently sintered into a hard ceramic.

The sheets obtained by the tape casting technique can also be processed (punched or laminated [Cui et al., 2003] to produce different shapes and sizes.

Fig. 22 illustrates the tape casting equipment and its basic principles: the reservoir (1) where the slurry (slip) is poured ends into a blade (doctor blade) (2) which is set to let a flow of the liquid from the gap (3). Once the carrier film (4) is in motion, the slip flows underneath the blade and is formed into tape (5) whose thickness is evenly calibrated.

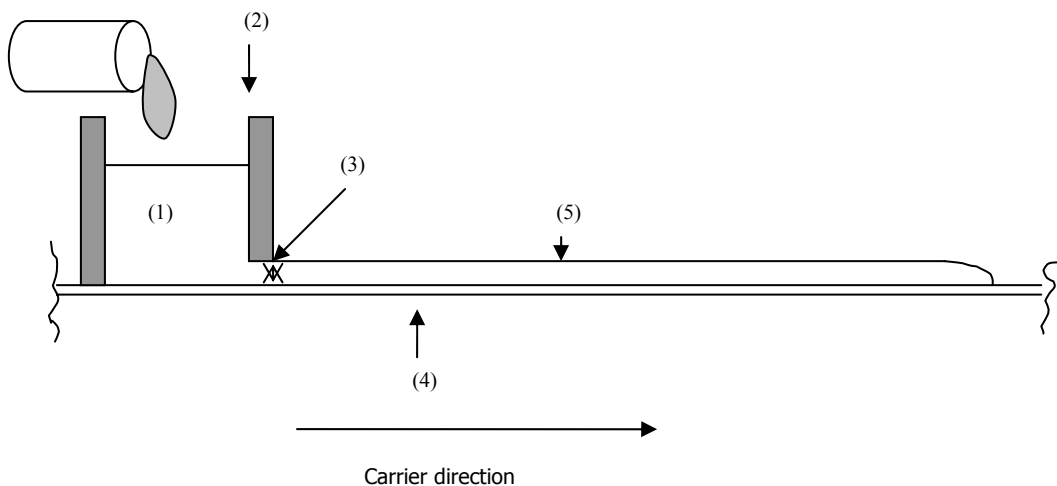


Fig. 22: Sketch of the mechanism at the basis of the tape casting equipment

The performance of the tape casting depends on many factors that can be grouped as:

- 1) the slurry chemical composition
- 2) the processing parameters.

The slurry composition should allow the ceramic to be well dispersed, creating a stable suspension which generates a homogeneous and compact green structure. The organic ingredients (additives) have to work individually to improve the tape characteristics (adhesion to the carrier during casting, easy release after drying and dispersion of the particles in the suspension), without interacting. The binder system has to improve the mechanical characteristics of the tape without compromising the green density or inducing flocculation.

Several processing parameters contribute to the quality of the tape and have to be controlled carefully to make the process reproducible.

The casting parameters:

- 1) the quantity of the slip determines the length of the tape, for a given gap height.
- 2) the speed of the carrier film and the gap height, which apply a shear stress on the slurry during casting, establish the thickness of the tape. As the level of the slurry in the reservoir increases the pressure on the head (P) and the flowing velocity of the slip out of the gap increase too.

This can be understood by considering the following relationships reported in Equation 7 for the shear rate under the blade ($\dot{\gamma}$) and l_r = length of reservoir

Equation 8 for the pressure on the casting head (P).

$$\dot{\gamma} = v / h_o; \quad v = \text{speed of carrier; } h_o = \text{gap height}$$

Equation 7

$$P = Q_r \times g / l h_o \quad g = \text{gravity acceleration; } Q_r = \text{slurry mass; } l_r = \text{length of reservoir}$$

Equation 8

- 3) the viscosity of the slip is another important factor that influences the tape thickness. The viscosity represents a definite resistance to change in form or “internal friction” of the fluid; it determines the extent of slip flow due to the forces acting on it. The lower the viscosity, the greater the deformation under the hydraulic force caused by the slip in the reservoir. The viscosity has such a large effect on the final cast tape that it is of primary importance to keep it under strict control during casting.

As illustrated in Fig. 23, in pseudoplastic slips (characterised by “shear thinning” behaviour typical of ceramic slurries, see section 2.6.4.1.2), the viscosity is strictly dependant on the shear stress applied. Changing the shear forces (gap height or carrier speed) modifies the apparent viscosity and thus the volume flow of the slip. Consequently, it is important to decide the correct casting conditions to have small perturbations.

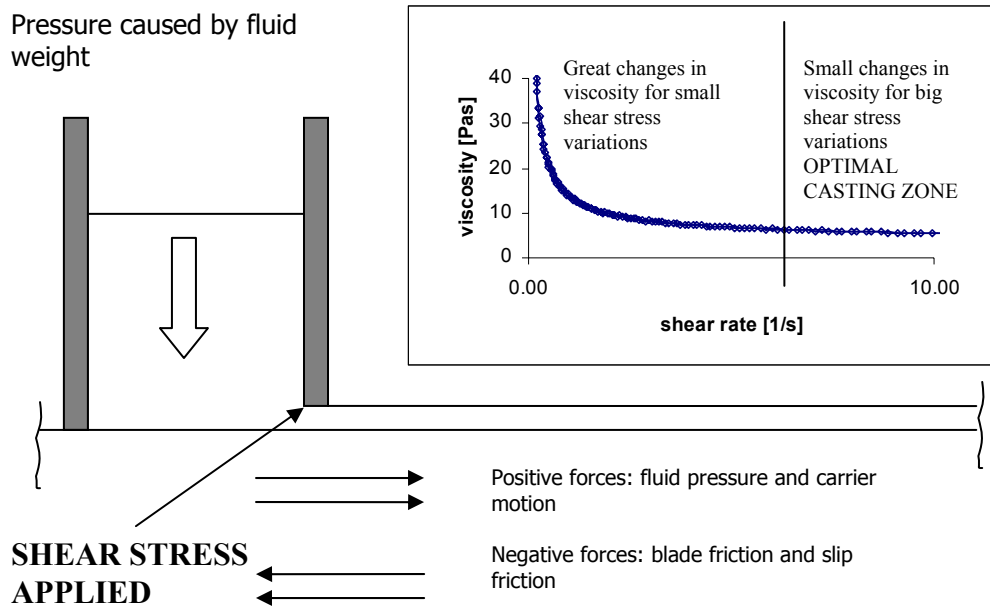


Fig. 23: Forces involved in the tape casting process

- 4) the level in the reservoir regulates the flow of material through the gap. Variations in the pressure (level) of the slip in the reservoir influence the casting performance. This effect can be reduced by using double doctor blade equipment which creates a “buffer reservoir” that controls the pressure. A “full capture” doctor blade has side walls that prevent slip flow out the sides and has a reservoir (‘buffer reservoir’) between the blades close to or equal to the reservoir to which slip is added (the 'fill reservoir'). In this case, the pressure under the blade is regulated (Fig. 24). This reduces the random error caused by the refilling operations.
- 5) the accurate control of the drying conditions (humidity and heat) helps in preventing the formation of cracks and defects.

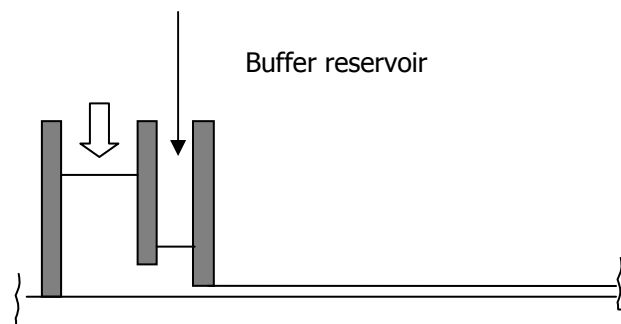


Fig. 24: Buffer reservoir scheme

2.4.4 Tape drying

Once cast, the tape is left to dry: the solvent evaporates and simultaneously the tape thickness decreases. Both gravity and the shrinkage of the organic system generate a packed structure and an increase in density. The drying process causes the particles to move closer together: the shrinkage in the lateral direction is negligible compared to the one in the thickness direction. The drying stage is crucial and stresses can build up into the tape. Cracks can develop as a result of the pressure gradient caused by capillary tension on the fluid.

The mechanism beyond the drying is led by surface evaporation and vapour internal diffusion and mainly it is developed into three different stages which were defined by Scherer in a review [1990] and are schematically shown in Fig. 25:

1) The constant rate period (CRP, Fig. 25a) during which the evaporation rate per unit area is constant (independent of the drying time but dependent on the temperature). The evaporation occurs at the body surface, which is continuously covered with a layer of liquid extracted from the internal part of the body. The transport of the vapour from the air layer just above the body surface and the ambient temperature also control the evaporation rate. Often, the diffusion rate of the liquid from the internal part of the body to the surface is far slower than the evaporation rate; this causes the formation of a dried layer on the top of the tape (skin) which limits the escape paths available for the liquid to reach the surface. Most of the shrinkage, if not all, happens in this stage. The shrinkage of the body is proportional to the amount of water lost.

The flow of the liquid towards the surface is due to local variations in particles packing: the smaller pores have a higher suction pressure due to capillary forces. This difference in pressure causes a rearrangement of the particle network within the ceramic.

The rearrangement of the particles happens laterally also and the diameter of the pores is reduced. Also, the meniscus radius shrinks up to a point when it has the same dimension as the pores. At this stage, the CRP ends.

2) In the first falling rate period (FRP1, Fig. 25b), the liquid withdraws into the porous body and the evaporation rate decreases with time. The drying still happens mostly at the surface (which is now recessed in the cavities of the green drying body), but some vapour diffusion occurs too. The body stops shrinking. The liquid-vapour meniscus becomes curved and the particles are covered by a thin layer of liquid allowing the flow. The thinner pores continue having a higher drying rate and the liquid is constantly transferred to them from the larger ones. When the flow of the liquid stops, the diffusion of the vapour is the only mechanism left and the FRP1 finishes.

3) In the second falling rate period (FRP2, Fig. 25c), the evaporation rate becomes less sensitive to the external conditions. The evaporation happens just by vapour diffusion internally to the body.

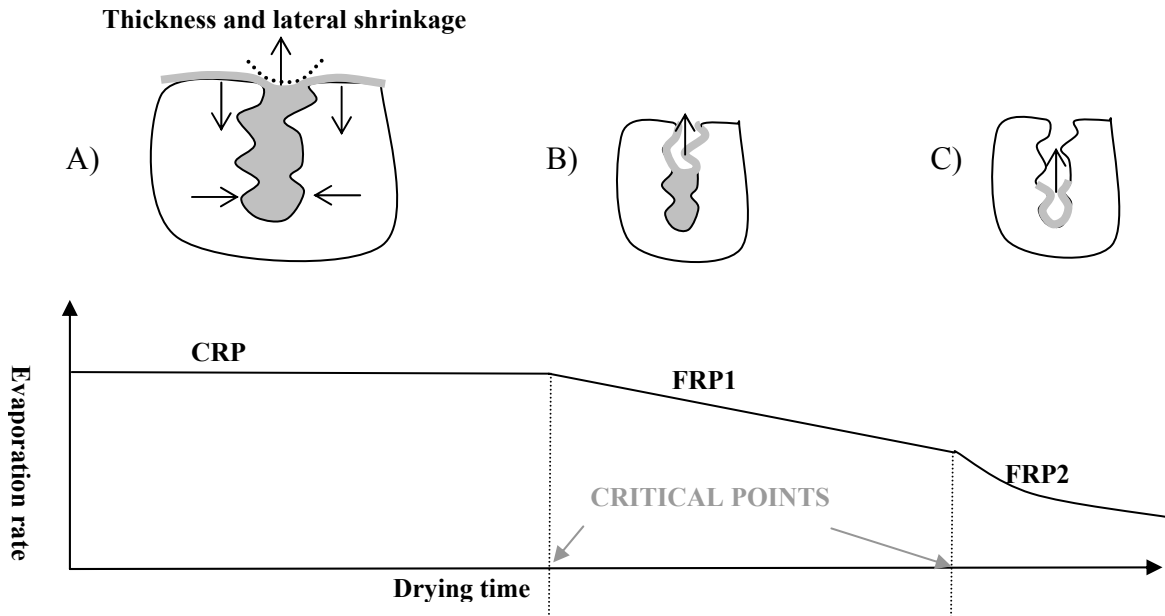


Fig. 25: Stages of drying and trend of the evaporation rate: A) The constant rate period; B) The first falling rate period, C) The second falling rate period.

Several parameters influence the quality of the dried tape such as: temperature, air flow, humidity, surface area, thickness of the tape, presence of binder and plasticizer. According to Briscoe et al. [1998] all these factors influence mostly the constant rate period, except for the thickness of the tape which affects more the second falling rate period.

Since evaporation is an endothermic reaction, raising the temperature both of the atmosphere and of the liquid, will supply higher energy for the surface liquid to evaporate, speeding the drying. Providing air flow above the tape will reduce the concentration of the evaporated liquid in the air layer above the tape, shifting the equilibrium towards the vapour and consequently increasing the evaporation rate. For the same reason very dry (in case of water based slurries) air surrounding the tape will promote drying.

Stresses during drying often result in tape defects. Cracking in the tapes are generally observed at the end of the constant rate period, when there is a differential shrinkage between the surface and the interior of the drying body. Stress development during drying can be caused also by a pressure gradient through the tape, due to the capillary forces in the liquid.

It is believed that a low evaporation rate reduces the risks of developing cracks and defects due to drying stresses. This because in this way the gradient of the pressure is minimised, and so are the stresses. A good quality tape shows no visible defects such as crow foot defects, pinholes, rails or cracks and it is evenly thickened; it has a homogeneous distribution of particles and a density comparable to 50% of the final sintering density.

The dried tape obtained is solid, can be cut into the desired shape or stored away awaiting for the final sintering stage. Quality controls of the wet tape thickness with a multi-teeth comb gauge, shown in Fig. 26, can help in predicting whether the resulting green tape is good enough to achieve the desired requirements after the sintering.



Fig. 26: Thickness comb gauge

2.4.5 Tape cast shaping

The desired shape of green ceramic is usually obtained by cutting or punching the dried tape. The technique is the most commonly used in industrial processes. It is also called blanking. The punch is pressed into the tape with the help of a hydraulic press. The sample is either pushed on the opposite part of the tape or retracted. The punches are usually made (or at least their cutting edge) of hardened steel or/and carbide material [Mistler and Twiname, 2000]. Other cutting tools can be employed such as cutting rollers and blades. Recently, the use of a computer controlled laser which can achieve very precise cuts has been suggested by Schwarzer et al. [1999].

2.4.6 Organics Burnout

Because of the relatively high amount of organics present in the tape cast (usually between 20 and 40% vol), their burnout is critical for the achievement of a good quality sintered ceramic. In particular, usually the binder is the most concentrated organic present.

Several strategies have been proposed to de-bind the ceramic components including thermal de-binding, wicking, solvent extraction, and supercritical fluid extraction. Of these, thermal de-binding (or binder thermolysis) remains the most widely utilized process in the manufacture of traditional and advanced ceramic components.

During binder thermolysis, many complex chemical and physical processes occur, often simultaneously. Decomposition of organic species, chemical interactions

between these species and the surfaces of ceramic powders, mass transport of reactants, volatile species, and degradation products through binder-filled and empty pores, changes in the distribution of condensed binder within the pore structure of the ceramic body are some examples.

In practice, binder removal can be difficult to control, thus leading to a variety of defects that reduce the yield of ceramic manufacturing processes. For instance, carbon retention, cracking, blistering, warping, anisotropic shrinkage, and delamination of fired bodies can all result from inadequate binder removal.

In practice, some balance between the time for removal of the binder which has to be as fast as possible and the prevention of defects is desirable.

Although the mechanism of burnout varies according to the polymer(s) present, in general, temperatures up to 500°C are enough to completely eliminate the organics from the green body.

The parameters which affect the binder burnout are: the molecular weight of the polymer, the interactions with the powder surface, the oxygen atmosphere, the gas flow and the heating rate.

The melted polymer and its fragments flow and diffuse through the ceramic body with mechanisms very similar to the one described for the liquid in the drying stage, but at a much higher viscosities. As well as in the drying stage, stresses can develop through the ceramic leading to deformities and cracks especially in non-homogeneous green bodies.

Some polymers melt before decomposing (for example PVA) and they decompose randomly creating fragments of various length whose degradation is difficult to control. Some polymers instead go back to the original monomer status (depolymerisation).

The thermogravimetric analysis (TGA) of the green tape provides valuable information about the heating path to be followed. Commonly a slow heating rate ($\sim 1^\circ\text{C}/\text{min}$) is used in the temperature range where the decomposition rate is rapid, while higher heating rates ($\sim 5^\circ\text{C}/\text{min}$) are used where the decomposition is slow.

When ceramics which need a conditioned atmosphere are sintered (as in the case of PZT), the complete burnout of the organics is complicated by the potential lack of oxygen in an insulated chamber. It is necessary that the polymer decomposes without leaving residuals that can contaminate the final ceramic and hinder the sintering. In most cases, the presence of oxygen is fundamental for this purpose.

PVA, according to the decomposition mechanism illustrated in section 2.3.1.4.1, can be destroyed both in presence and in absence of oxygen, presenting good flexibility characteristics in this respect.

2.5 Brief overview on the densification of ceramics (sintering)

The step after the forming or shaping of the green ceramic is the densification where the powder is compacted into a ceramic hard body. Nearly all ceramic materials need a high energy (high temperature and sometimes pressure) process

step to achieve densification. This processing step is called sintering or firing. Grains develop from the coalescence of several particles and from the removal of the porosity among them. Usually, the densification of a ceramic is accompanied by coarsening of the microstructural grains. Grain coarsening has its maximum during the final stage of the sintering, although it starts during the initial stage.

According to the mechanisms, sintering is generally divided in solid state and liquid-phase sintering.

Sintering results in the shrinkage of the green ceramic body as the interstitial porosity is removed. This happens through a matter transport mechanism, predominantly by atom diffusion (surface, volume, grain boundary diffusions) and plastic flow. For liquid phase the transport of matter happens both via capillary flow and diffusion.

2.5.1 Solid state sintering

Fig. 27 schematically illustrates the three typical stages of solid state sintering and the possible matter transfer mechanisms. In the initial stage (Fig. 27a) the particles are in tangential contact. The neck between the particles grows relatively quickly and it is accompanied by a substantial shrinkage as the curvature of the particles in contact diminishes. This stage is considered to last until the radius of the particles reaches about the half of the original size. The intermediate stage (Fig. 27b) is the longest stage. The densification happens by the shrinkage of the porosity which eventually will be isolated. This stage is considered to end when the ceramic density approaches approximately 90% of the theoretical density (i.e. the density of a perfectly sintered material with zero porosity). It corresponds to the density of the original powder). In the last stage, in Fig. 27c, the isolated porosity is completely eliminated.

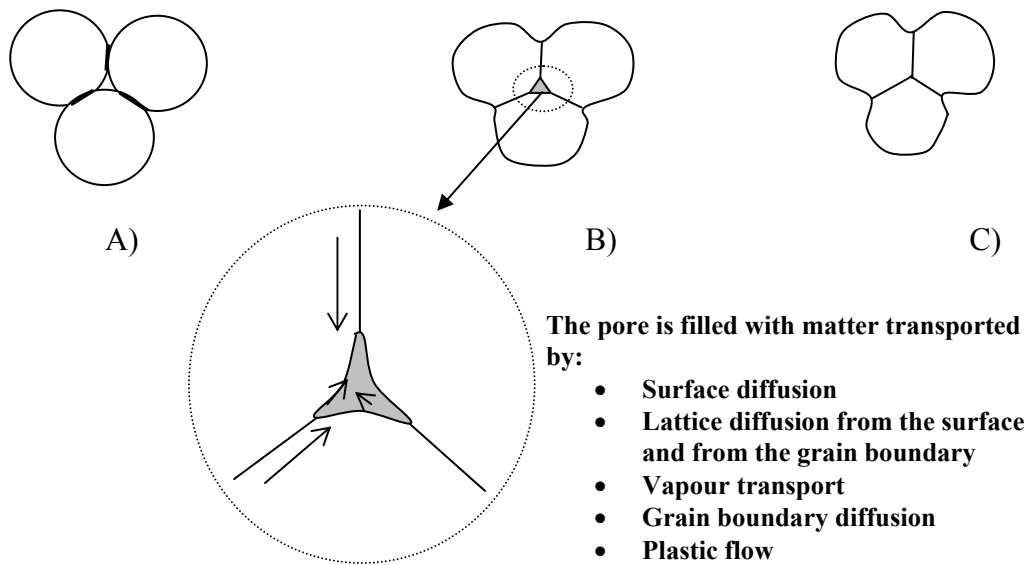


Fig. 27: Essential stages in the solid state sintering of particles, adapted from Rahaman [1995]

These stages in sintering have been used to develop mathematical models in order to describe the physical phenomena. All the models assume that the particles are spheres of the same size. This assumption provides an easy analysis, but neglects the influence of particle packing factor and the change of the shape of the particles during sintering. [Rahaman, 1995]

In general, the densification of the ceramic leads to an overall decrease of the free energy of the system, firstly by the densification of the body (when the matter is transferred from the grains into the pores) and secondly by the coarsening of the grains (when there is a rearrangement of the matter in different parts of the pore without any actual reduction of the pore volume).

2.5.2 Liquid phase sintering

Diffusion in solid state sintering might be difficult and, as a result, the grain coarsening may dominate, leading to relatively low sintered density. Sometimes, to improve the sinterability of some materials, an additive which melts at a relatively low temperature is added to the powder composition. The liquid phase created at the surface between the grains enhances the sintering. This type of sintering leads to a characteristic microstructure where an additional phase is visible at the grain boundaries.

In liquid phase sintering, the forces leading to the sintering are capillary and surface tension and the sintering temperature is usually far lower (about 3.5 times) than in solid state sintering. The liquid is normally present in concentrations below 5% and it behaves as a lubricant so that the particles movements and

rearrangements become easier. The liquid phase sintering mechanism can be subdivided in three stages which are sometimes overlapping: particles rearrangement, solution-precipitation and Ostwald ripening [Rahaman, 1995].

When the temperature has risen, the component of the composition with the lower melting temperature is the first to liquefy creating a liquid phase which wets the solid particles with a thin film. The rearrangement of the particles suspended in the liquid, driven by the surface tension forces, produces a more stable packing. The liquid between the particles will create a meniscus providing some compressive forces which make the particles rearrange rapidly. When the rearrangement has reached equilibrium, if the solid is soluble in the liquid, the solution-precipitation stage occurs. The solid diffuses through the liquid at the phase boundary and precipitates in other positions. This stage is driven by the chemical potential difference among sites and usually the precipitation of smaller particles on the biggest ones occurs. For this reason, this stage is accompanied by a shape variation (the grains become rounded if the liquid is abundant) and grain growth occurs.

The last stage, the Ostwald ripening stage, is characterised by a very slow densification rate because of the large diffusion distances due to the coarse grain structure. Consequently, it is the longer lasting stage. The liquid is often relocated and accumulated in the remaining pores.

2.5.3 Factors influencing the sintered microstructure

It can be generalised that a ceramic body with small and homogeneous grain size, high sintered density, little and small residual porosity is desirable as these requirements increase its mechanical and thermal resistance to stresses.

The growth of the grain can be classified as normal or abnormal. In normal grain growth, the size of the grains is fairly narrow and relatively homogeneous (there is not a big disproportion among grain size). In this case the porosity remaining is positioned on the boundary of the grains (triple points).

Abnormal grain growth instead sees a few grains increasing their dimension with a different rate at the expenses of the smaller grains. The residual porosity can lie within the grain. This type of porosity is difficult to remove.

Fig. 28 shows the difference between an exemplified normal grain growth and abnormal grain growth microstructures.

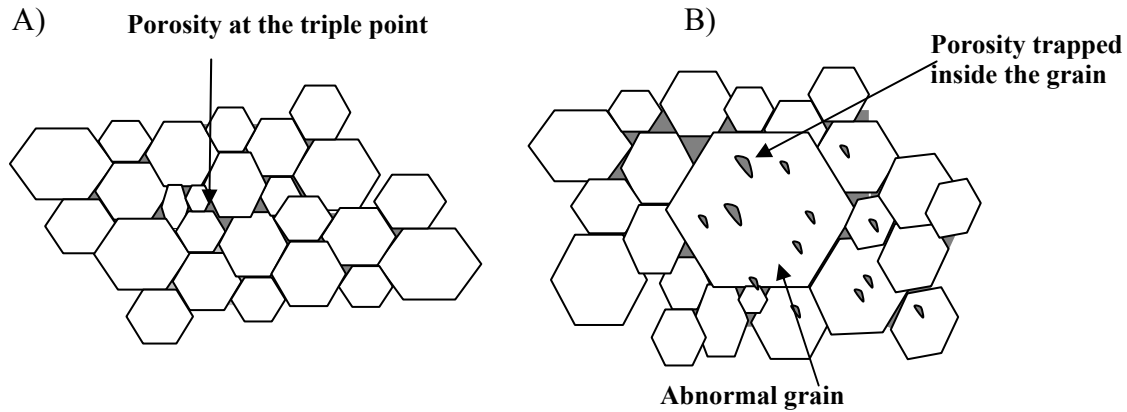


Fig. 28: The grain growth: A) normal grain growth, B) abnormal grain growth

The achievement of a controlled grain size is dependent on a slowed grain growth and simultaneous increase in the densification rate. Fast heating rate, homogeneous packing of the originating particles (of narrow size distribution) in the green body are examples of measures that favour the building of a normal grain growth. In some cases, dopants are added in order to slow down the grain growth.

In practice, the ceramic characteristics are strictly dependent on the microstructure and it is therefore necessary that the process is tailored in order to achieve what is desired. This could be accomplished by studying the influence of the sintering parameters on the final microstructure [Kingery, 1978]. Some of the most important processing parameters to be controlled in ceramic sintering are: the powder composition, the particle size, shape and distribution, the density of the green compact, the amount and the size of the pores in the green body, the heating rate, the sintering temperature, the sintering pressure, the sintering time and the gas atmosphere. Man F. Yan in 1981 reviewed the influences of some processing parameters on the production of ceramics for the electronic industry [Yan, 1981]. It was concluded that to have uniform and consistent microstructure in the sintered ceramic it was desirable to have:

- starting powders with small particle size, narrow particle size distribution, non-agglomerated particles with equiaxed shape
- uniform and defect-free green compacts
- a controlled chemistry which allows grain coarsening control
- well designed sintering profiles which permit the optimal grain growth and densification rates

The configuration of the ceramic particles in the green body has a very high influence on the quality of the sintered microstructure. The green density of a ceramic body has been proved to have a great effect on the sintering [Occhionero and Halloran, 1984]. Studies demonstrated that lack of homogeneity in the green

body can compromise the final characteristics of the sintered ceramic, developing cracks, large pores between relatively dense areas [Das and Maiti, 1999, Sacks and Tseng, 1984, Yeh and Sacks, 1988].

It has been shown that small and narrow particle size distributions increase the sintering rate and the final density [Das and Maiti, 1999, Yeh and Sacks, [Roosen and Bowen, 1988a].

The sintering of very porous solids has been investigated by Greskovich and Lay [1972]. The schematic mechanism is shown in Fig. 29. This leads to grains with elongated and unusual shapes, to big open porosity and low sintered densities.

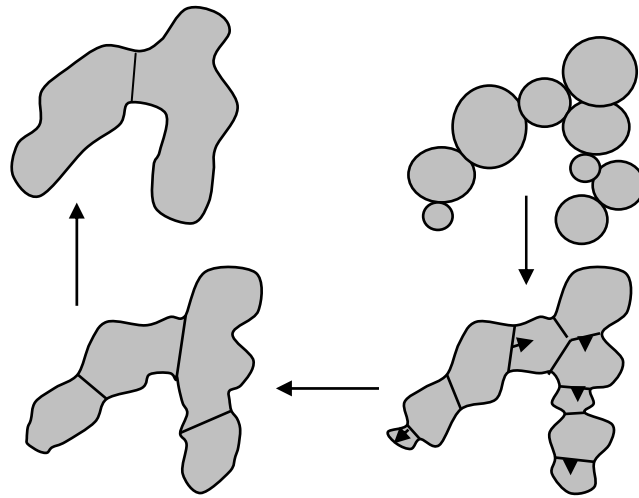


Fig. 29: Sintering mechanism of coarsely packed particles according to Greskovich and Lay

When particles of slightly different size are in contact, the neck grows mainly by surface diffusion, migrating from the contact plane, and consuming the smaller grain [Edelson and Glaeser, 1988]. This mechanism extended to a cluster of particles generates a large oblong granule. At this stage, both neck growth and the boundary relocation in the less porous areas would drive the coarsening of the grains. As sintering progresses, the ceramic microstructure will evolve areas of different density. If the grain-boundary migration is rapid, it can, for a certain green density, trap the pores in the cores of the grains. As new contacts between growing grains occur, less faceted grains are created.

The development of porosity is also dependent on the packing of the particles. The pores are surrounded by a different number (N , coordination number) of particles depending to their packing (Fig. 30). Pores which are surrounded by a small (between 3 and 6) number of particles (this happens in very well packed bodies) shrink during sintering. This phenomenon can be explained considering that, for this geometry, the decrease of the pores surface energy is greater than the increase in the grain boundary energy. In contrast, if the coordination number is 6 (critical pore coordination number), the pore is metastable which means that it doesn't grow or shrink. For any N greater than 6 the pores grow. Zheng et al.

found that it exists a critical ratio for pores in solid state sintering above which the pores can not completely eliminated with sintering, controlling the final density of the body [Zheng and Reed, 1989].

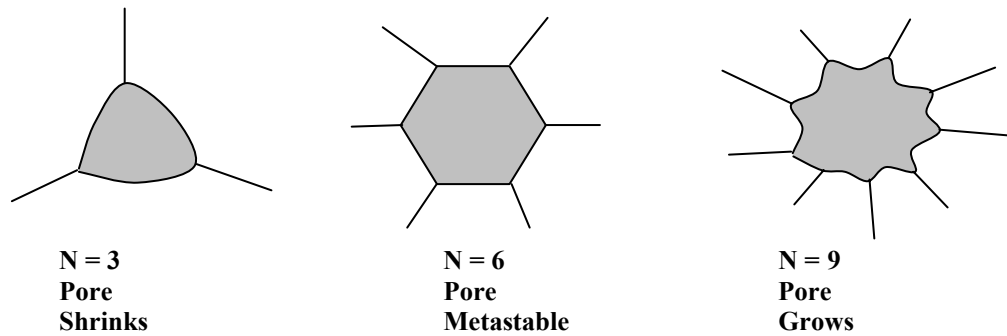


Fig. 30: Pores coordinated by grains-particles in a two-dimensional plane

By controlling the packing of the particles and the sintering conditions it is possible to modify the grain growth and the densification rates.

In addition, by increasing the heating rate one is able to diminish the grain growth. A very sudden increasing of the firing temperature is used in the sintering process called 'fast firing', where the ceramic is 'instantaneously' heated at the sintering temperature by being placed in a pre-heated furnace. This process improves the microstructure by hugely decreasing the grain growth at equal densification rates [She and Ohji, 2002].

PZT is thought to sinter through a liquid phase sintering mechanism [Corker et al., 2000, Kingon and Clark, 1983, Snow, 1974]. In the case of PZT, lead oxide (PbO) is added in excess to the powder composition in order to help the sintering both to provide the liquid phase and to prevent lead losses [Megriche and Troccaz, 1998]. In fact, PbO melts around 880°C, while PZT is usually sintered at higher temperature. It is well known that during the sintering of PZT ceramic, losses of PbO can occur [Northorp, 1967] changing the composition of the material and compromising the sintered structure and its electrical properties [Webster et al., 1967].

This problem can be limited by providing a PbO enriched atmosphere above the sample, as suggested by Kingon and Clark [Kington and Clark, 1983, Kingon et al., 1985]. A PZT powder rich in PbO is placed in the ceramic sintering furnaceware, so that the high partial pressure of the PbO in the atmosphere would reduce the evaporation rate from the sample.

2.6 Stabilisation of particles suspensions

To produce a green tape cast with the desired structure, a number of parameters must be carefully controlled. Generally speaking, one would like to have an as high as possible solids (powder) content combined with a relatively low viscosity for the slip to be easily cast. When a slurry is well dispersed, its maximum solids volume content can be raised up to 55-60%, while for flocculated (not well dispersed) slips it can be as low as 5%.

The structure of colloidal suspensions at rest depends on the balance of the forces acting between the particles. The liquid structure models depict a stable suspension as a disordered structure, similar to a liquid. The attractive forces are often large enough for the particles to collide and stick together creating clusters (i.e. flocs) which trap the solvent. Flocs behave like greater particles and pack heterogeneously leading to a poorly dense, non uniform green body [Rahaman, 1995]. In the deflocculated state particles are free to move around and they do not coagulate into stable flocs, while in the flocculated state, the small clusters grow into larger ones with time.

Attractive Van der Waals forces always act among the particles, but they are particularly relevant when the particle size is small (in the range of few microns – hundreds of nanometers). These attractive forces flocculate particles and cause the three-dimensional networks (gel structures) to form. At low solids content, three-dimensional networks may only form after individual particles have coalesced into flocs which settle and the three-dimensional network occurs in the sediment, where the particle's concentration is higher. At high solid content it is likely that the particles generate extended continuous fractal networks (gel structure) [Pugh and Bergström, 1994].

The strength of the gel structure can vary but it can break by applying a shear stress (e.g. in the tape casting, the shear stress of the casting blade). When the stress is not applied, the gel network 'freezes' the ceramic particles into a static position.

The techniques employed to prevent flocculation rely on the introduction of repulsive forces on the surface of the particles which can be electrostatic, steric or a combination of the two, as described in the section on the dispersant (2.3.1.3). In this section a brief overview on these stabilising principles is given.

2.6.1 Electrostatic stabilisation

In electrostatic stabilisation, the magnitude of the surface charges determines the intensity of the repulsion between the particles. When immersed in liquids, the particles can acquire surface charges by several mechanisms such as the preferential adsorption of ions, the dissociation of surface groups or the adsorption of electrolytes.

Information about the entity and the sign of the surface charge can be obtained by electrokinetic measurements in which the motion of the particles immersed in an electric field is detected.

The Zeta -potential (ξ), the electrical potential near the particles surface, is a measure of the repulsion intensity.

For oxide particles the main charging mechanism is the adsorption of ions from the solution in which they are immersed. Oxides are normally hydrated in water; at low pH the adsorption of H^+ ions produces a positive charge accumulated on the surface; at high pH instead, the OH^- ions are adsorbed and the overall charge will be negative. An intermediate pH exists when the adsorption of the H^+ and the OH^- will equilibrate and the total charge on the particle surface will be zero (point of zero charge or isoelectric point) as illustrated in the equilibrium in Fig. 31.

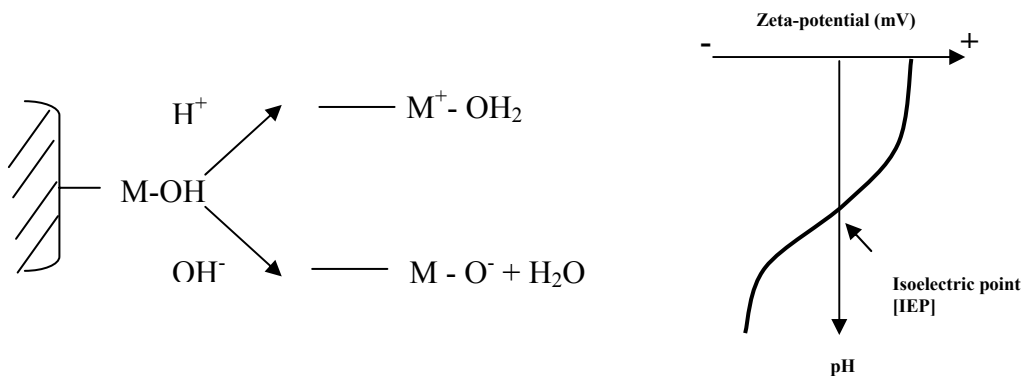


Fig. 31: Hydration of metal oxides and Zeta-potential variation with pH

When charges are adsorbed onto the surface, in absence of thermal motion, an equal number of counterions (ions of the opposite sign) would spontaneously be attracted towards the charged surface to neutralise it, forming a compact double layer.

Instead, because of the thermal motion, the external layer of counterions would diffuse in the surrounding medium creating a diffuse double layer as shown in Fig. 32. The double layer consists in of two regions: an inner zone where the ions are adsorbed onto the surface, and an extended diffuse region in which the ions are distributed according to the influence of the electrical forces and the random thermal motion.

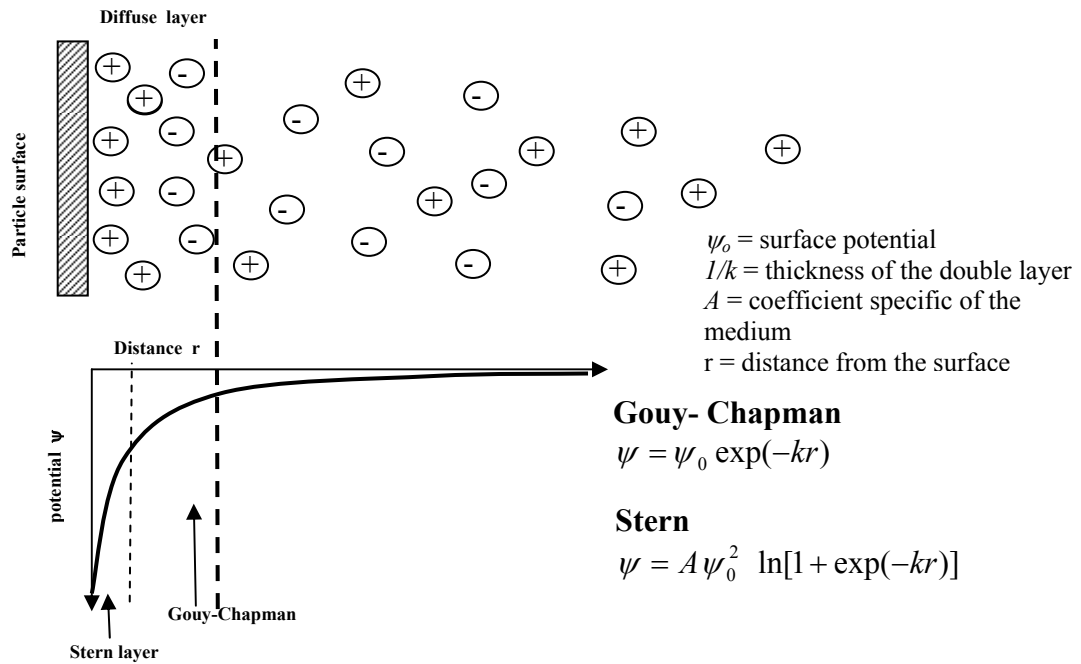


Fig. 32: Schematic representation of the diffuse double layer and potential profile according to the Gouy-Chapmann and the Stern models

Some models have been developed in order to estimate the potential variation with the distance from the surface. The simplest one was created by Gouy and Chapman [Rahaman, 1995] which assumes that the point charges are diminishing according the Poisson- Boltzman equation. According to this model the potential (ψ) decays exponentially with the distance (r) from the particle surface. A more accurate model has been developed by Stern dividing the double layer in two regions: one including a layer of adsorbed surface ions (compact Stern layer), and one diffuse as the Gouy-Chapman layer.

The experimental estimation of the potential ψ is very difficult and it is normally approximated with the Zeta -potential (ξ).

2.6.1.1 The DLVO theory

Two particles will begin to interact when their double layers overlap. The total electric potential (V_T) can be thought as the overlapping of two double layer potential curves; the effect is approximately additive and the potential in the centre is extremely augmented (Fig. 33), implying a repulsion.

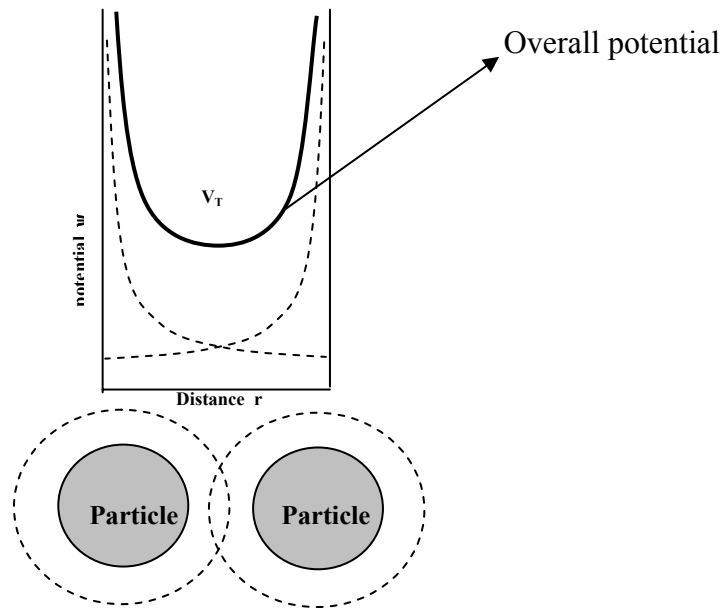


Fig. 33: Effect on the electric potential: two particles approach each other and the double layers overlap.

The general theory which tries to explain the interaction between particles double layers is called DLVO theory from the names of the developers Derjaguin, Landau, Verwey and Overbeek [Pugh and Bergström, 1994]. According to the DLVO theory, V_T would be the sum of the overall attractive forces (V_A , negative, Van der Waals), and the overall repulsive forces (V_R , positive, Double Layer) (Equation 9).

$$V_T = V_A + V_R$$

Equation 9

When V_T is smaller than zero, the attractive forces dominate and the particles coagulate; on the opposite, when the total potential is positive, the particles are kept far apart by the repulsive forces.

In Fig. 34 the total interaction potential V_T is plotted against the interparticle distance (r). Four different types of curves are drawn, according to the relative importance of the attractive and the repulsive parts of the potential.

Curve A represents the interparticle potential when the repulsion factor is very small, so the particles quickly collapse in a primary minimum. Curve B shows a maximum of potential (V_{max}) which prevents the particles from coagulating in the primary minimum. This curve has also a secondary minimum (V_{min}) which is cause of weak flocculation. Curve C represents a stable system since the primary minimum is not present and the energetic barrier to get to the secondary minimum is very high. In case of curve D the system is autonomously dispersed.

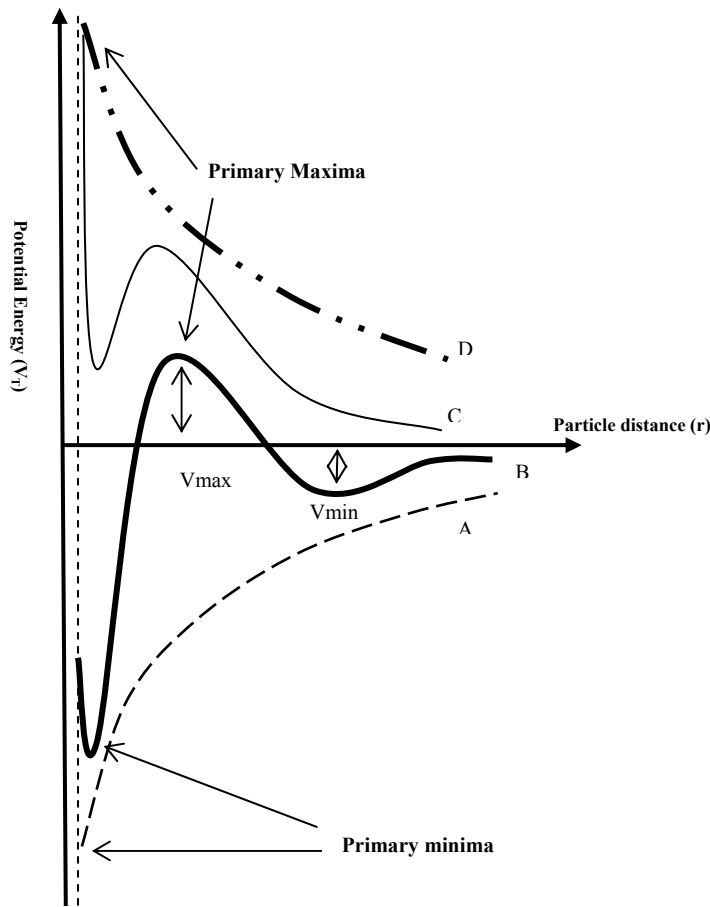


Fig. 34: Potential Energy curves against particle distance, showing different total interactions [Pugh and Bergström, 1994]

Anything which decreases the primary minimum and maximum will promote a flocculation of the particles. In general:

- The deeper the minimum, the stronger the cohesive tendency of the flocs and the higher the energy needed for their destruction.
- The smaller the maximum, the easier for the particle to overcome its energy barrier, falling into a minimum.

2.6.2 Steric Stabilisation

Polymers can induce flocculation as well as stabilisation.

In steric stabilisation, two mechanisms can be used:

- 1) The adsorbed or grafted polymer chains on the particles surface prevent them coming close enough for the Van der Waals forces to cause an irreversible attraction. (Fig. 35B)
- 2) A non adsorbing polymer can be located in the interstices among the particles preventing their contact. (Depletion stabilisation (Fig. 35D)).

On the other hand, polymers added to the dispersed particles can instead cause flocculation, following two mechanisms:

- 1) If the surface of the particle is not completely covered with the polymer, 'bridging' flocculation (contemporary grafting of the same polymer chains on two particles surface) can occur (Fig. 35A).
- 2) Non absorbing polymer can induce a depletion flocculation: the polymer can be evicted from the area between two surfaces, creating a gradient of concentration. This can cause an osmotic pressure which attracts the particles (Fig. 35C).

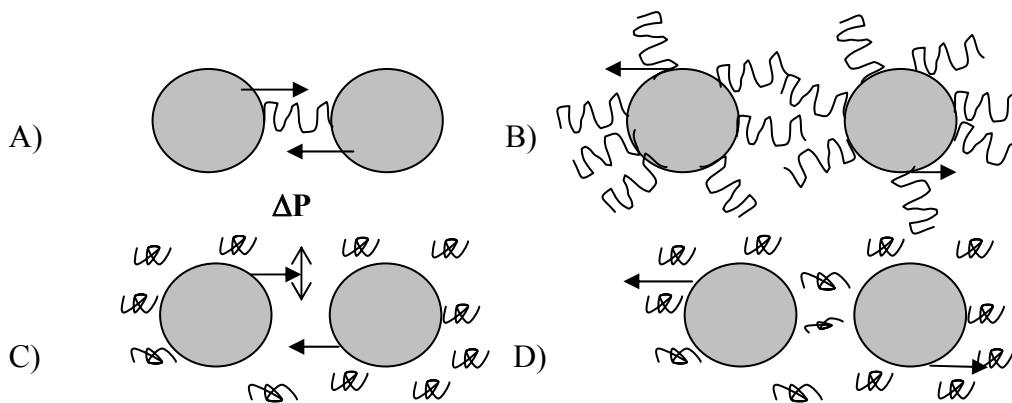


Fig. 35: Schematic representation of Polymers action on particles suspensions: A) Bridging flocculation; B) Steric stabilisation; C) Depletion flocculation; D) Depletion stabilisation

2.6.3 Electrosteric stabilisation

Suspensions can also be stabilised by electrosteric repulsion, using combined steric and electrostatic principles. The total effect can be achieved with:

- charged particles plus neutral polymers
- neutral particles plus charged polymers
- a combination of the two principles

The range of action of the electrostatic forces is longer than the steric forces, hence the electrostatic repulsion is active at long distances, while the steric is predominant when the particles are closer.

The most common dispersants which provide an electrosteric repulsion are referred as polyelectrolytes. They are commonly salts of polyacrylic and polymetacrylic acids. Their action has been briefly illustrated in section 2.3.1.3. As shown, the polyelectrolytes are subjected to a dissociation equilibrium (Equation 4) as well as the oxide particles (Fig. 31), which are influenced by the pH. Depending on these equilibria, both the particles and the ionic polymer develop charges. In case the charges of the particles and of the polyelectrolyte are

concordant (negative), the charged parts of the polymer are repulsed and the adsorption of the organic is limited (Fig. 36A). When the signs are discordant instead, the adsorption occurs because of the attraction of the opposite charges (Fig. 36B) [Funk and Dinger, 1994].

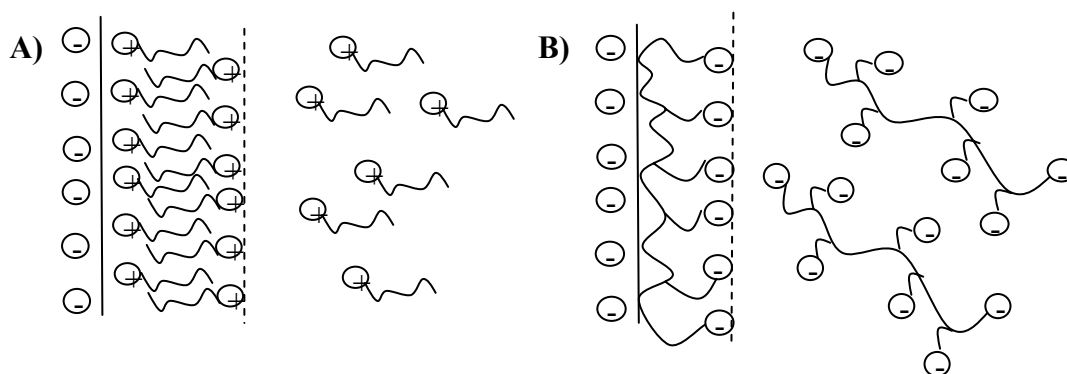


Fig. 36: A) Adsorption of a cationic copolymer on a negative particle surface; B) adsorption of an anionic copolymer on a negative particle surface

It has been shown that polyelectrolytes provide good stabilisation only if their amount is perfectly calibrated: in fact, the polyelectrolyte will be adsorbed onto the particles surface up to a point when it reaches its steric saturation; any dispersant added above this point would lead to undesired flocculation. This is because the free charged polymer, in fact a free charge, would reduce the double layer thickness as explained in the section describing electrostatic stabilisation [Rahaman, 1995].

2.6.4 Characterisation of particles suspensions: optimisation of the dispersing agent amount

As it has been explained in section 2.5.3, the achievement of a well stabilised ceramic suspension is highly desirable. The good stabilisation of ceramic dispersion is dependent on the employment of an adequate dosage of the dispersant and on the nature of the interaction induced by the other ingredients. Consequently, it is necessary to determine the optimum amount of dispersant to be employed in every ceramic process both for economic and (mostly) for processing requirements.

Different methods can be adopted to evaluate the best dispersant amount including, amongst others, electrokinetic experiments (e.g. Zeta - potential) or rheology.

The rheological method is described in the following section as it was employed in the present study.

2.6.4.1 Rheology

The rheology is the study of the deformation (strain γ) and flow of the matter under the influence of an externally imposed force (stress s) [Barnes et al., 1989]. The investigation of the rheological behaviour of ceramic suspensions is very helpful for understanding their structure, for determining the best dispersant dosage and to identify and understand the ideal processing conditions to minimise the batch to batch variation.

For liquids and suspensions, viscosity is commonly used to characterise the rheological behaviour.

The study of rheology has its origins back to the 17th century, with the works of Newton and Hooke.

In a perfect Hookean elastic solid, the material deforms when a force is applied and it relaxes (the opposite) at removal of the force. The energy is stored in the deformation and it is perfectly returned during the relaxation (elastic behaviour). In Newtonian viscous fluids, the deformation causes flow which ceases when the force is removed. In this case, the energy is completely dissipated as heat (viscous behaviour). Kelvin and Maxwell developed a theory which explains the behaviour of materials with both the elastic and the viscous characters.

In fact, any material can behave differently according to the relationship between the time-scale of the experiment and the natural time of the material. So, materials can be defined as viscoelastic material (i.e. responding partially in elastic and partially in viscous way to stresses).

Fig. 37 shows how a material can respond to a stress applied in a time t_0 . The response (hence the category) of any material depends from the ratio of the Relaxation Time (τ) and the experiment time t_0 , called Deborah number (De). The viscoelastic behaviour has typically $De \sim 1$.

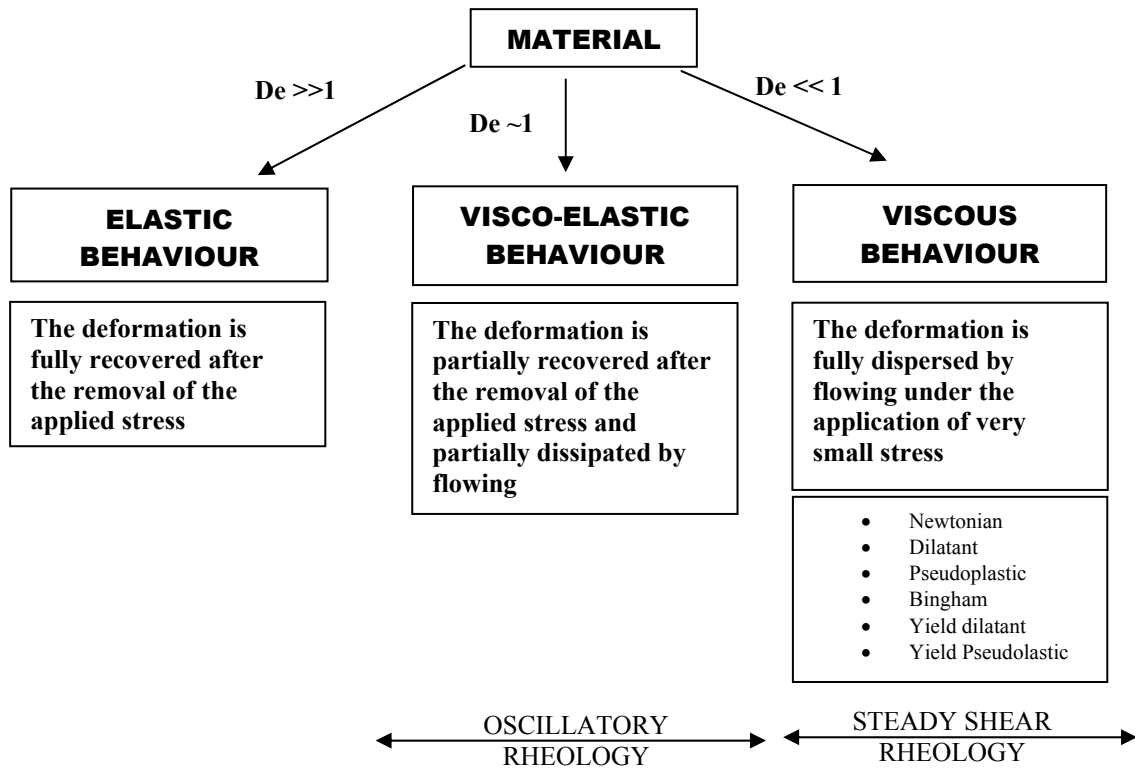


Fig. 37: Classification of rheological behaviour for any material

Rotational viscometers are commonly used in rheological measurements of particulate suspensions. These machines can work in control of the input stress or alternatively of the obtained strain. These instruments are consisting of two main parts one of which is rotated (or oscillated), and the other is stationary. The stress is transmitted from the part in motion to the stationary one through the sample and it is recorded.

A variety of geometries can be employed, but usually the basic ones used for ceramic are the so called ‘cup and bob’ and the ‘cone and plate’ (Fig. 38).

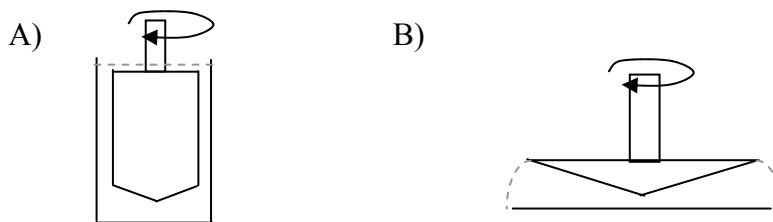


Fig. 38: A) Cup and bob, B) cone and plate configurations

2.6.4.1.1 Steady Shear rheology: the study of Viscous materials ($De \ll 1$)

Fig. 39 shows the shearing of a prismatic portion of liquid. The upper surface of area T of the prism is subjected on a force (F). The effect of the shearing results in a motion of the upper part of the prism against the lower part of it.

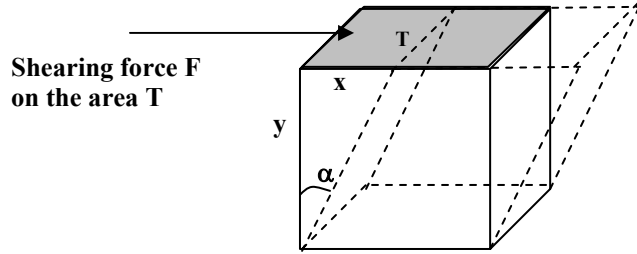


Fig. 39: Scheme showing the shearing of a prismatic portion of liquid and its effect on the shape of the prism (dashed figure)

The shear strain (γ) is defined from the deformation of the prism (Equation 10). The shear stress (s) corresponds to the ratio of the applied force F over the area T (Equation 11).

$$\tan \gamma = \frac{x}{y};$$

Equation 10

γ = shear strain
 x, y = deformation coordinates

$$s = \frac{F}{T};$$

Equation 11

s = shear stress
 F = applied force
 T = surface area

$$s = G \cdot \gamma$$

Equation 12

G = shear modulus
 γ = strain

The shear rate ($\dot{\gamma}$) is the gradient of the velocity between the upper and the lower prism surfaces or the increasing of the strain per time unit (Equation 13).

$$\dot{\gamma} = \frac{d\gamma}{dt}$$

Equation 13

Both the stress and the strain are in fact three dimensional tensors (i.e. having 9 components), but usually the rheological behaviour is analysed by relating the shear stress on the plane xy (s_{xy}) with the shear rate on that plane ($\dot{\gamma}$). This is commonly referred as steady shear rheology.

2.6.4.1.2 Viscosity of concentrated suspensions

Newton described materials that respond linearly to an applied shear stress (Equation 14).

$$s_{xy} = \eta \dot{\gamma} \quad \eta = \text{viscosity}$$

Equation 14

Many fluids, especially concentrated suspensions, deviate from the Newtonian behaviour and are no longer described by Equation 14. These systems' (non-Newtonian) apparent viscosity is dependent on the shear rate.

If the viscosity decreases with the shear rate, the system is defined as shear thinning, while if the viscosity increases with the shear rate it is called shear thickening.

The shear thinning behaviour of a particulate system can be explained by a gradual transition from a disordered to an ordered structure with increasing shear rate. Once stresses exceeding a yield value are applied, the flocs structure is broken into smaller pieces and the shear becomes easier (i.e. lower viscosity). The attractive forces will tend to rebuild the original flocs structure and the apparent viscosity measured is the balance of the shear force and the attractive forces.

At zero or very small shear rates the Brownian motion dominates the movements of the particles and the system is disordered; when the shear rate is increased, the particles will rearrange following the flow and the Brownian motion will lose importance. At a sufficiently high shear rate, the viscosity would not vary substantially with shear rate reaching a plateau as this effect has reached its maximum.

Then, if the shear rate is further increased, it can happen that the viscosity increases (shear thickening or dilatancy). The increasing of the viscosity, when the shear rate is augmented, is typical of highly concentrated suspensions and this phenomena usually occurs in a limited range of shear rates.

The phenomenon of shear thickening for highly concentrated suspensions can be explained considering that in these suspensions, at low shear rates, the particles are kept in a layered, closely packed structure where the repulsive forces are stronger than the viscous shear forces. When the shear rate increases the layered structure will be destroyed and more and more particles interactions (collisions) will take place. This friction generates a resistance to flow which is measured as a higher viscosity.

In Fig. 40, the summary of the interactions of particles in a suspension and the resulting rheology is pictured.

Line A (—) represents a shear thinning behaviour typical of gel structures under shear.

Line B (— ·) represents a shear thickening viscosity. The increasing of the apparent viscosity is due to the particle-particle collision. This factor is more relevant at high shear rates.

Line C (- -) represents a combined shear thinning – shear thickening

behaviour. At lower shear rates the suspension structure is broken by the shear force, while the attractive forces among the particles tend to rebuild the structure; at intermediate shear rates there is equilibrium between the breakdown and the build-up of the structure, so that the viscosity doesn't vary. At higher shear rates, the increase of the collision of the particles will augment the resistance to flow and hence the viscosity.

Line D (—) represents the case of very diluted suspension where the particles interaction is negligible.

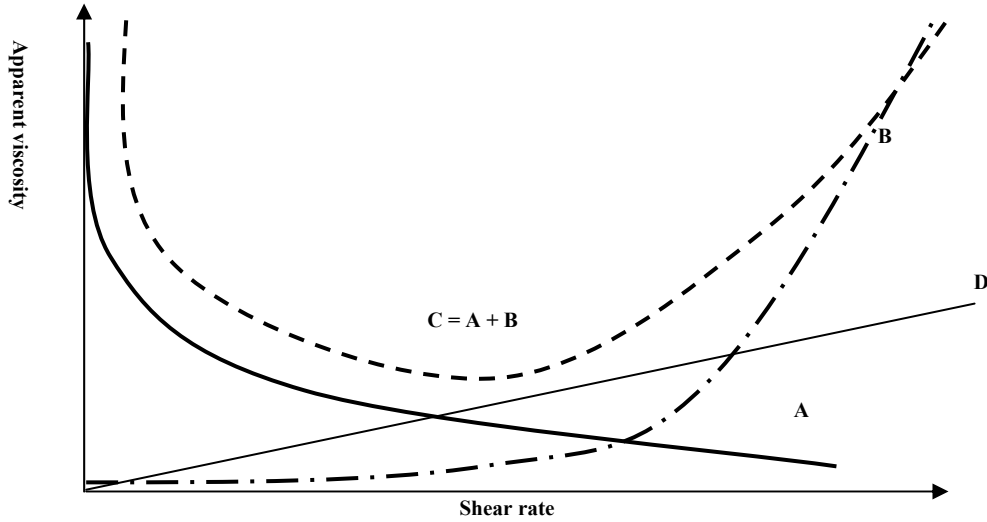


Fig. 40: Interaction of particles in a suspension and their contributions to the overall slurry rheological behaviours

Many colloid systems, among which are the ceramic suspensions, behave according to the classical Bingham or Casson shear thinning models (respectively Equation 15 and Equation 16), corresponding to the general behaviour of curve A in Fig. 40.

$$s = s_o + \kappa \dot{\gamma}$$

Equation 15

$$\sqrt{s} = \sqrt{s_o} + \sqrt{\kappa \dot{\gamma}}$$

Equation 16

where s_o is the plastic yield stress and κ is the plastic viscosity.

The plastic yield stress (s_o) is an extrapolation at zero shear rate of the shear stress. It represents the stress which has to be overtaken before the flow can occur. It is a measure of the strength of the structure network of the suspension. The plastic viscosity (κ) is calculated from the applied shear stress. It is a measure of how easily the body can flow after the yield stress has been exceeded.

The viscosity of a suspension is influenced by several factors, listed below in an approximate importance order:

- Particle – particle interactions (degree of dispersion)
- Particle concentration
- Particle size and distribution
- Particle morphology
- Rheology of the suspending medium

For suspensions with volume content of powder greater than 5%, the particle-particle interaction is the greatest factor influencing the viscosity. The status of the deflocculation is known to greatly influence the viscosity; this because the particles agglomerates trap some liquid and the whole suspension behaves as having apparent higher solids content. Consequently, the viscosity measurement is the most common method to determine the best amount of dispersant (polyelectrolyte) to be added to a suspension.

Fig. 41 shows an example of the viscosity variation when a polyelectrolyte is added. The dispersing effect decreases the viscosity up to a certain dispersant/powder ratio. Further additions increase the viscosity. The lowest viscosity point corresponds to the best approximation to the optimal dispersant amount.

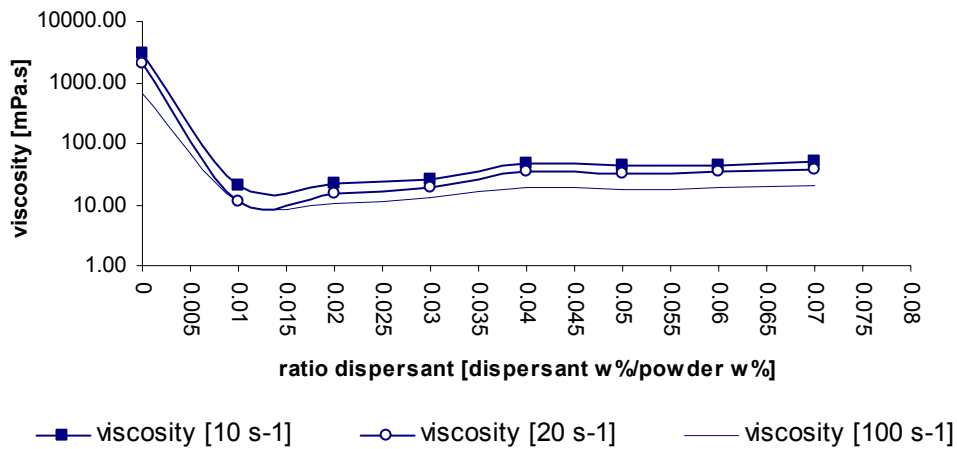


Fig. 41: Typical viscosity profile of ceramic slurries while sweeping the dispersant level. Example from current work.

Einstein [Pugh and Bergström, 1994] performed the first theoretical treatment of the effects of dispersed, spherical, hard, monosized particles on the viscosity for which he derived the Equation 17, highlighting the importance of the volume fraction of the particles in influencing the viscosity.

$$\eta = \eta_o (1 + 2.5\phi)$$

Equation 17

Where:

η = viscosity of the suspension

η_o = viscosity of the suspension extrapolated to zero particle concentration

ϕ = volume fraction of the particles

$\eta/\eta_o = \eta_r$ is referred as relative viscosity.

Many other developments to this model have been performed such as the Krieger-Dougherty or Quemada models [Pugh and Bergström, 1994]. These models are referred to particles that behave as hard spheres whose movement is affected just by Brownian motion and flow. Consequently, the interparticles forces and distances are not considered. These models are commonly referred as hard spheres models.

An improved model type, the soft sphere model, adds to the evaluation also the interparticle interactions: it is used for electrostatic, steric and electrosteric stabilised suspensions. Especially for stabilisations through the adsorption of polymers, this model considers the effective volume (ϕ_{eff}) occupied by the particles which includes the sterical hindrance (Δ) of the attached polymer.

In practice, ceramic suspensions usually have a volume content that oscillates between 30 and 60% in volume. In this region, the viscosity is greatly dependent on the volume fraction of solids. At a point in which the solids volume is increased and increased, the particles will form a three-dimensional network, making any flow impossible. The volume fraction at which it happens is called maximum packing fraction (ϕ_m) and it depends on the arrangement of the particles (cubic, hexagonal etc). Usually, the broader the particle distribution the higher is the maximum packing fraction.

The shape of the particles has also a great influence on the viscosity and on the maximum packing fraction. Deviations from the spherical shape generally make the ϕ_m to decrease.

2.6.4.1.3 Time dependent rheology: thixotropy

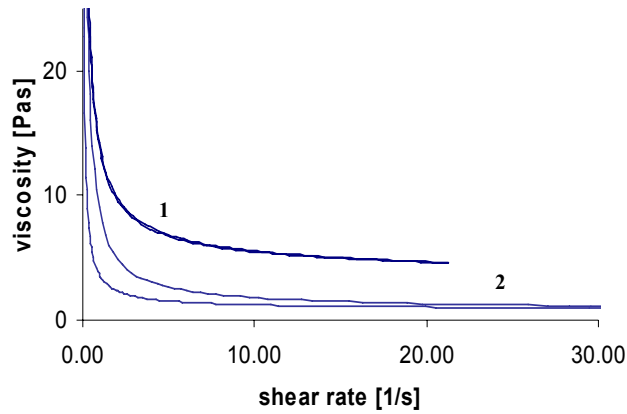
Thixotropy is the most common type of time dependent behavior and it is defined as a decrease of the viscosity under a constant shear stress, followed by a gradual recovery of the viscosity when the shear stress is removed.

This behavior is typical of gel flocculated structures whose network interaction is destroyed under the effect of a shear force, and it is progressively rebuild at rest. The speed of the rebuild depends on the nature of the interactions among the particles.

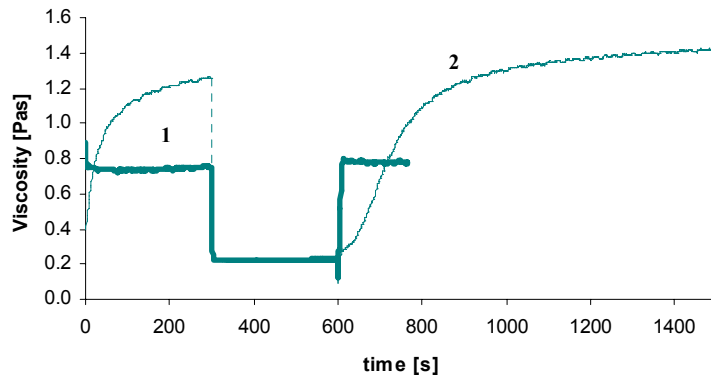
Usually, the assessment of the thixotropy happens by sweeping the shear rate in loops. If the viscosity curve doesn't coincide when the shear rate is increased and it is decreased, the slurry shows thixotropy.

Alternatively, another test is the step experiment, where the shear rate is varied 'instantaneously' from low to high and (after few minutes) a second step change is performed from high to a low shear rate.

The typical response to these tests on shear thinning slurries is shown in Fig. 42. In the figure, a comparison of a thixotropic and a not thixotropic behavior is made. In Fig. 42a, the profile shear rate/ viscosity are compared for slurries non thixotropic (1) and thixotropic (2). In Fig. 42b, the result of a step-shear experiment is reported for both thixotropic and non thixotropic slurries.



A)



B)

Fig. 42: A) Sweep of shear rates in loops; B) Step shear rate test; 1 = not thixotropic slurry; 2 = thixotropic slurry. Examples from current work.

2.6.4.1.4 Oscillatory rheology: the study of Visco-Elastic materials ($De \sim 1$)

In order to assess the viscoelasticity of a material, the most commonly used procedure is the oscillatory measurement technique.

The usefulness of oscillatory measurements in studying the particles interactions and the structure of concentrated dispersions has been demonstrated since many years [Tadros, 1990].

The material is subjected to a continuously oscillating strain over a range of frequencies.

The response stress (σ) is measured as a function of the time. The shift of the stress response to the applied strain is called delay time (δ). (Fig. 43)

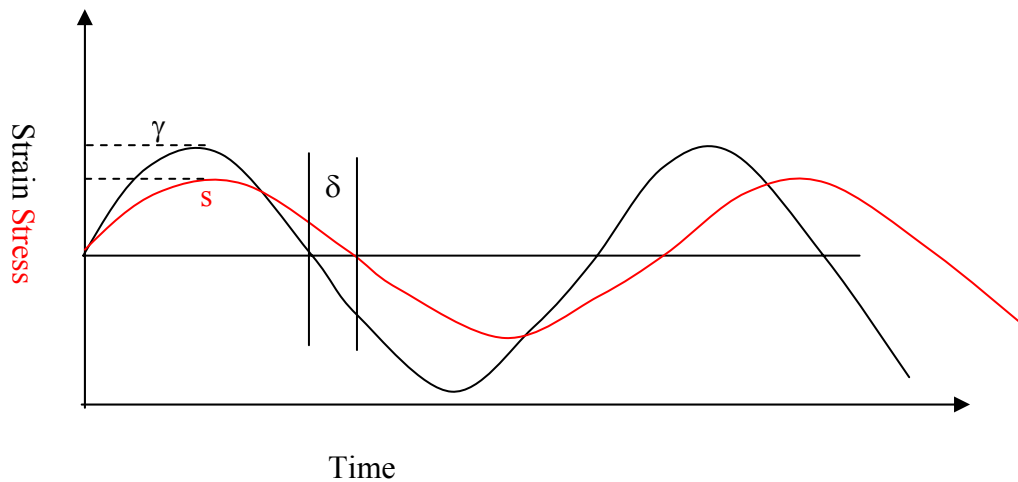


Fig. 43: The schematic response strain (γ) to an oscillating stress (s) applied to a material

In the *linear viscoelastic region* (LVR) a material behaves both viscously and elastically, but in addition its response to the applied forces doesn't depend to the extent of the force applied; it just depends on the time of the experiment. In fact, this happens only in a very limited region of applied stresses up to a maximum shear stress, T_c (critical shear stress), at which the elastic modulus G' begins to decrease with increasing shear rate.

The studies in oscillatory rheology are performed within the LVR (linear viscoelastic region); the responses in the LVR are useful as they:

- provide information on the structure of the material.
- are simplistic versions of the behaviour in the non viscoelastic region

The mathematical theory applied to the linear viscoelastic behaviour is based upon the 'superposition principle' (hence, strain is linearly dependent on the stress in any moment).

In this theory the equations are linear and the material parameters such as viscosity or rigidity modulus are constants (i.e. do not depend on the extent of the force applied).

The coefficients can assume various values, generating simplified models Hookean (the material is only elastic)

- Newtonian (the material is only ideally viscous)
- Kelvin and Maxwell (the material is both viscous and elastic) and combinations.

The simplest models of viscoelasticity (Kelvin and Maxwell) are treated as the combination of a spring and a dashpot behaviour respectively in parallel (Kelvin) and in series (Maxwell). More complex models can be assimilated to various combinations of these two models.

The complex dynamic modulus (G^*) in the linear viscoelastic region doesn't depend on the magnitude of the applied stress and it can be defined as in Equation 18.

$$G^* = s_0 / \gamma_0$$

Equation 18

where s_0 is the peak value of the stress and γ_0 is the relative strain (see Fig. 43). G^* can be split into its components G' and G'' : G' (Storage modulus) represents the elastic component (the energy that can be completely stored in the material) of the properties of the material and also the 'in phase' stress to strain ratio. G'' (Loss modulus) represents the viscous component of the properties of the material (the energy that is dissipated through the viscous flow) and also the 'out of phase' stress to strain ratio. (Equation 19)

$$G^* = G' + iG'' \quad (i = 1^{1/2})$$

Equation 19

G^* and its components G' and G'' vary with the frequency.

Suspensions show an increase of the elastic modulus as a response to an increase of the flocculation.

3 Methodology

This chapter aims to describe the methodology developed for the scale-up of a ceramic process around which the experimental work reported in this thesis has been developed.

In the following paragraphs, the terminology described in the literature review section 2.1 is used.

The laboratory scale process developed by Navarro [Navarro, 2001] was used as a case study for the design of a high-level methodology for the scale-up of ceramic processes.

The methodology that has been developed is summarised in Fig. 44.

A twofold approach has been adopted as the basis of the methodology to perform the process scale-up.

- Firstly, a “process focussed” approach was used that considered the sequence of processing operations, their feasibility on a larger scale and the potential problems foreseeable for a scaled-up process.
- Secondly, a “product focussed” approach analysed the quality of the product in respect to the customer requirements. This approach concerned also the analysis of the process potentiality to perform within essential tolerance interval.

The combination of the above two perspectives, run in parallel, provided a comprehensive view on the process issues during the scale-up, in agreement with the concurrent engineering philosophy of design.

Both the approaches (product and process) were conducted with sequential, iterative, phases denominated “conceptual” and “definitive” design phases.

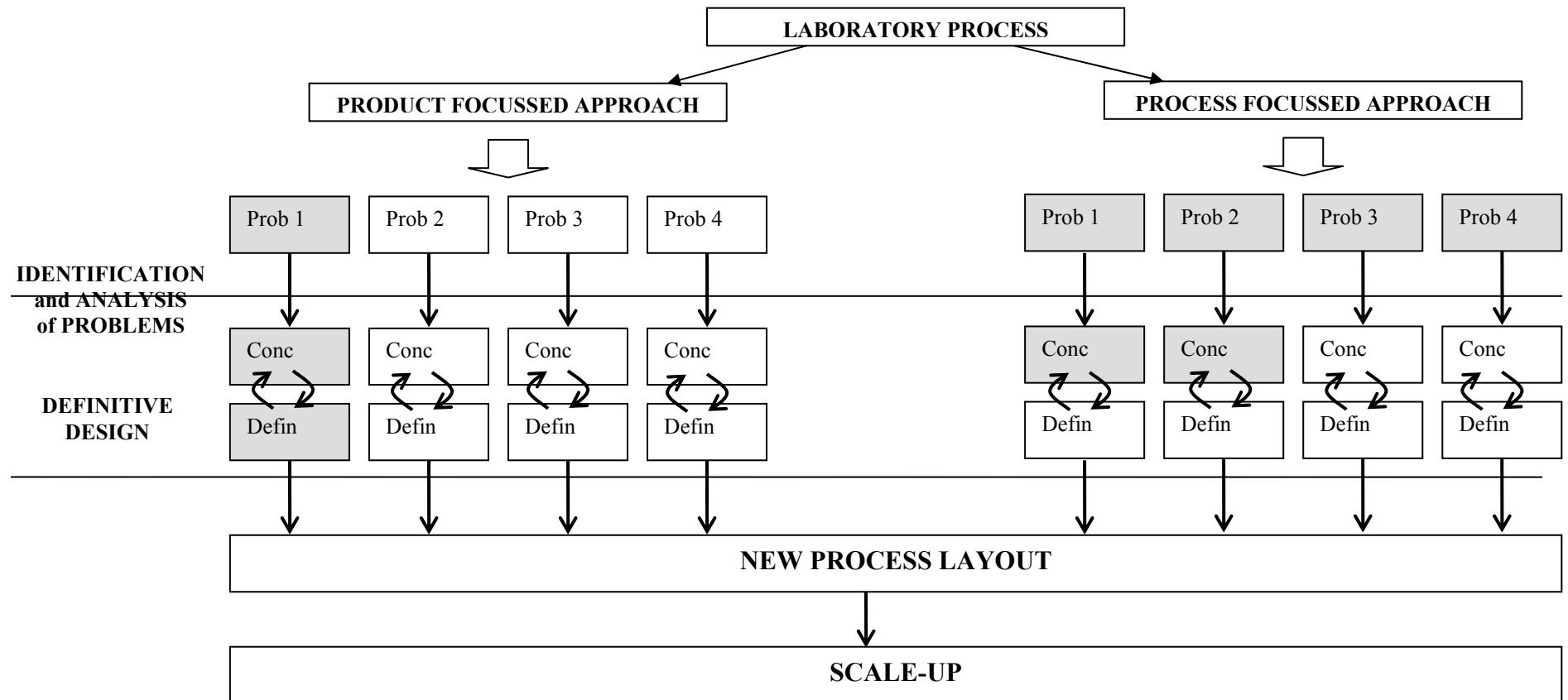


Fig. 44: Outline of the methodology towards the scale-up. The coloured boxes represent the specific steps taken in the case study at the basis of this work.

In the conceptual design stage, after the identification of the process problems in the light of the two approaches, potential solutions were found and tested:

- As most problems were usually ‘ill structured’, the solutions were found by means of a soft problem solving methodology.
- The obtained solutions were then tested at high level, providing a gross evaluation of their potential benefits and drawbacks.
- Among the solutions, few were chosen for deeper investigation. The selected solutions are the ones that provide the major benefits associated with the minor number of drawbacks.
- The solutions elicited underwent further tests to identify the single one to be promoted to the definitive design stage

In the definitive design stage, the chosen solution of the conceptual design stage underwent a further investigation to assess its capability to perform. In this stage, the key concepts of the Six Sigma philosophy became relevant. The tested solution had to be an ‘in control’ and ‘capable’ process, i.e. to run within pre-determined limits (tolerances), and to provide the required outcome (specification target).

In Fig. 44, the darkened boxes represent the stages developed in practice on Navarro’s process as described in detail in section 3.3

3.1 The twofold approach towards the scale-up

The process, described in detail in the Experimental section page 78, was analysed in the light of a scale-up to industrial production. Modifications were proposed and assessed in order to prevent problems at this larger scale.

This analysis has been done from two perspectives:

- Firstly, with a product focussed orientation.
The characteristics of the process outputs (i.e. the ceramic wafers) were compared with the specifications (i.e. a summary of deliverables and process requirements to fulfil the customer needs and expectations) to define the improvements needed for gaining a satisfactory product. In this context, the laboratory scale process performances were measured; the process outcomes were compared with the product specifications and an investigation of the main factors causing discrepancy was conducted.
- Secondly, the scale-up was approached from a process perspective.
The laboratory process was mapped. The diagrams were used in the identification of potential threats for yield on an industrial scale. Modifications were suggested and then assessed, to improve its efficiency and to minimise risk.

3.2 Methodology of the scale-up development

The process of scale-up followed the model shown in Fig. 45 adapted from the theory illustrated in the literature section page 8.

The first conceptual design was followed by a first definitive design phase; if the process resulting from these was still not satisfactory, then the whole cycle was repeated again in an iterative loop until the result of the work was satisfactory.

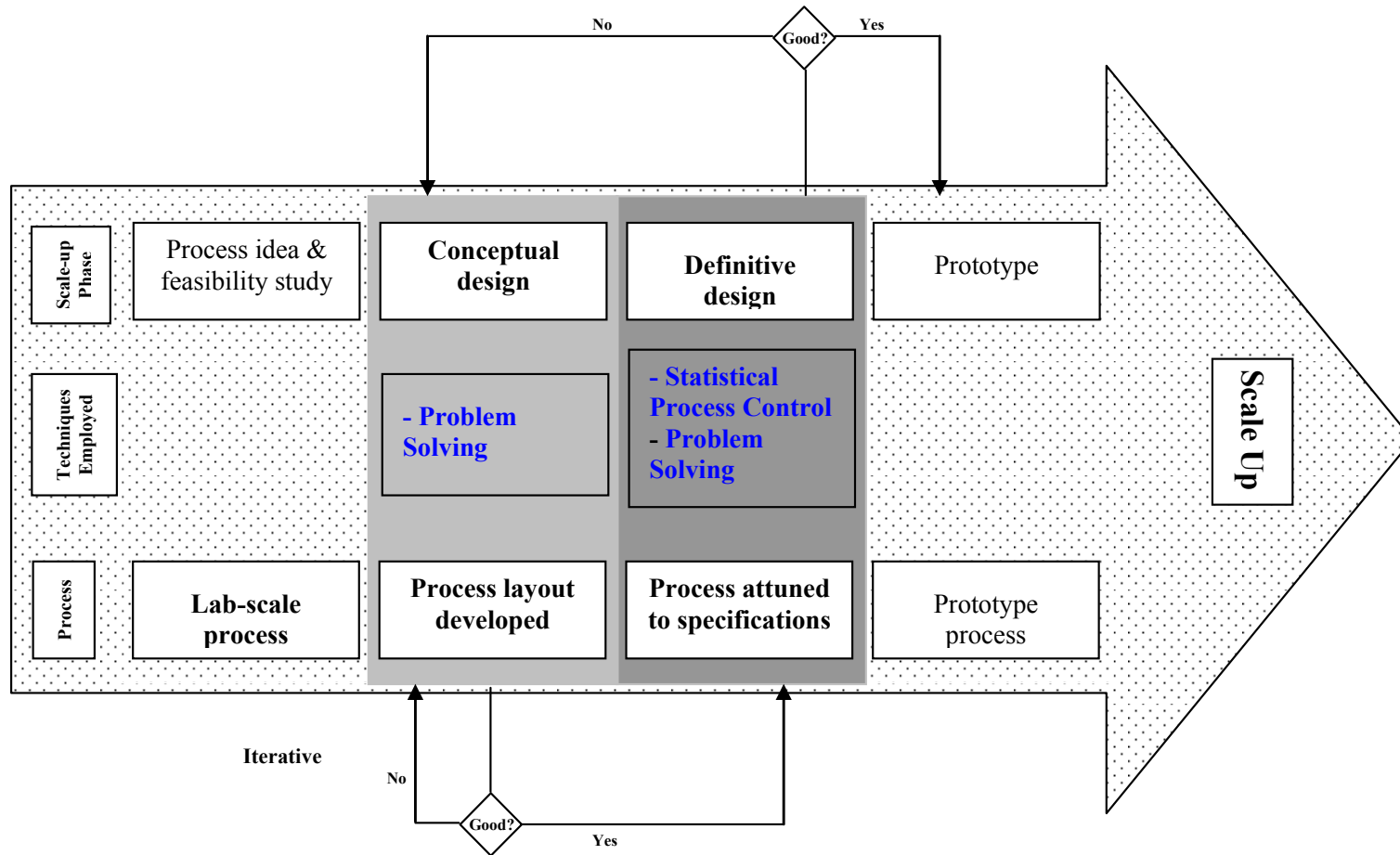


Fig. 45: Process development stages: specific progression of the research reported in this work and techniques employed (adapted from Rosenthal, S. [1992]).

In the conceptual design phase existing technological options to develop a product were evaluated and applied. An assessment of the issues regarding suitable manufacturing facilities was made.

Fig. 46 illustrates how the conceptual design developed processes solutions (i.e. modifications to the original process) which allowed the process performance to better approximate the specifications.

For example, if the process produced ceramic with characteristics (circle 1) far from the specifications (circle 2), a series of technical solutions (dotted circles) were conceptualised which predictably could achieve the product performances closer to the specifications. Among these, the best candidate (e.g. Sol 5, in Fig. 46) was chosen for the implementation and taken to the definitive design stage. The choice was made on the basis of both feasibility and low risk.

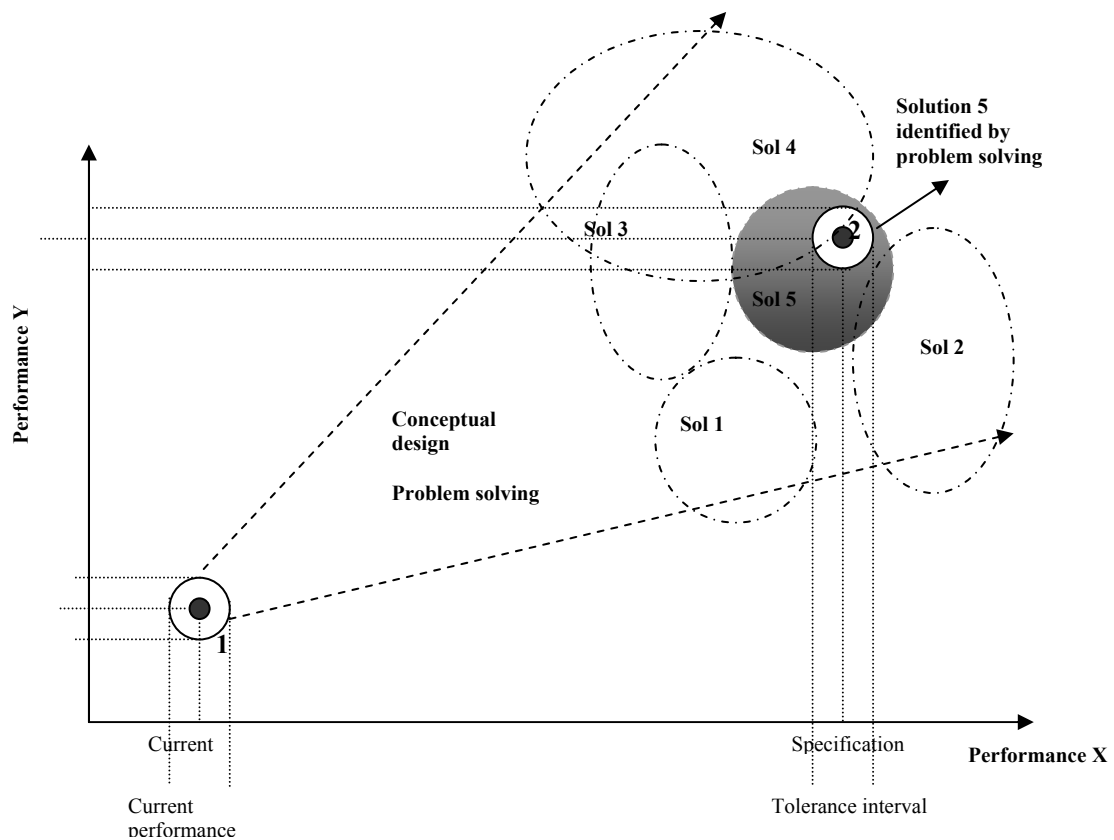


Fig. 46: The Conceptual Design phase: creative design of solutions which approximate the performances to the required value; the best one (e.g. Sol 5) is selected, according to criteria of feasibility and risk

The definitive design phase which followed aimed to refine the performance of the solution selected by the conceptual design stage to meet the product specification within the tolerance interval, as schematically illustrated in Fig. 47. With reference to the example before, this meant that the chosen technical solution (Sol 5) was analysed in detail to understand which conditions had to be used in order to increase its performances and to reduce its variation.

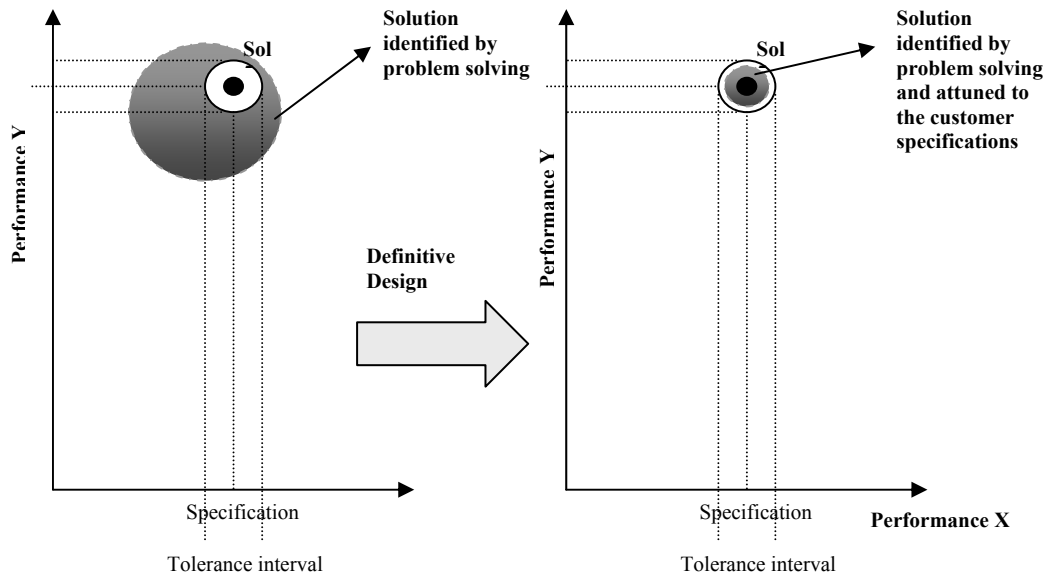


Fig. 47: The Definitive Design stage: attunes the performances to the required specifications so that the process becomes precise and accurate

Fig. 48 expands the definitive design stage as performed in this research. A single process stage was selected from the entire production process (represented in the flow charts) to be analysed (i.e. warm pressing).

The appropriate sampling technique was chosen and data were collected and analysed with the help of the Statistical Process Control tools (i.e. individual, mean and range charts, capability indexes) in the light of the specifications requirements. When the process was found to be out of control it was treated with a problem solving approach to develop process modifications.

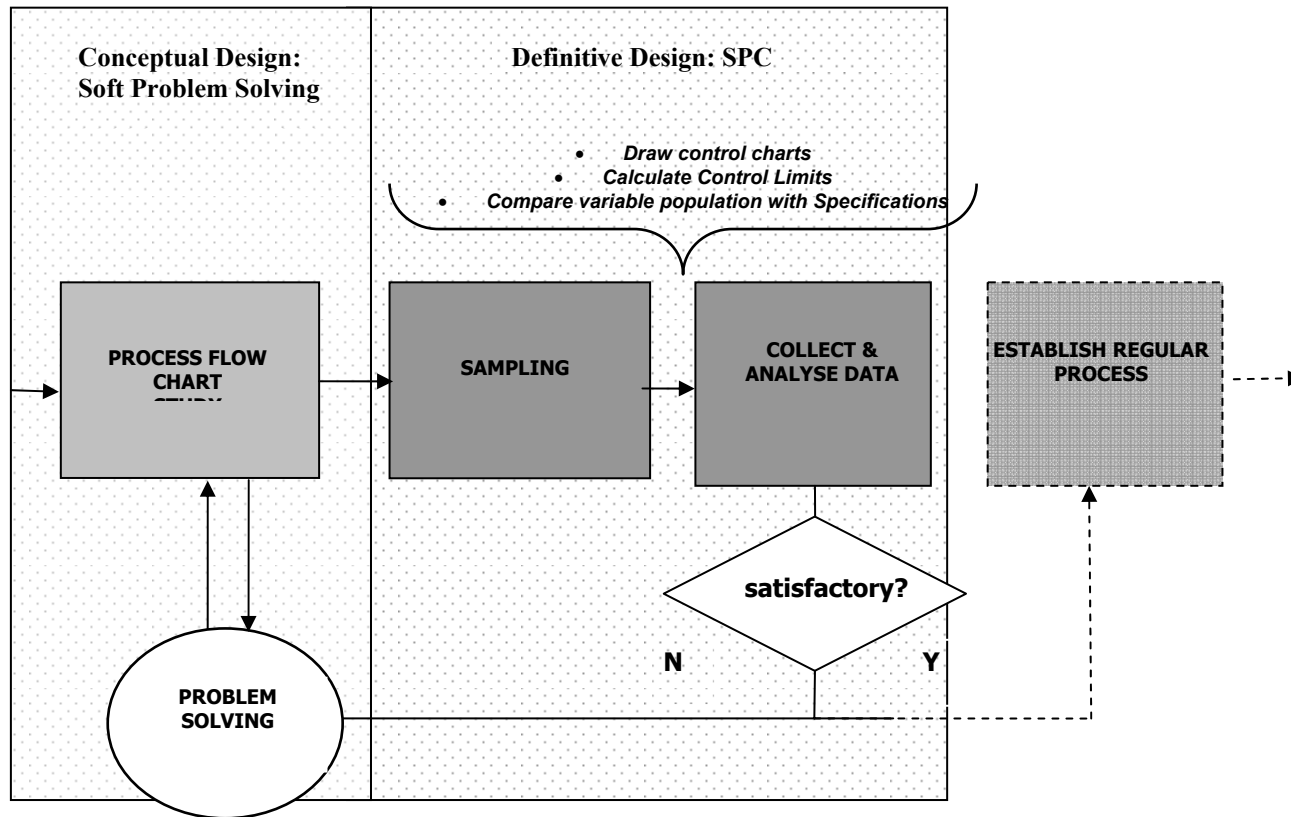


Fig. 48: Development of the Definitive Design stage

3.3 Description of the research

Due to the complex nature of the process and the limited amount of time and resources, for both the process and the product development, not all the issues were investigated in depth. Attention was primarily given to the factors judged as most important in influencing the process performances. In this respect the lack of strength in the ceramic material was judged as the most important factor for the success of the process scale-up.

Any other factor was judged of secondary importance and consequently was left behind.

It was possible to develop one complete loop, consisting of the conceptual and the definitive design (phase I), and part of a second loop with a conceptual design (phase II).

The diagram in Fig. 49 illustrates in detail the development of the research towards process scale-up, contextualising the experimental work reported in the following chapters and with a reference to future work.

3.3.1 The focus on the product characteristics

As explained extensively in section 7 (discussion), the achievement of a high mechanical resistance to stresses for the ceramic was identified as a primary importance factor for the scale-up success. Therefore, the main factors underpinning the ceramic mechanical characteristics, i.e. the microstructure characteristics, were extensively studied in the conceptual design phase I with the focus on the product characteristics. In this context, the achievement of high tape green density (above 61% of the theoretical density) was found to be a fundamental factor to attain a satisfactory ceramic microstructure.

The process designed by Navarro [2001] allowed green density of approximately 37% of the theoretical to be consistently achieved (see section 6.3.2.1), a low value in comparison to the approximate 50% theoretically expected and the 61 % required for the achievement of an adequate sintered microstructure.

The warm pressing of the tapes was considered in first instance as an adequate way to increase the green density, during the conceptual design phase I. Its capability to reliably deliver a green density of 5 g.cm^{-3} (approximately 61% of the theoretical density) was then analysed by means of the Statistical Process Control technique, during the definitive design phase I.

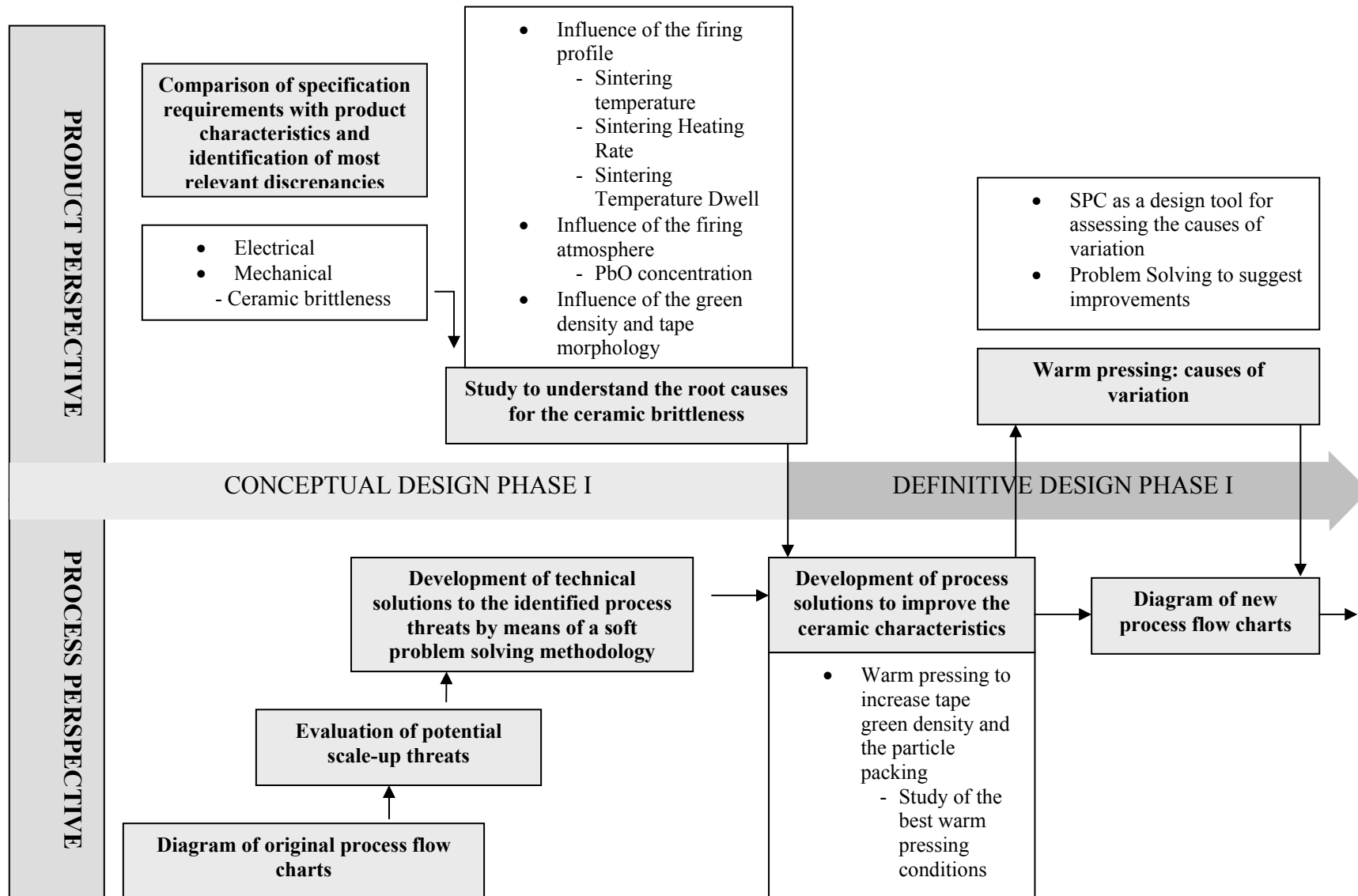
As a result of this complete loop, the feasibility of using the warm pressing technique to increase the tape green density was demonstrated. However, the use of warm pressing could have resulted in increasing of costs and complexity for the scale-up of the process.

Consequently, a second loop of conceptual and definitive designs was started, which aimed to discover the reasons behind the low green density figure achieved by the original process.

Consequently, a conceptual design phase II started with focus on the understanding the reasons underpinning the unsatisfactory green density of the tapes, to propose improving process modifications.

3.3.2 The focus on process efficiency

In the first cycle of the Conceptual and Definitive Design the flow charts of the original process were drawn. They were used to analyse and evaluate the potential threats and opportunities for waste reduction before the development of a larger scale process. Subsequently, several adjustments and technical modifications were proposed and introduced including the ones arising from the product focussed study. The chosen modifications were included in the process flow charts.



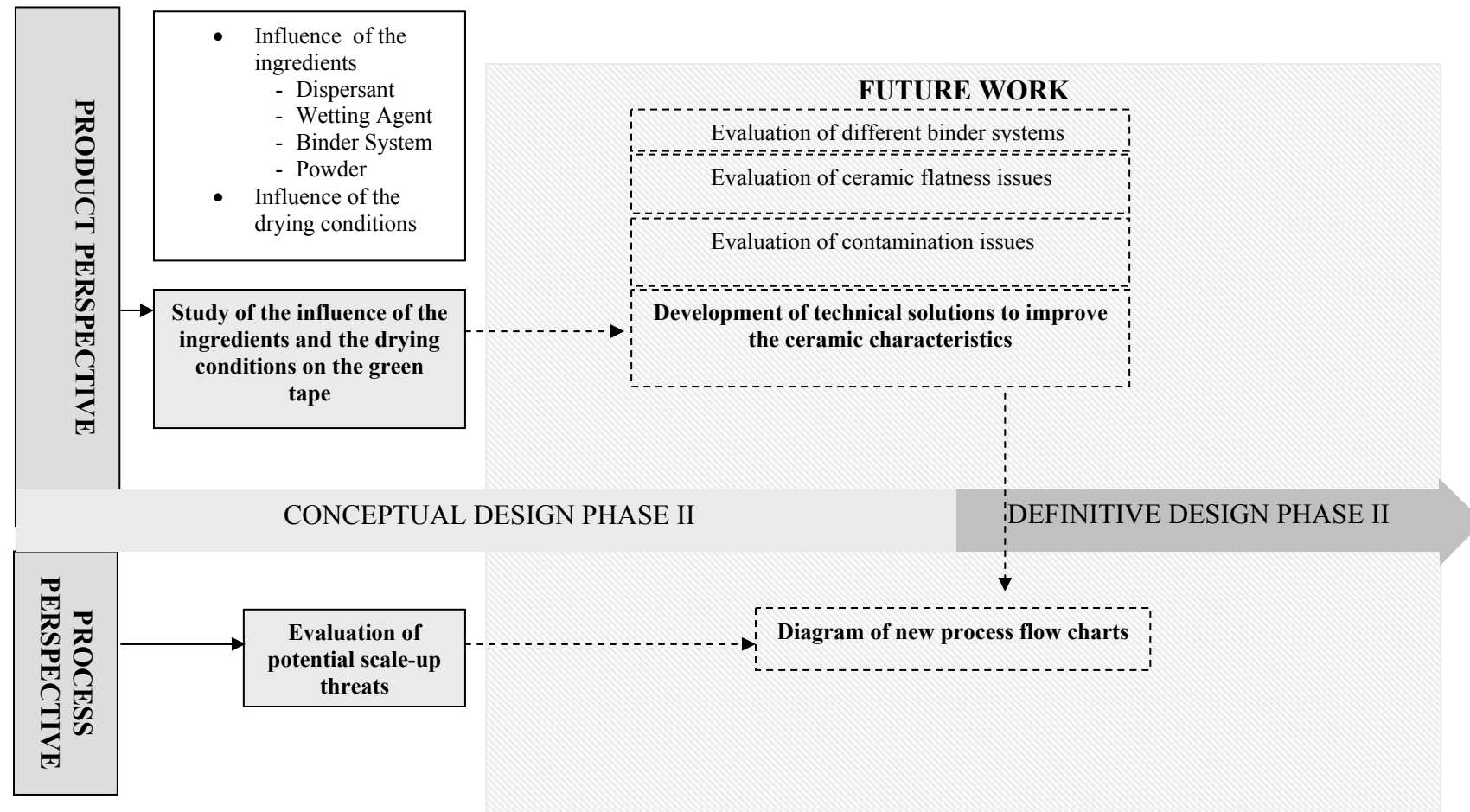


Fig. 49: Research development in detail. The bullet point items represent the experiments performed. In the grey boxes is a description of the experiment purpose. Future work is shown in dotted boxes

4 Experimental method

In this chapter, the general procedures used to produce the tape cast material, as found also in Navarro [2001], are described.

In addition, the general characterisation techniques employed during the investigation of the process are described in detail.

4.1 The original process

Fig. 50 shows a schematic diagram of the original process, which was adapted from the work of Navarro [2001].

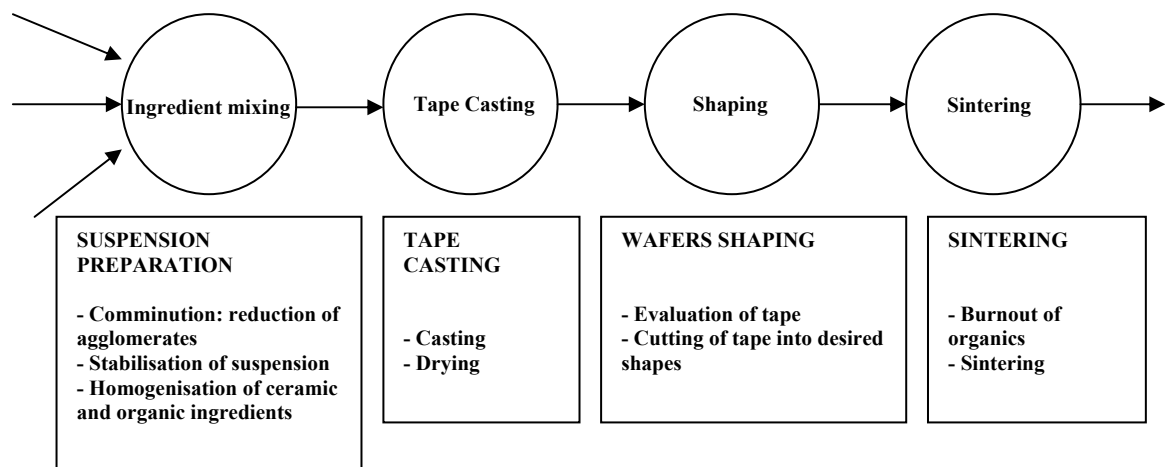


Fig. 50: Process steps for tape casting preparation

4.1.1 The materials

- **Powder:** The PZT [Uranium-doped $\text{PbZrO}_3\text{--PbTiO}_3\text{--Pb}(\text{Mg}_{1/3}\text{Nb}_{2/3})$] ceramic used in this investigation was produced as described by Stringfellow et al. [2002].

The powder was obtained by mixing lead (II) oxide (PbO , BHD, GPR), titanium (IV) oxide (TiO_2 – 325 mesh, Aldrich, UK), zirconium (IV) oxide (ZrO_2 , < 5mm, Aldrich, UK), magnesium niobate (MgNb_2O_6 prepared as in section 4.1.1.1) and uranium (V, VI) oxide (U_3O_8).

The ingredients were exactly weighted by using a Sartorius digital balance to make the composition $\text{Pb}[(\text{Mg}_{1/3}\text{Nb}_{2/3})_{0.075}(\text{Zr}_{0.925}\text{Ti}_{0.075})_{0.925}\text{U}_{0.01}]_3\text{O}_3$.

The reactants were ball milled in 0.75 litre polypropylene pots for 18 hours in an aqueous solution of 0.1% in wt. DISPEX A40 (Allied Colloids Ltd, UK), using cylindrical yttrium stabilised zirconia milling media.

The suspension was then dried at 80°C for 24 hours and then sieved to <300 μm . The powder was calcined in a furnace at 800°C for 6 hours.

After calcination the powder was sieved to <300 μm and milled for a second time for 18 hours with 450 cm^3 of the DISPEX solution. After drying and sieving as above the powder was taken up to 650 °C (dwell 0.1 minutes) to allow the burnout of the dispersant and of the pot contaminants.

Finally, the powder was sieved <75 μm .

- **Solvent:** Deionised water.

- **Dispersant:** Duramax D3021(Rohm and Haas): polyacrylic acid modified with substituted alkyl groups, pH 7, total solids 40%, counterion NH_4^+ , MW ~ 5000.

- **Wetting Agent:** Surfinol SE-F (Air products and Chemicals, Holland), formulation based on acetylenic glycol based surfactants and non-ionic emulsifiers.

- **Binder:** poly (vinyl alcohol) (PVA, 87–89% partial hydrolysis, MW=115,000 g/ mol) (Sigma-Aldrich UK).

- **Plasticizer:** Poly (propylene glycol) (PPG 400, Sigma-Aldrich, UK).

Table 5 indicates the proportions of the added ingredients in weight % for every processed batch. The water was added pure during the first milling stage. More water (amount indicated in the column with the asterisk) was added as part of the binder solution.

Addition stage	First milling			Second milling	Third milling			
						Binder solution		
Material	PZT	Dispersant	Water	Wetting Agent	Plasticizer	Binder	Water*	TOT
density (g.cm ³)	8.17	1.16	1	0.97	1.004	1.25	1	
quantity (g)	80.00	1.90	20.00	0.45	2.80	2.80	18.00	125.95
weight %	63.52	1.50	15.88	0.36	2.22	2.22	14.29	100.00

* water used to dissolve the PVA

Table 5: Slurry content of the original process

4.1.1.1 Preparation of magnesium niobate reactant

The magnesium niobate was prepared from basic magnesium carbonate [Mg(CO₃)·Mg(OH)₂·5H₂O] (Aldrich) and niobium (V) oxide (Aldrich, –325 mesh) in an initial step using the route described by Butcher and Daglish [Butcher and Daglish, 1993].

4.1.2 The procedure

All the tapes were produced following the given procedure except were otherwise specified. The flow chart diagram of the original process has been drawn using ANSI symbols and it is reported in section 5.2 (Fig. 58 page 96). In the following paragraphs the process operations will be numbered (Step 1, Step2, etc) with reference to the flow chart.

4.1.2.1 Slurry preparation

Step 1: PZT slips were prepared by ball milling the PZT powder in deionised water and ammonium polycarboxylate dispersant in 100 ml silicate milling jars with 200 g of cylindrical zirconia milling media for approximately 8 h.

Step 2: Surfynol SE-F wetting agent was then added to the slip and ball milled for a further 1 h.

Step 3a: Poly (vinyl alcohol) was pre-dissolved in a sufficient amount of water by heating and stirring the PVA solution in water to 95 °C for at least 2 h.

Step 3: The dissolved binder solution and the poly (propylene glycol) plasticizer were then added to the slip and ball milled, for a further 18 h to aid the dissolution of the organics into the slurry.

4.1.2.2 Slip conditioning

Step 4: The slurry was then separated from the media and transferred to a vacuum flask with a 38 µm sieve.

Step 5: De-airing was performed using a low vacuum diaphragm pump (Vaccubrand, model ME2) at a pressure of 100kPa. During the de-airing the slip was kept under agitation using a magnetic stirrer and heated at 30°C. (See Fig. 51)

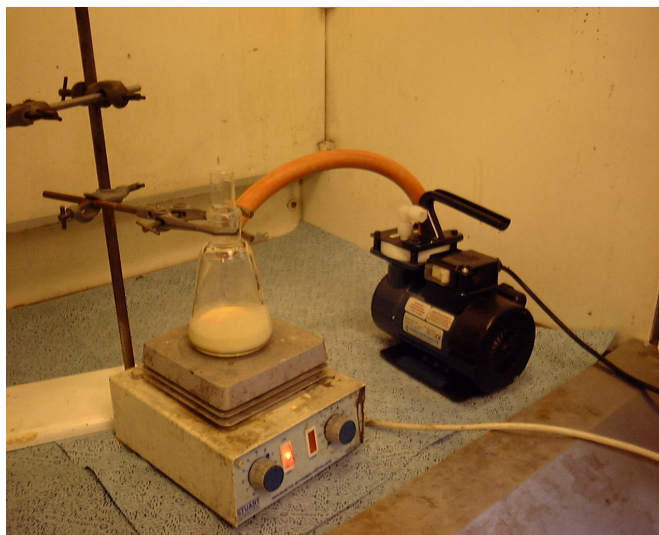


Fig. 51: Laboratory scale de-airing equipment

4.1.2.3 Casting Conditions

Step 6 and 7: The slurry was poured in the tape casting equipment reservoir. A table-top tape caster equipment (TTC-1000 from Mistler Inc. USA – dimensions 5' x 12") was used with a stationary double blade casting head, schematically pictured in Fig. 52. The front doctor blade height above the carrier surface was set at 550 μm and the reservoir blade at 1100 μm .

The speed of the polypropylene carrier (Western Wallis, CA) was 0.75 cm.s^{-1} giving a shear rate under the front blade of 13.6 s^{-1} .

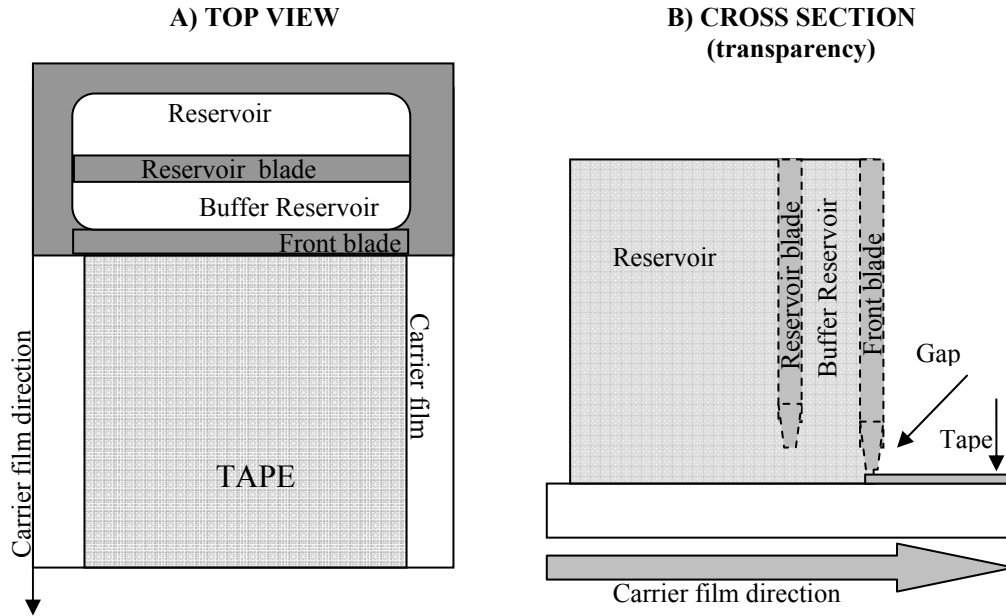


Fig. 52: Schematic representation of the doctor blade: A) top view and B) cross section with view of the blades positions

4.1.2.4 Drying conditions

Step 8: The tapes were dried at room temperature, with a constant current air flow at 50°C at approximately 0.5 m/s for the first hour after casting.

4.1.2.5 Samples cutting

Step 9 and 10: The green tape was separated from the carrier film and its characteristics were evaluated. The tape thickness was measured at regular intervals (approximately every 8 cm) along its length and its depth (approximately every 3 cm), as schematised in Fig. 53. For the measurement of the tape thickness a micrometer gauge with a tolerance of 5 μm was used.

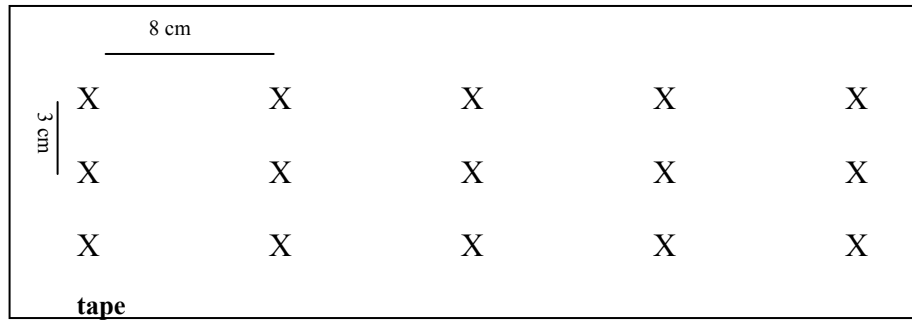


Fig. 53: Schematic outline of the green tape thickness measurements

Step 11: The green ceramic was stored in plastic sealed bags, waiting for the shaping.

Step 12 and 13: Squared samples (8 by 8 cm.) were cut from the tape in selected homogeneous (i.e. were no defects were visible at naked eye) and evenly thickened areas ($220 \pm 5 \mu\text{m}$), by means of a razor blade. To help the cutting, the outline of the sample shape was lightly drawn on the tape with a pencil with the help of a rule (tolerance $\pm 0.5 \text{ mm}$).

4.1.2.6 *Wafers burnout and sintering conditions*

4.1.2.6.1 *Samples sintering configuration nomenclature*

As in the process designed by Navarro, the samples were sintered with the configuration illustrated in Fig. 54, to limit samples curling. In this work, the samples' side A corresponds to the upper side during casting and to the lower side during sintering where it was in contact with the alumina support. The B side was the carrier side of the green tape. It was in contact with the carrier film during casting but it was the upper one during sintering.

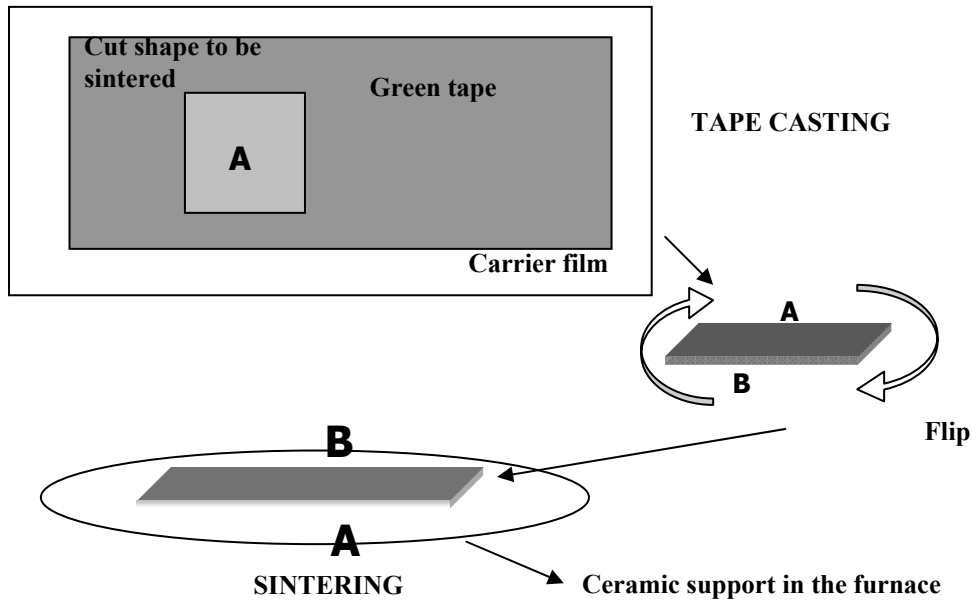


Fig. 54: Standard configuration for the casting and sintering of the samples

4.1.2.7 Samples sintering

Step 14: The cut samples were individually positioned as illustrated in Fig. 55 and on a flat sintered alumina (alumina min 99.7%) plate preconditioned with PZT powder. The pre-condition was provided by a layer of PZT powder deposited on the alumina with a wet cloth and pre-heated at 1270 °C.

The samples were surrounded by spacer pots containing a PZT powder enriched with 5% w/w PbO as also shown in Fig. 55.

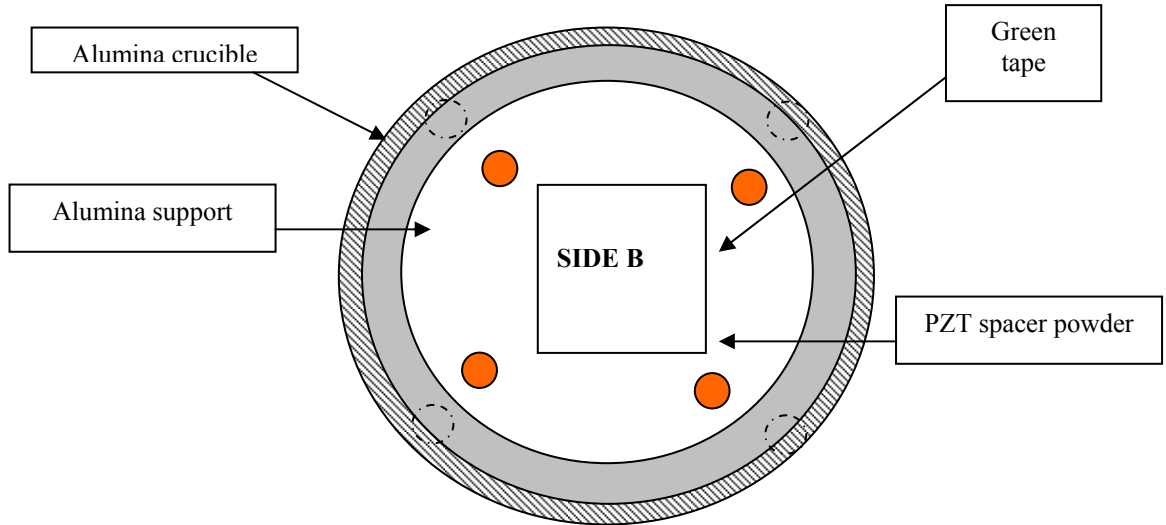


Fig. 55: Schematic representation of a top view for the placement of an individual sample on the sintering support

Step 15: The burn-out profile was performed in a furnace as reported by Table 6.

	Heating rate	Temperature	Dwell time
1	2°C/min	260°C	1 hour
2	1°C/min	500°C	1 min
3	10°C/min	Room Temperature	-

Table 6: The burnout profile

Step 16: After the samples have been cooled at room temperature, a preconditioned alumina crucible was placed on top of the plate to create a sealed environment, rich in PbO. The sintering profile was then run as shown in Table 7.

	Heating rate	Temperature	Dwell time
1	3°C/min	1270°C	45 min
2	10°C/min	Room Temperature	-

Table 7: The sintering profile

4.2 General characterisation techniques

4.2.1 Green density

The green density (GD) of the tapes and the sintered density (SD) were expressed also in terms of percentage of the theoretical density (TD) as shown by Equation 20.

$$TD = \frac{GD \text{ or } SD}{8.17 \text{ (g.cm}^{-3}\text{)}} \times 100$$

Equation 20

Where 8.17 g.cm⁻³ is the powder density theoretically calculated from the crystal cell.

The green density (GD) of the tapes and the sintered density (SD) of the samples were calculated using the following equation:

$$GD \text{ or } SD = \frac{w}{V} = \frac{w}{T \times h}$$

Equation 21

Where w is the sample weight, T is the sample area and h is the sample thickness.

The samples weight w was measured with a Mettler balance within the range of ± 0.0001 g.

The dimensions were measured with a ruler within a range of ± 0.5 mm and the area was geometrically determined.

The accuracy of this method was assessed by evaluating the area with an Image Analysis technique (Leica Q500MC image analysis software) on selected samples.

The samples thicknesses were determined with a micrometer gauge with an accuracy of ± 5 μ m.

4.2.2 Sintered density

Some sample's sintered density was evaluated following both the Archimedes methodology [Kwan and Alcock, 2002] and the geometric method. This allowed a comparison of the two methods and to test the precision of the volumetric method. The sintered density was calculated as: sample weight divided by sample volume (Equation 21), but the volume was obtained as in **Error! Reference source not found.**.

$$V = \frac{\text{dry weight} - \text{wet weight}}{\text{water density}}$$

Equation 22

4.2.3 Microstructure and Morphology

The following techniques were employed for the green tape, the sintered material and the brown tape obtained by burning out the organics of the green tape at 500°C for 1 hour.

Both a Scanning Electron Microscope (SEM) Philips XL series Scanning and an Optical Microscope Nikon (Japan) 143650, equipped with 3-CCD Camera by JVC, were used to analyse the sample's microstructure.

For the SEM imaging, portions of samples were held on an SEM stud and coated with several nanometers of gold-palladium. Samples were pictured on both free surfaces and on the cross section (obtained fracturing the samples).

The size of single grains was obtained graphically on the pictures, by drawing a horizontal line across the grains (from boundary to boundary), measuring its size and comparing it with the length of the scale-bar reported on the picture.

The calculated average grain size (d) of the imaged samples was obtained with two methods:

1) By counting the grains intercepted by a standard line drawn on the pictures taken at the same magnification and using Equation 23.

$$d = \frac{l}{m}$$

Equation 23

where l is the length of the drawn line (in the scale the picture was taken) and m is the number of grains intercepting the line (including portions of grains).

2) By averaging the measurements of single grains obtained as noted above of 20 grains, for each microstructure.

4.2.4 Flatness and roughness measurements

Flatness and roughness measurements were performed on sintered ceramic wafers with a Form Talysurf equipment (Model 4, Rank Taylor Hobson). The flatness was measured across 50 mm length in two perpendicular directions, on the same side of the samples, as illustrated in Fig. 56.

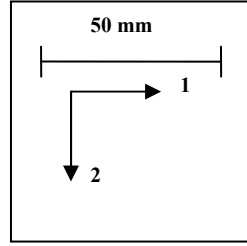


Fig. 56: Schematic diagram for wafer's flatness measurements

The average roughness (R_a), i.e. the peak to valley distance, was measured across 10 mm on the two wafer's edges (side A and B).

4.2.5 Electrical characteristics

The sintered tapes were coated with a temporary metallic electrode (Cu/Au, approximately 150 nm) on both surfaces, via evaporative method, using an Edwards coater.

The poling of samples was performed at 120°C in an oil bath by applying 445 V for approximately 10 minutes with a Keithley 6517 electrometer. After cooling the oil at room temperature, the wafer was washed and annealed for 12 hours at 70°C with short-circuited electrodes.

The samples capacitance and loss ($\tan \delta$) were measured before and after poling at room temperature (20 °C) with a Genrad RLC Digibridge (Model 1689M) at 1V. The measurements were performed at 30 Hz in 50 cycles to obtain an average value.

The capacitance was used to calculate the relative permittivity (ϵ_r) by the relationship in Equation 24, where ϵ_0 is the permittivity of the vacuum (8.854×10^{-12} F/m).

$$\epsilon_r = \frac{\text{Capacitance} \times \text{wafer thickness}}{\text{wafer area} \times \epsilon_0}$$

Equation 24

The DC resistivity of the unpoled samples was measured at room temperature using a Keithley 6517 electrometer, under vacuum. A voltage of 2V was applied and the resistivity was calculated using Equation 25

$$\Omega = \frac{\text{electrode area} \times 2V}{\text{wafer thickness} \times I}$$

Equation 25

where Ω is the sample's resistivity and I is the current flowing through the sample.

The pyroelectric current response of each sample was measured using the Byer–Roundy method on a custom-built computer controlled rig. This used a thermoelectric heater/cooler to ramp the specimen temperature within the range 26–24 °C, whilst under reduced pressure. The pyroelectric coefficients reported here are the averages of those measured on heating and on cooling. The heating/cooling rate was 1 °C/minute. The resultant current was measured using Keithley 6517 Electrometer. At least 3 cycles were done.

The figures of Merit F_v and F_D were obtained as in the equations below:

$$F_v = p / (c' \epsilon_0 \epsilon)$$

Equation 26

$$F_D = p / (c' (\epsilon_0 \epsilon \tan \delta)^{0.5})$$

Equation 27

Where:

p = pyroelectric coefficient

ϵ = dielectric permittivity at the frequency of device operation

ϵ_0 = dielectric permittivity at the frequency of free space

$\tan \delta$ = volume specific loss at the frequency of device operation

c' = specific heat capacity

4.2.6 Rheological characterisation of ceramic suspensions

The rheological properties of the slurries described in this thesis were characterised using a Bohlin CVO rheometer (stress controlled rheometer). The ceramic suspensions containing water, ceramic and dispersant were tested only under steady shear conditions, using a cup and bob configuration (C14 DIN 53019). For slurries which included the organic system, a cone and plate configuration (CP 4°/40 mm diameter) was instead employed.

4.2.6.1 Viscoelastic properties

In order to determine the linear viscoelastic region (LVR), the samples containing of the complete slurry were analysed with a stress sweep experiment from 0.05 to 200 Pa at 1 Hz frequency. Then a frequency sweep (from 0.1 to 10 Hz) experiment was carried out within the limits of the LVR.

4.2.6.2 Steady shear rheology

Slurries were pre-sheared at 50 s^{-1} for 60 seconds and then left to rest for 3 minutes. Then they were tested under steady shear conditions ascending and descending stress ramps between 0.8 and 50 Pa. The data on viscosity presented in this work were referred at 20 s^{-1} shear rate.

The thixotropy of the suspensions was assessed with two methods:

- 1) By a step experiment, varying ‘instantaneously’ the shear rate from 2 to 250 s^{-1} and (after 5 minutes) a second step change to 2 s^{-1} . Both, the ‘recovery’ time (the time required for the viscosity to re-gain a steady value, and the rate of recovery (to which extent the viscosity was recovered after the step shear) were considered indicative of the thixotropy.
- 2) By evaluating the thixotropy coefficient. A figure calculated by the rehometer software by integrating the area included between the viscosity curves obtained in ascending and descending the shear stress.

4.2.7 Assessment of the PVA adsorption onto the particles’ surface

Samples of the slurries produced following the above methodology were centrifuged at 6000 RPM in order to separate the ceramic from the liquid phase. Aliquots of the supernatant were diluted to a known extent and examined following the standard procedure for the PVA determination in products described in literature [Finch, 1973]. The method suggests the spectrophotometric determination of the PVA – iodine complexes, created in presence of boric acid [Finley, 1961].

4.2.8 The assessment of the tapes glass transition temperature (T_g)

The organic phase of the tapes glass transition temperature was evaluated with a Differential Scanning Calorimeter DSC2920, Modulated DSC (TA instruments), by sweeping the sample’s temperature up and down between -25 and +45 °C at 3°C/minute.

5 Results and Discussion of the process focused approach

The aim of this section was to show how ‘unstructured’ problems (i.e. problems which can not be clearly defined) were treated during the conceptual design phases.

This section describes the process focused approach to the research (see methodology section page 66).

The detailed descriptions of the process to which this work refers and its conditions are described in the experimental method section “The Original Process” at page 78.

The results of the product focused approach are given in the next results sections, where the core of the experimental work is described.

5.1 Process charts

The original process was mapped using layout and flow charts in order to achieve a full view, highlighting weaknesses that might have caused potential failure in the scaled-up process.

Then an analysis of the threats to the scaled-up process was performed, and potential modifications were suggested using a soft problem solving approach, following the method noted in the literature review section at page 14.

5.1.1 Process layout

The process layout overview of process presented in Fig. 57 shows the succession of the operations and times in producing the item. The rectangles represent the material processed and the arrows indicate the activities.

The laboratory process lasts in total more than 100 hours (more than 4 days). A break-down of task times is shown on the diagram.

Three main stages are shown Fig. 57, associated with the time needed for each activity. They are:

- 1) Slip preparation - lasting 29 hours
- 2) Tape casting, drying and shaping – lasting 26 hours
- 3) Burning out the organics and sintering – lasting 48 hours

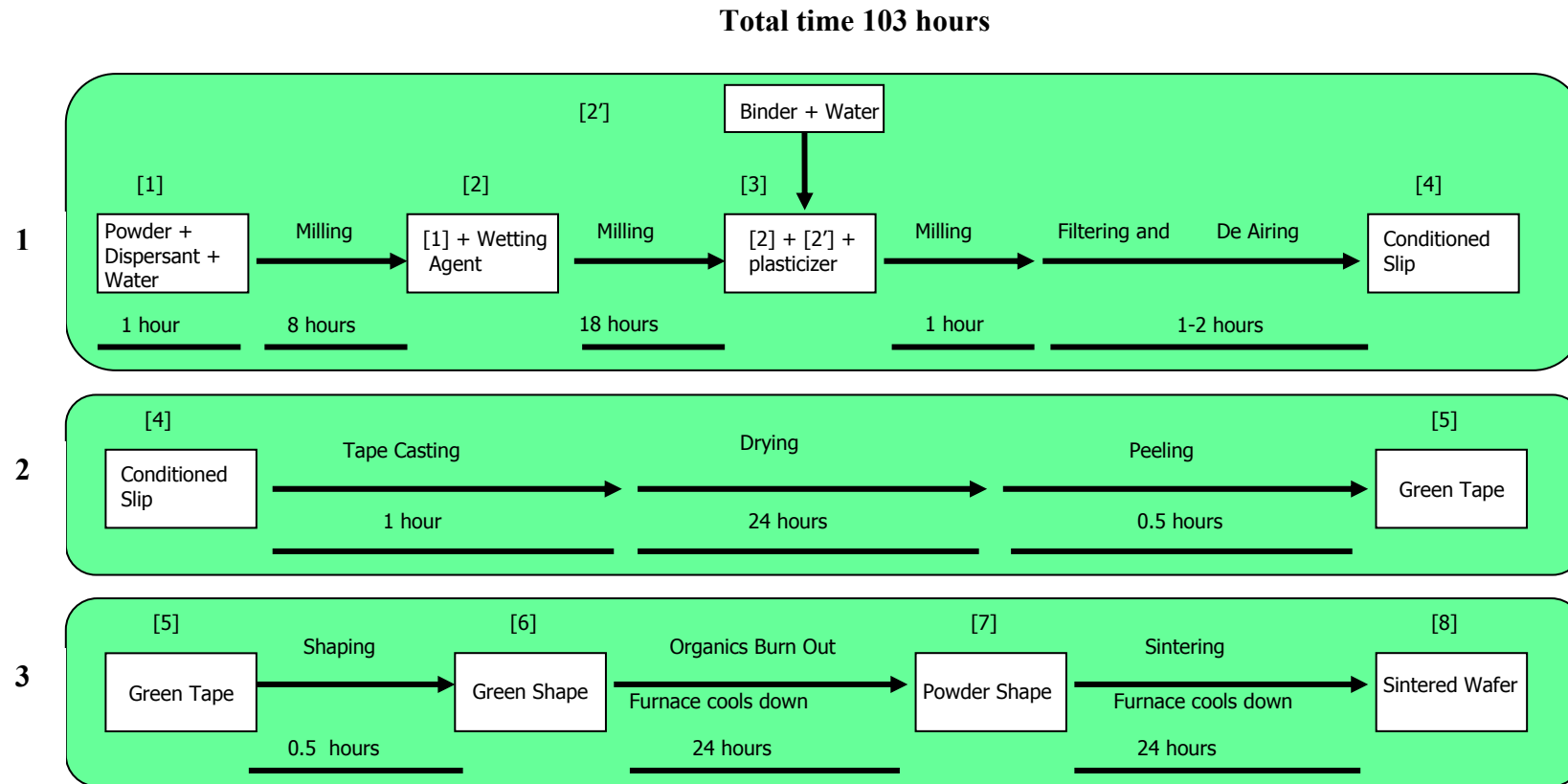
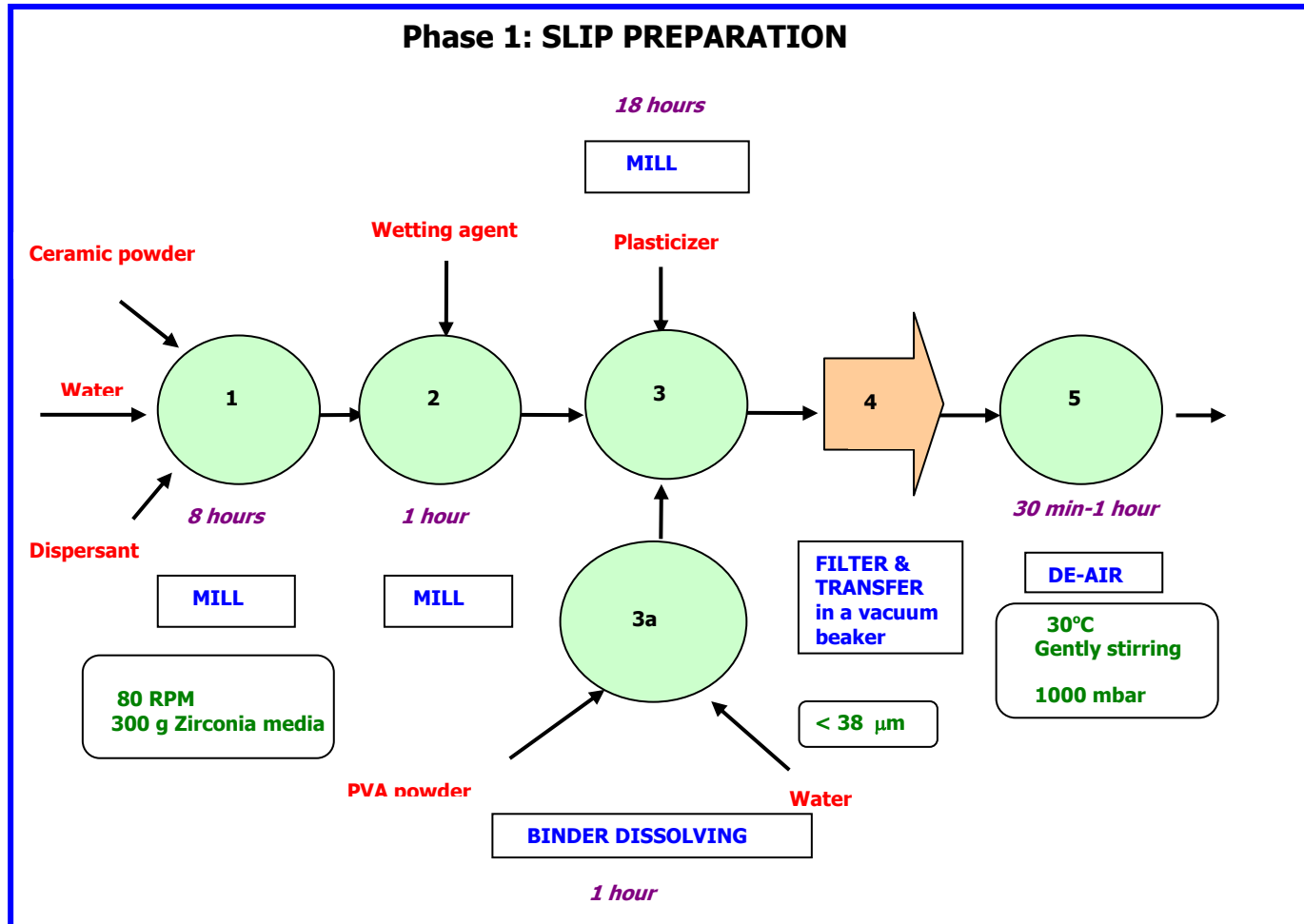
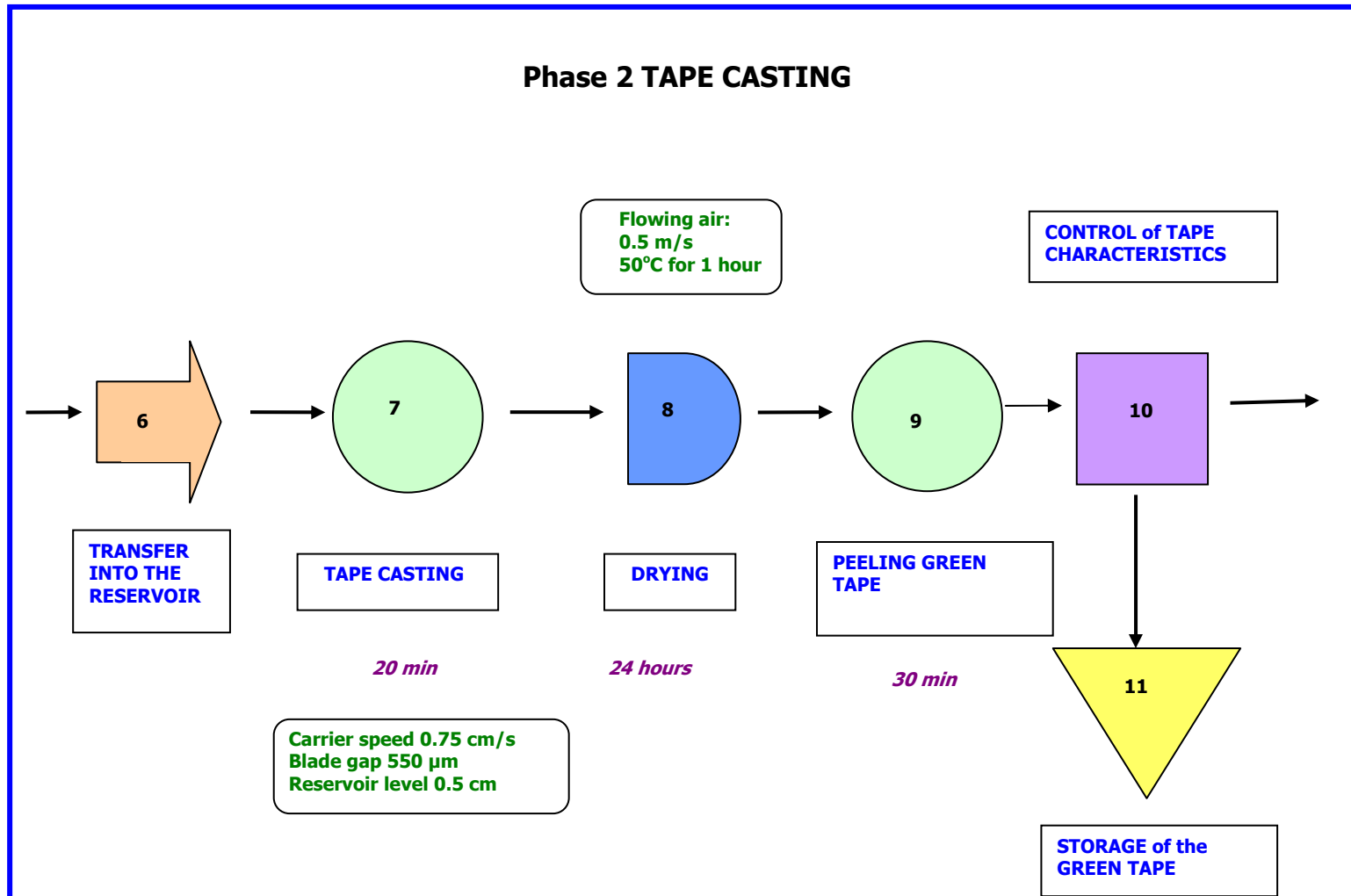


Fig. 57: Layout of the process (focusing on time flow)

5.1.2 Process flow chart

A material flow chart was also drawn (Fig. 58), which describes what happened to the product during manufacturing with details of operations, material transfers and process conditions. Standard symbols, which are published by ANSI, the American National Standard Institute, were used to construct the chart.





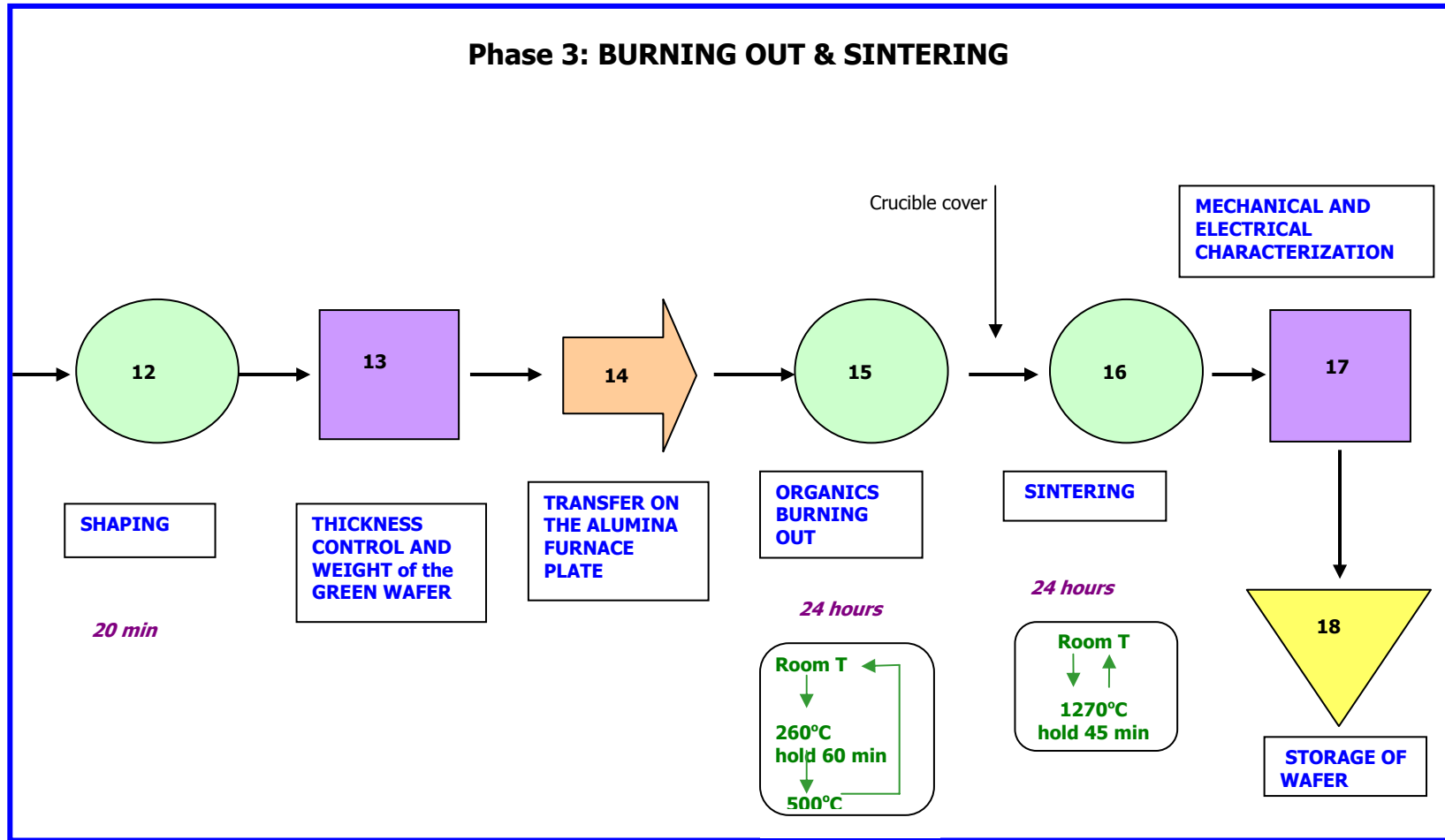


Fig. 58: Original Process Flow Charts

5.2 Process Analysis

5.2.1 The process yields, times and wastes

An analysis was performed focussing on the variation of the ceramic powder mass.

The Total Process Input was 80 g of ceramic powder.

The Total Process Output was a 5.9 g ceramic wafer plus 44 g of powder formed as green tape cast.

The yield of a 103 hours cycle was approximately 7.3% (one wafer of 5.9 g). The yield of the single phases was much higher oscillating between 78 and 98%.

The inputs, outputs and wastes of the three process phases are reported in Table 8.

Phase	Time	Perc. on tot time	Phase Input	Phase Output	Phase Waste	Phase yield	Output on tot mat.	Waste on tot mat.
	[h]	[%]	[g]	[g]	[g]	[%]	[%]	[%]
Slip preparation	29	28	80	64	16	80	80	20
Tape Casting	25.5	25	64	50	14	78	62.5	28
Burnout & Sintering	48.5	47	6	5.9	0.06	98	7.3	1

Table 8: Inputs and outputs of material for each stage

About 37.5% (approximately 30 g) of the total input material was wasted during the process. The material was principally wasted in the slip preparation and in the tape casting phases.

The 5.9% yield figure, i.e. the output of the entire process per run, can be explained by the fact that the majority of the material was not taken up to the end of the process, but was stored as green tape.

This was a limitation of the equipment/process in use that could sinter one wafer at a time. Hence, if all the green material was taken to the final sintering stage, the yield would rise to about 62% of the initial input (49.5 g of sintered samples versus 80 g of powder initially processed). However, processing the entire ceramic green tape, with the current equipment, would increase the process time from 103 hours to approximately 454.5 hours (54.5 for slip preparation and tape casting and approximately 400 hours for obtaining the sintered ceramic).

5.2.2 Analysis of the potential causes of low yield

As explained in the methodology section (page 69), in the conceptual design phase, after the analysis of the risks for the process scale-up, potential solutions to improve the process problems were conceived and assessed with a problem solving methodology.

The potential causes of low yield are summarised in Table 9, together with the threats to the scaled-up process.

Phase	Risk Type	Description
Slip preparation (Phase 1):	Low yield	Three milling steps were designed elongating the milling time and increasing the safety risks
	Threat	The de-airing method used was difficult to scale up
	Low yield	The material transfer to the de-air equipment inevitably led to waste of material
Tape casting (Phase 2):	Low yield	The slip was again transferred poured into the reservoir (increasing the waste of material)
	Increase of time	The drying time for the green tape was very high keeping the bench engaged for a long time (24 hours)
	Low yield	The length of the tape casting bench might have a limit to the achievable yield
Burning Out & Sintering (Phase 3):	Increase of time	Burning out of organics and sintering were achieved separately. This because of the necessity firstly of burning out organics in presence of excess of oxygen and secondly because of the need of creating a controlled atmosphere rich in lead oxide during sintering.
	Low yield	Using the laboratory system it was possible to sinter only one ceramic piece (or maximum few) at a time. This was the biggest bottleneck in the process.

Table 9: Potential threats to the scale-up of the original process

5.2.3 The problem solving: an example

All the problems noted above afflicted the process and would have to be solved in order to provide a new, more efficient and simpler layout.

This section describes the problem solving approach used to solve the most important problems affecting the process and generating the greatest bottlenecks.

Phase 3 was identified as containing the greatest time penalty.

In this context, two main problems were considered, and treated with a soft problem solving methodology:

Problem 1: The burnout and the sintering were using the same equipment but two different profiles were run.

Problem 2: The yield of the sintering step reduces the yield of the entire process, which produced 1 single ceramic wafer at a time.

Once identified, the problems were analysed considering their impact on the entire process.

5.2.3.1 Problem 1

a. Root definition (Unlinked furnace steps):

- *What is the problem?* Time was wasted in two heating and cooling cycles.
- *What is the target?* The time for this stage should be reduced whilst avoiding wasteful operations. Preferably, the risk of damage to the ceramic piece should be also reduced. The ceramic is extremely fragile after the burn out of binder and plasticizer.
- *Which were the reasons for the original process?* 1) The burn out phase was performed on an uncovered alumina support because of the necessity of burning out organics in presence of excess of oxygen. 2) Subsequently, an alumina cover was placed on top of the samples to create a controlled atmosphere, rich in PbO, during sintering. This prevented lead losses at high temperature.

b. Conceptual modelling (Possible solutions):

Various solutions for the problem were considered to reduce the number of heating cycles to one.

- 1) To place on the sample the alumina cover at the beginning of the heating cycle and set an appropriate temperature profile to reach the sintering temperature.
- 2) To find spacer material to sustain the alumina crucible while the burnout of the organics in the samples occurred, which burns at higher temperature than the binder system.
- 3) To design an automatic system capable of lowering the crucible at the right moment.

c. Comparison and debate (of solution 1):

In Table 10, the high-level assessment and comparison of the three potential solutions is given.

Solution	Quick assessment	Risk	Feasibility
Crucible from the beginning	PVA degrades with no residue even in absence of oxygen [Literature review, page 28]. A possible threat was linked to an incomplete burn of the other organic material, especially if multiple samples were treated simultaneously.	Medium	High
Spacer material to support the crucible and then to be burnt	Providing that it was possible to find the material with appropriate physical characteristics, the risks for sample contamination was high. In addition, if an uncontrollable burning of material made the crucible to collapse on the support, the risks of a rupture of the crucible shell was quite high, leading to potential serious threats for health and safety and to inevitable increasing costs	Very High	Medium
Automatic system for lowering the crucible from the outside	Lowering the crucible from the outside would involve the use of materials resistant to high temperature (e.g. Platinum) which are very expensive. The lowering of the crucible had to be very precise not to compromise the sample(s) and the crucible. This is relatively complicated to achieve from the outside, without vision.	Medium	Low

Table 10: Comparison of the potential solutions of case 1

Given the relatively lower risk and higher feasibility of the potential solution 1, this was analysed further:

- *Is the solution feasible?* A series of laboratory tests were set to check the feasibility of this solution. As a result ceramic pieces with similar mechanical and electrical characteristics to the one produced with the original process were obtained.
- *What are the possible risks?* An unsatisfactory burn out of the organics could lead to the formation of undesirable fumes and also residues that might affect the sintering stage, creating defects. To check the limiting amount of tape to be burnt out at a time, several samples were sintered together. It was shown that it was possible to sinter up to 7 samples at a time without causing sintering problems. It was impossible to increase the samples number further, due the laboratory equipment in use.
- *What is the outcome?* By setting the new profile operations 15 and 16 in Fig. 58 were condensed. This reduced Phase 3's time from 48.5 to 28 hours (a reduction of about 42 % of Phase 3 time and approximately 20% of total process time).

d. Conclusion: Among the potential solutions to the problem, the example discussed here appeared to be the more feasible. It was shown also to reduce significantly the processing time. In order to be in control of the process, it would be necessary to continue the assessments, to detect exactly the amount of material to be processed at a time.

5.2.3.2 Problem 2

a. Root definition (Sintering of multiple samples):

- *What is the Problem?* Only one piece of ceramic was sintered at a time, leading to a very small throughput.
- *What is the target?* To achieve the sintering of a quantity of green tape per furnace cycle as close as possible to the amount of the tape cast.
- *Which were the reasons for the actual process?* PZT tapes adhere if placed in contact during sintering. The dimension and the shape of the alumina support allowed only one sample to be sintered at a time.

b. Conceptual modelling (Possible solutions):

- 1) From a literature review a possible solution was noted in the work of Feng et al. [2001] who were able to sinter several samples at a time, separated by a tape cast buffer sheet made by coarse (about 18 μm) zirconia powder and binder. (Fig. 59A)
- 2) Another option was to stack several alumina plates as illustrated in Fig. 59B.

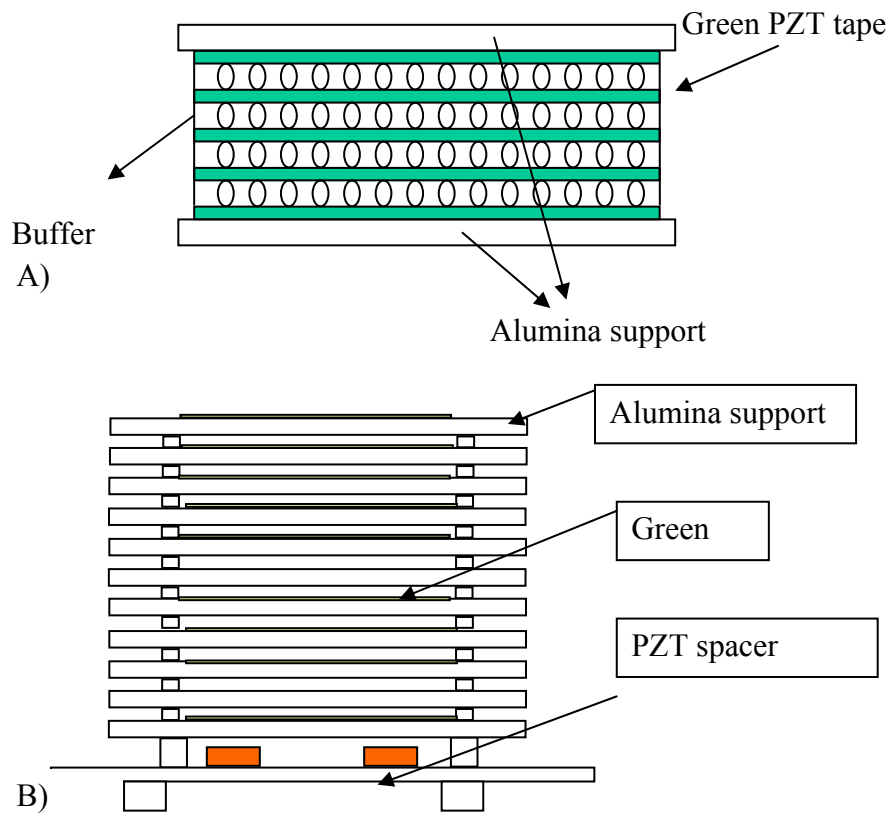


Fig. 59: A) The buffer configuration as suggested by Feng; B) the stack configuration proposed

c. Comparison and debate:

In Table 11, the high-level assessment and comparison of the two solutions is given.

Solution	Quick assessment	Risk	Feasibility
Buffer Sheets	For a successful result an in depth study is necessary to find the right buffer material to be tape cast and the conditions for the processing. The multiple sample sintering might lead to unevenness, marks and lack of uniformity in the samples.	Medium	Medium-Low
Stack of plates	The limits of this solution are the cost (very high for pure alumina supports) and the potentially precarious equilibrium of the configuration.	Low	Very High

Table 11: Comparison of the potential solutions of problem 2

The second potential solution was presenting the lowest risk combined with the highest feasibility. It was consequently chosen for a more in depth assessment. The detailed discussion follows:

- *Is the solution feasible?* The feasibility has been demonstrated by producing up to 7 samples using the configuration shown in Fig. 60.

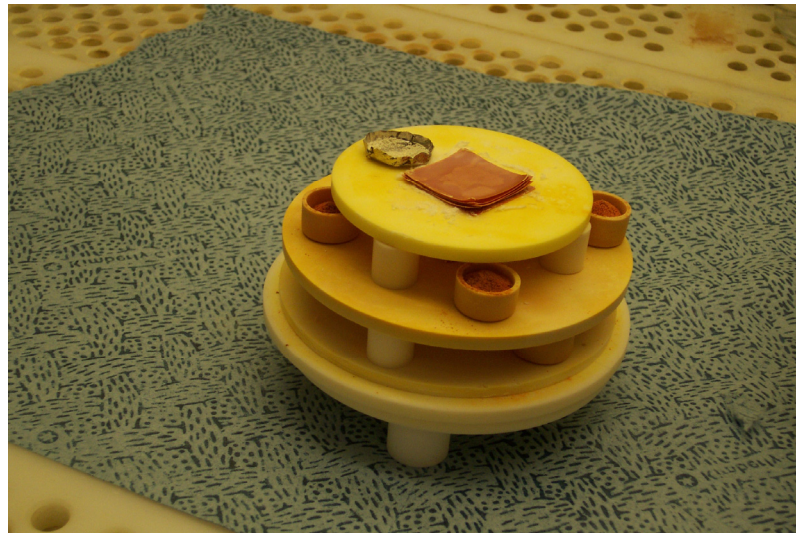


Fig. 60: Sintering configuration of multiple samples

- *What are the possible risks?* a) The multilayer structure has a precarious equilibrium, which would become more precarious as the number of stack increases. b) The cost of the high purity alumina support would be now high, and

it would be uncertain how long the ceramic could resist thermal shocks without breaking.

- *What is the outcome?* It was shown that it was possible to sinter several samples at a time.

d. Conclusion: Among the various ideas to solve the problem the solution 2 appeared to be the more feasible. By improving the design of the alumina plates and maximising the stability of the stack, it would be possible to stack the ceramic supports more effectively, If the number of the supports required justified the design of a mould for slip casting, the costs for each shelf could be reduced substantially.

e. Problem solving stage conclusions of the problems here reported:

By combining the solution of problem 1 and problem 2 it would be possible to reduce the Phase 3 step time by a total of 20% and increase the throughput by producing more samples at a time. The increase of the throughput would depend on the design of the ceramic sintering support. The newly obtained layout is shown in Fig. 61.

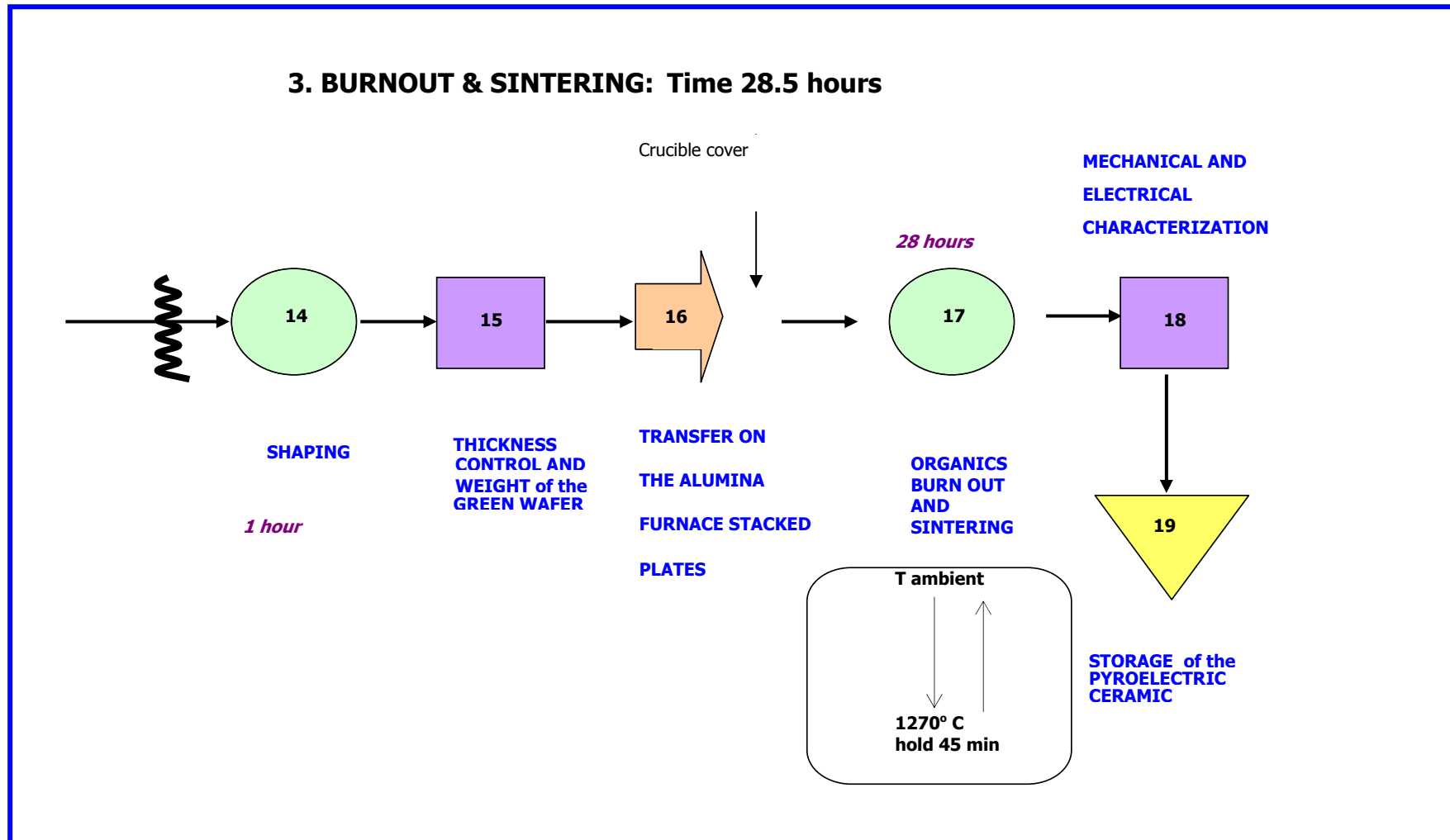


Fig. 61: The proposed new process

5.2.4 The newly designed process

After a sequence of problem solving loops that modified the original material flow (Conceptual Design), a new flow chart was drawn. It is represented in Fig. 62. This process resulted from both the product and the process approaches and represents the development after the first cycle of conceptual and definitive design.

In contrast with the original process (See Fig. 58), six main process steps were involved:

- Slip preparation
- Tape casting
- Warm Pressing
- Sintering and Poling
- Powder recycling
- Binder preparation

In addition to the examples given in the previous sections, other process steps were evaluated using the same methodology:

- Filtering and De-airing
- Cutting & Shaping
- Recycling of powder

The process phase ‘Warm Pressing’ was designed as a result of the product focused approach, to improve the product characteristics (refer to Fig. 49 in the methodology section). The work relative to its development is reported in the section 1 page 1 and discussed in section 7 page 197.

Furthermore, control measurement techniques were established to increase the rigour in the monitoring of the process. The rhombohedra symbols signify decision points using the results of the control measurements.

Appendix A describes the chart operations.

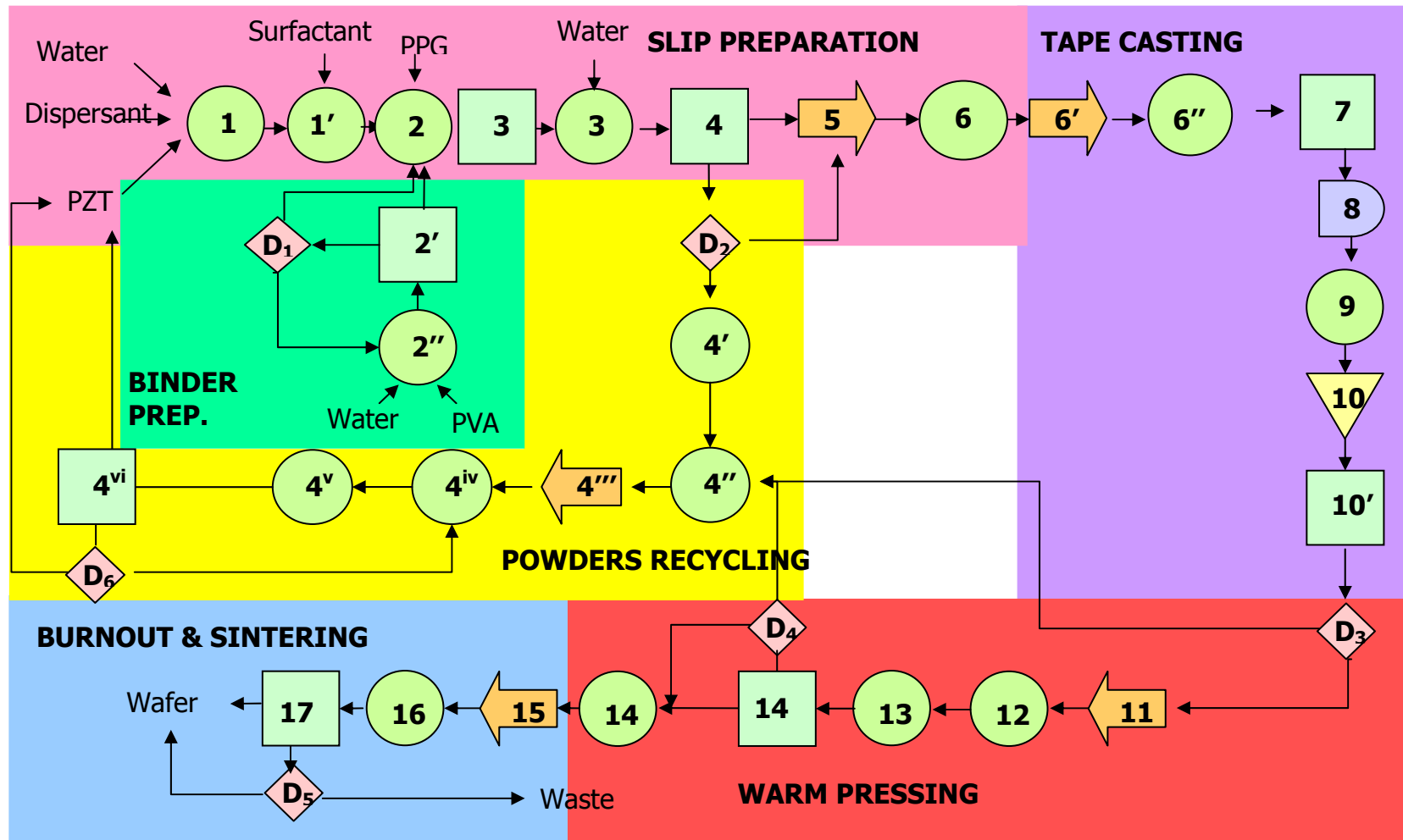


Fig. 62: Process as designed through the Conceptual Design Phase I

5.3 Considerations about the process scale-up

5.3.1 The evaluation of the process yield

The yield of the newly designed process has been evaluated, considering the results on the laboratory scale. Twenty samples were produced up to the sintering stage which showed acceptable characteristics in respect to the specifications reported in section 1.2.1. Among these, four were tested in the following processing stage, the poling and dicing.

The scheme in Fig. 63 shows the yield data, in percentage, referred to the original weighed powder.

It can be noted that the yield of the ceramic process studied, encompassing slurry preparation, tape casting and sintering, was about 35%. This value was thought to be strictly dependant on the laboratory scale of the process, where a maximum of 240g of powder had been processed. In fact, the laboratory scale equipment didn't allow a steady state of the tape casting step to be reached as the length of the tape was limited by the length of the tape casting bench. As a result, the tape cast areas with uniform thickness, i.e. $345 \pm 15 \mu\text{m}$, were extremely limited. Following on from this, it seemed verisimilar to assume that in a larger process scale, the yield would increase.

However, the 65% of the material was not completely wasted up to this stage, since it was possible to recycle up to 55% of the raw powder through the designed recycling process. No ceramic was wasted in the sintering stage.

The target yield figure of 50% given in section 1.2.3 refers to the following stages in the sensor processing: ceramic poling, wafers dicing and print-run (i.e. the deposition of the array of electrodes and of the conductive bonds on each wafer that allow the integration with a silicon chip). The figure encompasses more process steps than the ones strictly related to the ceramic process evaluated in this research. However, the analysis of these process yields gives a perception of the conformity of the product to the industrial needs.

Poling and dicing had a 75% yield(1), according to the results of a test conducted on 4 wafers. In other words, 3 out of 4 wafers were successfully poled and diced and could be taken to the next process stage (print run). This value was 25% higher than the requested 50% .

A precise data on the yield(2) for the print run stage couldn't be obtained, due to a because, for time constraints, a small number of arrays that could be mounted on silicon and tested. However, estimations were made of the factors and that could affect the yield(2) on the basis of the trials made on four arrays in total. Localised defects in the bulk of the ceramic or powder contamination could reduce the yield(2). An additional factor which could lead to the failure of some devices was a limited flatness of the samples that might reduce the contact of the ceramic with the circuit on the silicon. Fig. 88 at page 148 shows how the samples were slightly bowed, as confirmed by the data of flatness reported in Table 26 at

page 147. This latter was estimated as the biggest threat for the achievement of a yield that met the requirements. The considerations on the samples flatness are given in the discussion of the product focused approach, in section 7.1.1.

In order to achieve a successful scale-up of the process, further studies were needed to investigate the flatness or contamination hypotheses and to improve the yield at this stage. A new phase of the conceptual design, investigating these problems could have started at this point.

However, although the final yield value was uncertain, there wasn't a definitive impediment to the process utility.

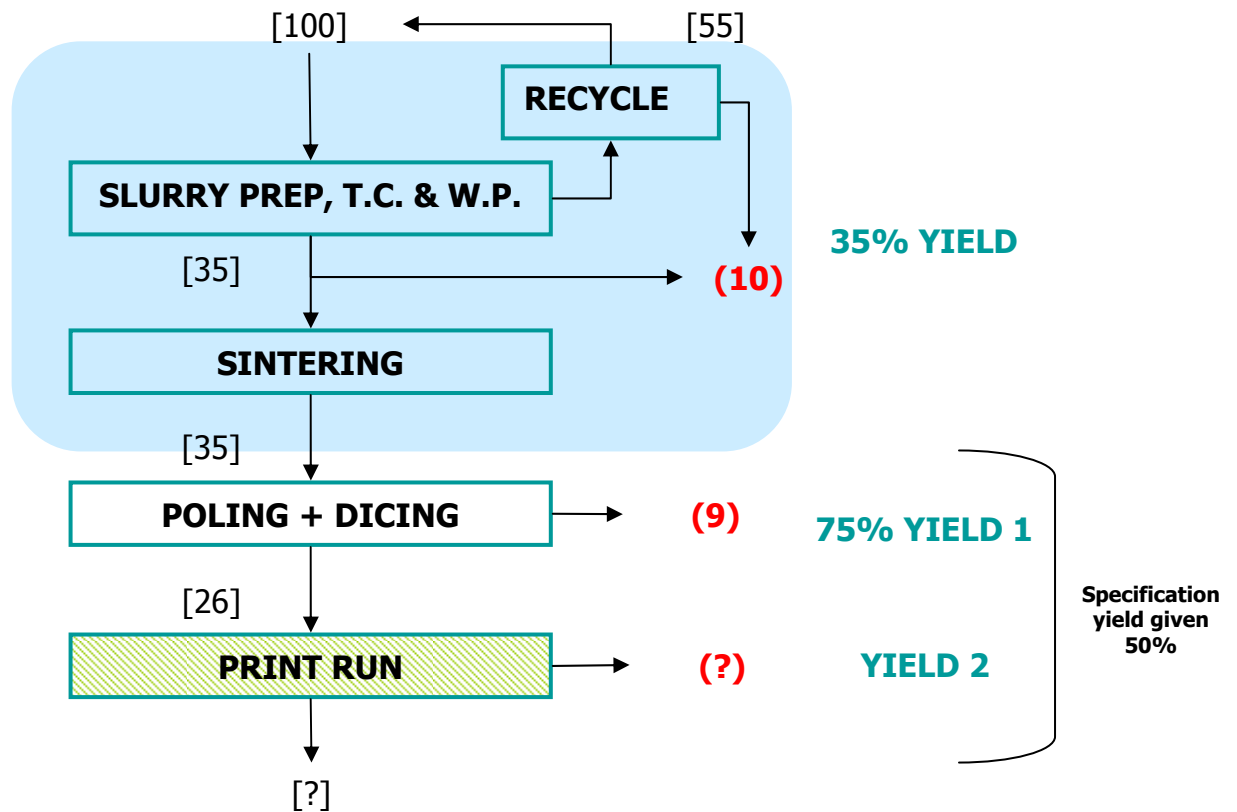


Fig. 63: The evaluation of the process yields. The ceramic process studied in this research is evidenced by the shadowed area. Its yield was 35%. The values in the square brackets represent the input and the output of each stage, in percent. The bold values in the round brackets represent the waste. Yield 1 corresponds to the yield of the process step poling and dicing. Yield 2 refers to the 'print run' step, which was estimated.

5.3.2 The estimated yearly throughput

On the basis of the newly designed process, an estimation of the throughput was made.

The estimation took into account the casting of a 650 g powder batch on an extended tape casting equipment, longer than 5' like the one employed in this study. For evaluating the worst case scenario, the 35% yield figure obtained by the laboratory trials was reduced further to 30%.

The results of the throughput per batch are shown in Table 12.

Total process time/ batch [days]	4
Powder processed/ batch [g] (50% virgin /50% recycled)	650
Green tapes obtained (8 x 8 cm) [N°] Uniform thickness ($345 \pm 15 \mu\text{m}$) Green density $\sim 3.0 \text{ g.cm}^{-3}$	40-50
Green pressed tapes (7 x 7 cm) [N°] Uniform thickness ($240 \pm 20 \mu\text{m}$) Green density $\sim 5.0 \text{ g.cm}^{-3}$	35-40
Sintered samples (6.5 x 6.5 cm) [N°] Uniform thickness ($210 \pm 20 \mu\text{m}$)	30-35
Yield [% on the original powder]	~ 30
Poled and diced ceramic wafers [N°]	22-26 considering yield (1) = 75%
Waste [% on the original powder]	10-15

Table 12: Estimate of process batch throughput

By processing 650g of powder, 50% virgin and 50% recycled, it could be estimated that 40 to 50 squared samples approximately $345 \mu\text{m}$ thick and with 8 cm side could be produced. After the warm pressing 35 to 40 samples would have been taken to the sintering stage, once their edges were reduced to 7 cm to eliminate any border effect. The sintering stage would yield 30 to 35 samples for poling and dicing. This could have been achieved by using 2-3 furnaces in parallel and with the configuration suggested in section 5.2.3.2. Up to this point the yield on the powder would have been $\sim 32\%$. 10 to 15% of the original powder, i.e. approximately 65g, would be wasted.

Considering a 75% yield of the polishing and dicing stage obtained before, the number of samples to be mounted on silicon wafers would be approximately 22 to 26 for each tape casting batch.

By performing 4 to 5 batches per week, shifted by a day, the total wafers per year would be between 6240 and 4224.

The estimation indicated the capability of the process to meet, and largely overcome, the short-term targets of producing between 500 and 1000 wafers per year.

In order to evaluate the economy of this process, more defined yield figures for the print run as well as the production costs, including the cost of waste disposal, would be necessary.

6 Results of the product focused approach

This chapter summarises the detailed results obtained during the investigation with the product focused approach.

6.1 Microstructure characterisation of the ceramic achieved by the original process

The ceramic wafers obtained with the original laboratory process were characterised and their main electrical and mechanical properties were compared with the product requirements (see section 1.2 in the introduction chapter). Among the product characteristics, a particular source of concern was the brittleness of the samples, which constituted a threat for the achievement of a satisfactory yield, as detailed in the discussion section at page 197. As strength in ceramic is thought to be dependant on its microstructure, in this thesis the microstructural characteristics of the produced wafers have been the subject of an extensive study.

6.1.1 Sintered density

The average sintered density of ceramic wafers was estimated with the Archimedes method as $7.82 \pm 0.07 \text{ g.cm}^{-3}$ (95.7% of the theoretical).

6.1.2 Ceramic surface microstructure

Fig. 64 shows optical microscope and Fig. 65 SEM images of the surfaces of a typical tape cast and sintered sample.

As described in the experimental section page 83, in this thesis the surfaces of a sintered sample are:

- A in contact with the support during sintering
- B upper side of the sample during sintering.

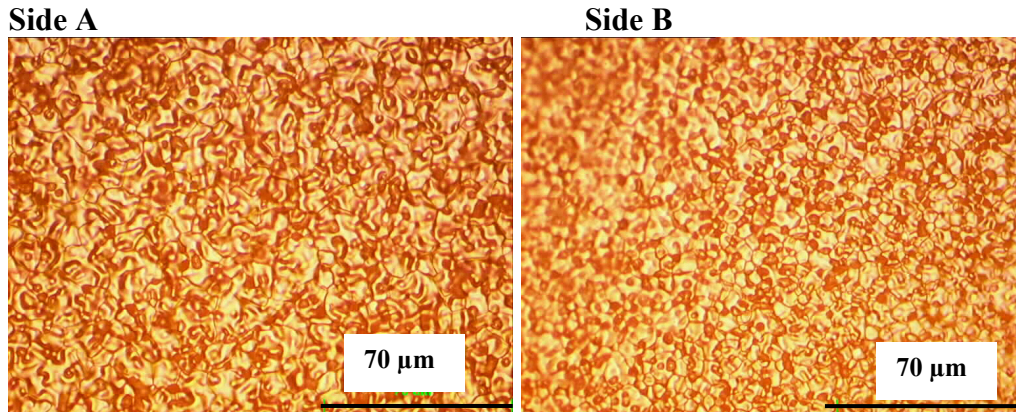


Fig. 64: Optical microscope images of the surfaces of a sintered ($T = 1270^{\circ}\text{C}$) tape-cast sample obtained with the original process. (Side A in contact with the support during sintering and side B free to air)

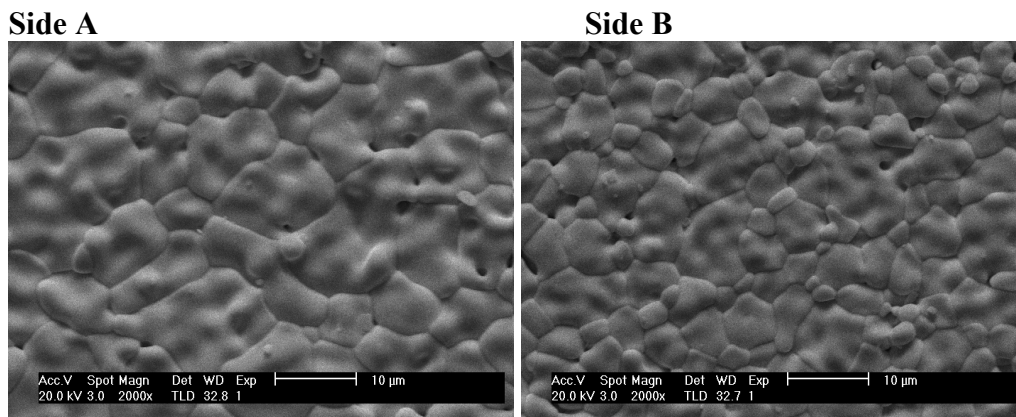


Fig. 65: SEM images of the surfaces of a sintered ($T = 1270^{\circ}\text{C}$) tape-cast sample obtained with the original process. (Side A in contact with the support during sintering and side B free to air)

6.1.3 Ceramic cross-sectional microstructure

Fig. 66 shows the cross sectional appearance of the sintered tapes in proximity of the surfaces and in its central area.

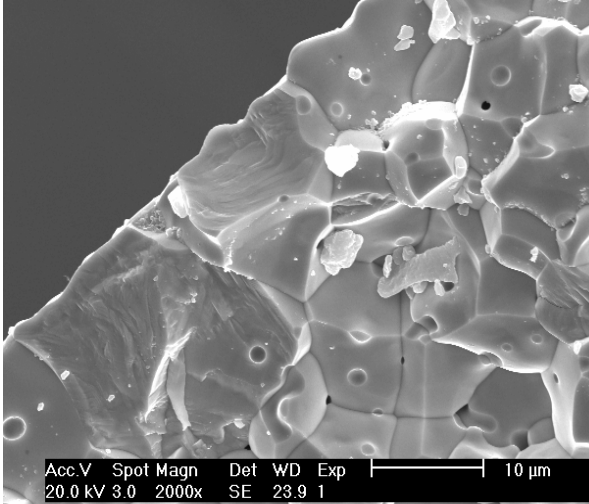
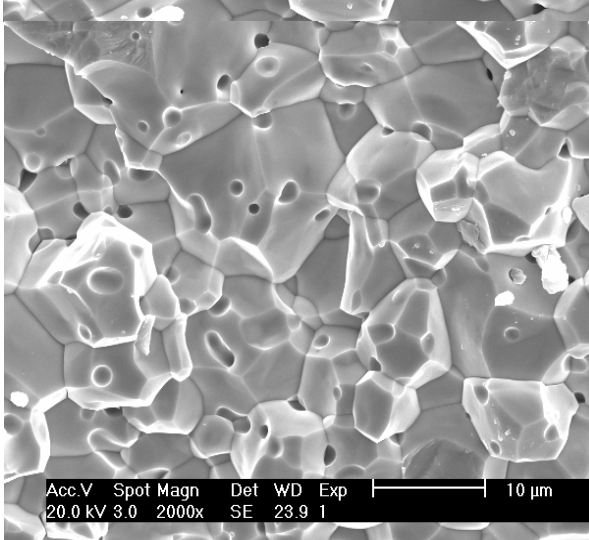
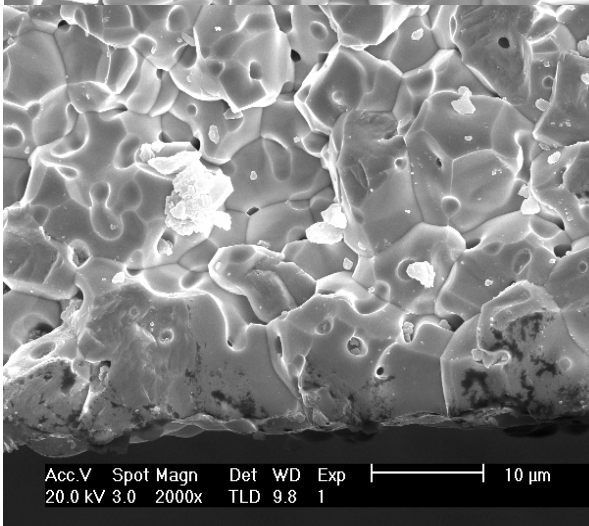
	SURFACE A In contact with the alumina support during sintering	
	Thickness of the layer	20-30 μm
	Grain size	$\sim 10\text{-}20 \mu\text{m}$
	Microstructure description	<p>The surface of the wafer was almost fully dense. The ceramic porosity was located both at the triple points and within the grains.</p> <p>The grains were larger than in the rest of the structure.</p> <p>The fracture path didn't follow the grain boundary, but it developed through the grain.</p>
	INTERNAL AREA	
	Thickness of the layer	100-150 μm
	Grain size	5 –15 μm
	Microstructure description	<p>Porosity was located both at the triple point and within the grains. The shape of the porosity was irregular.</p> <p>The grains were smaller than on the surfaces.</p> <p>The fracture path followed the grain boundary.</p>
	SURFACE B Free surface during sintering	
	Thickness of the layer	15-20 μm
	Grain size	8-15 μm
	Microstructure description	<p>The surface of the wafer was almost fully dense but the surface appeared rougher than surface A.</p> <p>Porosity was present mainly at the triple points.</p> <p>The grains were larger than in the internal area.</p> <p>The fracture didn't follow the grain boundary, but it developed through the grain.</p>

Fig. 66: Typical sample cross section with description.

The microstructure of all the samples analysed presented the following characteristics:

- The grain sizes on both surfaces were large compared to the particle size after milling shown in Fig. 75 (about 0.5 microns, see).
- Both the surfaces A and B appeared almost fully dense and denser than the central area.
- The dimension of the grains, although larger than in the central area, was smaller on side B (approximately 15-20 μm), respect to the side on surface A (approximately 20-30 μm).
- The cross section image showed a change in microstructure morphology starting from approximately 20 μm from both the surfaces. In this central area the grains were smaller (approximately 5-15 μm) than on the surfaces (approximately 15-30 μm). In addition, the micrographs showed an apparently not completely dense microstructure where pores were present both on the triple points and internally to the grains. The porosity was sometimes irregular in shape.
- There is evidence that the crack morphology is not homogeneous in the structure. The fracture path is more intragranular at the surfaces and intergranular in the centre of the sample.

6.1.4 Samples Flatness and roughness (Ra)

The samples average roughness, measured for 3 samples across 10 mm, was 205 nm on side A and approximately the double (412 nm) on side B, as reported in Table 13.

The table also reports the values of the samples flatness, measured for the same 3 samples, across 50 mm in two perpendicular directions (direction 1 and direction 2).

These values were comparable, with Navarro's results if not more satisfactory (see Introduction chapter 1.1.1, page 1)

	Roughness			Flatness		
	Side A	Side B	Sides Average	Direction 1	Direction 2	Directions Average
	nm	nm	nm	μm	μm	μm
Average	205	412	309	75	95	85
Standard deviation	19	27	-	17	28	-

Table 13: Values of samples flatness and roughness

6.1.5 Resistance to stresses

95% of the sintered samples obtained broke when taken to the poling or dicing stage. The samples were fragile enough to allow cracks to develop easily.

6.1.6 Crack morphology

Fig. 67 shows the typical sintered microstructure and an example of crack (indicated by the arrow) development into the ceramic. The sample imaged was voluntarily stressed until it broke. The picture was taken with the SEM in the wafers central area. It is visible how the crack, which mostly followed the grain boundary, occasionally broke intergranularly. The crack seemed to develop in in proximity of grains which broke intergranularly.

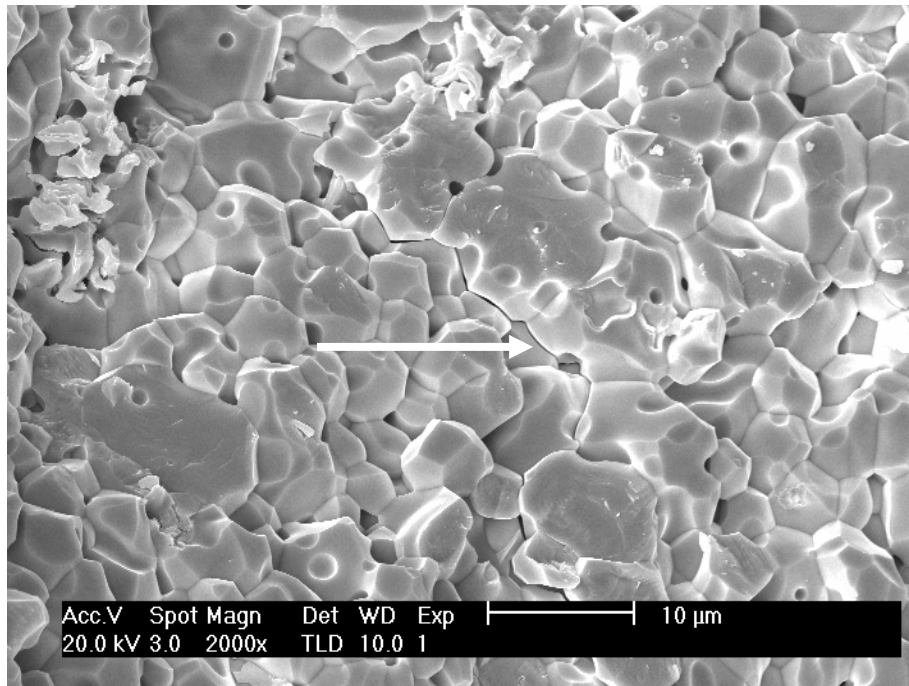


Fig. 67: A crack developing through the ceramic microstructure

6.2 Electrical characteristics of the tape cast material

Table 14 reports the average and the standard deviation of the electrical characteristics of six sintered wafers. The wafers were selected from six cast tapes obtained by using two different batches of powder.

Results

The characteristics across the material were comparable with the ones obtained by Navarro (see Introduction, chapter 1.1.1, page 1). In addition, the values of the standard deviations suggested that the process gave reproducible results.

Before poling				After poling					
	ϵ_r (30 Hz)	Tan δ (30 Hz)	ρ	ϵ_r (30 Hz)	Tan δ (30 Hz)	p	p/ϵ	F_v	F_D
		%	$\Omega m \times 10^{-9}$		%	$Cm^{-2} k^{-1} \times 10^{-4}$	$Vm^{-2} K^{-1} \times 10^5$	$m^2 C^{-1}$	$Pa^{-1/2} \times 10^{-5}$
	298	1.5	2.4	237	2.1	2.5	1.2	0.049	2.3
St.d	9	0.4	0.4	22	0.2	0.2	0.1	0.005	0.3

Table 14: Electrical characteristics of the wafers achieved following Navarro's process. These values were obtained by averaging the measurements of six different wafers coming from six different tape cast batches. Two different powder batches have been employed.

6.3 Conceptual Design Phase I: Study on the factors influencing the ceramic microstructure

Strength in ceramics is dependent on peak flaw size and therefore on the grain size and porosity of the microstructure [Richerson, 1992]. A small grain size and, generally, a high final density, contribute to high strength. The attainment of such a final microstructure in the ceramic is the result of many factors, which could be grouped in two main categories: the green ceramic characteristics and the sintering conditions [Rahaman, 1995], as described by the Cause-Effect diagram in Fig. 68.

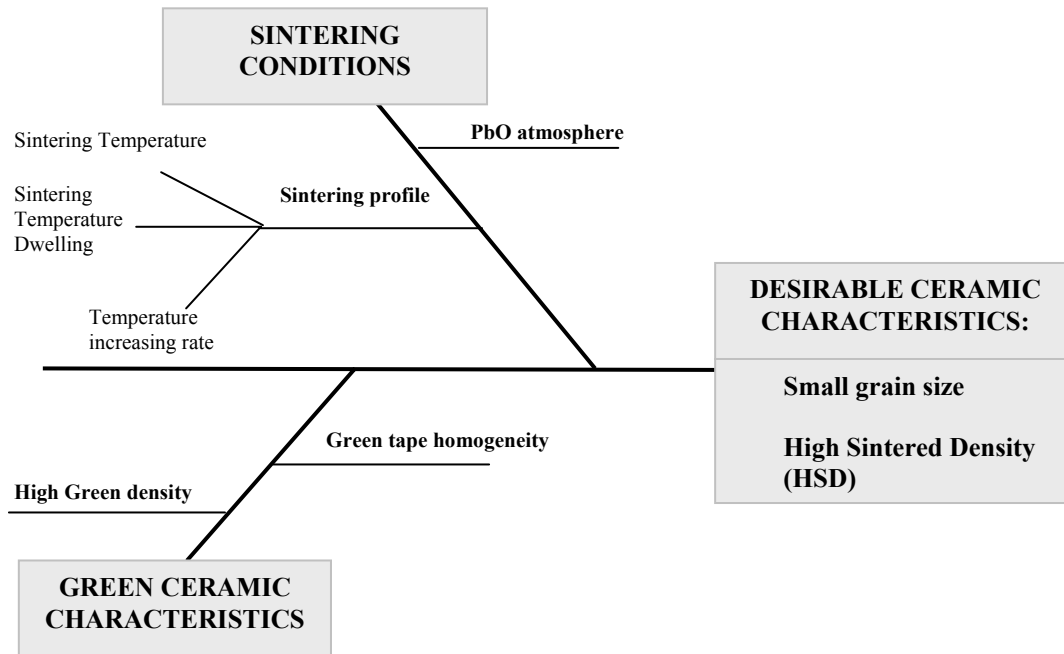


Fig. 68: Ishikawa (cause-effect) diagram for the characteristics of the sintered ceramic

In this work the influence of the sintering conditions, specifically the sintering temperature, the dwell of the sintering temperature and heating rate, and the green density influence on the sintered microstructure were investigated. The effects of the variation of the sintering atmosphere on the ceramic characteristics could not be evaluated due to technical limitations in measuring effectively the lead oxide atmosphere and evaporation rate in the crucible during sintering.

6.3.1 Study of the effects of the sintering temperature and dwell time on the ceramic characteristics

6.3.1.1 Method

Two experiments were conducted to separate and compare the effects of the sintering temperature and the dwell time. Fig. 69 represents the method used to investigate the two factors.

In the first experiment, six samples were sintered, decreasing the sintering temperature, starting from the temperature of original process.

In the second experiment, two samples were produced by reducing the dwell time for two sintering temperatures (1250 and 1270 °C).

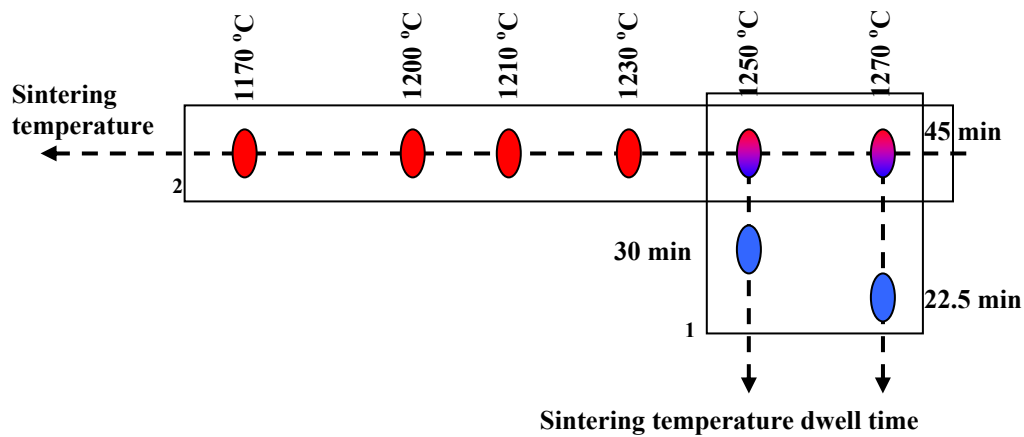


Fig. 69: Methodology for determining the effects of sintering temperature and dwell time. The rectangles represent the two experiments

The samples' density was measured. The cross section of each sample in its central area was pictured with the SEM. An evaluation of the average dimension of the grains was performed with the graphical method illustrated in the experimental method section.

6.3.1.1.1 Sintering Temperature Dwell

Four samples with green density 3.03 g.cm^{-3} were sintered varying both the sintering temperature and the sintering temperature dwell time, as reported in Table 15.

Sample	Green Density	Sintering Temperature	Sintering Temperature Dwell time
	[g.cm ⁻³]	[°C]	[min]
1	3.3	1270	45
2	3.3	1270	22.5
3	3.3	1250	45
4	3.3	1250	30

Table 15: Sintering conditions to study the effects of the sintering temperature and the sintering temperature dwell time

6.3.1.1.2 Sintering Temperature

The sintered density of wafers at decreasing temperature was evaluated with the Archimedes method. In each case the starting green density was 3.3 g.cm⁻³. As reported in Table 16, the dwell time was 45 minutes. The heating rate was 3°C/min. The temperatures were 1270, 1250, 1230, 1210, 1200 and 1170 °C.

Sample	Green Density	Sintering Temperature	Sintering Temperature Dwell time
	[g.cm ⁻³]	[°C]	[min]
1	3.3	1270	45
2	3.3	1250	45
3	3.3	1230	45
4	3.3	1210	45
5	3.3	1200	45
6	3.3	1170	45

Table 16: Sintering conditions to study the effects of the sintering temperature

6.3.1.2 Results

6.3.1.2.1 Influence of the sintering temperature dwell time

The data gathered from the microstructure analysis of the samples obtained varying the dwell time for two sintering temperatures are summarised in Table 17. Fig. 70 reports the SEM images of the microstructure of the samples taken in the central area of their cross sections. The table reports the sintered density, the calculated average grains dimension, the maximum and the minimum grains observed. All the grain sizes have been evaluated graphically with the methods explained before in the method paragraph 6.3.1.1.

Sample	CONDITIONS		RESULTS			
	Sinter. Temp.	Sintering time	Sinter. Density	Calc. Grain size	Max grain size	Min grain size
	[°C]	[g.cm ⁻³]	[g.cm ⁻³]	[µm]	[µm]	[µm]
1	1270	45	7.9	6.6	16.2	4.7
2	1270	22.5	7.2	8.9	31.4	6.8
3	1250	45	7.8	6.6	15.3	4.7
4	1250	30	7.2	7.3	18.4	5.3

Table 17: Characteristics of the samples sintered varying the dwell time for two sintering temperatures

For both the sintering temperature used, the calculated grain size (d) increased when the dwell was reduced. When the sintering temperature was 1270 °C and the dwell time was reduced to 22.5 min, the calculated average grain size moved from 6.6 to 8.9 µm, with an increase of about 40%. Both the maximum and the minimum grain size observed increased. Especially the maximum grain observed was the largest of the series being approximately 31.4 µm. The same trend was found for the samples sintered at 1250°C when the dwell time was reduced by 15 minutes. In this case the increases were more modest. The average grain size increased by approximately 10% (from 6.6 to 7.3 µm) and the maximum grain size observed was 18.4 µm, the second largest in the series.

By decreasing the sintering temperature from 1270 to 1250 °C, the sintered density remained almost constant for either dwell times.

For both sintering temperatures a reduction in their dwell time decreased their sintered density appreciatively. The reduction were from about 96.4% to about 87.6% of the theoretical density for 1270 °C and from about 96.1% to about 88.6% o the theoretical density for the samples sintered at 1250 °C.

There wasn't any substantial difference in the microstructure characteristics of the samples. All the samples were characterised by irregular grains with porosity trapped within the grain. The size of the porosity increases when the sintering dwell is shortened. This effect is visible in particular at the highest temperature by comparing sample 1 and 2 micrographs in Fig. 70.

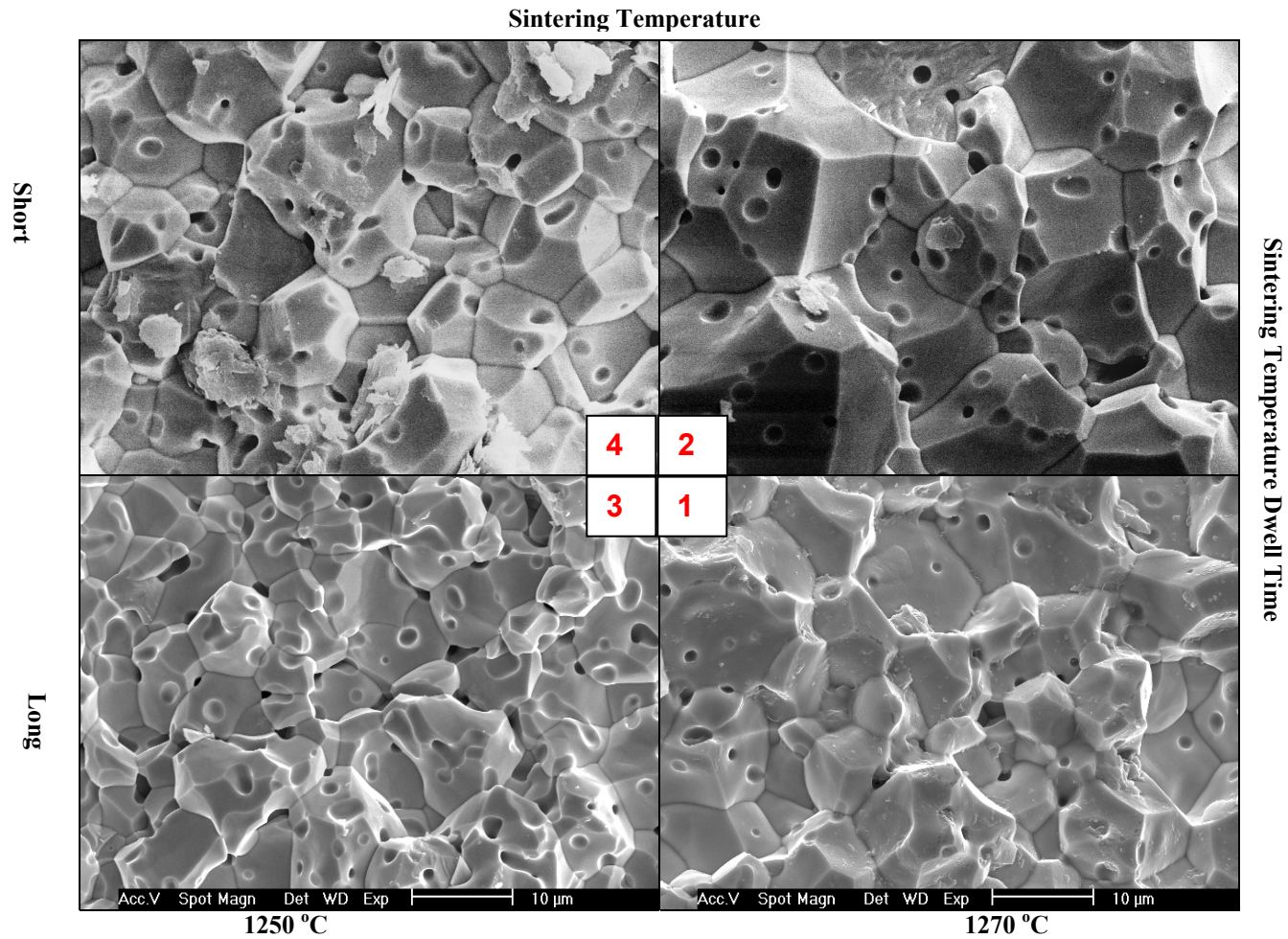


Fig. 70: Microstructure of central areas of samples cross sections, obtained at decreasing sintering temperature and dwell time

6.3.1.2.2 Influence of the sintering temperature

The densities and the data gathered from the microstructure analysis of the samples obtained varying the sintering temperature are summarised in Table 18. The table reports the sintered density, the calculated average grains size, the maximum and the minimum grain size observed. All the grain sizes have been evaluated graphically with the methods explained in the experimental method session (page 87).

Sample	CONDITIONS		RESULTS			
	Sinter. Temp.	Green Density	Sinter. Density	Calc. Grain size	Max grain size	Min grain size
	[°C]	[g.cm ⁻³]	[g.cm ⁻³]	[µm]	[µm]	[µm]
1	1270	3.3	7.7	6.6	16.2	4.7
2	1250	3.3	7.5	6.6	15.3	4.7
3	1230	3.3	7.4	4.4	10	4.1
4	1210	3.3	7.1	3.3	8.1	3.2
5	1200	3.3	6.9	2.8	6.4	2.3
6	1170	3.3	N/A	2.3	8.3	1.9

Table 18: Characteristics of the samples sintered at decreasing temperature. Micrographs can be found in Fig. 72.

Fig. 71 graphically summarises the trends of the sintered density and the calculated average grain dimension with the sintering temperature.

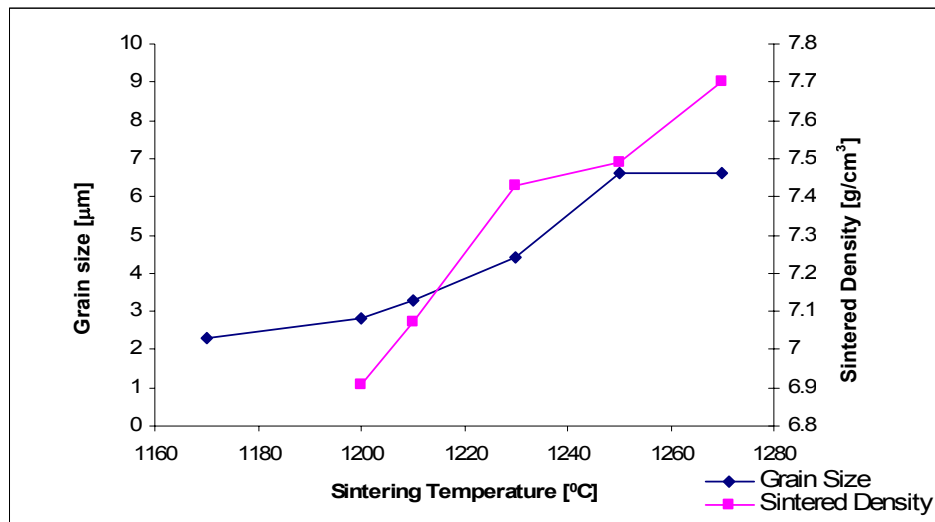


Fig. 71: Trend of the calculated grain size and of sintered density with temperature

As shown in Fig. 71, the calculated average grain size (d) value showed a gradual increase with temperature.

The calculated average grain size varied from 2.3 to 4.4 μm , in the samples sintered at temperatures between 1170°C and 1230°C. The value was augmented more steeply in the sample sintered at 1250°C, which reached 6.6 μm with just 20°C sintering temperature increase. A further 20°C step in the sintering temperature didn't produce any sensible difference in the calculated grain dimension as it remained 6.6 μm in the sample sintered at 1270°C.

As shown in Fig. 71, the sintered density of the sample sintered at 1170 °C was not obtained, as the wafer was too fragile to be handled. For the wafers sintered at 1200, 1210 and 1230 °C the sintered density increased progressively.

The sintered density varied from 6.9 $\text{g}\cdot\text{cm}^{-3}$, about 84.6% of the theoretical density, to 7.4 $\text{g}\cdot\text{cm}^{-3}$, about 90.9% of the theoretical density. For a further 20°C temperature raise, with sintering temperature of 1250 °C, the rate of increase in density decreased, reaching 7.5 $\text{g}\cdot\text{cm}^{-3}$, about 91.7% of the theoretical density. A density of 7.7 $\text{g}\cdot\text{cm}^{-3}$, about 94.2 % of the theoretical density, was achieved at 1270 °C.

Fig. 72 reports the SEM images taken from the central area of the samples cross sections. Below, examples of the individual microstructures are described.

In Fig. 72 n° 1 the microstructure obtained at 1270°C is shown. The grain size oscillated from a maximum of approximately 4.7 μm (line a) to a minimum of approximately 16.2 μm (line b). The shape of the grains was predominantly irregular. Most grains had inclusions of pores as shown in circle 1. Some pores were positioned at the triple point. As indicate by the arrow visible cracks were present following the grain boundary. The fracture path followed mainly the grain boundary. As it is visible in circle 2, some grains broke intragranularly.

Fig. 72 n° 2 shows an example of microstructure obtained at 1250 °C. The microstructure was very similar to that of 1270 °C. The maximum grain size was approximately 4.7 μm (line a) and the minimum was approximately 15.3 μm (line b). The shape of the grains was mostly irregular. Some pores were positioned at the triple point. But almost all the grains included pores, as evidenced by circle 1. The amount of porosity appeared higher than in the sample sintered at 1270 °C. In this case, no cracks were visible.

Fig. 72 n° 3 is relative to a microstructure obtained at 1230°C. The image shows grains which vary between approximately 4.1 μm (line a) and approximately 10 μm (line b). In this microstructure, the porosity was positioned both at the triple point and within the grain structure, as highlighted by circle 1. The pores reached a maximum dimension of approximately 4.8 μm (line c). The inclusion of the pores in the grains was also visible as indicated by circle 2.

The microstructure of a sample sintered at 1210°C is shown in Fig. 72 n° 4. It was characterised by an abnormal microstructure. The smaller grains were approximately 3.2 μm as highlighted by line a. Line b indicates that the diameter

of the biggest grain reached approximately 8.1 μm . The larger grains were mostly very irregularly shaped, with curved surfaces and pores trapped inside the grains (circle 1). The fracture path followed mostly the grain boundaries. However, as in the case of circle 2, it fractured some grains internally. As shown by circle 3, the abundant porosity presented sometimes a very irregular shape.

Fig. 72 n° 5 shows the microstructure of the samples obtained at 1200 °C. Areas of high density were alternated with ones where the porosity was very abundant, as shown in circles 1 and 2 respectively. The size of a typical grain was approximately 4 μm (line a) in diameter. The maximum grain observed, indicated by line b, was approximately 6.4 μm in diameter. The minimum grain observed was approximately 2.3 μm in diameter. Some grains and some pores were irregularly shaped as the one in circle 3. The pores were abundant, generally positioned at the grain boundary. Some pores were large as the one indicated with line d which had a diameter of approximately 6 μm .

An example of the microstructure obtained at 1170 °C is shown in Fig. 72 n° 6. It was rather inhomogeneous as clusters of grains more densely packed (circle 1) were alternated with groups of grains containing pores inclusions (circle 2). Small grains of approximately 1.9 μm in diameter alternated with larger ones of approximately 8.3 μm in diameter, as highlighted. The grain shape was also irregular as some grains deviate from a polyedric shape (circle 3). The porosity was abundant and it was positioned almost generally at the triple points.

Generally, raising the sintering temperature increased both the density of the samples and the grain size. The porosity was mainly positioned at the triple point in the sample sintered at the lowest temperature (1170°C). It moved gradually to positions inside the grains as the sintering temperature increased to 1250 and 1270°C. Although the sample sintered at the highest temperature (1270 °C) was denser, the structure appeared weakened as cracks were evident (See Fig. 72, n° 1).

The shape of the grains was more regular at the lowest temperatures. It gradually turned into a more asymmetrical shape with pores trapped on the surfaces as the temperature was increased to 1230 °C.

Sample	Central area microstructure
1 1270 °C	
1250 °C	
1230 °C	

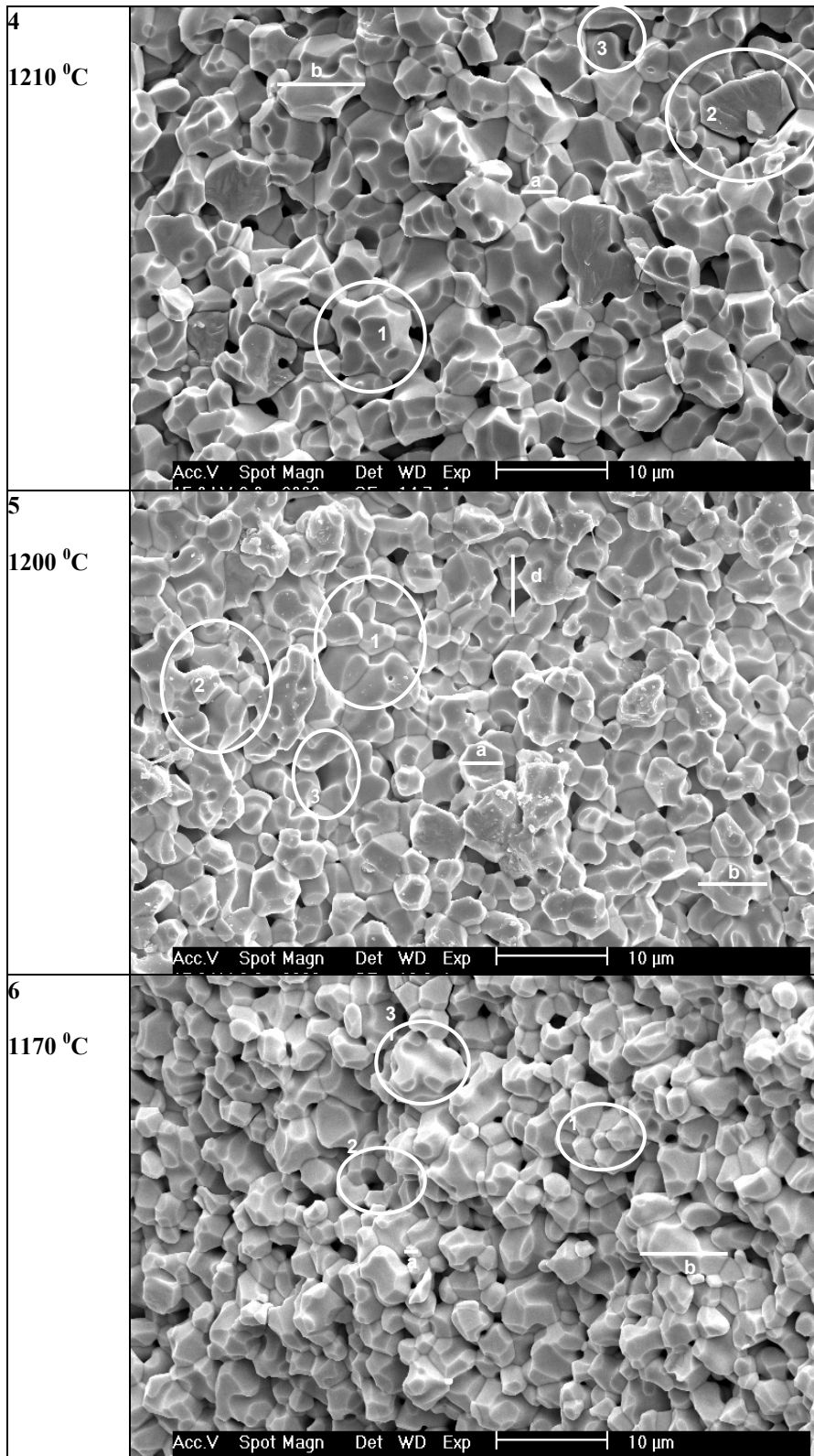


Fig. 72: Microstructure of central areas of samples obtained at decreasing sintering temperature. In the pictures the distinctive characteristics are highlighted with circles and lines

6.3.2 Study of the effects of the green density and the sintering temperature on the ceramic characteristics

In the following sections, the study of green density influence on the sintered microstructure is reported. The increase of green density was obtained using the warm pressing technique, as detailed in the following sections.

6.3.2.1 *Characterisation of the green tape as resulted from the original laboratory process*

The green density was determined as described in the experimental section (page 86). The average green density was 3.2 g.cm^{-3} (with a standard deviation $\sigma = 0.193$), corresponding to approximately 38.7% of the theoretical density. The green density results showed consistency as the difference between the highest and the lowest value was less than 0.4 g.cm^{-3} , corresponding to approximately 5.3% of the theoretical density (Table 19).

Highest GD	3.4 g.cm^{-3}
Lowest GD	2.9 g.cm^{-3}
Average GD	3.2 g.cm^{-3}
Standard deviation	0.193
Theoretical density	8.17 g.cm^{-3}
% of Average green density on theoretical	38.7%

Table 19: Density of green tapes

The microstructures of a typical green tape surfaces are shown in Fig. 73(1) and (2): the tapes were highly porous showing pores up to approximately 5 microns in diameter. The side of the tape in contact with the carrier (Fig. 73(1)) shows a higher content of organic phase and its macroscopic naked-eye aspect is shinier and smoother.

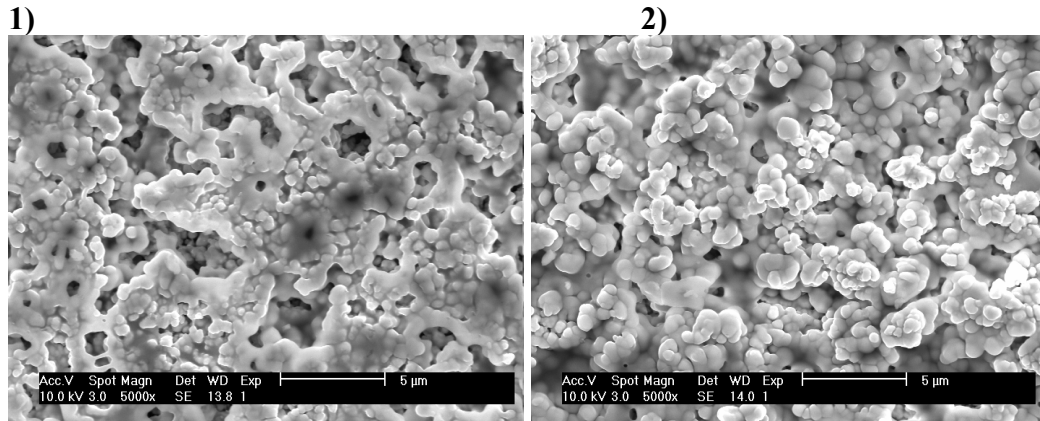


Fig. 73: SEM pictures of 1) carrier side and 2) upper side of the cast tape.

In Fig. 75, SEM images of the cross sections of a green tape microstructure are shown. The tape appeared inhomogeneous across the entire thickness, with areas where the porosity is larger in size or/and greater in quantity alternated with apparently more dense zones. Some areas showed an apparently higher concentration of organic phase. The ceramic particles were agglomerated in dense, discrete clusters covered with the organic phase. Overall the tape structure appears deriving from the packing of the clusters, rather than the packing of the single particles.

Fig. 74 shows the powder particles obtained after a complete milling cycle. The primary particles looked equiaxed and not characterised by hard agglomerates. Their diameter was smaller than 1 µm.

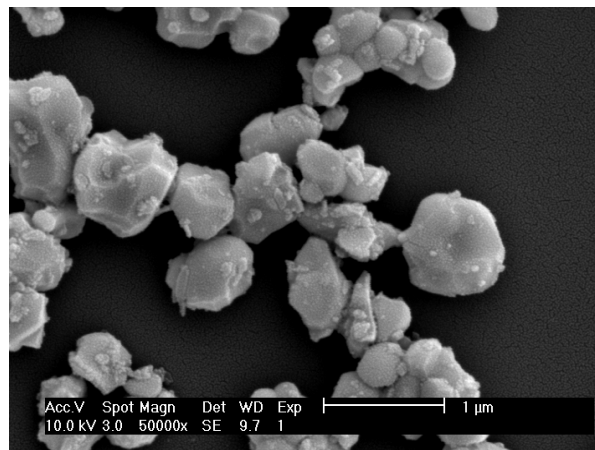


Fig. 74: SEM picture of the ceramic powder after a complete milling cycle. The particles look equiaxed with diameter smaller than 1 µm.

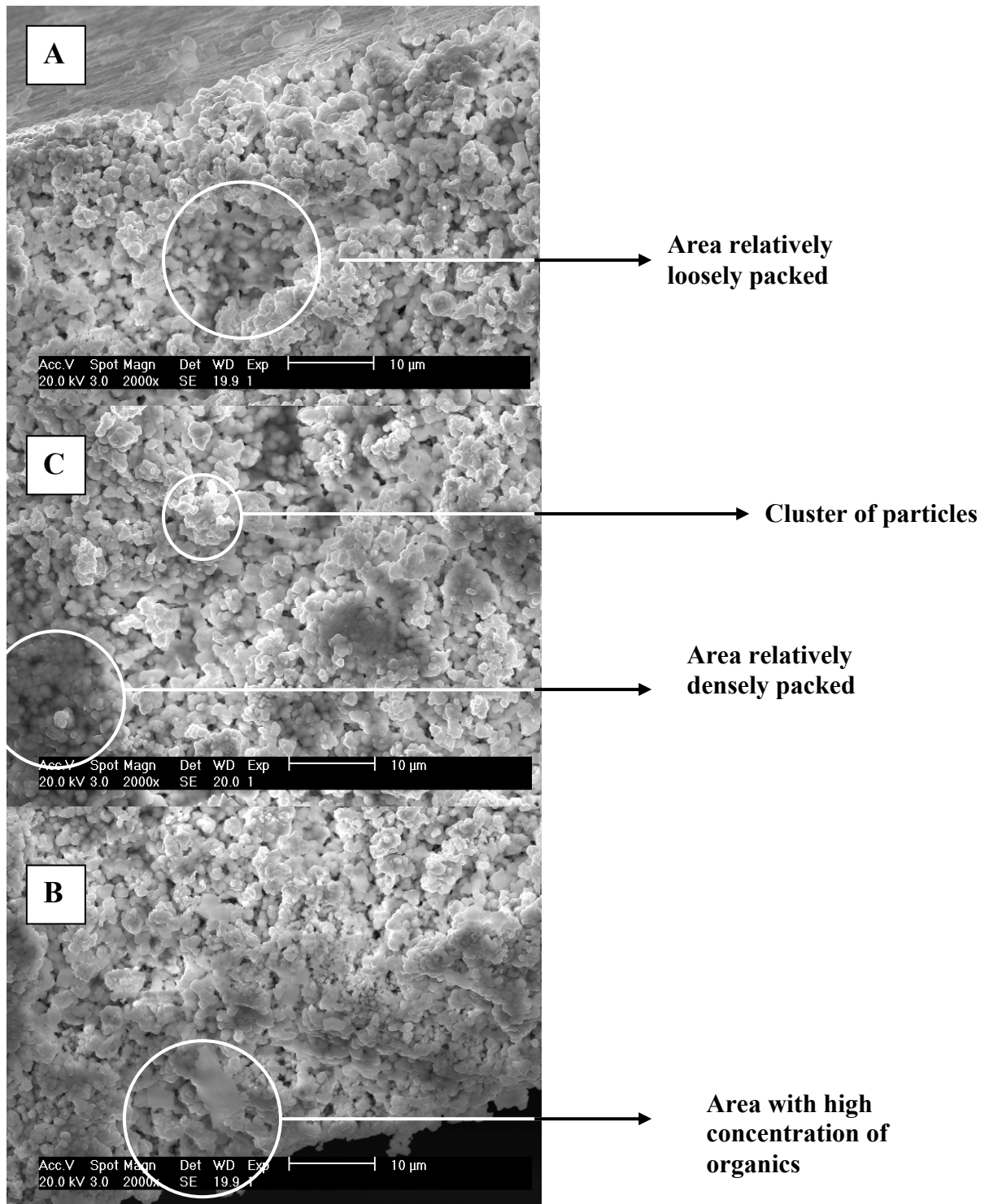


Fig. 75: SEM picture with details of the cross section of a green tape along its fracture surface: A) close to the carrier surface, B) close to the free surface, C) in a central area

6.3.2.2 Method

Tapes with different green densities (one per green density) were warm pressed in order to achieve a gradient of green density as shown in Table 20.

The samples were divided in two halves and were sintered for 45 minutes at 1210°C and 1170°C respectively. The heating rate was 3°C/min. Their microstructure and their sintered characteristics were evaluated.

Fig. 76 represents the method used to investigate two factors in combination: the sintering temperature and the green density.

	Sintering temperature	Green density	Green density *
	[°C]	[g.cm ⁻³]	[%]
A1	1170	3.0	37.1
B1	1170	4.8	58.6
C1	1170	5.3	64.7
A2	1210	3.0	37.1
B2	1210	4.8	58.6
C2	1210	5.3	64.7

* Percentage of the Theoretical Density (8.17 g.cm⁻³)

Table 20: Experimental conditions to study the effect of green density

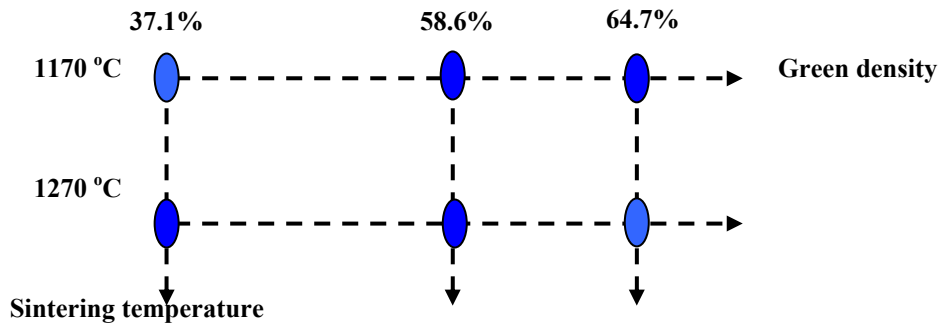


Fig. 76: Methodology for determining the effects of sintering temperature and Green density.

6.3.2.2.1 Optimisation of the pressing conditions

The warm pressing technique was identified as a suitable option in order to increase the green tape's density by the problem solving technique.

Consequently, a study aiming to identify the best pressing conditions was necessary. The study is reported below.

The warm pressing was performed with a press by G.E.Moore (UK). The equipment allowed to apply different pressures. The platens could be pre-heated and kept at a constant temperature during pressing.

In Fig. 77, the configuration of the samples between the platens is shown in the case of a single sample. Each sample was positioned in the press, separated from the others and from the platens by polymer sheets.

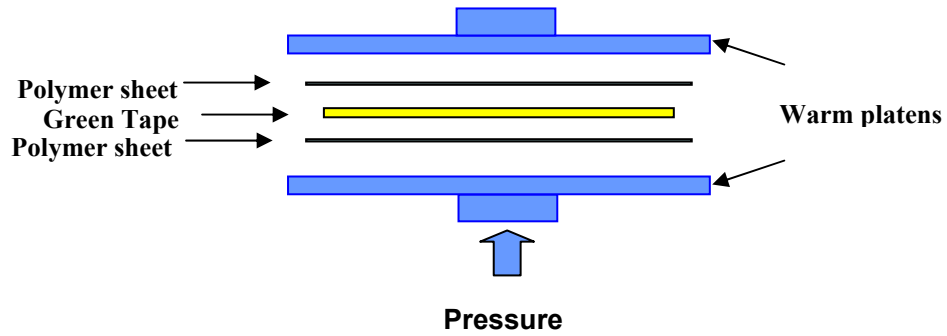


Fig. 77: Pressing configuration of green samples

Below, the study of the optimisation of the pressing conditions is reported. In particular, several factors were assessed:

1. The repeatability of the results
2. The influence of the pressure applied to the individual samples
3. The influence of the temperature during the pressing
4. The influence of the pressing dwell time
5. The best configuration for the pressing of multiple samples

After the pressing, the green density of each sample was determined as explained in the experimental section.

1. For the assessment of the repeatability of results, green tapes samples with green density 3.0 g.cm^{-3} were singularly pressed at 20°C and 65 MPa for 15 minutes and their green densities were compared.
2. To identify the influence of the pressure applied to individual samples, tapes with a starting green density of 3.0 g.cm^{-3} were pressed with pressures between 65 and 160 MPa. The pressures were applied for 15 minutes while the temperature was kept constant at 20°C .
3. The importance of the temperature during pressing was assessed by pressing samples with green density of 3.0 g.cm^{-3} at increasing temperature. The temperature was varied between 20 to 50°C , keeping applied a pressure of 65 MPa for 15 minutes.
4. The relevance of the pressing time increase to the green density was determined by extending the pressing time from 10 to 25 minutes, for samples with green density equal to 3.0 g.cm^{-3} pressed at 65 MPa and 50°C .

5. In order to determine how to increase the area possible to be pressed at once, a study was conducted on the best configuration of the samples under the platens. Side by side and stack configuration were obtained as illustrated in Fig. 78. Stacked and side-by-side configurations efficiencies were compared by evaluating the green density of samples.

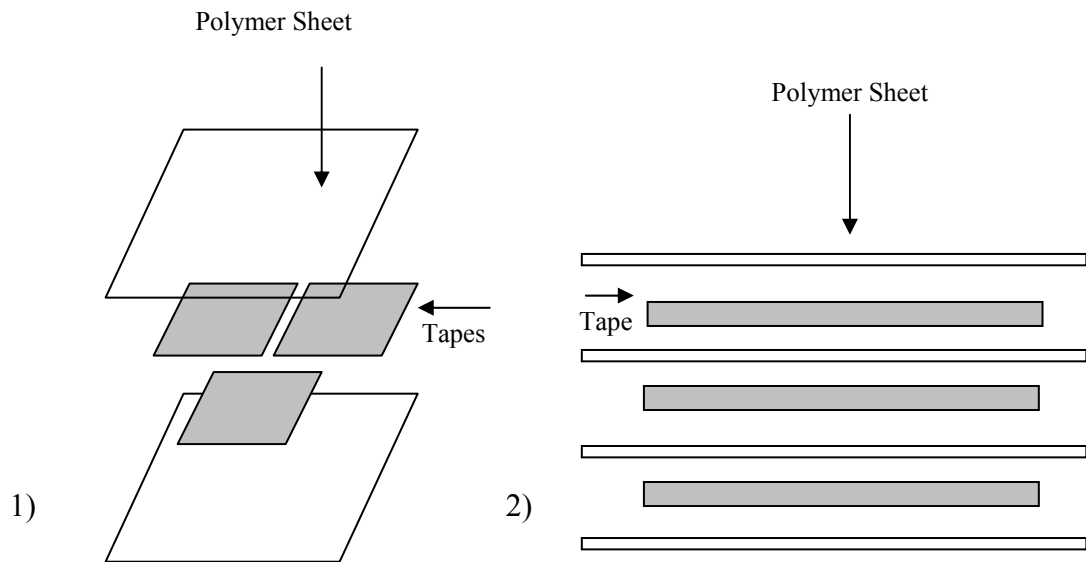


Fig. 78: Samples configuration under the press. 1) Side by side; 2) stack

6.3.2.3 Results: effects of the green density on the ceramic microstructure

Samples with different green densities, 3.0, 4.8, 5.3 g.cm⁻³ were chosen among these obtained with the warm pressing studies. Each sample was cut in two parts. A part of each sample was sintered at 1210 °C and the other at 1170 °C.

The microstructure of the green tapes and sintered ceramics was examined by SEM. The average grain size and the standard deviation of the grain sizes were calculated from measurements of 20 grains for each microstructure. Table 21 reports the data of sintered densities, and grain size for three different green density samples sintered at 1170 and 1210 °C. Fig. 79 shows pictures of the ceramic microstructures taken in the central area of their cross section.

	Sintering Temp.	Green Density	Green Density % of Theor. Density	Sinter. Density	Sinter. Density % of Theor. Density	Grain size aver.	Stand. Dev.	Grain size range
		[g.cm ⁻³]	[%]	[g.cm ⁻³]	[%]	[μm]		[μm]
A1	1170	3.0	37.1	6.8	83.7	3.9	2.12	1.6 – 8.4
B1	1170	4.8	58.6	7.6	93.3	7.3	2.64	3.1 – 12.2
C1	1170	5.3	64.7	7.9	97.3	7.0	2.16	3.4 – 10.3
A2	1210	3.0	37.1	6.9	84.6	5.5	1.75	3.1 – 9.1
B2	1210	4.8	58.6	7.6	93.6	9.1	2.67	2.8 – 12.2
C2	1210	5.3	64.7	7.8	95.7	8.3	2.58	4.1 – 13.1

Table 21: Densities and grain sizes of green material and sintered tapes

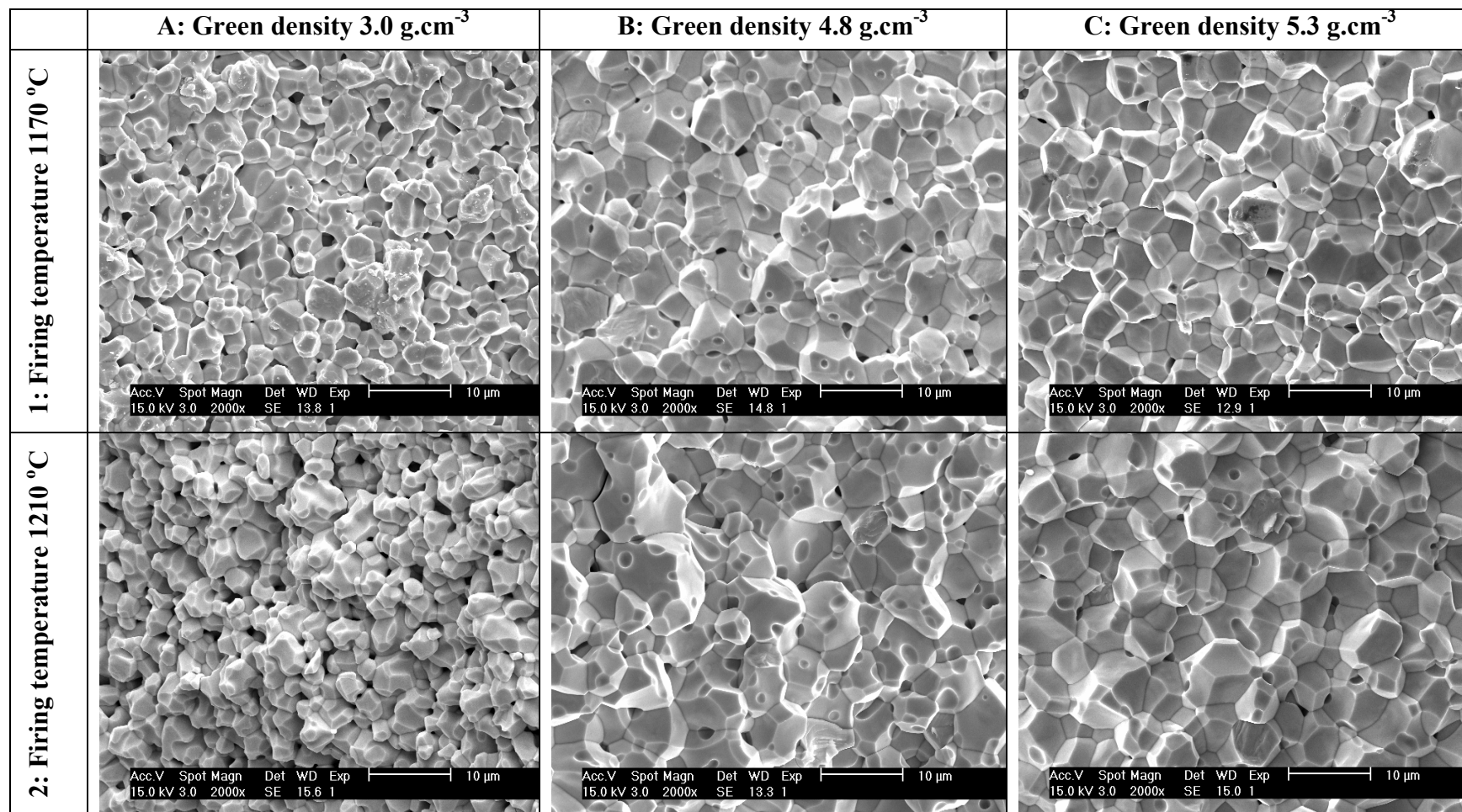


Fig. 79: Fracture surfaces of sintered microstructures

Fig. 80 illustrates the development of the sintered density as a function of green density. Fig. 81 reports how the average grain size varied with the green density.

There was a strong correlation between high green density and high sintered density. However, the 40 °C variation in sintering temperature had little effect on density. The average grain size appeared to be influenced by both the variation in the firing temperature and by the increase in green density.

At 1210 °C a 27.6% increase in green density, from approximately 37% (A1) to 65%(C1), gave an improvement in the sintered density of 11%, while at 1170 °C it gave an increase of 13.6%.

General trends of the development of the ceramic microstructure whilst varying the green density (A), (B) and (C) could be observed for both sintering profiles (1) and (2), as described below:

- Green density of 3.0 g.cm⁻³: Tapes of 37% (A) green density produced a fired density of approximately 84%. The porosity was still abundant and positioned in the triple point. The grains had average dimensions of 3.9 and 5.5 µm respectively, with non uniform shapes. Dense areas, alternated with more porous ones.

- Green density of 4.8 g.cm⁻³: Tapes of 59% (B) green density produced a sintered density of about 93%. The microstructure showed average grain size with averages of 7.3 and 9.1 µm respectively, higher than in the case of the tapes with lower green density. These microstructures revealed also an apparent lower amount of porosity. The microstructure was compatible with an over-sintered state: the porosity was closed and positioned both at the triple points and in the cores of the grains. The grains exhibited strong coarsening.

- Green density of 5.3 g.cm⁻³: The samples obtained from the 65% (C) green density tape showed high sintered density, 95-97% of the theoretical and an improved microstructure. The grain size averages were 7.0 and 8.3 µm. There was evidence of little residual porosity, located mainly at the triple points.

In contrast, the increase of sintering temperature from 1170°C to 1210°C, for a constant green density, produced a negligible change in the final sintered density of 1%, for the 37% green density. For 65% green density the sintered density diminished by 1.6%.

Firstly, varying the sintering profile from 1210°C to 1170°C, the grain size was reduced. Secondly, the average grain size showed a smaller decrease for the samples sintered from the highest green density thick film. Thirdly, in the samples sintered at the lowest temperature, the porosity appeared smaller in size.

It is evident for the tapes at the lowest and intermediate green density that, by starting from a low density ceramic the grain coarsening effect was dominant in comparison to the increasing of the ceramic density.

While for the lowest green density tapes the sintering temperature was insufficient for complete densification, the intermediate density achieved a state of apparent

over-sintering. However, the samples with the highest green density showed a different correlation between densification and grain growth, exhibiting smaller grains and higher density.

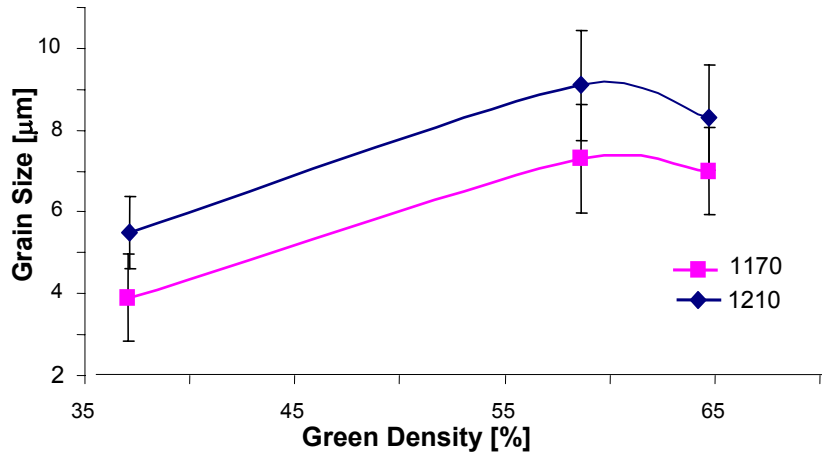


Fig. 80: Graph of the variation of the calculated average grain size against the variation of the green density

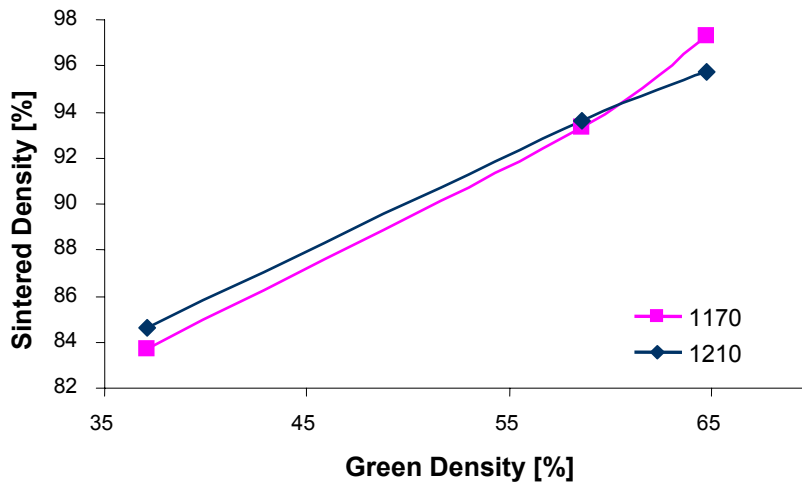


Fig. 81: Graph of the variation of the sintered density, expressed as a percentage of the theoretical, against the variation of the green density

6.3.2.3.1 Optimisation of the pressing conditions: scoping study

The data reported in the following section refer to the optimisation of the warm pressing conditions for increasing the green density of the samples. The experiments described here intended to illustrate which settings and samples configuration under the press can give the highest green density, at high level. The

variability of this technique has been studied by means of the Statistical Process Control technique and the relative results are reported in section 6.4. The error in the green density measurements was 0.2 g.cm^{-3} , as reported in section 4.2.1, in the Experimental section.

Firstly, the repeatability of the method was tested, by pressing 4 samples. Secondly, the effects on the green density of the variation of the applied pressure, the pressing temperature and the pressing time were investigated. One sample was pressed for each condition. The results are summarised in Table 22. The green density values obtained are also expressed as a percentage of the theoretical density. The percent increment on the starting green density is reported. Thirdly, in Table 23, the results of the study of the best samples configuration for pressing multiple samples are reported.

Sample	CONDITIONS			RESULTS		
	Press. Temp.	Pressure	Pressing time	Green Density	Increase on the starting GD	Percent. of the TD
Nº	[°C]	[MPa]	[min]	[g.cm ⁻³]	[%]	[%]
1	-	-	-	3.0	0.0	37.1
1/a	20	65	15	3.5	15.2	42.7
1/b	20	65	15	3.5	14.8	42.6
1/c	20	65	15	3.5	15.5	42.8
1/d	20	65	15	3.5	15.5	42.8
2/a	20	65	15	3.5	15.2	42.7
2/b	20	90	15	4.1	36.3	50.5
2/c	20	115	15	4.2	39.6	51.8
2/d	20	160	15	4.5	47.8	54.8
3/a	20	65	15	3.5	15.2	42.7
3/b	40	65	15	3.8	25.4	46.5
3/c	45	65	15	4.3	40.6	52.1
3/d	50	65	15	4.7	54.8	57.4
4/a	50	65	10	4.4	46.2	54.2
4/b	50	65	15	4.7	54.8	57.4
4/c	50	65	18	5.1	70.0	63.0
4/d	50	65	20	5.3	75.0	64.9
4/e	50	65	25	5.4	77.0	65.6

Table 22: Results of the pressing conditions study

6.3.2.3.1.1 Repeatability of the green density with pressing

Four green tapes samples (series 1 in Table 22) with green density 3.03 g.cm^{-3} were individually pressed at 20°C and 65 MPa for 15 minutes. As a result, their green density was increased to 3.5 g.cm^{-3} . This corresponds to an increase of about 15 % of the original green density. The deviation standard among the four samples was 0.0096. The maximum green density variation among the samples was 0.02 g.cm^{-3} , which was lower than the error.

6.3.2.3.1.2 Effects of the applied pressure on the green density

In this experiment, pressures of 65, 90, 115 and 160 MPa were applied for 15 minutes to individual samples (series 2 in Table 22) with a starting green density of 3.0 g.cm^{-3} . The temperature was kept constant at 20°C . As shown in Fig. 82, the largest change in green density occurs between the samples pressed at 65 and 90 MPa. When the pressure was raised by 25 MPa from 65 to 90 MPa, the green density increased by 0.64 g.cm^{-3} , from 3.5 to 4.1 g.cm^{-3} . A further 25 MPa increase raised the green density by just 0.1 g.cm^{-3} . When a pressure of 160 MPa was used, i.e. an additional 45 MPa were applied, the green density was incremented by only 0.2 g.cm^{-3} . This gave the highest green density of the series, 4.5 g.cm^{-3} , corresponding to 55% of the theoretical density.

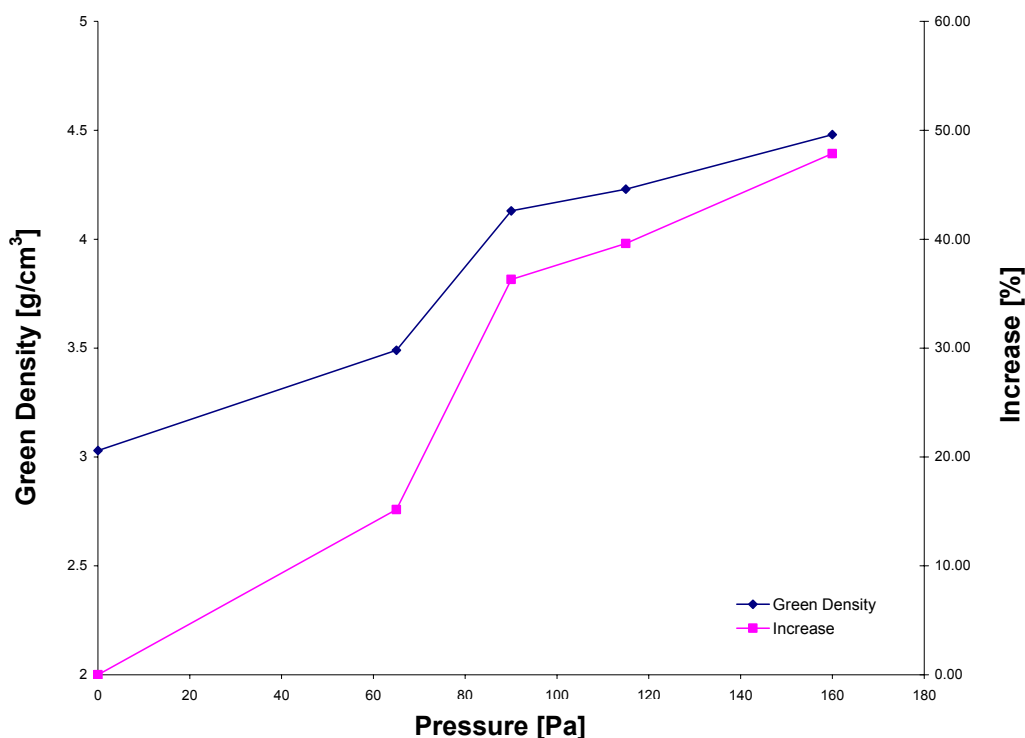


Fig. 82: Increasing of the green density by warm pressing with rising pressures at room temperature

6.3.2.3.1.3 Effects of the pressing temperature on the green density

The Differential Scanning Calorimetry (DSC) analysis of the green tape found that the T_g (glass transition temperature) of the polymeric system was found 39°C.

Samples (series 3, Table 22) were pressed at temperatures between 20 and 50 °C. A pressure 65 MPa, was applied for 15 minutes. When the temperature was raised from 20 to 40°C, the green density reached 3.8 g.cm⁻³, with a 0.3 g.cm⁻³ step. With 6 °C increase above the T_g (45°C), the green density increased by 0.5 g.cm⁻³, reaching 4.3 g.cm⁻³. With further 5 °C increment, i.e. with a 50°C temperature, the green density reached 4.7 g.cm⁻³, showing an almost linear trend visible in the graph in Fig. 83. The maximum green density obtained in this series was 4.7 g.cm⁻³, 57.4% of the theoretical density.

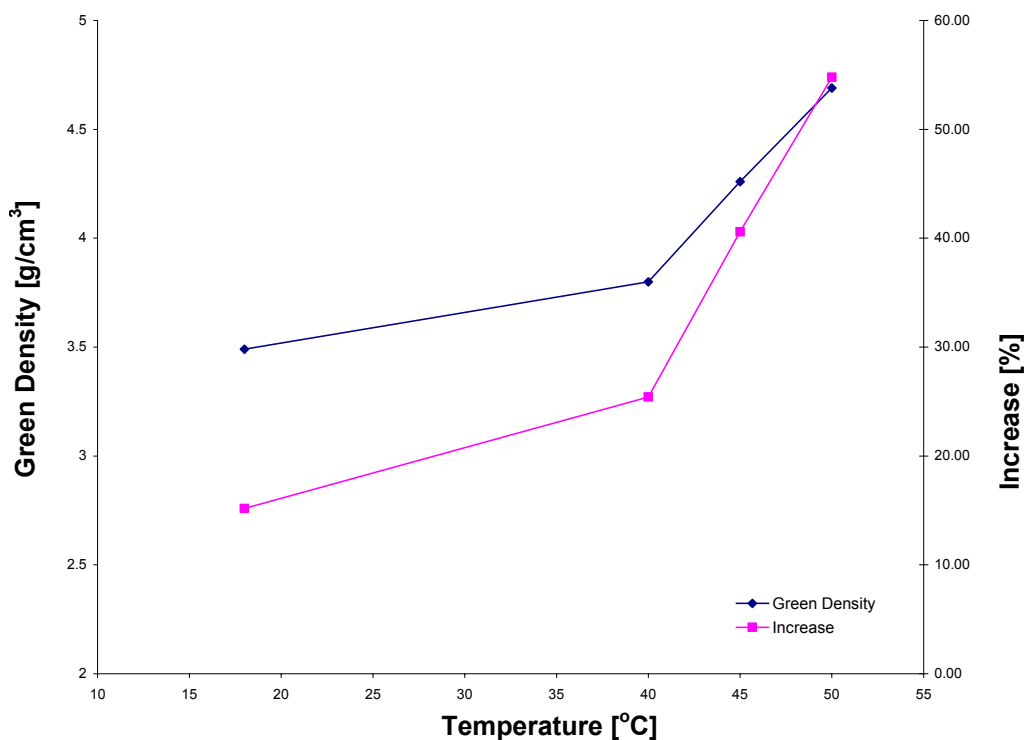


Fig. 83: Increasing of the green density by warm pressing with 65 MPa pressure at rising temperature

6.3.2.3.1.4 Effects of the pressing time on the green density

Fig. 84 illustrates the trend of the green density for the series 4 samples in Table 22. The green density figure increased in the first 20 minutes from 4.4, to 5.3 g.cm^{-3} . There was an increment of 0.1 g.cm^{-3} , from 5.3 to 5.4 g.cm^{-3} between the samples pressed for 20 and 25 minutes. The highest green density value of this series, 5.4 g.cm^{-3} , corresponded to approximately 65.6% of the theoretical density.

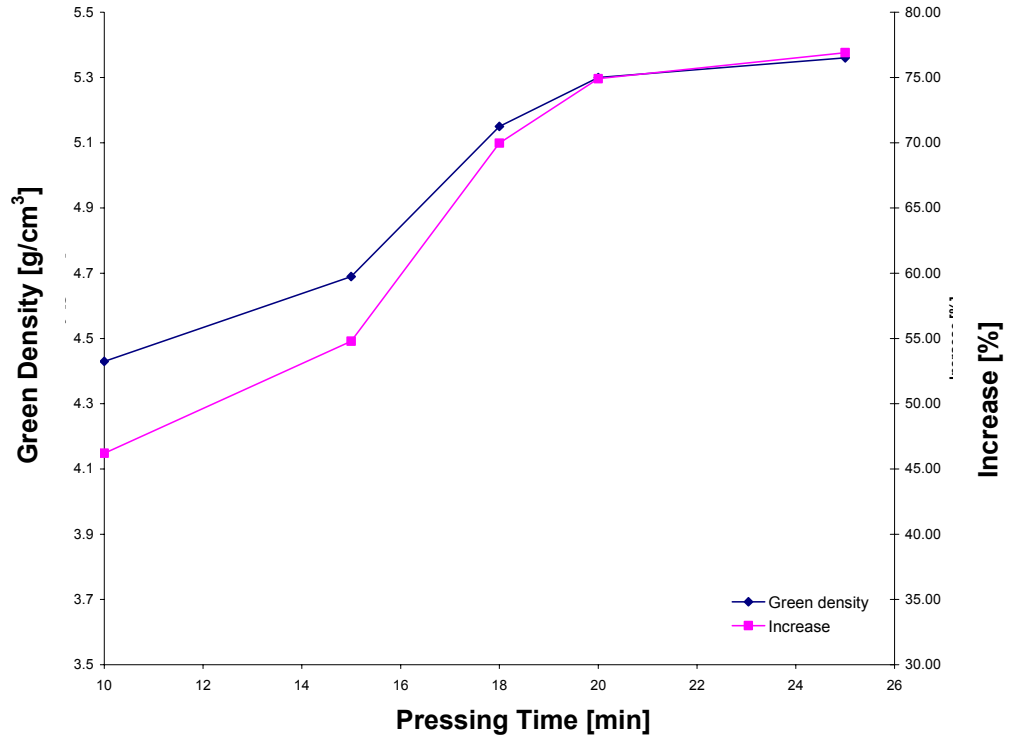


Fig. 84: Increasing of the green density with increasing pressing time at 65 MPa and 50°C

6.3.2.3.1.5 Effects of the configuration of the samples under the platens on green density

In order to increase the area possible to be pressed at once, a study was conducted on the effects of the samples configuration under the platens on the green density. Samples were positioned under the platens in a ‘side by side’ (series 5, Table 23) and in a ‘stack’ (series 6, Table 23) configuration, as illustrated in Fig. 78. The table reports the pressing conditions, the samples characteristics and the pressed green density which was also expressed as a percentage of the theoretical density.

Config.	Sam.	CONDITIONS				RESULTS		
		Pressure	Average Pressure on Sam.	Sample Area	Sam. Thick.	Press. green density	Green density Increa.	Perc. theor. density
	N°	[MPa]-	[MPa]	[cm ²]	[μm]	[g.cm ⁻³]	[%]	[%]
Not pres.	1	-	-	-	-	3.0	0.0	37
Side by side	5/a	220	73	13.7	281	4.4	44.5	54
	5/b	220	73	13.7	291	4.9	60.4	60
	5/c	220	73	13.7	294	5.1	67.0	62
Stack	6/a	73	73	13.7	264	4.7	56.1	58
	6/b	73	73	13.7	275	4.7	56.1	58
	6/c	73	73	13.7	246	4.8	58.4	59

Table 23: Green density of samples pressed for 15 minutes at 20 °C in different configurations

With the side by side configuration, the green density was increased up to an average of 4.8 g.cm⁻³, approximately 58% of the theoretical density. Although the samples were pressed simultaneously, the green density obtained varied from a minimum of 4.4 g.cm⁻³, approximately 54 % of the theoretical density, to a peak of 5.1 g.cm⁻³, approximately 62%, of the theoretical density.

The stack configuration allowed a similar average green density to be obtained, 4.7 g.cm⁻³. In this case, the green density across the three samples was more consistent, as it oscillated from a minimum of 4.7 g.cm⁻³, to a maximum of 4.8 g.cm⁻³, with a maximum variation of the theoretical density of approximately 1%.

3.6.2 Microscopic appearance of the pressed tape

Fig. 85(1) shows a sample with a green density of 3.0 g.cm^{-3} .

Fig. 85(2) illustrates the structure of a green sample pressed at 65MPa and 50°C for 20 min, with resulting density of 5.1 g.cm^{-3} . The porosity has been noticeably reduced in size and amount. The quantity of polymer in the two cases is the same, but its volume fraction is higher in Fig. 85(2) as the air amount has been reduced.

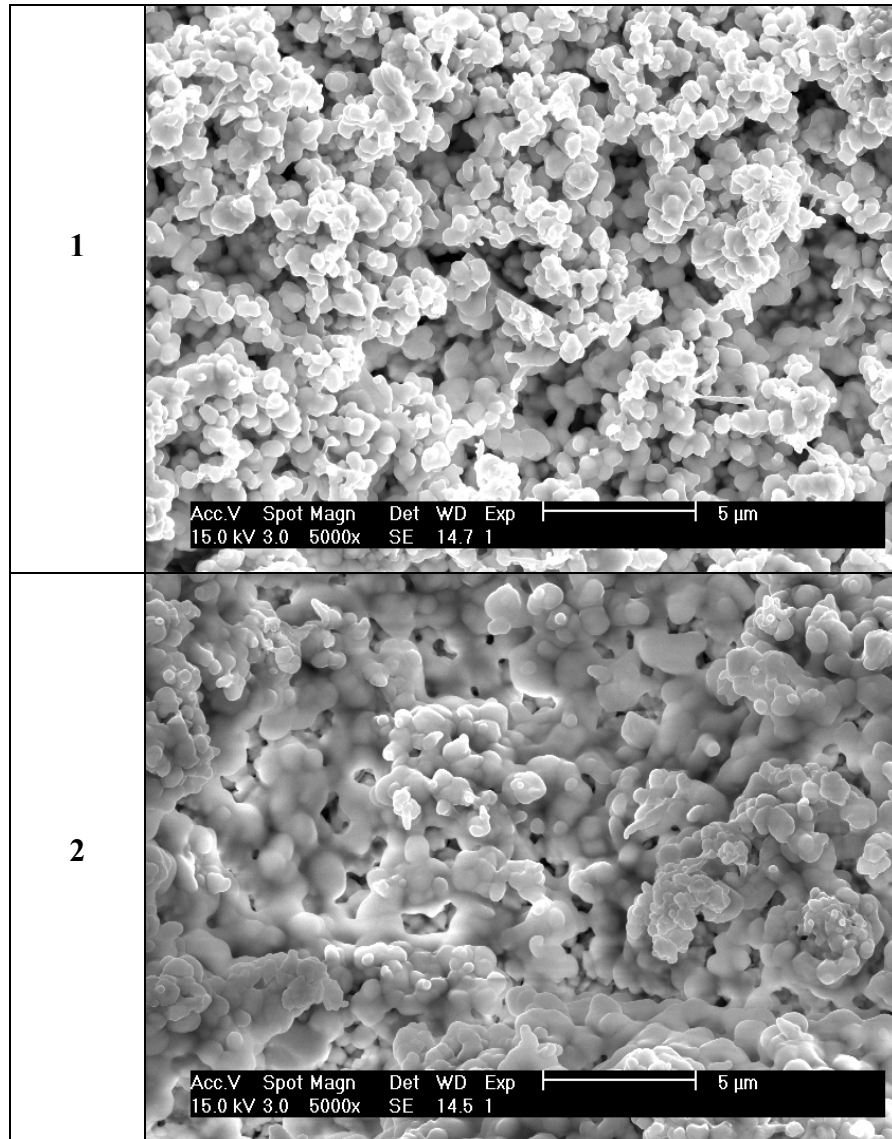


Fig. 85: 1) Fracture surface of not pressed tape cast thick film with green density of 3.0 g.cm^{-3} ; 2) fracture surface of warm pressed tape cast thick film with green density of 5.1 g.cm^{-3}

6.3.3 Study of the effects of the sintering heating rate on the ceramic characteristics

6.3.3.1 Method

Portions of a tape with green density of 5.2 g.cm^{-3} , warm pressed at 50°C and a pressure of 65 MPa, for 20 minutes, were sintered at 1170°C for 45 minutes. The heating rates were from $3^\circ/\text{min}$, to $6^\circ/\text{min}$ and $10^\circ/\text{min}$. Their microstructure and their sintered characteristics were evaluated.

6.3.3.2 Results: Effects of the heating rate on the ceramic microstructure

The data gathered from the microstructure analysis of the samples sintered with different heating rate are summarised in Table 24. The table includes an evaluation of the average dimension of the grains performed by averaging the measurements of 20 grains with the graphical methods illustrated in the Experimental Method section.

Sam.	CONDITIONS		RESULTS				
	Temp	Heating rate	Sintered density	Average grain size (method 2)	Standard deviation (method 2)	Max grain size (method 2)	Min grain size (method 2)
	[$^\circ\text{C}$]	[$^\circ\text{C}/\text{min}$]	[g.cm^{-3}]	[μm]		[μm]	[μm]
1	1170	3	8.0	6.1	0.2	8.6	2.5
2	1170	6	8.0	5.0	0.2	10.0	2.5
3	1170	10	8.0	4.8	0.2	7.5	2.0

Table 24: Characteristics of the samples sintered at increasing heating rate. Micrographs can be found in Fig. 86 .

The average grain size figures were decreasing with the increasing of the heating rate. The standard deviation values show that the grain size varied more in the microstructure obtained with the 6°C heating rate profile.

The samples' sintered density didn't appreciatively vary. And remained in the range of 8.0 g.cm^{-3} .

The cross section of each sample, imaged with the SEM, is reported in Fig. 86. In all three samples, the microstructure was similar: in the majority of the cases, the grain structure was apparently dense with the little residual porosity positioned at the triple points. In particular, the microstructures of samples sintered at 3 and 6°C appeared similar while the grain size in the sample obtained at 10°C appeared slightly smaller.

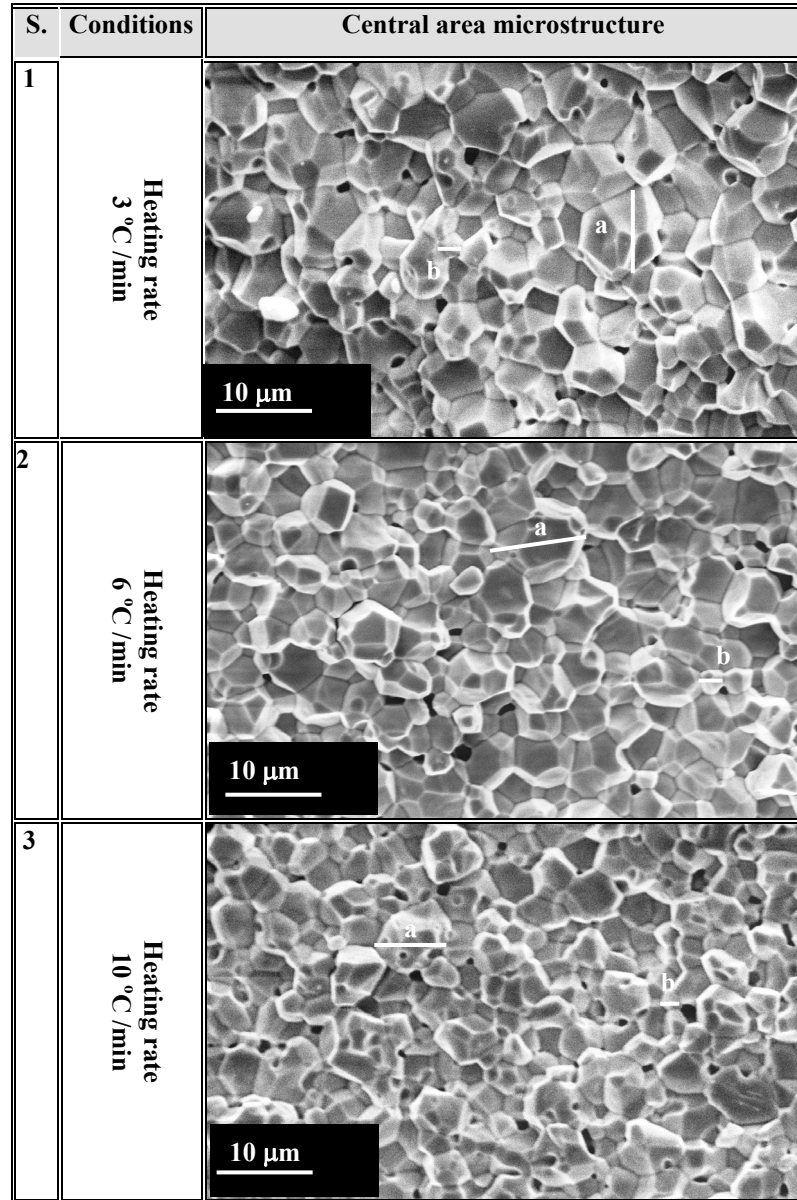


Fig. 86: Microstructure of central areas of samples sintered with an increasing heating rate

6.3.4 Results of the studies on the factors influencing the sintered microstructure

As expected, the sintered microstructure of the tape cast PZT was influenced both by the sintering conditions and the samples green density.

By modifying the processing conditions, the ceramic microstructure was transformed from the one shown in Fig. 87(1) to the one in Fig. 87(2), using the conditions listed in Table 25.

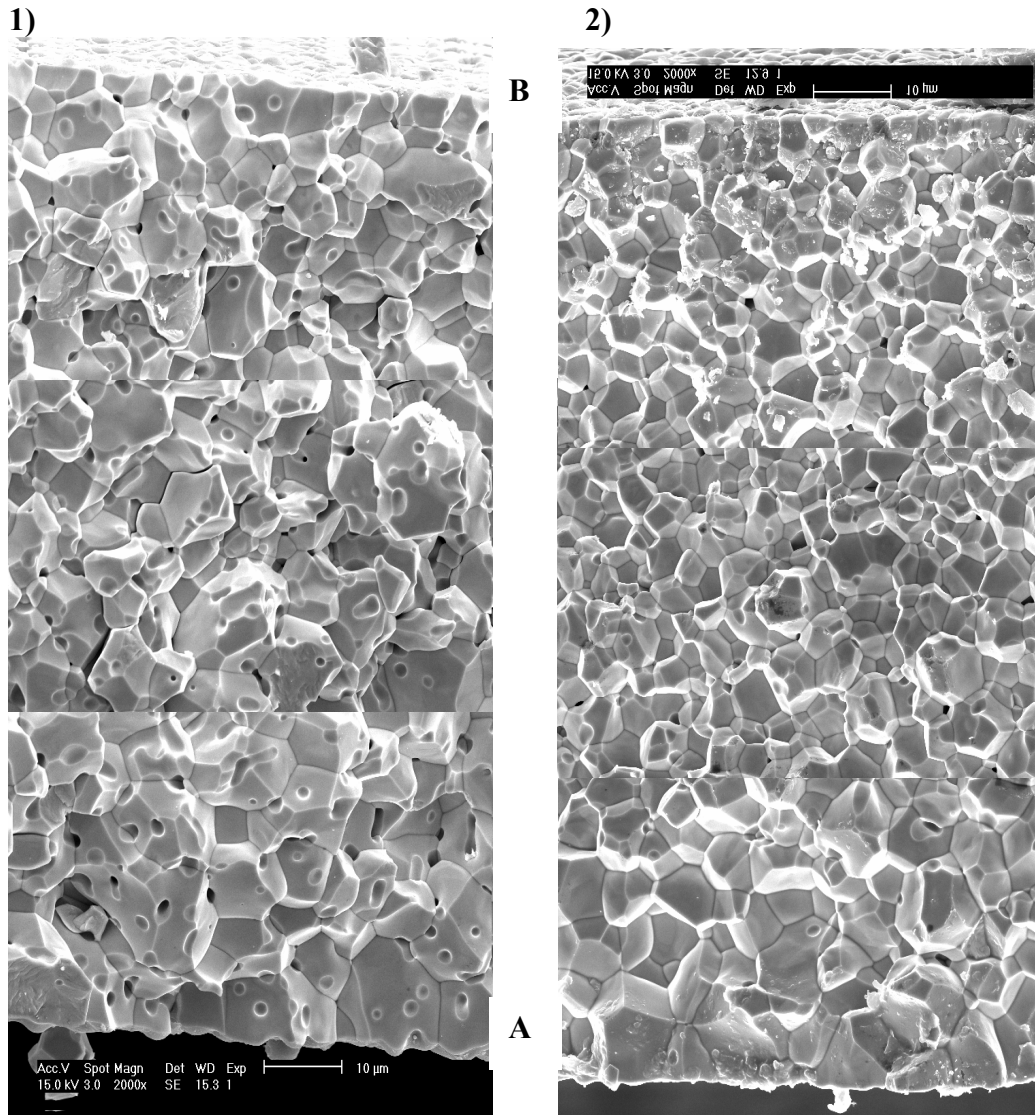


Fig. 87: 1) Original microstructure as obtained before the sintering studies; 2) microstructure achieved after the modification of the sintering conditions

	Before the study	After the study
Typical green density [g.cm^{-3}]	3.0	5.0
Sintering Temperature [$^{\circ}\text{C}$]	1270	1170
Dwell time [min]	45	45
Heating rate [$^{\circ}\text{C}/\text{min}$]	3	6
Pressing conditions:	-	
Pressure [MPa]	-	65
Dwell time [min]	-	20
Temperature [$^{\circ}\text{C}$]	-	50
Configuration under the platens	-	stack

Table 25: Processing conditions before and after the study

The samples produced with the newly developed profile showed a sintered density of approximately 7.9 g.cm^{-3} on average (approximately 97% of the theoretical density) with a standard deviation of 0.16, against the previously achieved of approximately 7.7 g.cm^{-3} approximately 94% of the theoretical density. The porosity was substantially reduced and its position shifted primarily to the triple point. Overall, the grain size was diminished and cracks were not visible in the images of the cross section.

Table 26 reports the data of flatness and roughness of a sample obtained with warm pressed material, in comparison with the data from the material achieved with the original process.

	Roughness			Flatness		
	Side A	Side B	Sides Average	Direction 1	Direction 2	Directions Average
	nm	nm	nm	μm	μm	μm
Average before pressing	205	412	309	75	95	85
After pressing (on 1 sample)	220	230	225	70	82	76

Table 26: Samples flatness and roughness characteristics before and after pressing

The sintered samples were $210 \pm 20 \mu\text{m}$ and tended to bow naturally during sintering, curling as shown in Fig. 88.

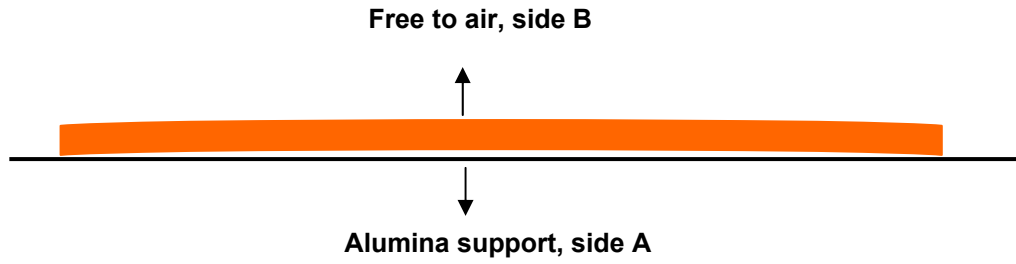


Fig. 88: Wafers profile, after sintering

6.3.4.1 The electrical characteristics of the pressed material

Table 27 reports a cross comparison of the electrical specifications (1) originally given for the process, the data by Navarro [2001] (2), the data from the repeatability study on the laboratory process (3) with their standard deviation (4) and the values of the samples obtained with the warm pressing step and the re-designed sintering profile (5) with their standard deviation (6).

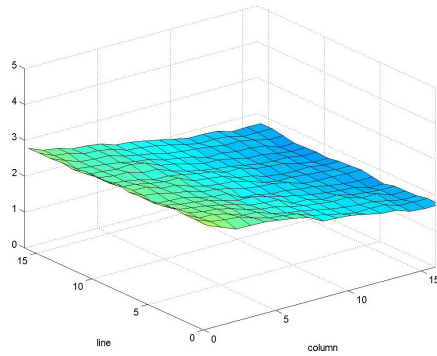
	Before poling			After poling					
	ϵ_r (30 Hz)	Tan δ (30 Hz)	ρ	ϵ_r (30 Hz)	Tan δ (30 Hz)	p	p/ϵ	F_v	F_D
		%	$\Omega m \times 10^{-9}$		%	$Cm^{-2} k^{-1}$ $\times 10^{-4}$	$Vm^{-2} K^{-1}$ $\times 10^5$	$m^2 C^{-1}$	$Pa^{-1/2}$ $\times 10^{-5}$
1	250 ± 50	< 2	2 ± 0.5	250 ± 50	<2	2.5 ± 0.3	>1.1	-	-
2	277	1.7	3.1	220	1.6	2.5	1.3	0.051	1.8
3	298	1.5	2.4	237	2.1	2.5	1.2	0.049	2.3
4	9	0.4	0.4	22	0.2	0.2	0.1	0.005	0.3
5	300	1.9	2.0	250	2.3	2.5	1.1	0.048	2.4
6	16	0.2	0.1	12	0.1	0.3	0.1	0.001	0.2

Table 27: Comparison electrical characteristics. 1) Electrical characteristics as from specification. 2) Values for wafers from Navarro's study. (see section 1.2.2). 3) Values from Navarro's process repeatability study (see section 6.2). 4) standard deviation for the original process samples (on 6 samples, 2 tape batches), 5) Average figures for pressed material (on 3 samples, from 2 tape batches), 6) standard deviation of the pressed material samples.

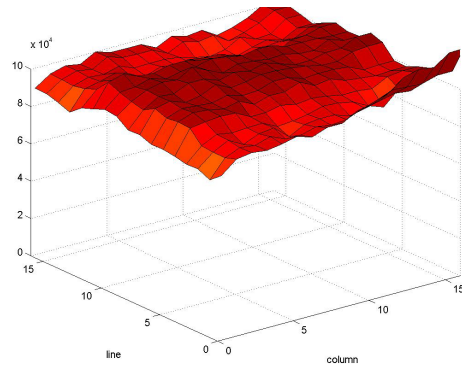
In Fig. 89, additional data are reported which compare the performances of a reference material, typically employed in IR devices, and the tape cast obtained with the warm pressing step. The typical response of the tape cast material was approximately 85% of the reference material.

In Fig. 90, a thermal image is reported taken with a device mounting the tape cast material.

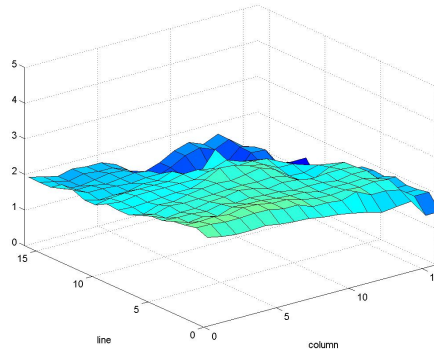
Offset reference material



Response reference material



Offset tape cast material (warm pressed)



Response tape cast material (warm pressed)

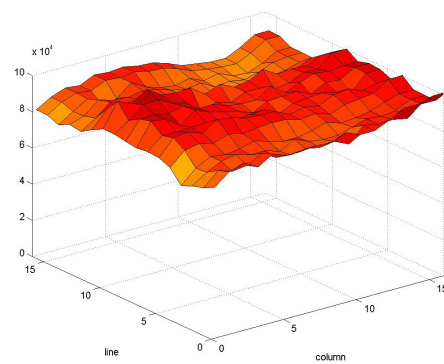


Fig. 89: Direct comparison between a reference material (a different pyroelectric ceramic) and the tape cast material performances in application

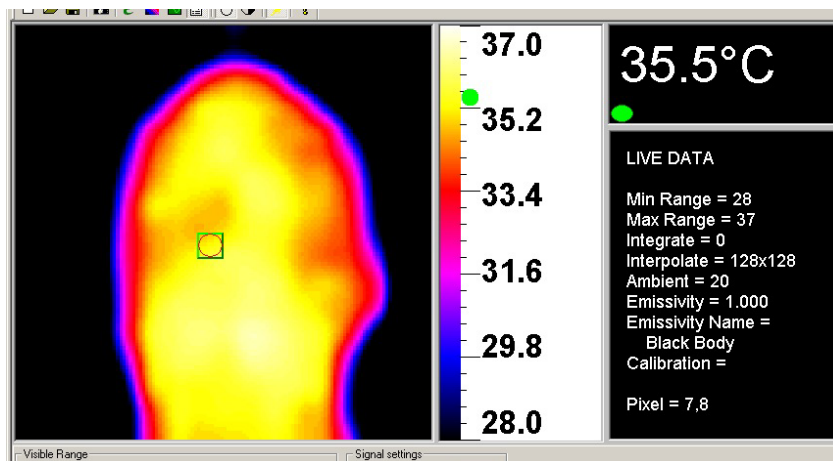


Fig. 90: Thermal image acquired with device mounting the tape cast material, resulted from the modified process

6.4 Definitive Design Phase I: The Statistical Process Control to assess the sources of variation in the warm pressing stage

The study previously reported assessed the warm pressing technique as a suitable method for increasing the green density of tape cast ceramic. Green densities up to approximately 66% (5.4 g.cm^{-3}) of the theoretical density were obtained. The Statistical Process Control technique has been selected as a tool to assess and monitor the variation in the green density figures achieved with the warm pressing process. In the following section, the results of this study are reported.

6.4.1 Method

100 samples were pressed with a pressure of 65 MPa applied for 20 minutes. The samples were stacked as illustrated in Fig. 91. The samples were stacked between platens pre-heated at 50°C . The sets included 5 stacked samples, separated by layers of poly propylene plastic to avoid lamination. The total number of stacks (n) was 20. The sample area was 16 cm^2 . The experiment was conducted over a time of 4 days. Each day the setting of the press were re-inputted.

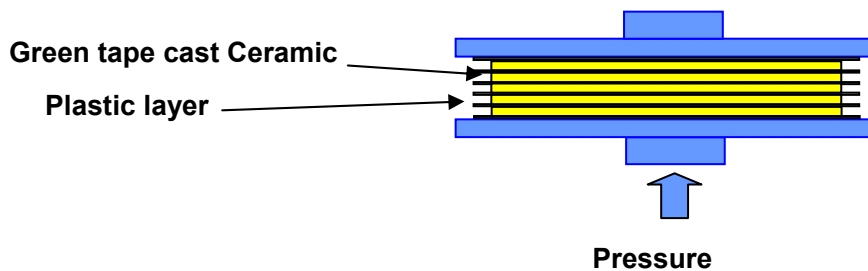


Fig. 91: Samples stacked in the pressing configuration

The sample thickness was taken as the process parameter to be monitored. The thickness was measured using a micrometer gauge with a tolerance of $5 \mu\text{m}$.

From the data of thickness, the density of each sample was calculated geometrically as noted in experimental section. The samples area didn't vary with the pressing.

Basic tools of the SPC technique (such as individual observation, mean and range charts as described in the literature review section) were used to analyse the green density data. The data were assumed to approximate a normal distribution. The green density achieved by pressing was used as the variable plotted in the process charts.

A green density of 5.0 g.cm^{-3} , 61% of the theoretical density was decided to be the optimum compromise for a satisfactory sintered microstructure. This value was decided in consequence of the pressing conditions optimisation study, where it appeared to be the highest value of green density achieved more often.

An Upper Specification Limit (USL) and the Lower Specification Limit (LSL) were 4.9 and 5.1 g.cm^{-3} respectively. Hence, the specifications tolerance limit was 0.2 g.cm^{-3} . These values were decided arbitrarily for the scope of the experiment.

The statistics were analysed and compared with the specifications and the required tolerances. The capability indexes were also calculated as explained in the literature review section.

6.4.2 Results

6.4.2.1 Individual observation chart

The graph in Fig. 92 reports the individual observations of samples' pressed density. The Upper (UCL) and Lower (LCL) Control Limits were positioned at 3σ from the mean line (\bar{X}). The warning limit lines (UWL and LWL) were drawn at 2σ from the mean line on the figure.

The pressed green density of a sample of tape varied between a minimum of 4.4 and a maximum of 5.0 g.cm^{-3} . The average green density of all the samples (mean, \bar{X}) was 4.7 g.cm^{-3} . The standard deviation (σ) of all the samples was 0.15 .

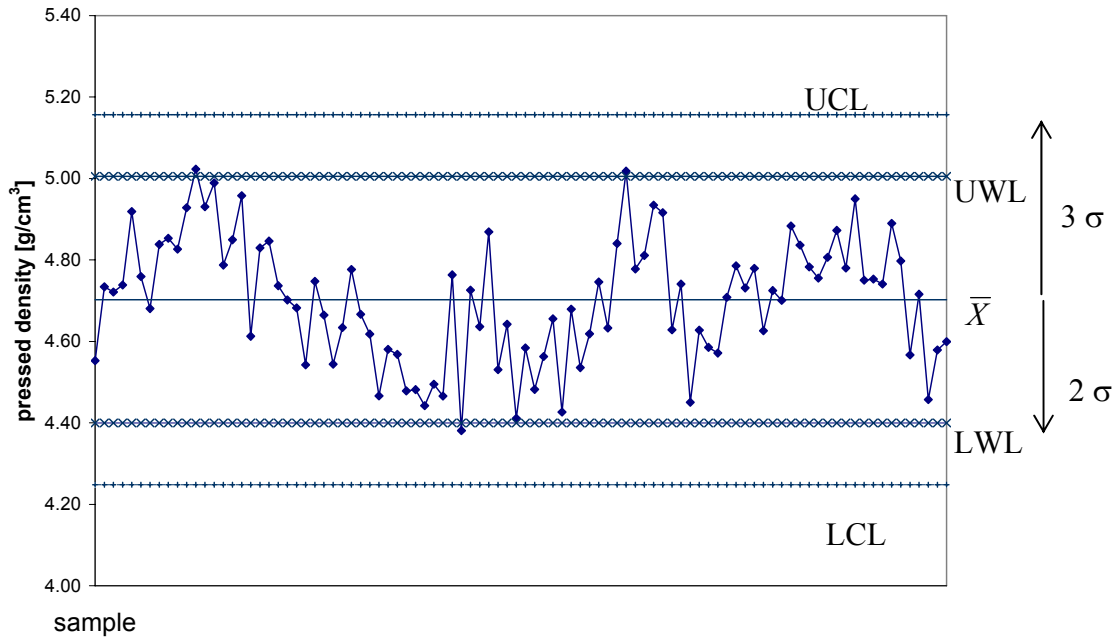


Fig. 92: Individual observation chart: upper and lower control limits (UCL, LCL) lines, mean line \bar{X}

The individual observation chart indicates that no values were out of the LCL to UCL range. However, in some circumstances densities were found outside of the 2σ warning lines. Moreover, rows of points, greater than 8 in succession, were located on the same side of the mean.

6.4.2.2 Mean and Range charts

The means and ranges of the sample densities were calculated for each stack of tapes and they are reported in Table 28: Raw data of green density for each sample of each stack with calculated statistical figures for each stack, together with the data of green density of the single samples.

The relevant mean (\bar{X}) and range (R) charts were subsequently plotted. They are reported in Fig. 93(1) and Fig. 93(2), respectively. These charts report the value of the mean of each stack (\bar{X}) and the difference between the highest and the lowest value of the green density in the stack (range, R).

The lines corresponding to the calculated mean of the means ($\bar{\bar{X}}$) and the mean of the range ($\bar{\bar{R}}$) of the stacks were drawn on the charts.

The Upper and the Lower Control Limit lines (UCL and LCL respectively) were placed respectively at $3\sigma(n)^{-1/2}$ above and below the average values of the mean of the means ($\bar{\bar{X}}$) and the mean of the range ($\bar{\bar{R}}$). Table 29 reports the values of the main figures used for the analysis.

6.4.3 Capability Indexes

The capability indexes for the studied process C_{pk_u} , was 1.02; C_{pk_l} was -0.51. C_p was 0.25.

Results

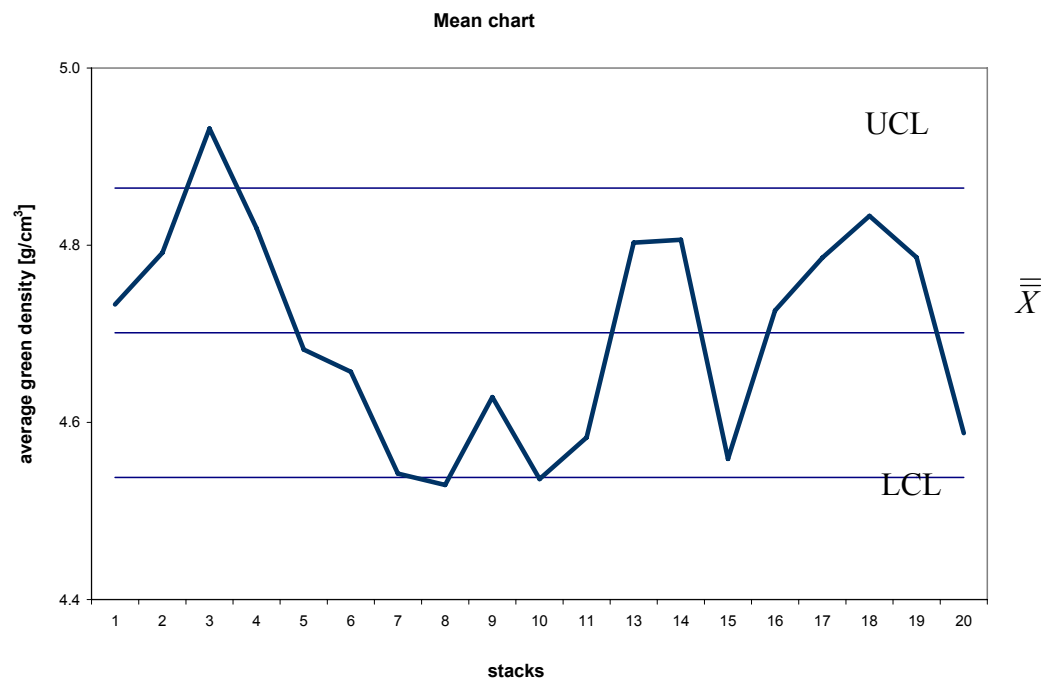
Stack	1	2	3	4	5	6	7	8	9	10	11	12	13	14	15	16	17	18	19	20
Sample																				
1	4.55	4.76	4.93	4.85	4.74	4.66	4.62	4.48	4.38	4.64	4.66	4.75	4.81	4.45	4.71	4.73	4.76	4.75	4.57	4.62
2	4.73	4.68	5.02	4.96	4.70	4.54	4.47	4.44	4.73	4.41	4.43	4.63	4.93	4.63	4.79	4.70	4.81	4.75	4.72	4.47
3	4.72	4.84	4.93	4.61	4.68	4.63	4.58	4.49	4.64	4.58	4.68	4.84	4.92	4.59	4.73	4.88	4.87	4.74	4.46	4.58
4	4.74	4.85	4.99	4.83	4.54	4.78	4.57	4.47	4.87	4.48	4.54	5.02	4.63	4.57	4.78	4.84	4.78	4.89	4.58	4.57
5	4.92	4.83	4.79	4.85	4.75	4.67	4.48	4.76	4.53	4.56	4.62	4.78	4.74	4.60	4.63	4.78	4.95	4.80	4.60	4.48
Statistics																				
Mean (\bar{X})	4.73	4.79	4.93	4.82	4.68	4.66	4.54	4.53	4.63	4.54	4.58	4.80	4.81	4.56	4.73	4.79	4.83	4.79	4.59	4.54
Range (R)	0.37	0.17	0.24	0.34	0.21	0.23	0.15	0.32	0.49	0.23	0.25	0.38	0.31	0.18	0.16	0.18	0.20	0.15	0.26	0.15
Standard Deviation (σ)	0.13	0.07	0.09	0.13	0.08	0.08	0.07	0.13	0.19	0.09	0.10	0.14	0.13	0.07	0.06	0.08	0.08	0.06	0.09	0.07

Table 28: Raw data of green density for each sample of each stack with calculated statistical figures for each stack

UCL (\bar{X})	LCL (\bar{X})	Mean of the Means ($\bar{\bar{X}}$)	UCL (R)	LCL (R)	Mean of the Ranges (\bar{R})
[g.cm ⁻³]	[g.cm ⁻³]	[g.cm ⁻³]	[g.cm ⁻³]	[g.cm ⁻³]	[g.cm ⁻³]
4.86	4.54	4.70	0.38	0.38	0.38

Table 29: Calculated values for UCL, LCL, and means for the Mean and Range charts

1)



2)

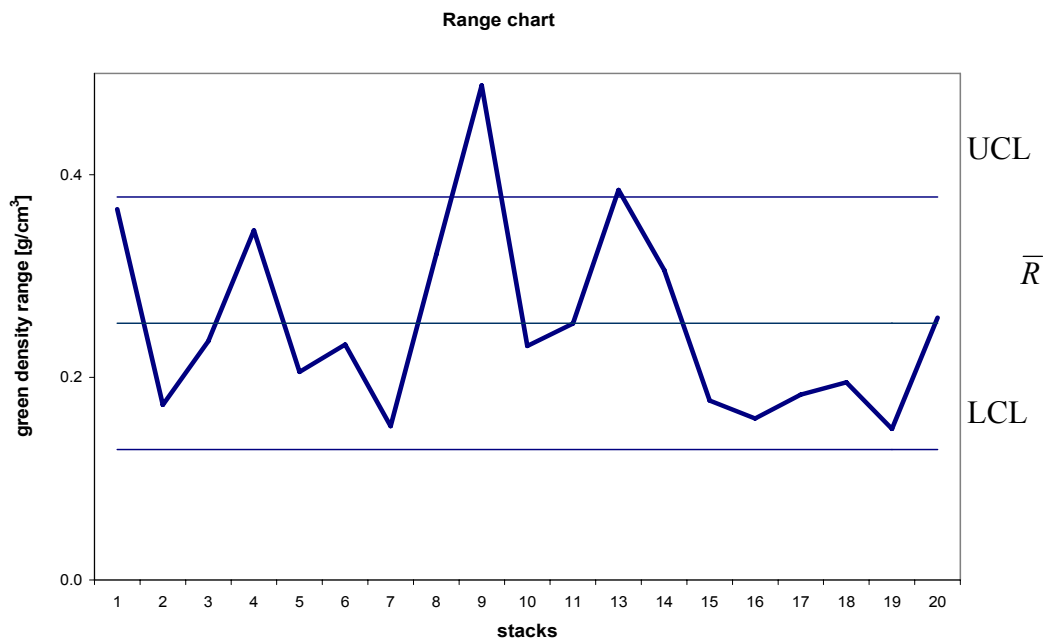


Fig. 93: Mean (1) and Range (2) charts

6.5 Conceptual Design Phase II: the influence of the ingredients and the drying conditions on the green tape

The second conceptual design phase was a study on the effects of the slurry ingredients and the drying conditions on the ceramic green tape.

The amount of the individual ingredients was varied to study their particular effects. The analysis of the ingredient effects was performed with a combination of techniques.

Below the individual experiment description and motivation are reported.

Firstly, the effects of the dispersant were studied by varying its amount in the slip composition. In this case two slurry preparation routes were used and compared. Route 1 was the procedure described for the original process (see section 4.1, page 78). In this case the powder was ball milled in presence of different amounts of dispersant.

In the powder preparation Route 2, the powder was pre-milled in excess of water and subsequently different quantities of dispersant were added.

This methodology allowed the separation of the dispersant effects in stabilising the suspension and in acting as comminution aid.

For both the preparation routes, the interactions with the binder were investigated.

Thirdly, the effects of different binder-plasticizer ratio on the tape cast were investigated. For this study, slurries prepared following Route 1 with a constant rate of dispersant were added with different binder/plasticizer ratios.

Fourthly, the variation in ceramic powder concentration on the green tape characteristics was assessed. Keeping the dispersant/powder and the other organics/ powder ratios constant, slurries at different powder concentrations were prepared. In this case all the slurries were prepared following Route 1.

6.5.1 Method

6.5.1.1 The effects of the dispersant amount and of the interactions with the binder system on the green ceramic

Two preparation procedures were used (Route 1 and Route 2) which allowed the separation of the dispersant effects in stabilising the suspension and in acting as comminution aid.

The suspensions were tested for their rheological characteristics. The microstructures of the cast ceramic were imaged with the SEM as compared as cast and after the elimination of the organic ingredients by burnout. In case of the slurries produced with Route 1, the absorption of the binder (PVA) onto the particle surfaces was also tested.

6.5.1.1.1 Route 1: comminution and stabilisation effects combined

Route 1 followed the procedure described as “original process”. A detailed operational description of this process was made in the experimental section (page 78).

Fig. 94 reports a flow chart representation of this procedure.

The powder was ball milled in presence of four different amounts of dispersant. As it can be noted also on the picture, the slurries at this stage of preparation are referred as “samples NB”.

Subsequently, the other ingredients were added and milled. The complete slurries are referred as “samples B”.

Table 30 indicates the proportions of the added ingredients in weight %. In the table, the dispersant amounts are also expressed as ratios of total dispersant weight over powder weight, including the water which it contains (the dispersant is a water solution 40% in weight of active material).

	Samples B							
	Samples NB							
	PZT	Disp.	Water(1)*	Surf.	PPG	PVA	Water(2)*	disp/powder
	w%	w%	w%	w%	w%	w%	w%	w%/w%
1	64.00	0.29	16.41	0.32	2.22	2.22	14.54	0.0046
2	64.00	0.78	15.92	0.32	2.22	2.22	14.54	0.0122
3	64.00	1.52	15.18	0.32	2.22	2.22	14.54	0.0238
4	64.00	2.40	14.30	0.32	2.22	2.22	14.54	0.0375

- Water(1) used for the milling of the powder with the dispersant (1st milling)
- Water(2) used to dissolve the PVA.

Table 30: Slurries ingredients of process following Route 1

All the slurries had a powder volume content of about 18%, an overall solid content of about 26% and an organic volume content of about 9%.

For all the slurries, the rheological properties and the cast tapes’ characteristics were investigated. The absorption of the Binder (PVA) onto the particle surfaces was also tested. The dried cast tapes were imaged with the SEM at both free and onto the carrier surfaces. SEM images of brown tapes, after the burnout of the organics at 500 °C for 1 hour, were also obtained. Their microstructure was characterised.

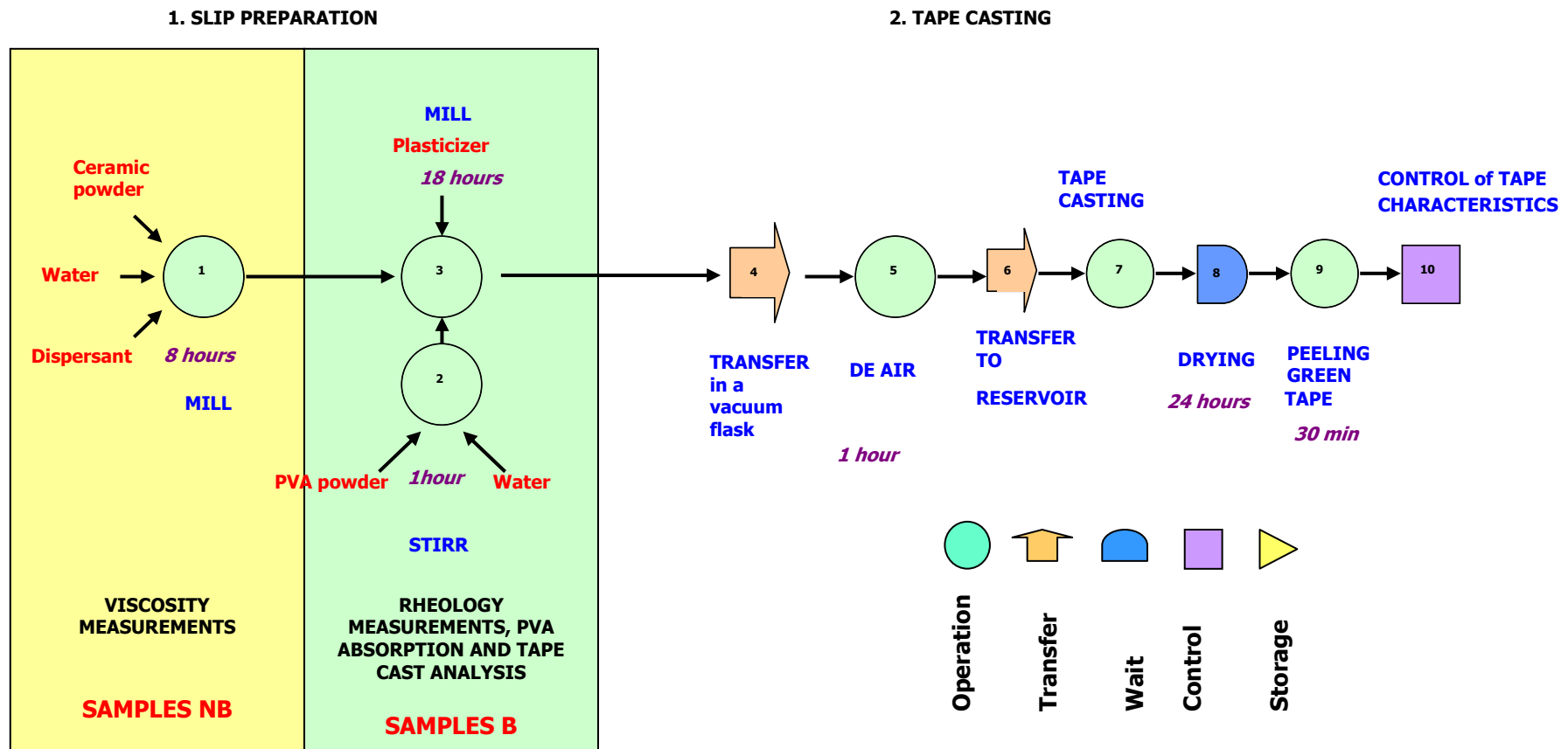


Fig. 94: Process flow sheet for the slurry preparation and the tape casting [Route 1]

6.5.1.1.2 Route 2: dispersant's stabilisation effect

Route 2 followed the steps described in Fig. 95.

The PZT powder was ball milled in an excess of water for approximately 24 hours in a 100 ml silicate milling jar with 200 g of cylindrical zirconia milling media. No dispersant was added.

The slurry was then centrifuged at 1000 RPM for 10 min in order to increase the powder concentration. This concentrated suspension was then divided into two portions and each of them 5 aliquots. Different dispersant and water amounts were added to each, in order to obtain slurries at different dispersant and powder concentrations, as illustrated by Table 31.

Five reached a powder content of about 73% in weight and five of about 82.5% in weight. The samples were stirred continuously for 24 hours with a magnetic stirrer, in order to permit the absorption of the dispersant on the particles surface. In this case, as in the samples produced with Route 1, the samples were named “samples NB” as they contained water, dispersant and powder.

In order to assess the repeatability of the results, the experiment was repeated three times at the lowest powder concentration, and 1 time for the higher concentration. However, as every experiment implied a different milling process, for consistency of the results it was chosen to evaluate every experiment independently, paying more attention to the trends in rheological parameters than to the absolute values of the rheological figures obtained. For this reason, in the results section 6.5.2.1, two of the experiments, e.g. final powder concentrations 62% and 68% w., are reported in detail, as representative of the series. Also, comprehensive graphs are added which show how the trends throughout the experiments were consistent.

The rheological characteristics of these slurries were measured as detailed in the experimental method section (page 86).

Samples	Dispersant/powder ratio	FINAL POWDER VOL 15%		FINAL POWDER VOL 21%	
		NB	B	NB	B
		Powder concentration	Powder concentration	Powder concentration	Powder concentration
	[w%/w%]	[w%]	[w%]	[w%]	[w%]
1	0.0043	73 ± 3	62 ± 3	82.5	68
2	0.0085	73 ± 3	62 ± 3	82.5	68
3	0.0146	73 ± 3	62 ± 3	82.5	68
4	0.0247	73 ± 3	62 ± 3	82.5	68
5	0.0553	73 ± 3	62 ± 3	82.5	68

Table 31: Samples powder and dispersant content for Route 2

Subsequently, the other ingredients of the binder system were added to each suspension, maintaining the binder/powder and the binder/plasticizer ratios in weight constant (0.035 and 1 respectively). The suspensions (samples B) were stirred for 24 hours with a magnetic stirrer, in order to allow reaching an equilibrium condition.

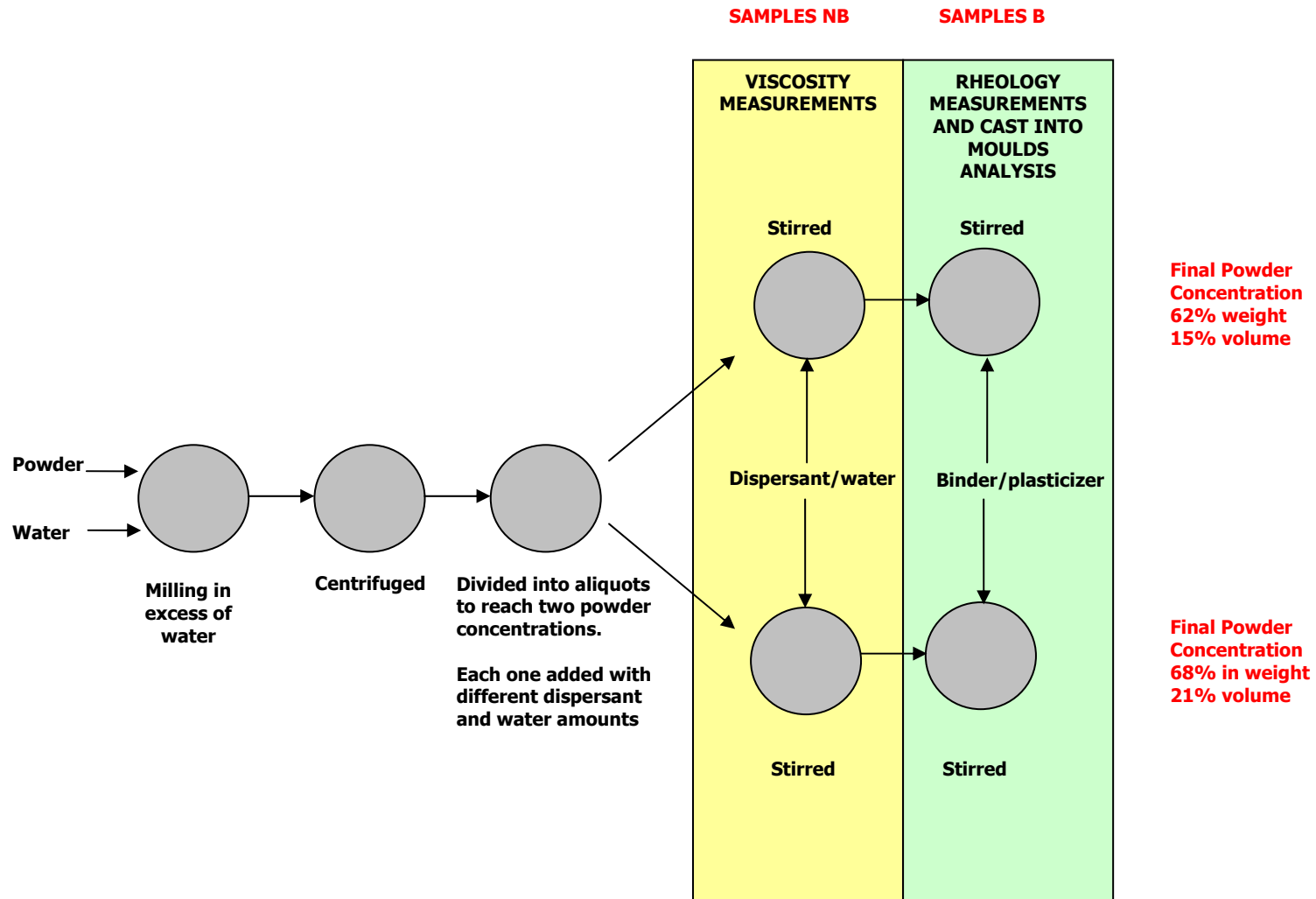


Fig. 95: Route 2: procedure

6.5.1.2 The effect of the binder/plasticizer ratio and the powder content

This experiment was performed by comparing the tapes cast from slurries prepared with the same ratio of dispersant/powder and binder/powder but which differ for two basic characteristics:

1. powder content
2. plasticizer content (in substitution of water) (PPG/PVA = 2:1)

Table 32 reports the composition of the slurries.

The slips were prepared according to Route 1 and then tape cast. The dried tapes' microstructures were compared also after the burnout of the organics.

Sample	PZT	Disp.	Water	Surf	PPG	PVA	Water (2)*
	w%	w%	w%	w%	w%	w%	w%
1	64.00	1.50	15.45	0.32	2.22	2.22	14.29
2	72.22	1.71	10.67	0.36	2.52	2.52	10.00
3	72.22	1.71	8.15	0.36	5.04	2.52	10.00
4	64.00	1.50	13.23	0.32	4.44	2.22	14.29

*Water(2) used to dissolve the PVA.

Table 32: Composition of the slurries for the assessment of the influence of the binder system and the powder content

6.5.1.3 The effects of the drying conditions

5 g aliquots of slurry, produced according to Route 1 with the ingredients proportion listed in Table 5 at page 23, were cast into plastic moulds and let to dry in different conditions as reported in Table 33.

Sample	Conditions		
	Temperature	Humidity	Flowing air
		[%]	
1	3	< 50	No
2	17	75	Yes
3	18	76	Yes
4	19	82	No
5	20	73	No
6	36	< 50	No
7	>>50	n/a	No

Table 33: Drying conditions

The sample's weight loss was monitored and plotted against time.

From the dried samples two regular pieces (1 by 1 cm) were cut and the green densities and their average were calculated.

6.5.2 Results

6.5.2.1 Study of the dispersant effects on the slurry preparation: Route 1

6.5.2.1.1 The steady shear rheology

All the slurries showed pseudoplastic behaviour. Fig. 96 show the profiles of viscosity of the slurries after the organics addition.

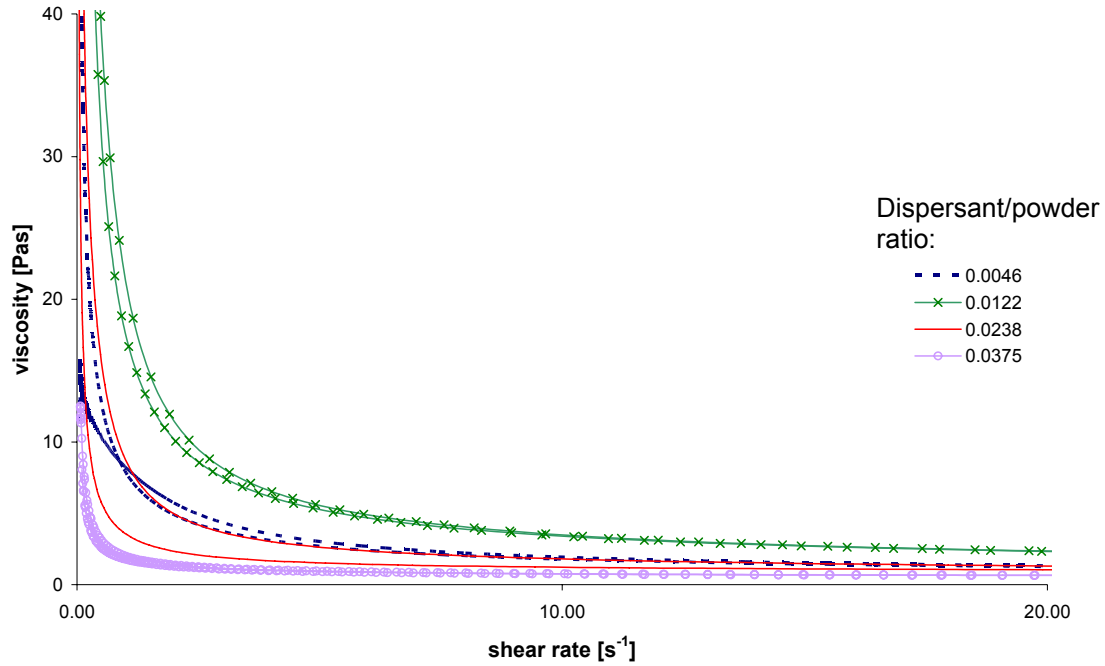


Fig. 96: Viscosity profiles of slurries prepared with different dispersant amounts containing the binder system

The interpolation of the viscosity curves showed affinity with the both the Bingham and the Casson models. These models relate the stress s to the shear rate $\dot{\gamma}$.

The parameter s_0 represents the yield stress after which the material flows with constant differential viscosity, while κ is the plastic viscosity, which describes the slurry's flow at high velocity. The Bingham and Casson models equations are reported in Equation 14 and Equation 15 respectively in the literature review section.

The parameters obtained by fitting the viscosity curves for the complete slurries (samples B) with the Bingham and the Casson models are listed in Table 34 and plotted in Fig. 97

Sample	Dispersant/powder ratio	Bingham			Casson		
N ^o		s_0	κ	R^2	s_0	κ	R^2
	[w ^o /w ^o]	Pa	Pa.s		Pa	Pa.s	
1	0.0046	4.9	0.9	0.9651	2.3	0.6	0.9852
2	0.0122	1.8	0.5	0.9989	0.5	0.4	0.9990
3	0.0238	3.6	0.9	0.9806	1.9	0.6	0.9863
4	0.0375	6.9	2.4	0.9998	4.2	1.5	0.9401

Table 34: Parameters and correlation coefficient for all the slurries (samples B)

Generally, the correlation coefficient R^2 was close to 1, indicating that both the models approximate the viscosity curves.

Both the yield stress s_0 and the plastic viscosity κ of the two models follow an identical trend. They decrease towards a minimum, reached for 0.0122 dispersant over powder ratio, after which they increase for any other addition of dispersant.

Plasticity for suspensions is secondary data defined by the ratio yield stress (s_0) above plastic viscosity (κ), a decrease in the plastic viscosity κ , associated with an increase in the yield stress, indicates an increase in the suspension plasticity. It is a measure of the rigid structure that develops at zero shear rate in an open continuous structure of colloidal particles. Fig. 98 reports the data of plasticity calculated for both the models, using the values in Table 34.

For the Bingham model the plasticity values were higher. In both cases the trends had a minimum in correspondence of 0.0122.

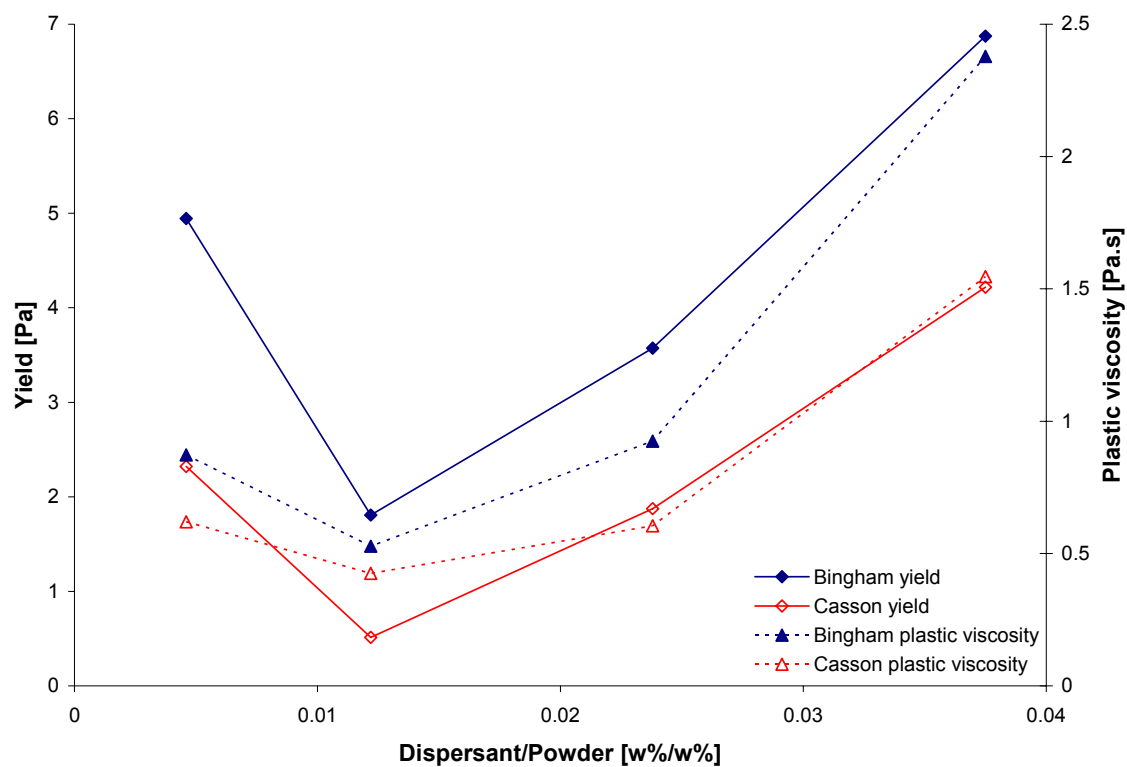


Fig. 97: Trends of the parameters obtained by fitting the viscosity profiles with the Bingham and the Casson Model: Yield (s_0), Plastic viscosity (κ)

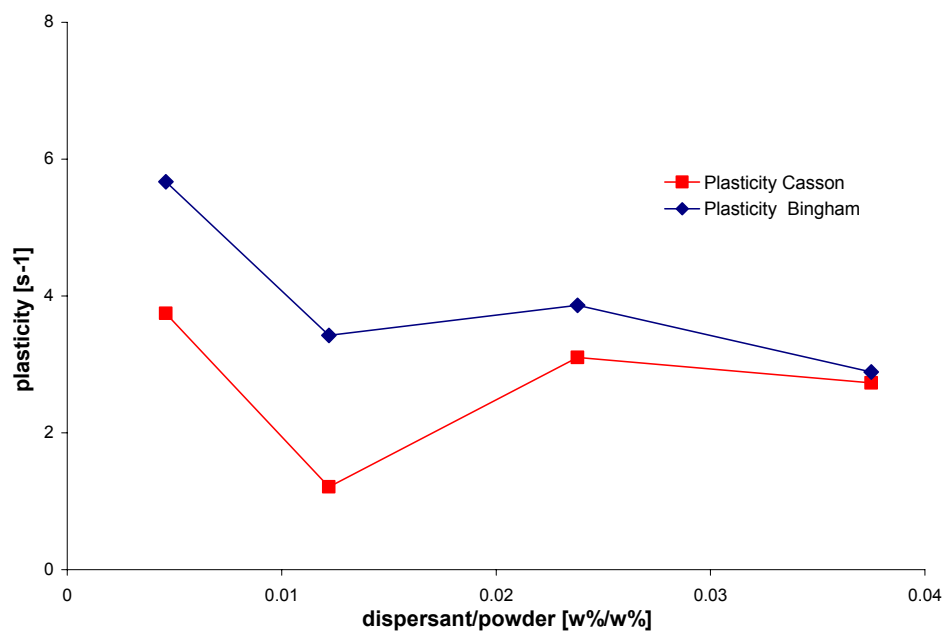


Fig. 98: Plasticity calculated for the Bingham and Casson coefficients

6.5.2.1.2 The viscosity and the green density trends

Table 35 summarizes the rheological and green density data collected for each cast sample. These data are also plotted in Fig. 99.

		Samples NB: without binder system	Samples B: with binder system	
Samples	Disp./pow der ratio	Viscosity (20 s ⁻¹)	Viscosity (20 s ⁻¹)	Green Density
	[w%/w%]	[Pa.s]	[Pa.s]	[g.cm ⁻³]
1	0.0046	3.3	1.9	3.4
2	0.0122	0.2	3.5	2.9
3	0.0238	1.3	1.8	3.0
4	0.0375	0.9	0.8	2.7

Table 35: Viscosity data of slurries prepared according Route 1 and relative green density values

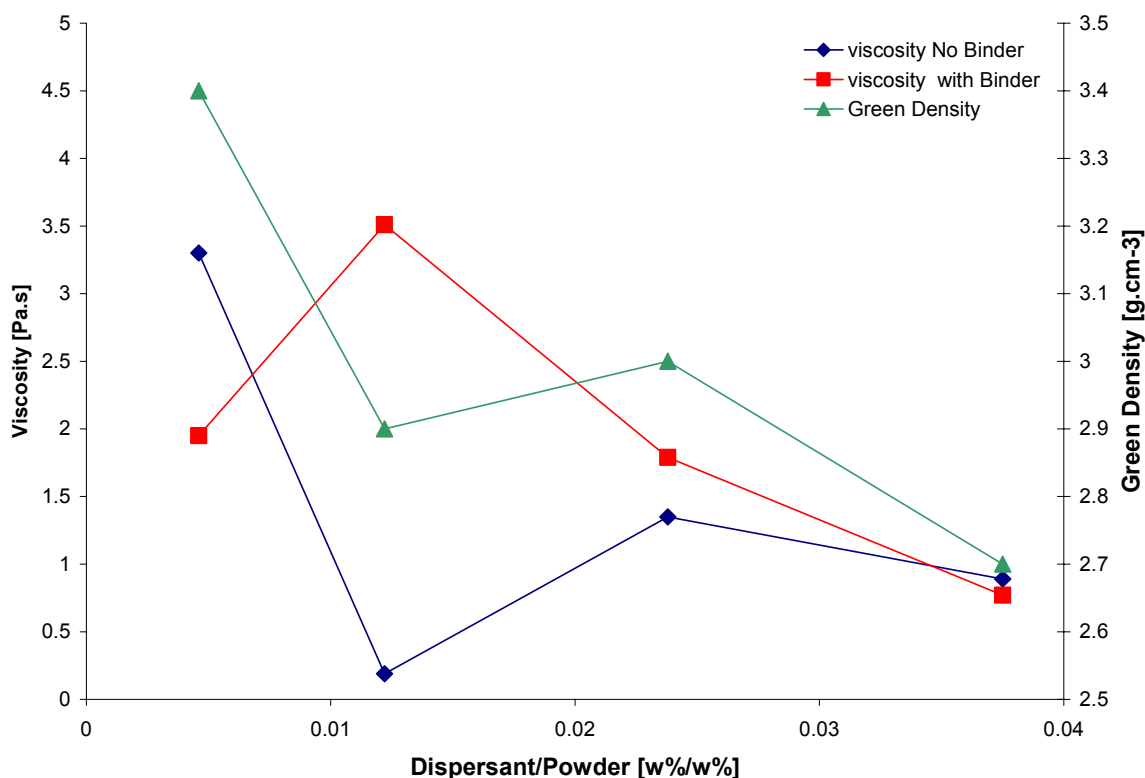


Fig. 99: Viscosity trends (at 20 s⁻¹) for slurries prepared according to Route 1 with and without binder, associated with green density figures

The viscosity of the slurries with no organic phase, samples NB, varied between 3.3 and 0.2 Pa.s. It decreased up to a minimum of 0.2 Pa.s, reached at 0.0122 dispersant ratio. Ulterior dispersant additions, up to 0.0238 and 0.0375 dispersant ratio, increased the viscosity to 1.3 and 0.9 Pa.s respectively.

The viscosity of the slurries after the addition of the polymers, samples B, showed an opposite trend. In this case the viscosity oscillated between 3.5 and 0.8 Pa.s. The maximum of viscosity was 3.5 Pa.s, found for 0.0122 dispersant ratio. This maximum was in correspondence of the dispersant amount giving a minimum for the viscosity trend of samples NB, with no organics.

The green density of the tapes cast from samples B oscillated between 2.7 and 3.4 g.cm⁻³. The green density of the tapes cast followed a similar trend as the viscosity of samples NB, when no binder was added. A minimum in the green density trend was found for 0.0122 dispersant ratio.

6.5.2.1.3 The oscillatory rheology

Table 36 reports data gathered with oscillatory measurements, made on slurries containing the binder system (samples B).

The table lists G'_{\max} , characterising the linear viscoelastic region: G'_{\max} is the elastic modulus in the linear viscolastic region. In addition the elastic modulus G' at 1.13 Hz obtained in the frequency sweep measurements within the linear viscoelastic region is reported.

Sample	Disp./pow der ratio	Max. Elastic Modulus in the LVR (G'_{\max})	Elastic modulus at 1.13 Hz (G')	Viscosity (20 s ⁻¹)
N ^o	[w%/w%]	[Pa]	[Pa]	[Pa.s]
1	0.0046	175	154	1.9
2	0.0122	1840	2097	3.5
3	0.0238	150	153	1.8
4	0.0375	100	88	0.8

Table 36: Rheological parameters obtained with oscillatory tests

As shown in Fig. 100, the trends of rheological figures achieved with oscillatory techniques follow analogues patterns than the viscosity of the slurries with binder system, visible also in Fig. 99. For all the figures, the maximum values are coincident with 0.0122 dispersant amounts.

The elastic modulus in the linear viscoelastic region G'_{\max} varies between 100 and 1840 Pa. The maximum, 1840 Pa, was obtained for the samples with 0.0122 dispersant ratio. This value was an order of magnitude higher than the other results. The same comments could be made describing the elastic modulus G' obtained at 1.13 Hz in the frequency sweep in the linear viscoelastic region. G' oscillated between 2097 and 88 Pa. Also in this case the maximum value was found for the samples with 0.0122 dispersant ratio. For this dispersant amount, the G' was one order of magnitude bigger than for the other dispersant ratios.

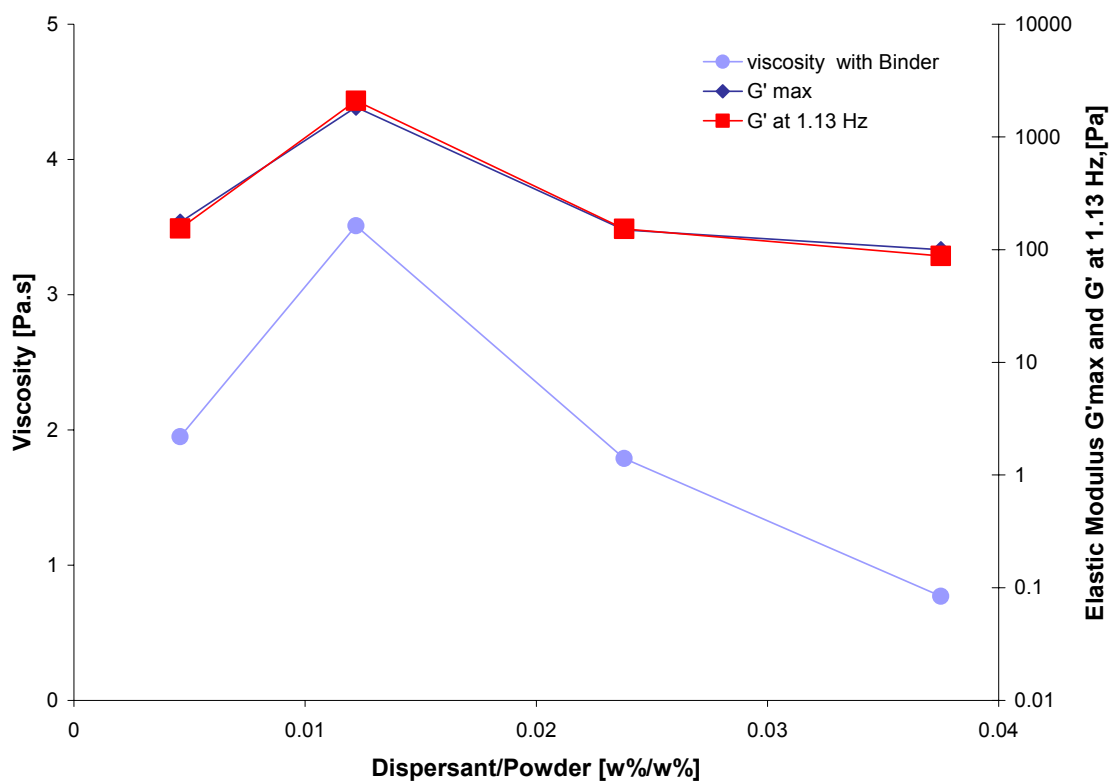


Fig. 100: Comparison of rheological figures of slurries containing the binder system (Samples B) prepared following Route 1

6.5.2.1.4 Time dependent rheological characteristics

The time-dependent viscosity of the slurries containing all the ingredients (samples B) is illustrated in Fig. 101. The graph shows the profiles of the instantaneous viscosity when the shear rate was varied suddenly from 2 s^{-1} to 50 s^{-1} and vice versa.

Table 37 reports the values of the instantaneous viscosity at critical times. Firstly, at 2 s^{-1} , just before the increase in shear rate. Secondly, at 50 s^{-1} . Thirdly, again at 2 s^{-1} , when the viscosity had stabilised. In addition, the recovery time, i.e. the time employed for the viscosity to regain an equilibrium value after the higher shearing, is reported for each slip. The last column of the table lists a thixotropy coefficient calculated by the rheometer software by integrating the area included between the viscosity curves obtained by sweeping ascending and descending the shear stress.

Sa m.	Disp/pow der ratio	Instantaneous Viscosity at 2 s^{-1}	Instantaneous Viscosity at 50 s^{-1}	Instantaneous Viscosity at 2 s^{-1}	Recov. time	Thixotropy Coefficient *
Nº	[w%/w%]	[Pa.s]	[Pa.s]	[Pa.s]	[s]	[Pa/s]
1	0.0046	5.6	0.6	5.6	50	66
2	0.0122	10.7	0.9	10.8	138	40
3	0.0238	3.4	0.6	3.0	475	217
4	0.0375	1.3	0.5	1.3	12	24

* calculated for the curves shear stress vs. shear rate

Table 37: Data of the step shear experiments for slurries containing all the ingredients and prepared as in Route 1

In all the cases, the viscosity value is fully recuperated after the removal of the 50 s^{-1} shearing.

The slurry with the lowest dispersant content, 0.0046, showed a little evidence of thixotropy as the viscosity value recuperated in about 50 seconds after the high shear was removed.

In contrast, if the concentration was intermediate (0.0122 or 0.0238), the viscosity showed a strong component of thixotropy. This was especially evident for the slurry with 0.0238 dispersant ratio. For 0.0122 dispersant amount, approximately two minutes were needed for the viscosity to recuperate completely.

Approximately 8 minutes were needed if the dispersant was 0.0238 ratio.

The slip with higher dispersant content, 0.0375, was the slurry which exhibited the lowest degree of thixotropy. The recovery time was less than 12 seconds.

Fig. 102, the trends of the thixotropy coefficient calculated on the viscosity curves and the recovery time are compared. In both cases, the 0.0238 dispersant ratio slurries showed the maximum thixotropy.

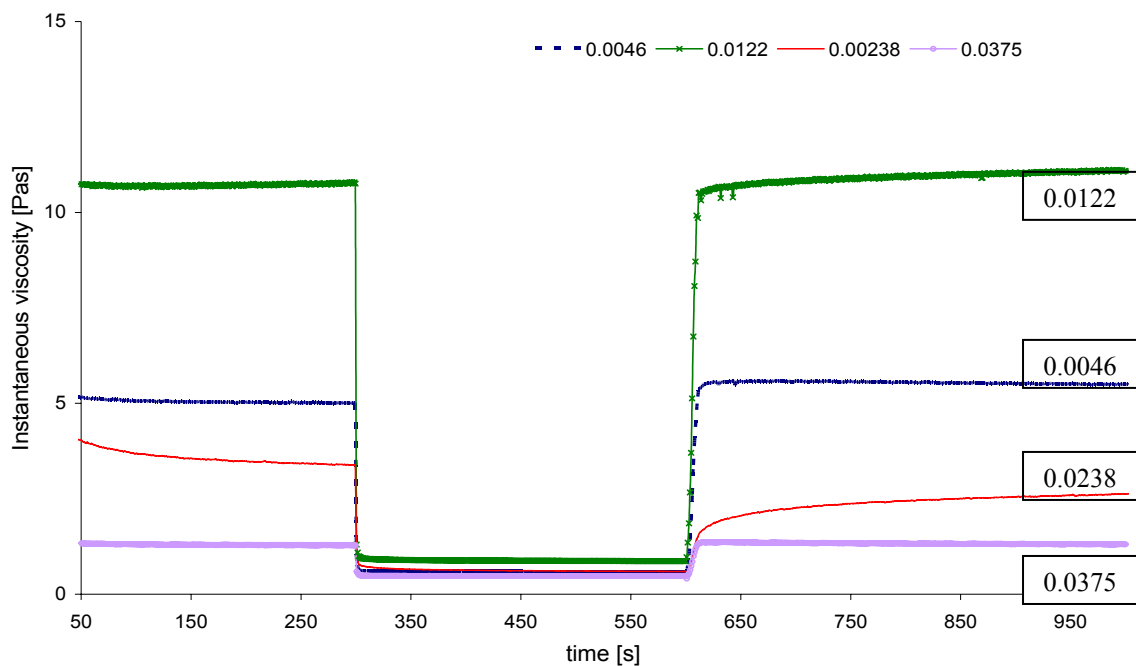


Fig. 101: Time-dependent behaviour for the slurries prepared with Route 1, tested at 2 and 50 s⁻¹ shear rates

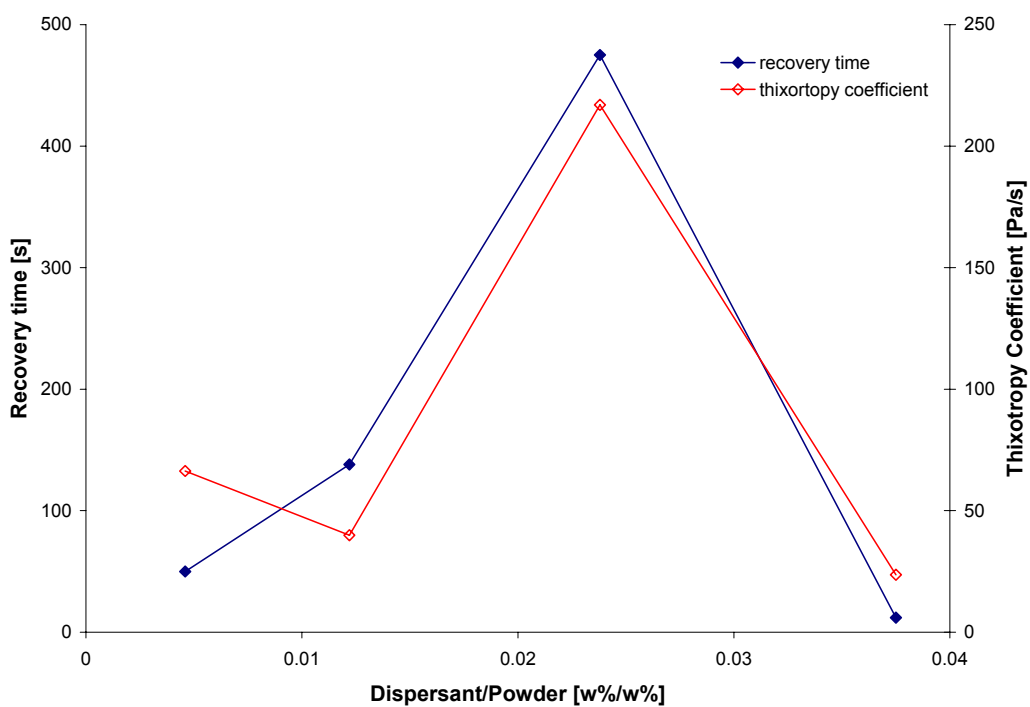


Fig. 102: Trends of thixotropy. Comparison of recovery time and thixotropy coefficient

6.5.2.1.5 Analysis of the brown tape microstructure

Fig. 103 shows the microstructures of the burnt out tapes. The SEM images were taken on both tapes surfaces, i.e. on side A of the tapes next to the polymer carrier and side B, the free upper side. The figure also reports the green density of each tape.

Table 38 summarises the data of the maximum particle size observed and the green density figures.

Dispersant /powder ratio	Green Density	Max particle diameter observed		
		carrier	top	Δ particle size up -carrier
[w%/w%]	[g.cm ⁻³]	μm	μm	μm
0.0046	3.4	3.6	3.6	0
0.0122	2.9	2.7	1.2	1.5
0.0238	3.0	1.3	1.1	0.2
0.0375	2.7	1.5	1.3	0.2

Table 38: Green density of the tapes and max particle size observed

- Sample 1 prepared with dispersant ratio equal to 0.0046, showed a similar microstructure on both sides of the tape. Its green density, 3.4 g.cm⁻³, was the highest achieved in the series. The maximum particle size of this sample was the largest among the series, approximately 3.6 μm visible on both tape surfaces.

- Sample 2 prepared with dispersant over powder ratio of 0.0122, had a different appearance on the two sides of the tape.

The carrier side microstructure was similar to sample 1's, although the size of the particles was slightly reduced. The maximum particle diameter observed on side A was approximately 2.7 μm .

In contrast, on the top surface (side B), the particles were considerably smaller with the maximum particle diameter of 1.2 μm . On this side the microstructure appeared more homogeneous.

The green density of this tape was reduced to 2.9 g.cm⁻³, approximately by 15%.

- Sample 3 was prepared with dispersant ratio of 0.0238. Like sample 1, it showed an uniform microstructure on both sides. The particle size was notably reduced compared to Sample's 1. Its largest particle diameter was approximately 1.1 μm on the surface B and 1.3 μm on the carrier side. The green density was approximately 3.0 g.cm⁻³.

- Sample 4's was obtained from dispersant ratio 0.0375 slurries. Its microstructure was comparable to sample 3's. In this case the porosity seemed to be slightly increased in size compared to sample 3. This observation was in accordance with the green density figure. The green density was lower in sample 4 by approximately 10% at 2.7 g.cm⁻³. This green density value was overall the lowest achieved. The dimensions of the particles on the two sides were comparable, 1.3 and 1.5 μm on the free and carrier side respectively.

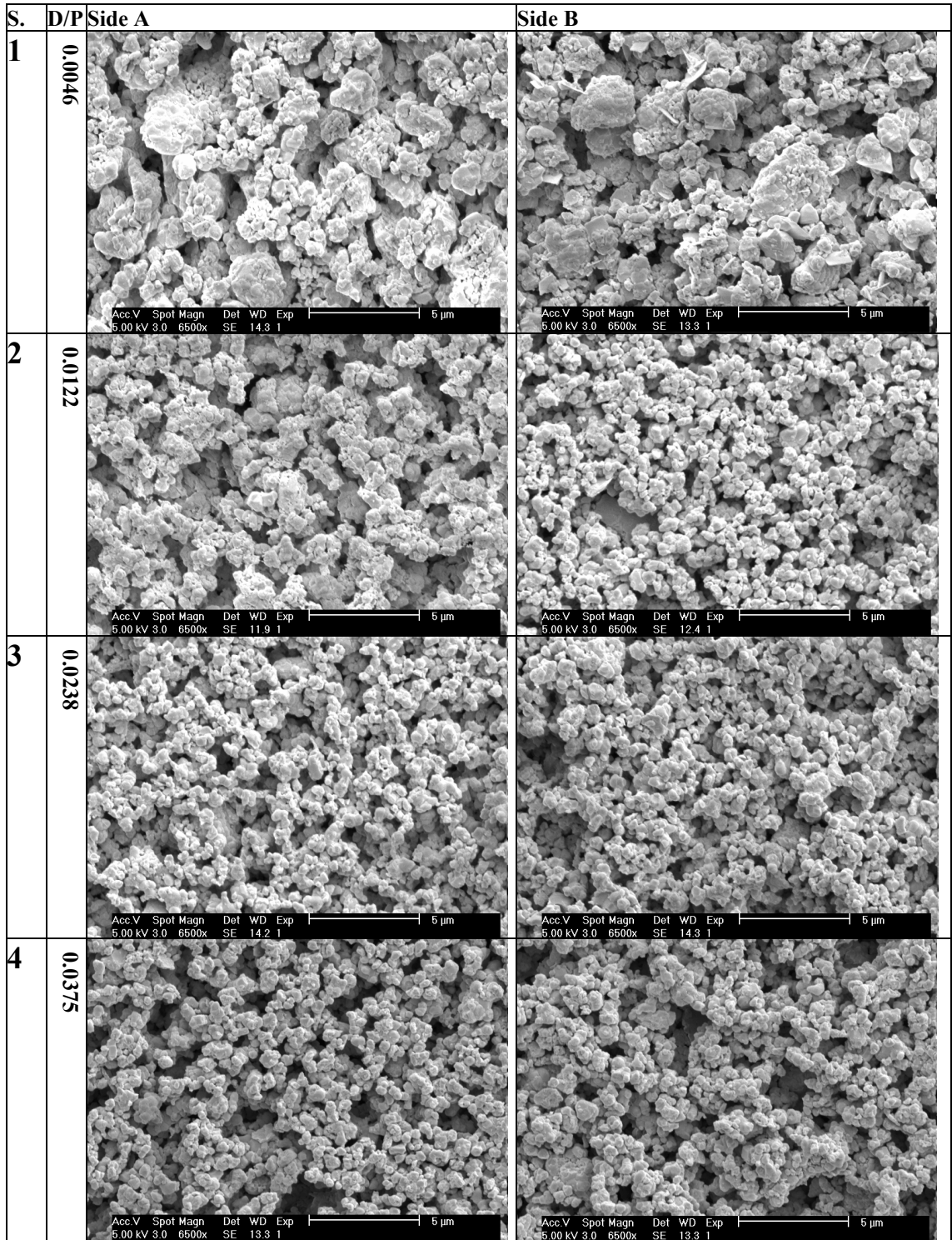


Fig. 103: Variation of the microstructure of the burnt out tapes produced with different amount of dispersant

6.5.2.1.6 Analysis of the green tapes microstructure: the binder distribution

Fig. 104 shows the green tapes before the burnout of the organic system.

The binder to powder ratio was constant in the slurries.

The carrier sides of all the samples showed a higher ratio of organic phase. Whilst this was very evident in sample's 2, 3 and 4, it was less clear in sample 1.

Increasing the dispersant ratio from 0.0046 to 0.0122 to 0.0238 seemed to reduce the binder amount visible with this kind of analysis. The peak of this trend was reached in sample 3 where the top surface appeared particularly binder free.

An additional increment in the dispersant amount to 0.0375 reversed this situation as sample 4 exhibited more binder phase, notably on the carrier side.

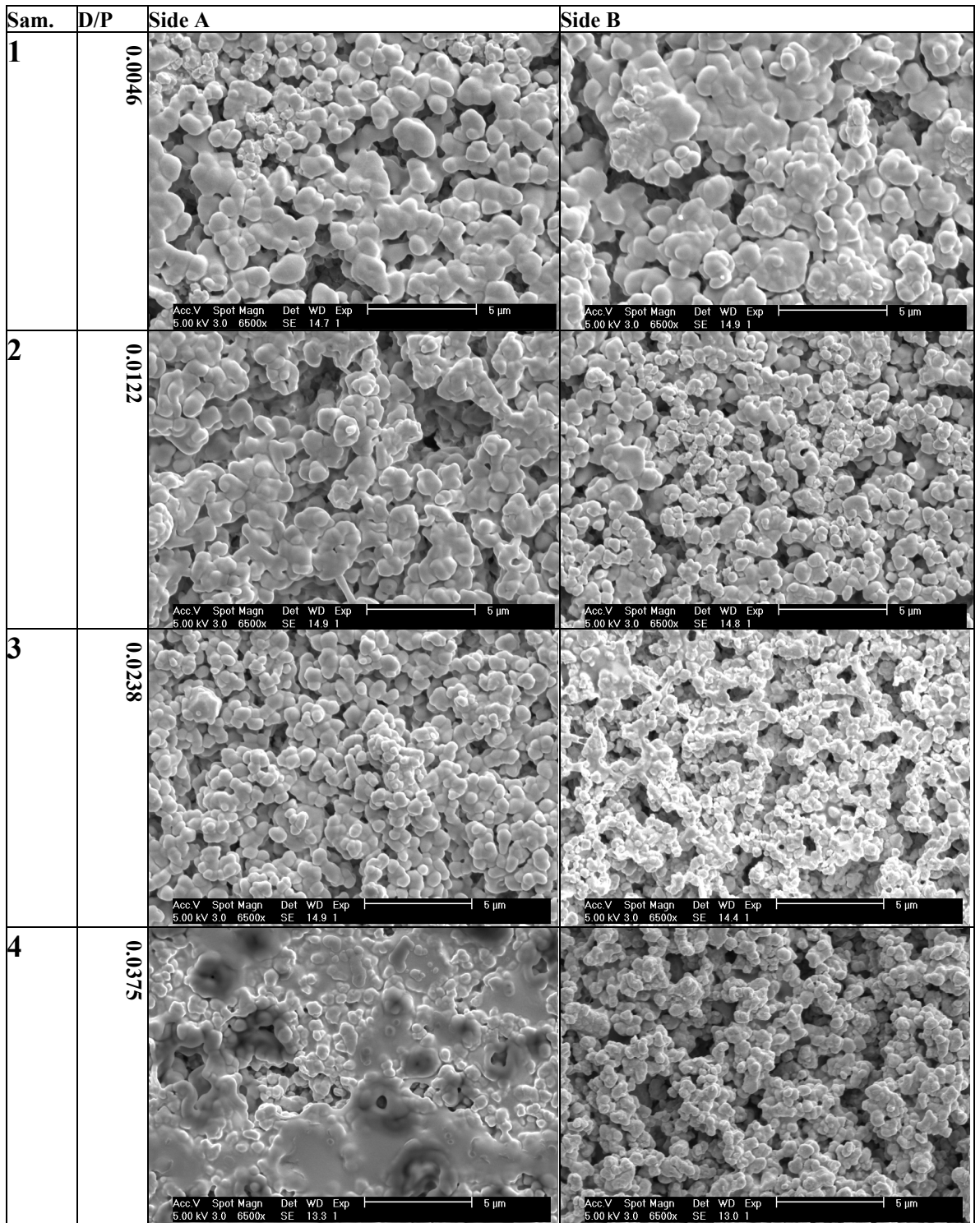


Fig. 104: Variation of the microstructure of the green tapes produced with different amount of dispersant.

Fig. 105 shows a high magnification of the particle surfaces after the burnout of the organics. The sample milled with 0.0046 dispersant ratio had primary particles

clustered to form bigger particles, while the sample milled at higher dispersant concentration, 0.0238, exhibited free primary particles.

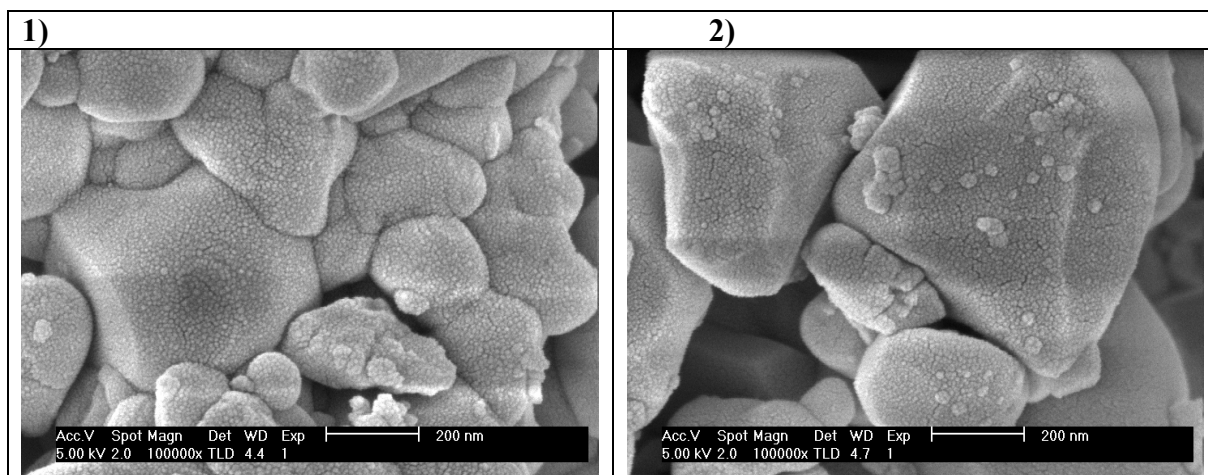


Fig. 105: High magnification micrographs of the particle surfaces after the organic burnout. 1) Tape 1 milled with 0.0046 dispersant ratio. 2) Tape 3 milled with 0.0238 dispersant ratio

6.5.2.1.7 Evaluation of the binder (PVA) absorption onto the particles surface

Fig. 106 plots the percentage of binder absorbed onto the particle surface and the maximum particle size observed in each sample (see table Table 38).

Expressed as a percentage of the amount added to the slip, the percentage of binder absorbed was evaluated by subtracting the free amount of binder found in the slurries before casting from the amount originally added.

The PVA adsorbed increased from 43.1% of sample 1 (0.0046 dispersant ratio) to 66.7% and 71.9% respectively of samples 2 and 3 (0.0122 and 0.238 dispersant ratio). The absorbed amount decreased to 44.4% for sample 4 prepared with 0.0375 dispersant ratio.

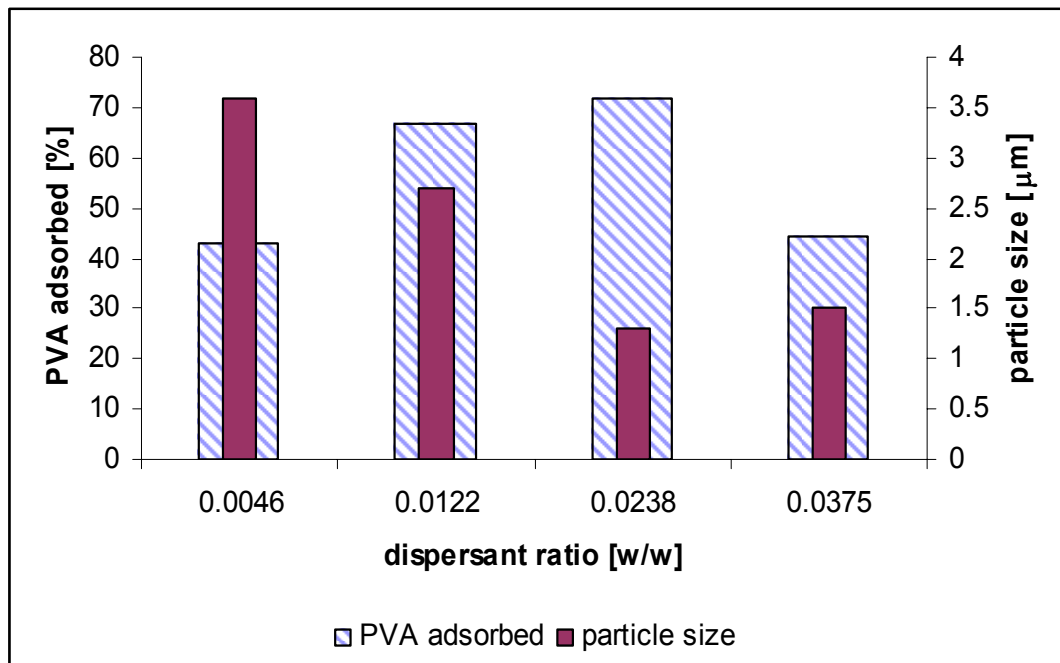


Fig. 106: Plot of PVA adsorbed and particle size versus dispersant concentration

6.5.2.2 Route 2: study on the effects of the dispersant amount on the suspension stabilisation

Samples were prepared according to Route 2 as explained in details in the Method section at page 159. In the following pages, the detailed results achieved for 2 of the experiments conducted

6.5.2.2.1 The steady shear rheology

All the slurries, both before and after the addition of the organic ingredients, showed pseudoplastic behaviour. Fig. 107 shows the viscosity for the slurries, before the organics addition for the samples at the lowest powder concentration.

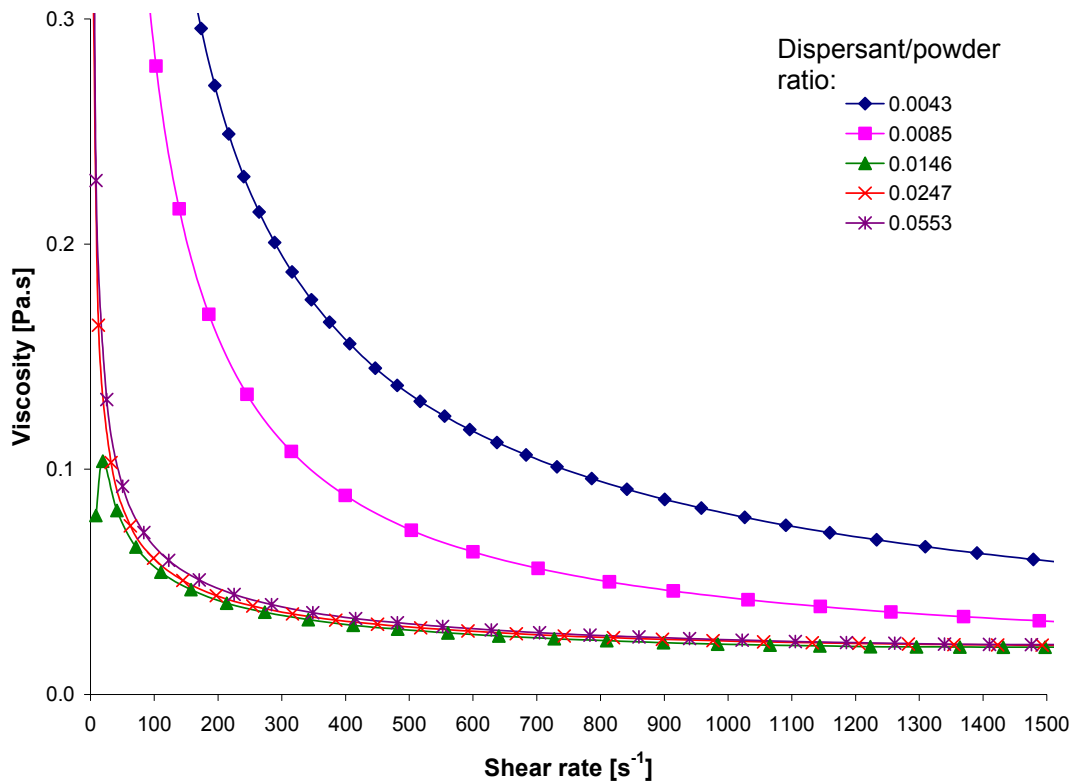


Fig. 107: Viscosity profiles of slurries without binder (samples NB). The dispersant was varied between 0.4% and 5.5%

The parameters obtained by fitting the viscosity curves with the Casson model and the relative correlation coefficient R^2 are listed in Table 39 and plotted in Fig. 108.

Generally, the correlation coefficient R^2 was close to 1. It can be noted that the R^2 was lower for

- samples B, containing the organic phase, and dispersant ratios in the range of 0.0146 and 0.0247,

- samples NB, slurries without binder system, with dispersant ratios between 0.0043 and 0.0085.

As observable in Fig. 108(1), the yield stress s_0 increased by increasing the powder concentration. This could be observed by comparing the dashed lines for samples without binder, samples NB at 73 and 82.5 w% powder content and the continuous lines for samples B with powder content of 62 and 68 w%.

In the case of samples NB, at 73% powder concentrations, the value of the Casson yield stress decreased from 18.9 to 1.1 Pa when the dispersant ratio increases from 0.0043 to 0.0146. For further additions the yield values remained almost constant. Similarly, in the case of samples NB with 82.5% powder content, the yield stress s_0 decreased up to 1.1 Pa, reached for 0.0247 dispersant amount. A further addition of dispersant up to 0.0553 ratio gradually increased the yield stress value to approximately 2.0 Pa.

The trend of the yield stress for samples B, containing binder system, is observable in Fig. 108(1) following the continuous curves. In this case, the yield stress increased its value. The maximum values of these curves were found at 0.0146 and 0.247 for the 62 and the 68 w% samples respectively. The maximum values in both cases coincided with the minimum values for the samples NB.

In Fig. 108(2) the trends of the plastic viscosity (κ) are observable.

Typically, the plastic viscosity value increased with the powder content.

κ was also higher for samples B with the organic phase rather than for the samples NB with no binder system. This is noticeable comparing the continuous lines with the dashed lines on the graph.

The plastic viscosity for samples with no binder system (samples NB) decreased to a minimum at 0.0146 dispersant ratio, for both powder concentration.

Also, in case of samples B with binder system at both the powder concentrations, the plastic viscosity had a minimum for 0.0146 dispersant concentration.

	no binder NB						Binder B					
Powder [w%]	73%			82.5%			62%			68%		
	s_0	κ	R^2	s_0	κ	R^2	s_0	κ	R^2	s_0	κ	R^2
Disp/powder ratio	[Pa]	[Pa.s]		[Pa]	[Pa.s]		[Pa]	[Pa.s]		[Pa]	[Pa.s]	
0.0043	18.9	0.2	0.9353	35.4	0.01	0.9403	3.2	0.4	0.9992	9.5	2.0	0.9791
0.0085	11.3	0.1	0.9167	77.6	0.04	0.6967	3.4	0.7	0.9996	3.8	4.4	0.9592
0.0146	1.1	0.01	0.9982	4.9	0.02	0.9974	28.9	0.3	0.7584	16.4	2.2	0.9808
0.0247	1.3	0.01	0.9991	1.1	0.03	0.9998	20.8	0.6	0.7510	58.5	3.8	0.8235
0.0553	1.5	0.01	0.9986	2.0	0.03	0.9998	0.2	0.7	0.9998	3.5	4.4	0.9573

Table 39: Parameters and correlation coefficient for the fitting of the viscosity profiles of samples prepared with Route 2 with the Casson model

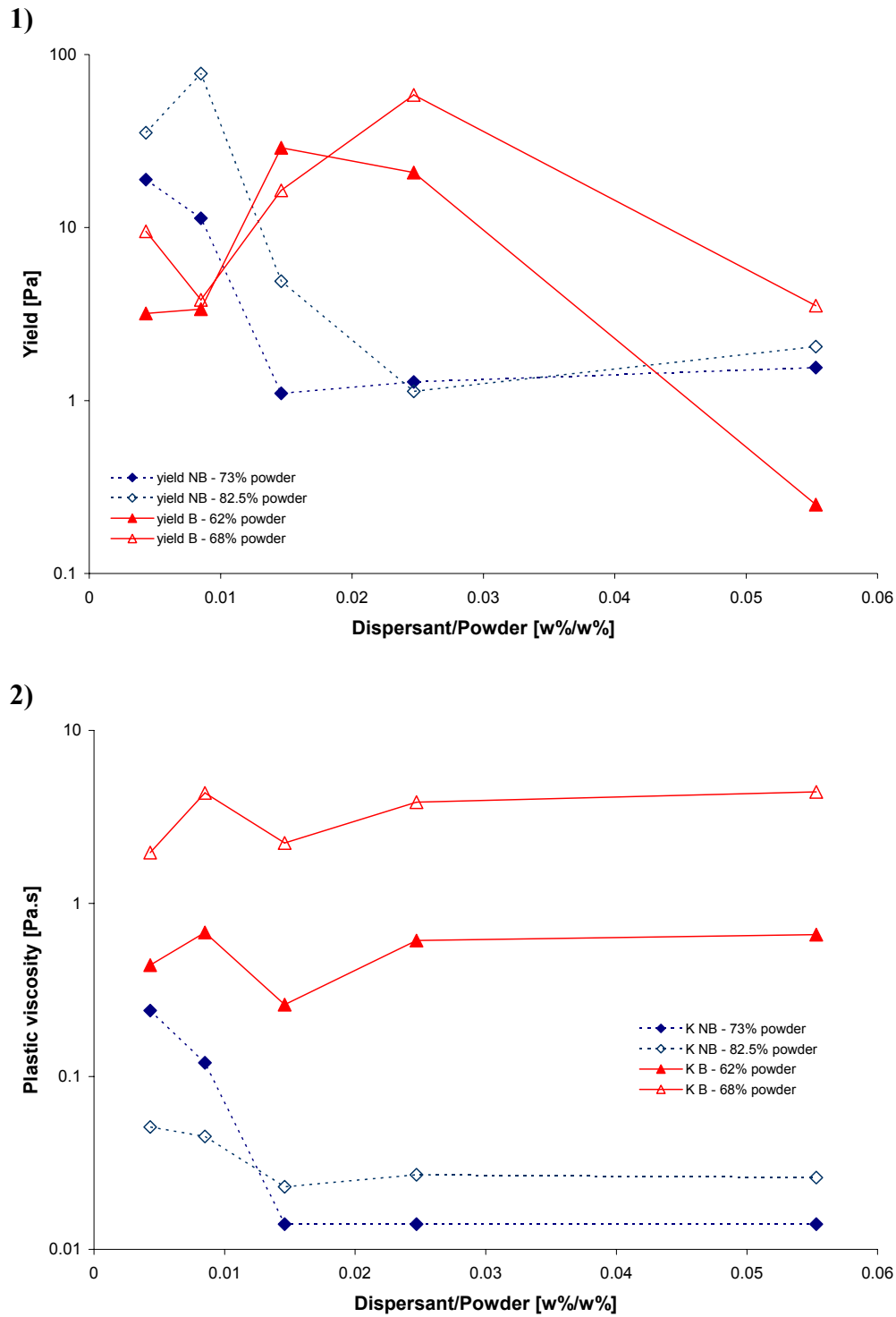


Fig. 108: Parameters obtained by fitting the viscosity profiles with the Casson Model: 1) Yield (s_0), 2) Plastic viscosity (κ)

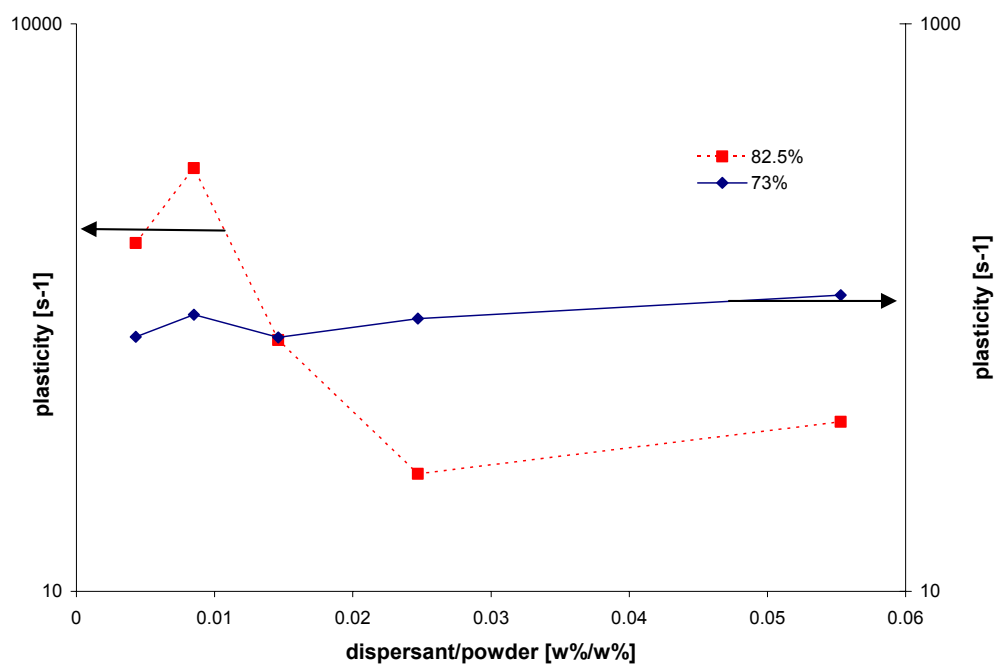


Fig. 109: Variation of plasticity with dispersant amount for samples NB

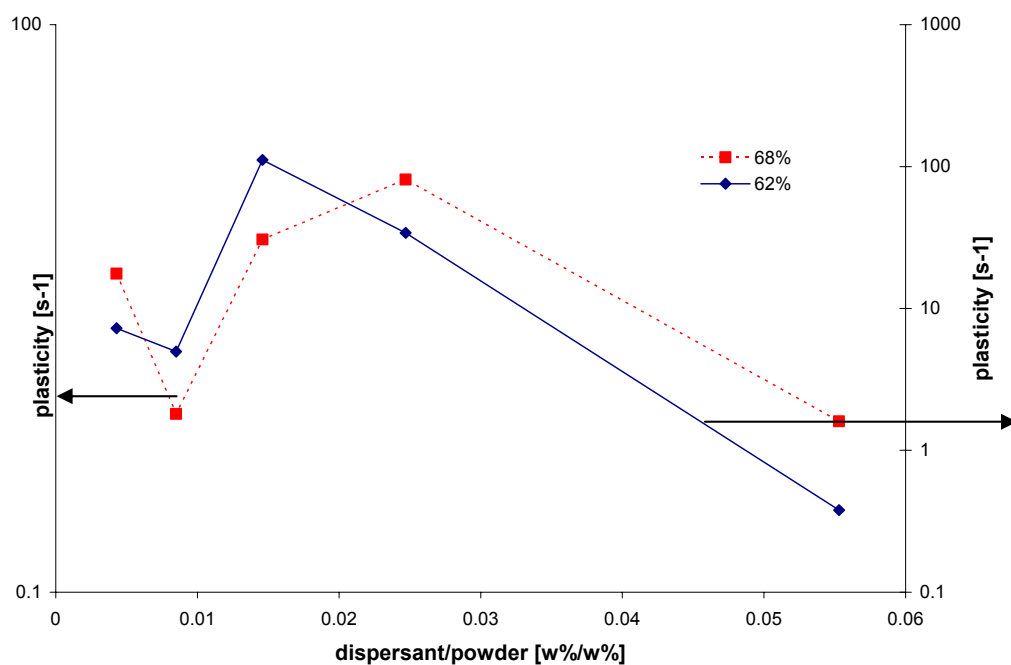


Fig. 110: Variation of plasticity with dispersant amount for samples B

Fig. 109 and Fig. 110 plot the plasticity as calculated for the ratio yield stress above plastic viscosity from the data in Table 39.

In the case of the binderless suspensions, the plasticity was the lowest in correspondence of the 0.0146 and 0.0247 dispersant ratio for the 73% and the 82.5 % powder content respectively. When the binder was added the trend was inverted. In fact, for the same dispersant amounts, i.e. 0.0146 and 0.0247, the curves showed a maximum instead of the minimum.

In addition, while the plasticity increased with powder content in the case of the binderless slurries, the samples with lower powder content had higher plasticity when the binder was added.

6.5.2.2.2 The viscosity and the green density trends

Table 40 summarizes the rheological and green density data collected for each samples.

Samples NB		Samples B			Samples NB: without binder system	Samples B: with binder system	
Approximate Powder content		Approximate Powder content		Disp./pow der ratio	Viscosity (20 s ⁻¹)	Viscosity (20 s ⁻¹)	Green Density
[w%]	[vol%]	[w%]	[vol%]	[w%/w%]	[Pa.s]	[Pa.s]	[g.cm ⁻³]
73	25	62	15	0.0043	2.8	2.8	3.5
				0.0085	2.0	3.5	3.1
				0.0146	0.9	11.8	2.6
				0.0247	1.5	10.6	2.8
				0.0553	2.5	1.2	2.8
83	37	68	21	0.0043	15.9	5.6	3.6
				0.0085	4.8	5.8	2.8
				0.0146	1.3	8.0	2.7
				0.0247	0.2	20.1	2.7
				0.0553	0.4	5.7	2.7

Table 40: Viscosity data of slurries prepared according Route 2 and green density values.

Fig. 111 and Fig. 112 show the trends of the viscosity with dispersant content. The values reported were measured at 20 s⁻¹.

As it can be observed, for both the formulations with final powder volume of 15 and 21%:

- The viscosities of the slurries with no organic phase showed a progressive decrease to a minimum followed by a subsequent increase with increasing dispersant content.
- The viscosity of the slurries containing binder showed an opposite trend. The viscosity increased with increased dispersant content a progressive increase of the values with increasing dispersant. A peak viscosity was reached at 0.0146 and 0.0247 dispersant ratio respectively for the slurries at 15 and 21% volume of powder. These corresponded to the dispersant contents at which a minimum viscosity was observed for the binderless slurries.

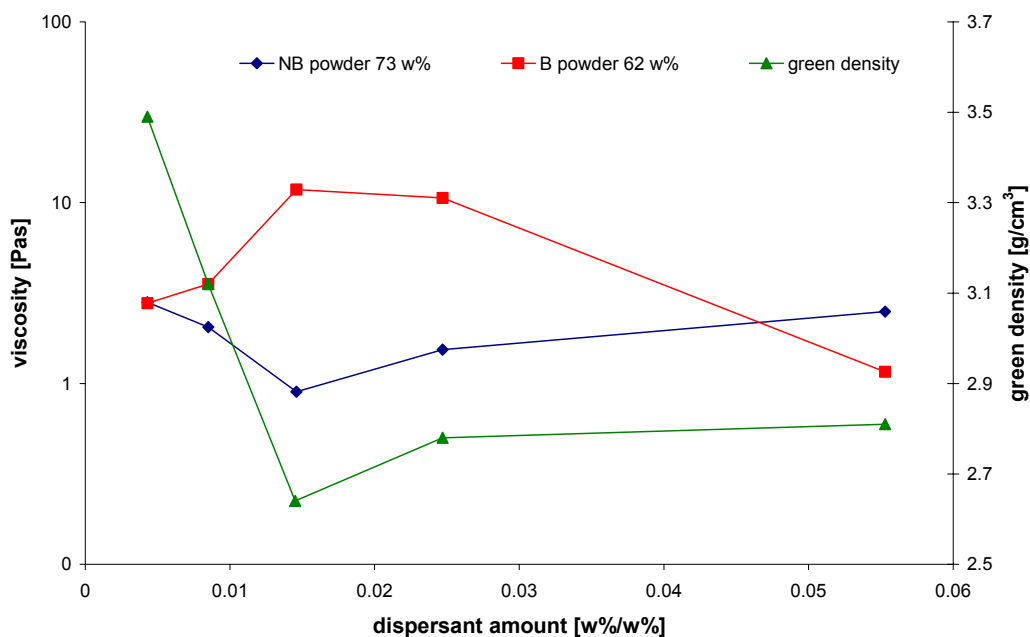


Fig. 111: Viscosity trends (at 20 s^{-1}) for slurries prepared according to Route 2 at the lowest powder content, associated with green density figures

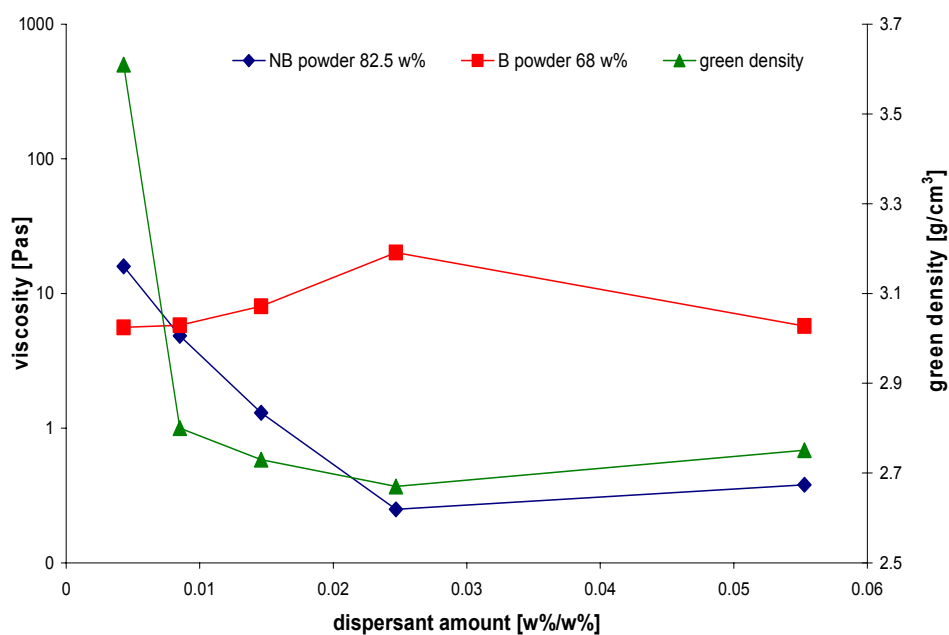


Fig. 112: Viscosity trends (at 20 s^{-1}) for slurries prepared according to Route 2 at the highest powder content, associated with green density figures

The points of discontinuity, i.e. minimum for the ‘no organics’ slurries and maximum for the ‘organics’ slurries, were in correspondence of 0.0146 dispersant/powder ratio for the slurry at 15% volume powder content. For the slurries at final 21 vol % powder content were shifted to 0.0247.

As the forming mechanism was different than the tape casting and the samples couldn't be de-aired before casting, the absolute value of green density was taken as purely indicative. More attention was paid to the trends of green density across the series.

The green density of the samples cast into plastic moulds follows a similar trend as the viscosity when no binder is added. This is observable both in Fig. 111 and Fig. 112. The green density reached a minimum, i.e. 2.6 g.cm^{-3} at 0.0146 dispersant ratio for the 15% powder volume. Similarly, the minimum green density, i.e. 2.7 g.cm^{-3} , was obtained at 0.0247 dispersant content for the 21% of powder volume.

The maximum green densities, i.e. 3.5 and 3.6 g.cm^{-3} , were achieved in both cases with the slurries prepared with 0.0043 dispersant ratio.

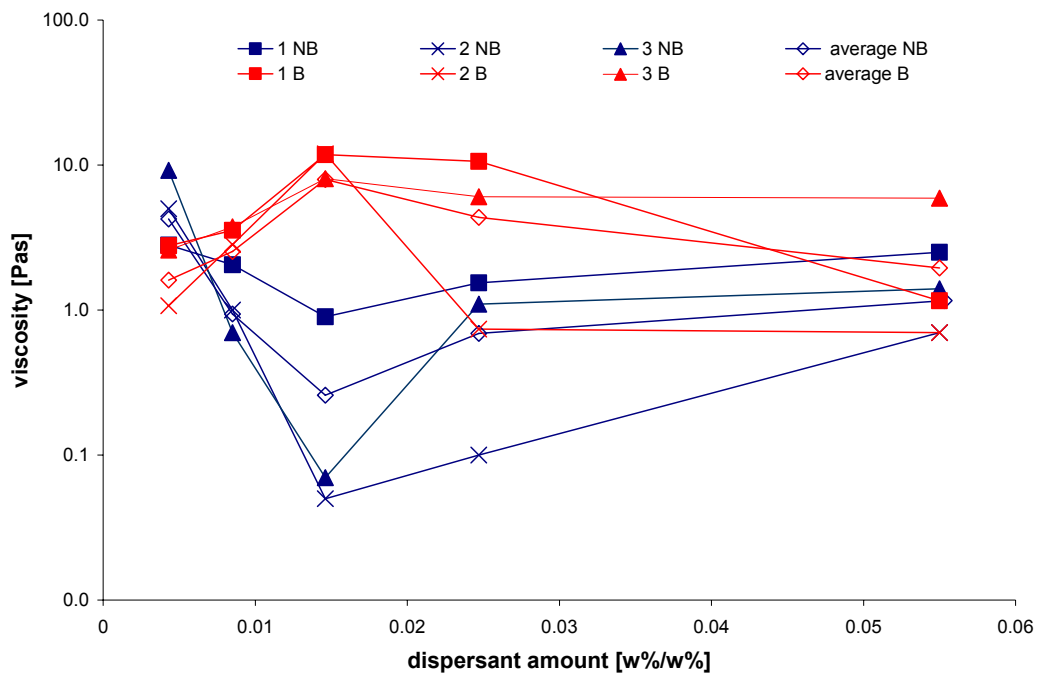


Fig. 113: Comparative graph reporting the trends for binderless samples (blue) and samples with binder (red) of the three experiments performed at the lowest powder content (final amount = $62 \pm 3\%$).

Fig. 113 shows the viscosity trends obtained for the three experiments performed at the lowest powder concentration ($62 \pm 3\%$). It can be noted that the profiles were coherent with discontinuity points coincident with 0.0146 dispersant amount.

6.5.2.2.3 The oscillatory rheology

Table 41 reports data gathered with oscillatory measurements: the elastic modulus in the linear viscoelastic region (G'_{\max}) and the elastic modulus (G') measured at 1.13 Hz in the frequency sweep within the linear viscoelastic region.

Samples NB		Samples B		Disp./pow. ratio	Max elastic modulus in LVR (G'_{\max})	Elastic modulus at 1.13 Hz (G')	Viscosity (20 s^{-1})
[w%]	[vol%]	[w%]	[vol%]		[Pa]	[Pa]	[Pa.s]
73	25	62	15	0.0043	7	7	2.8
				0.0085	74	162	3.5
				0.0146	374	257	11.8
				0.0247	215	213	10.6
				0.0553	39	62	1.2
83	37	68	21	0.0043	25	223	5.6
				0.0085	218	894	5.8
				0.0146	257	1120	8.0
				0.0247	468	987	20.1
				0.0553	108	350	5.7

Table 41: Rheological parameters obtained with oscillatory tests on samples B prepared with Route 2

As shown in Fig. 114 and Fig. 115, the trends of rheological data produced are similar to these of the viscosity data of the slurries with binder system, also reported on the graphs. The maximum values are coincident with 0.0146 and 0.0247 dispersant ratios for 15% vol. and 21% vol. respectively.

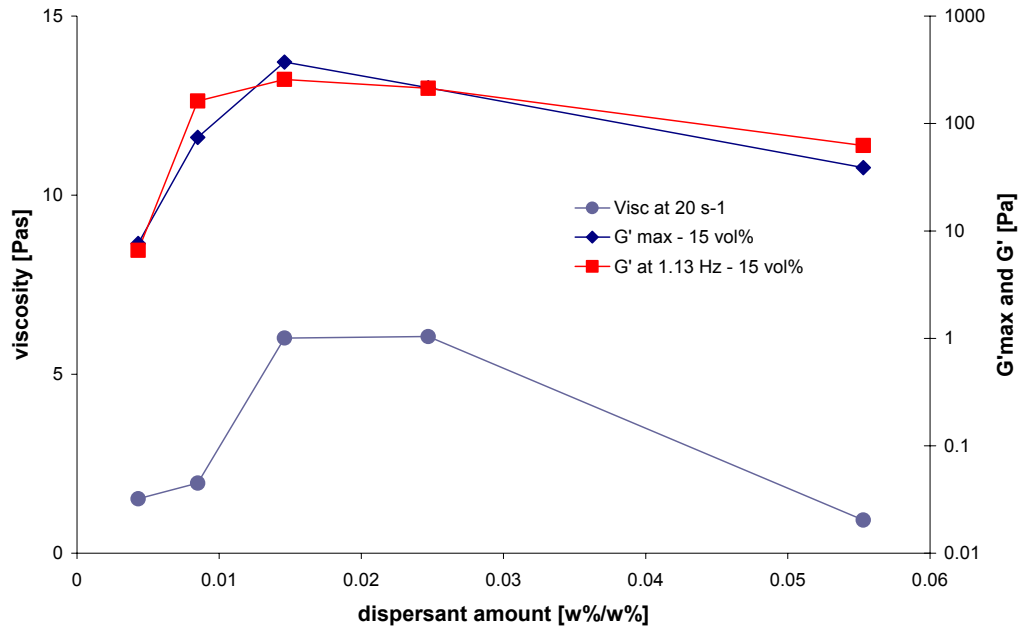


Fig. 114: Comparison of rheological figures of slurries containing the binder system (Samples B) prepared following Route 2 at 15% volume of powder

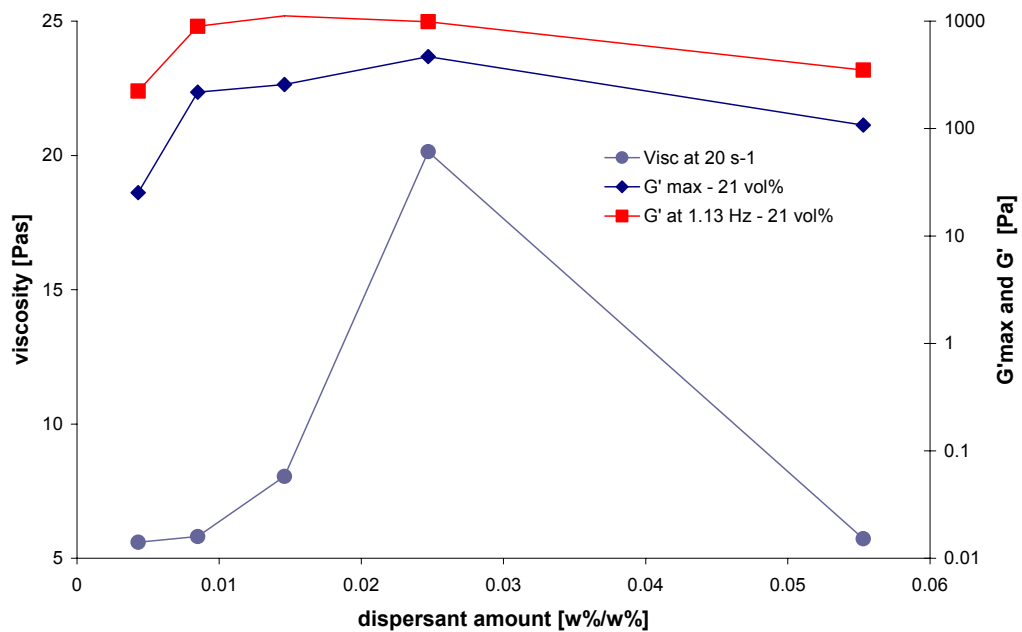


Fig. 115: Comparison of rheological figures of slurries containing the binder system (Samples B) prepared following Route 2 at 21% volume of powder

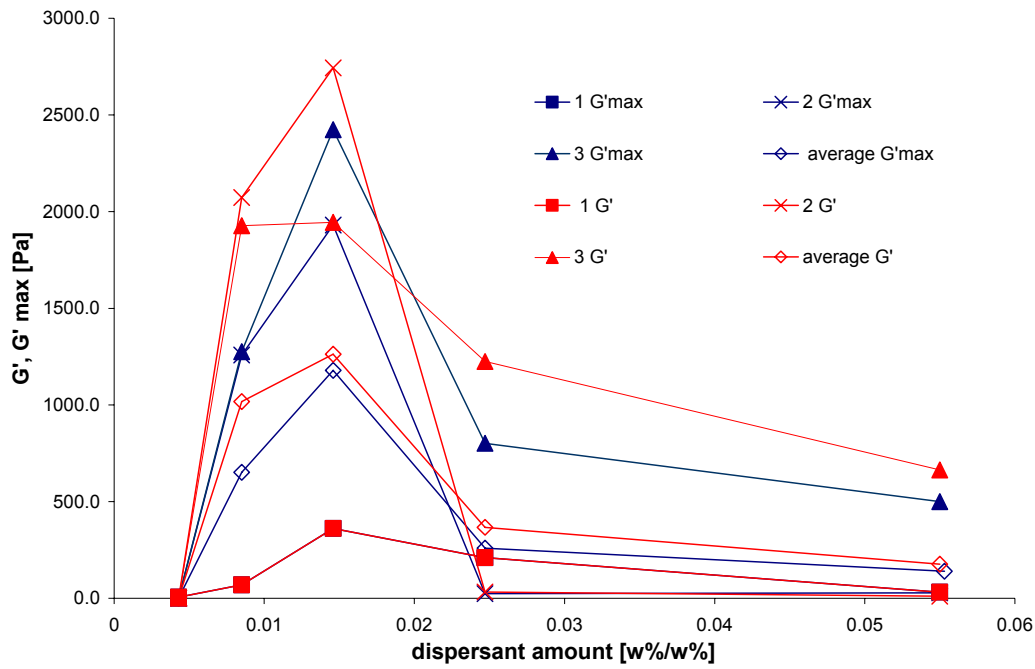


Fig. 116: Comparative graph reporting the trends for Elastic modulus (G') (red) and Max Elastic modulus (G'_{max}) (blue) of the three experiments performed at powder content $62 \pm 3\%$.

Fig. 116 shows the G' and G'_{max} trends obtained for the three experiments performed at the lowest powder concentration ($62 \pm 3\%$). It can be noted that, although the absolute values of the rheological parameter varied, the profiles were coherent with maximum points coincident with 0.0146 dispersant amount.

6.5.2.2.4 Time dependent rheological characteristics

The time-dependent viscosity of the slurries at 21% vol. powder concentration is shown in Fig. 117. The graphs show the profiles of the instantaneous viscosity when the shear rate was varied suddenly from 2 s^{-1} to 50 s^{-1} and vice versa.

Table 42 reports the values of the instantaneous viscosity at critical times. Firstly, at 2 s^{-1} , just before the increase in shear rate. Secondly, at 50 s^{-1} . Thirdly, again at 2 s^{-1} when the viscosity had stabilised. In addition, the recovery time, i.e. the time employed for the viscosity to regain an equilibrium value after the shearing, is reported for each slip. The last column of the table shows a thixotropy coefficient calculated by the rheometer software by integrating the area included between the viscosity curves obtained by sweeping ascending and descending the shear stress.

Disp/powder ratio	Instantaneous Viscosity at 2 s^{-1}	Instantaneous Viscosity at 50 s^{-1}	Instantaneous Viscosity at 2 s^{-1}	Recovery time	Thixotropy Coefficient*
	[Pa.s]	[Pa.s]	[Pa.s]	[s]	[Pa/s]
0.0043	3.8	0.6	4.1	32	26
0.0085	4.4	0.9	4.5	22	38
0.0146	14.2	0.8	5.3	27	68
0.0247	12.6	1.0	6.9	64	705
0.0553	1.3	0.7	1.4	21	47

*calculated for the curves shear stress vs. shear rate

Table 42: Data of the step shear experiments for slurries prepared as in Route 2 at 21% powder in volume

The time dependent viscosity profiles for the slurries at 21% volume of powder are illustrated in Fig. 117.

The slurries with the lowest dispersant content, i.e. 0.0043 and 0.0085, showed little or no evidence of thixotropy. The viscosity value recuperated in 20 - 30 seconds after the high shear was removed. The same can be said for the slurry with the highest dispersant ratio (0.0553).

In contrast, if the dispersant concentration was intermediate, i.e. 0.0146 or 0.0247 ratios, the viscosity showed a component of thixotropy. If the recovery of the viscosity at the removal of the high shear was fast, the high viscosity values obtained before the strong shearing were not recuperated completely. Moreover, during the first constant shearing at 2 s^{-1} , the viscosity was not constant, but it decreased progressively with time.

As shown in Fig. 118, both the recovery time index and the thixotropy coefficient agree in indicating the slurry with 0.0247 dispersant ratio as the more thixotropic. The thixotropy indexes increased progressively up to a maximum in correspondence of 0.0247 dispersant ratio, and it was reduced substantially for further additions of dispersant.

Results

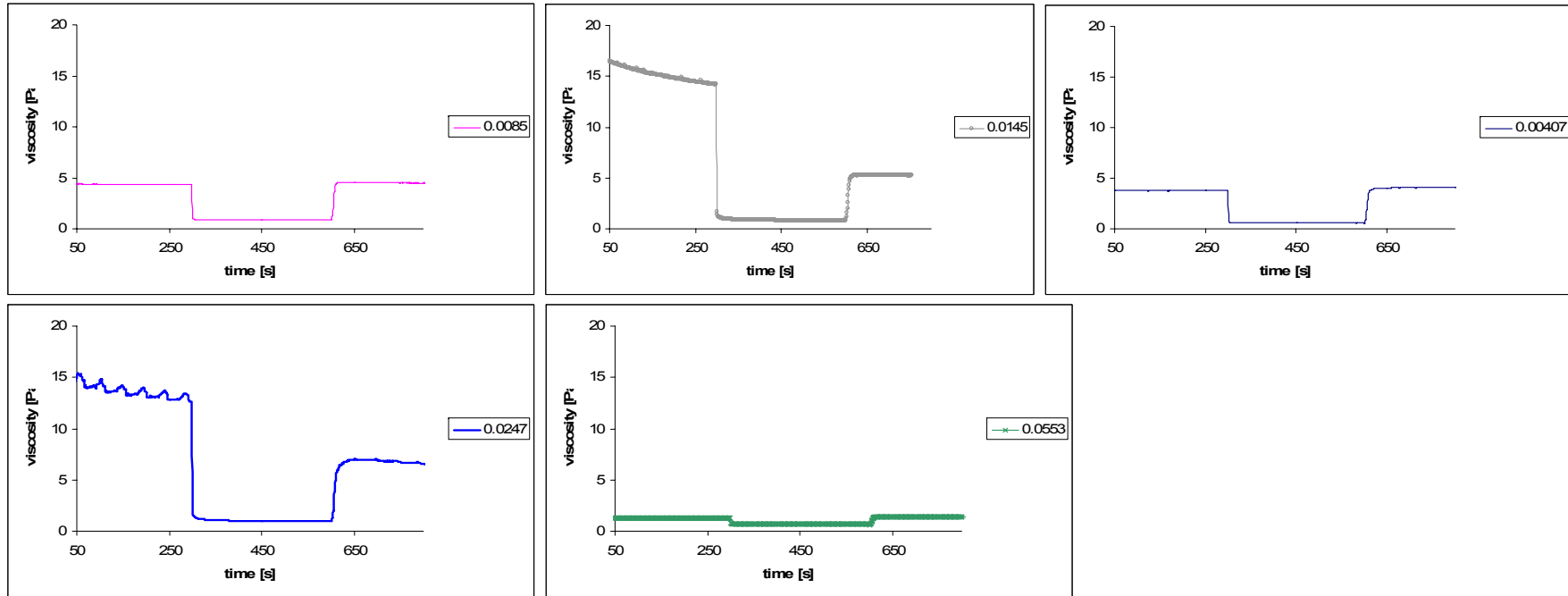


Fig. 117: Time-dependent behaviour for the slurries at 21% vol. powder content, tested at 2 and 50 s⁻¹ shear rates

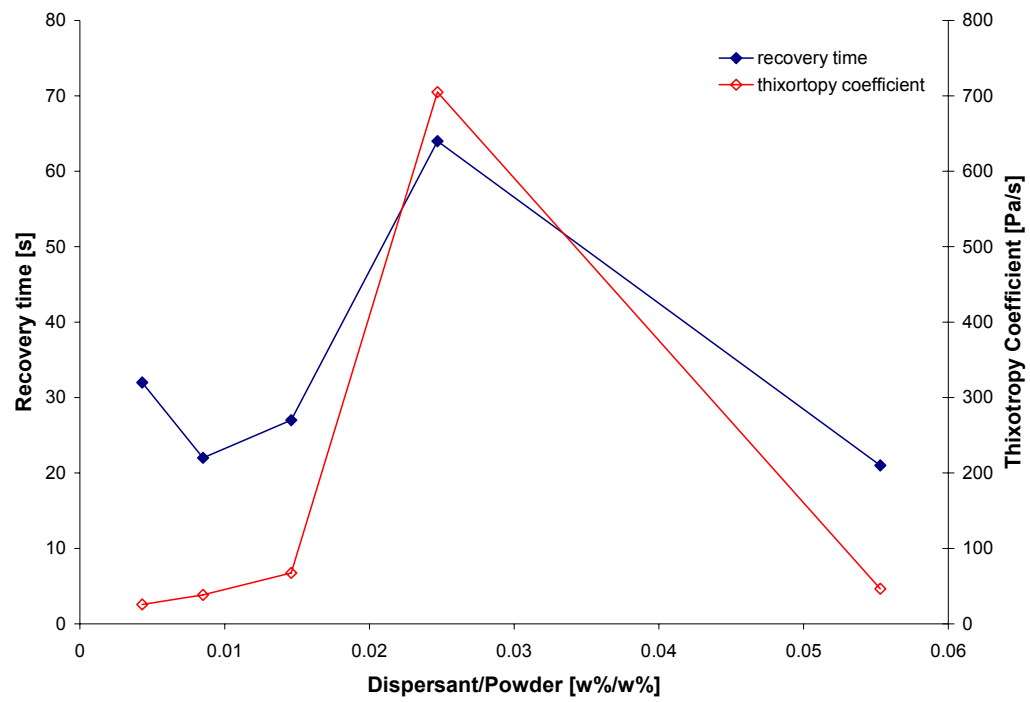


Fig. 118: Recovery time and thixotropy coefficient trends for the slurries at 21% volume of powder

6.5.2.2.5 The distribution of the binder system

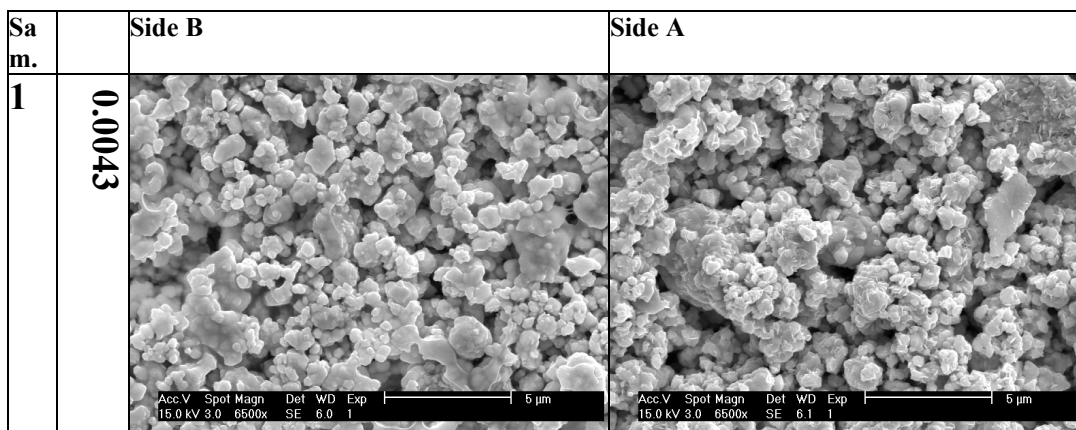
In Fig. 119 the images of the green bodies obtained by casting the slurries (samples B) with 21% volume of powder into plastic moulds. The relative green densities are reported in Fig. 112. The images were evaluated qualitatively to provide information on the binder distribution. As the forming mechanism was different than the tape casting and the samples couldn't be de-aired before casting, the absolute value of green density and the evaluation of the packing were taken purely as indicative. More attention was paid to the trends of green density, packing, porosity and binder distribution across the series.

The more uniform binder distribution was obtained for the sample with the least amount of dispersant, i.e. 0.0046. On the two surfaces the amount of visible binder was similar. On both surfaces agglomerates were visible, some of them 3-5 μm large.

With an increase in the dispersant amount up to 0.0085 and 0.0146 the difference between the binder amount on the top and the bottom of the samples increased. The lower side was richer in binder system. On the top surface agglomerates were visible with dimension in the range of 0.25- 4 μm .

At 0.0247 dispersant amount, apparent amount of binder appeared reduced on both sides. Almost negligible amount of free binder was visible on the lower side of the sample. In addition the agglomerates on both sides appeared reduced in size and more uniformly distributed. Larger pores were visible on the carrier side of this sample than in the rest of the series.

A further increase in dispersant created a huge difference in the binder distribution. The lowest side of the sample was almost continuously characterised by free binder which interconnected the particles. On the top, the evident binder amount was reduced. However, the top surface appeared slightly richer in binder than the sample with 0.0247 dispersant amount.



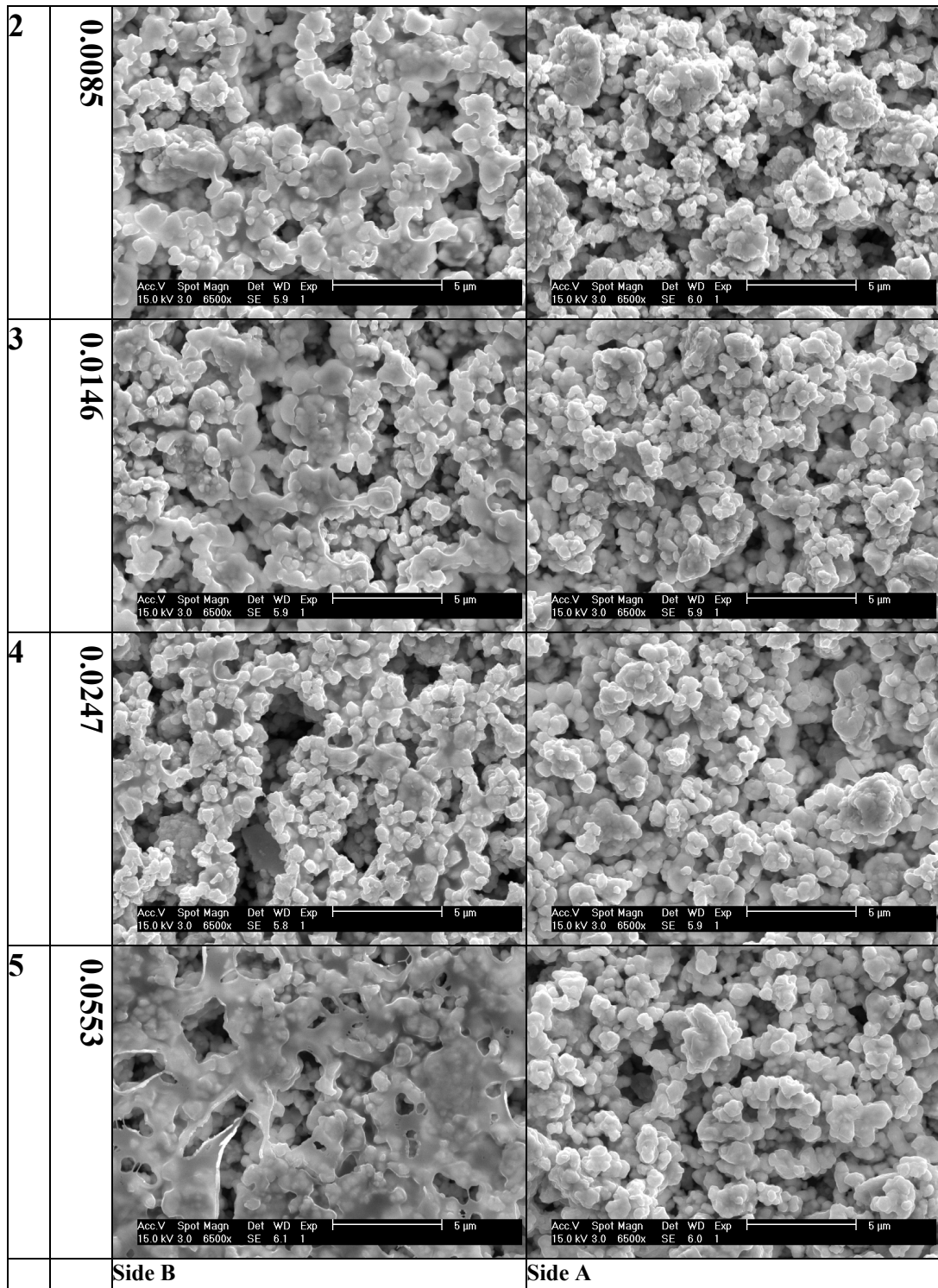


Fig. 119: SEM pictures of the green bodies as cast into plastic moulds. Side B was the lower side of the green body, in contact with the mould. Side A was the free to air surface

6.5.2.3 The effect of the binder/plasticizer ratio and the powder content

Slurries were prepared according Route 1 as explained in details in the Method section at page 161. These experiments aimed to evaluate the influence of both the binder/plasticizer ratio and the powder concentration on the tape cast.

For all the slurries, the ceramic powder was milled in presence of the same amount of dispersant. After the addition of the wetting agent, different amounts of binder and plasticizer were added and milled.

As explained in the method section 6.5.1.2, the recipes were formulated in order to vary two parameters:

- The total powder amount
- The ratio binder/plasticizer

The green tapes's microstructures were observed with the SEM microscope before and after the burnout of the organics.

6.5.2.3.1 The green density and the samples microstructure

The green density figures, relative to the tapes, are reported in Table 43.

	Powder	Plasticizer/binder	Binder/powder	Green density
Tape	[w%]	[w%/w%]	[w%/w%]	[g.cm ⁻³]
1	64.0	1	0.03	2.9
2	72.2	1	0.03	3.1
3	72.2	2	0.03	3.2
4	64.0	2	0.03	3.1

Table 43: Green density figures of the tapes obtained varying plasticizer and powder contents

The green densities of the tapes vary from a minimum of 2.9 g.cm⁻³, approximately 35.5% of the theoretical density, obtained for sample 1, to a maximum of 3.2 g.cm⁻³, approximately 39.4% of the theoretical density, for sample 3. The total maximum variation was about 4% of the theoretical density.

In Fig. 120 the microstructure of the free to air side, side B, of the as cast tapes obtained by varying the plasticizer and the powder amounts are shown. In Fig. 121 the microstructures of the tapes's sides B after the burnout of the organics are shown.

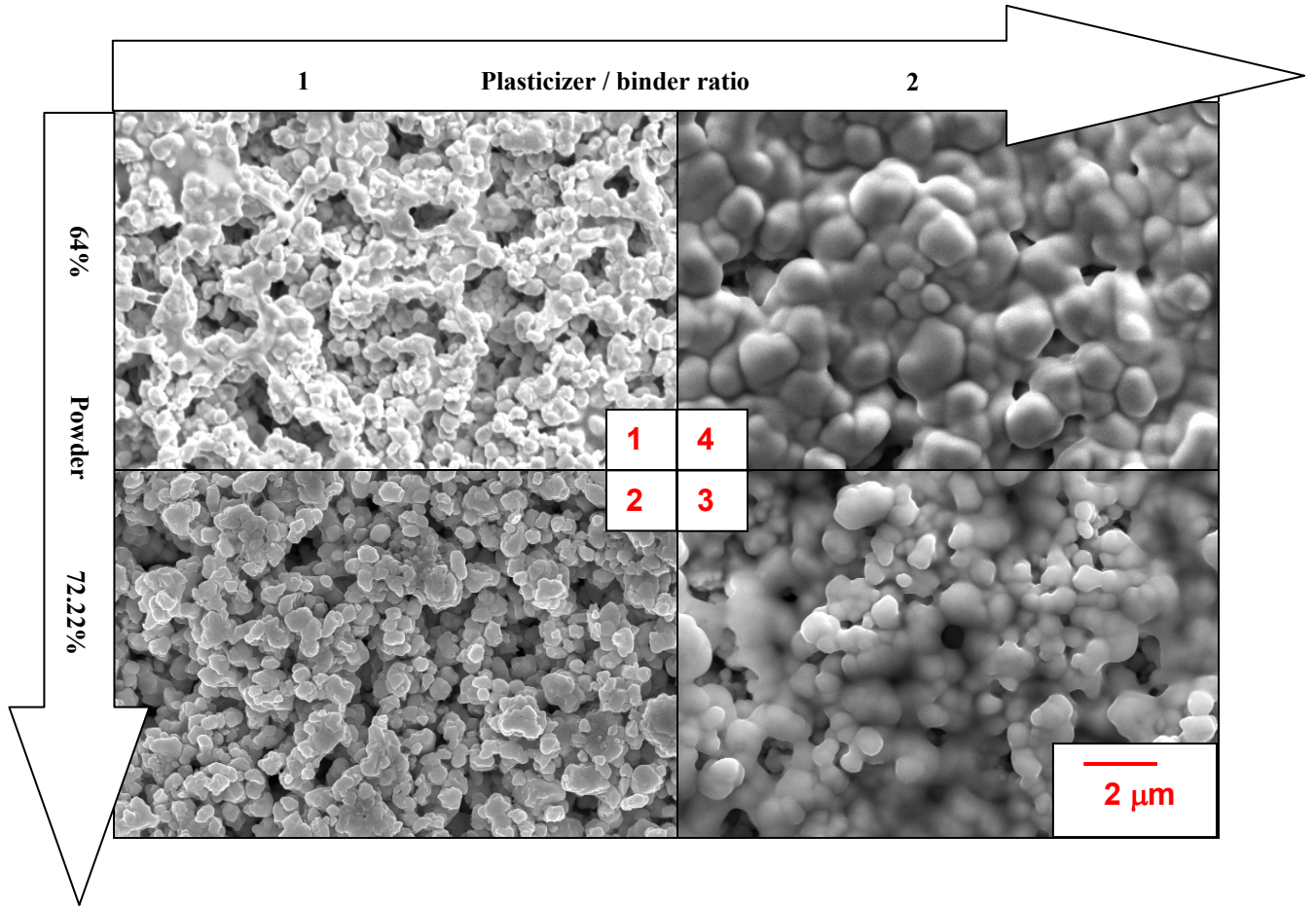


Fig. 120: Microstructure of green tapes produced varying the powder and the plasticizer content

In both tape 1's and tape 2's pictures the organic phase was less evident than in sample 3 and 4. Both sample 1 and 2 showed porosities several microns large. The polymeric phase in sample 1 appeared less homogeneously distributed than in sample 2, with traces of organic phase linking the particles. Sample 3 and 4 showed a relatively denser microstructure with smaller pores. The organic phase covered homogeneously the particles with a layer of polymer. Both samples show agglomerates; sample 4's agglomerates are bigger than sample's 3.

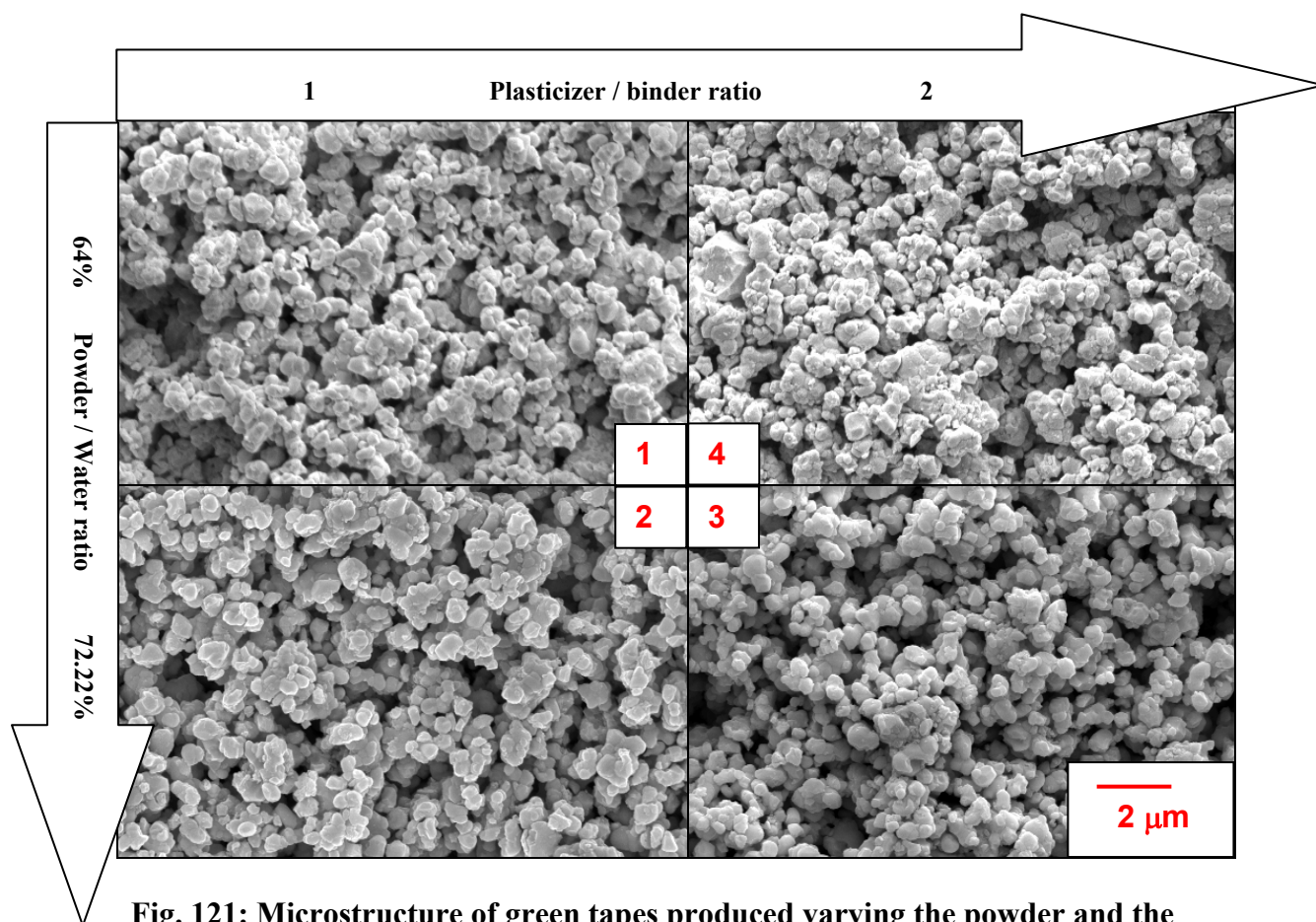


Fig. 121: Microstructure of green tapes produced varying the powder and the plasticizer content, after the organic burnout

The microstructures of the four cast tapes after the organics have been removed didn't show appreciable differences. All the samples showed pores surrounded by several particles.

6.5.2.4 The effects of the drying conditions

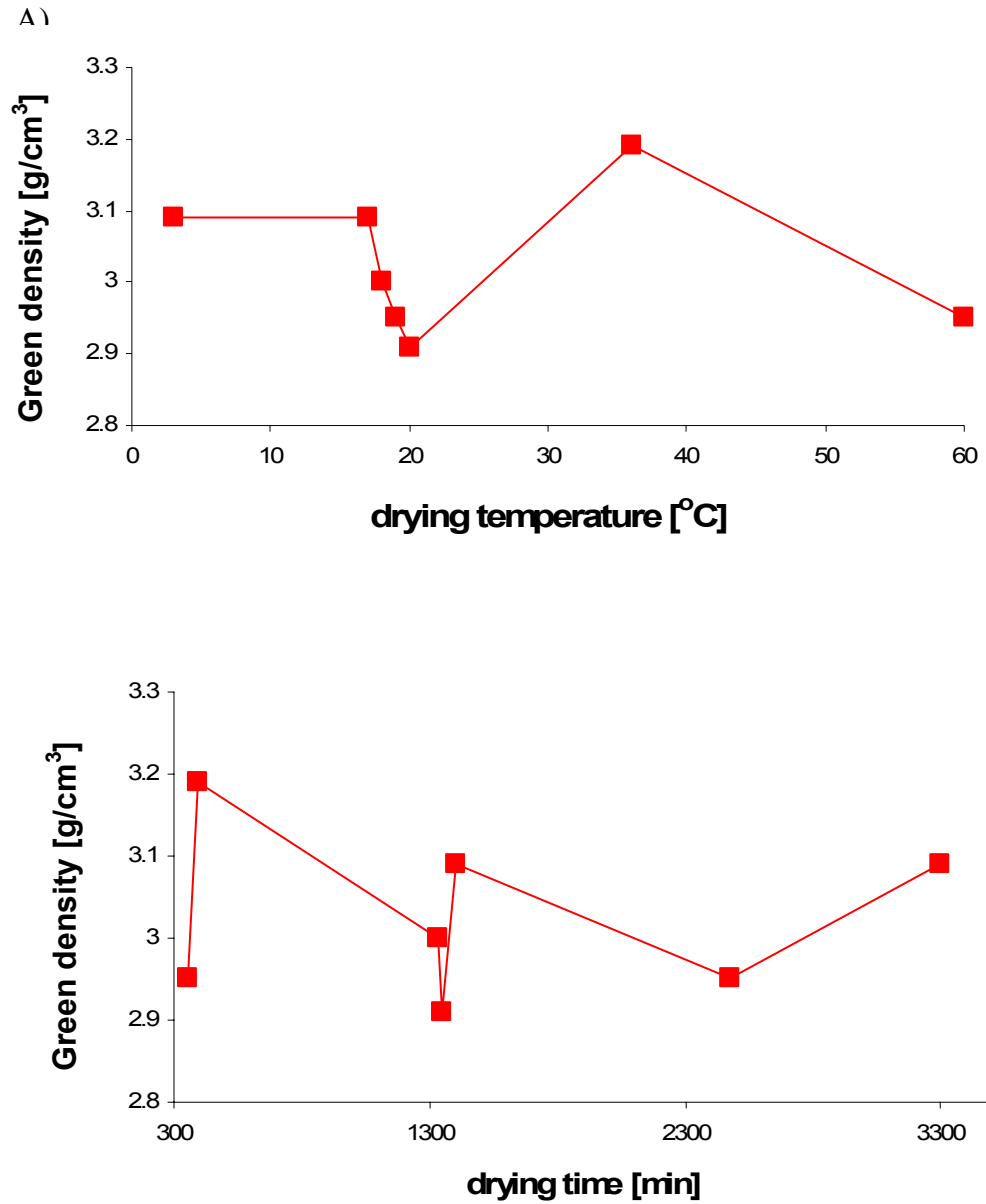
In order to evaluate the influence of the drying conditions on the tape cast green density, a slurry was prepared according Route 1, as explained in details in the experimental method session at page 78. It was then cast into plastic moulds and left to dry under various conditions of temperature, humidity and air flow. The sample's final green density and drying time are reported in Table 44.

Conditions			Results	
Temperature	Humidity	Flowing air	Drying time	Green density
	[%]		[min]	[g.cm ⁻³]
3	< 50	No	3300	3.1
17	75	Yes	1400	3.1
18	76	Yes	1335	3.0
19	82	No	2475	2.9
20	73	No	1350	2.9
36	< 50	No	395	3.2
>>50	n/a	No	355	2.9

Table 44: Green density and drying time figures of tapes

The green densities of the tapes vary from a minimum of 2.9 g.cm⁻³ was obtained for the sample dried in 1350 min at 20°C and 73 % of humidity. This green density was approximately 35.6% of the theoretical density. The maximum green density achieved was 3.2 g.cm⁻³, corresponding to approximately 39.0% of the theoretical density. This green density was obtained in 395 minutes drying time at 36°C in a very dry condition.

The total maximum variation was approximately 3.4% of the theoretical density. In Fig. 122 the green densities achieved were plotted against drying temperatures and drying times.



B)

Fig. 122: Green densities achieved with different drying conditions. A) Green density plotted against drying temperature. B) Green density plotted against drying time.

7 Discussion of the product focused approach

The laboratory process studied in this work was designed to produce thin wafers of pyroelectric ceramic for electronic devices by using the tape casting technique. This production route presented an alternative to the one commonly used in the manufacture of ceramic sensors. The most used processing technique makes use of sawing and lapping to obtain thin, flat wafers from a bulk material sintered by hot pressing. The original laboratory scale process, described in details in the Experimental Method, had previously demonstrated its capability to deliver operating sensors on a laboratory scale [Navarro, 2001].

As explained in the Methodology chapter at page 66, the experimental work herewith discussed was carried out in the context of the development of the scale-up of this ceramic process.

Two parallel approaches to the scale-up have been adopted to provide a more holistic view of the process, as suggested by the concurrent engineering approach to the design:

- A process-focused approach was taken which evaluated the potential threats posed to the development into an industrial scale. The results of this approach are described and discussed in the section Process Analysis and will not be treated in this chapter.
- At the same time, the work carried out with a product-focused approach assessed and improved the quality of the product (i.e. the ceramic wafer) in the light of the industrial requirements. This latter focus led to an in-depth investigation of the ceramic characteristics and of the processing techniques. The study was conducted through consecutive loops of conceptual and definitive design phases (see Methodology section, page 69). This chapter discusses the results, reported in section 1, obtained during this investigation.

7.1 The Conceptual Design Phase I: study of the factors which influence the sintered ceramic microstructure

The first step in the product focused approach was to assess the product characteristics and to compare them with the product specifications provided by the electronic industry.

A special concern was caused by the high rate of ceramic fracturing. The 95% rate of the wafers breaking during handling or processing, was evaluated as a high impact threat for a satisfactory process yield. This was especially in consideration of the highly stressful operations that the material typically undergoes for the creation of infrared devices, such as poling, jig clamping or dicing. Consequently, the efforts in the product focused approach herewith described were directed to the understanding and to the elimination of the causes underpinning the low strength.

7.1.1 The sintered material characterisation

An analysis of the characteristics of the wafers produced by the original process highlighted several factors which could have underpinned the lack of adequate strength. The data about the characterisation of the ceramic can be found in the results section at page 112. In general it was found that:

- The ceramic sintered density was low. The sintering density was typically about 95.7% of the theoretical density. It was noted that the residual porosity was completely closed. Pores were trapped within the grains and were consequently very difficult to eliminate during sintering. The samples presented non uniform density across the thickness. The material appearance on the surfaces suggested a close to fully dense condition (See Fig. 65) while the internal area was showing abundant porosity (See Fig. 66).
- The presence of grains over 20 μm in diameter, with trapped porosities, suggested a discontinuous grain growth happening in the third stage of the sintering. This is usually an indication that the grain boundaries have moved faster than the relocation of the porosity. As a consequence the small grains were consumed. Thus, some grains appeared with many highly convex sides.
- Structural discontinuities in the body were present which could act as localized stress raisers. In particular the wafers had:
 1. Non uniform grain size. The samples were characterised by a “sandwich” structure with dense large-grains layers corresponding to the 20-30 μm close to the external edges. These superficial areas were limiting an internal bulk with grains 5-15 μm .
 2. Non uniform porosity distribution. The placement of the porosity was both at the triple points and inside the grains.

The role of the microstructural discontinuities in the crack development could be noted especially in Fig. 67. It shows the development of a crack in a perpendicular direction of the main sample fracture surface. It could be observed that the fracture of the larger grains was mostly transgranular. Where the grains were smaller, more homogeneously sized and with the porosity placed at the triple points the fracture path followed the grain boundary. The transgranular ruptures happened mainly in correspondence of the external surfaces. In particular this happened on side A, in contact with the alumina support during sintering, where the grain size was largest and many pores were trapped within the grains.

A similar phenomenon, where the ceramic presented different appearances on the surfaces in contact with the support during sintering and free-to-air, was observed by [Bitterlich and Heinrich, 2002] in silicon nitride tape cast ceramics. Also in that occasion, as in the case under study, the side of the sintered ceramic in contact with the support showed a denser, apparently more sintered side. The causes of such changes in morphology were hypothesised by Bitterlich to be related to the green tape's variation between the free-to-air and on the carrier

sides. The bottom side of the tape was smoother than the free-to-air side. It also had regions of increased polymer concentration. Alternatively, Bitterlich suggested, that the appearance of the grains in free-to-air surface derived from a reaction of evaporated silicon and nitrogen during cooling.

The PZT ceramic under study presented similar green tape features those observed by Bitterlich, with a smoother and more binder-rich carrier side, and rougher upper side with a reduced presence of the organic phase (see Fig. 73, section 6.3.2.1 at page 128). However, the configuration of the ceramic material under study was inverted during sintering (Fig. 54), as suggested by Navarro [Navarro, 2001]. This led to the hypothesis that the “sandwich” microstructure was associated with side effects of the sintering configuration, rather than with the green tape’s features. One of the potential alternative explanations was that the phenomenon was associated with the conditioning of the crucible with lead oxide enriched PZT powder. The conditioning of the crucible and the addition of PZT spacer pots could have created different lead oxide concentration at the surfaces, modifying the sintering mechanism for the 10-20 microns external layers in comparison with the internal bulk material. In particular, the surface in contact with the alumina support (A), featuring larger grains, appeared to be in a more advanced sintering stage than the free-to-air surface (B).

The diverse appearance on the two faces suggested an explanation for the samples bowing as a different grain growth rate at the edges, might have led to asynchronous shrinkage rates. This argument was supported by the experimental evidence that the sample bowing decreased with increased thickness, for which any effects constrained to the edges would have been less important.

7.1.2 Study on the factors influencing the ceramic microstructure

According to the literature normal microstructures, small grain size and high sintered density can enhance the ceramic’s mechanical properties and are desirable [Yan, 1981].

The grain size is believed to strongly influence the strength of the material with a factor of $1/\sqrt{d}$, where d is the grain size (i.e. the smaller the grain size, the stronger is the ceramic) [Rahaman, 1995].

An almost fully sintered density as close as possible to the theoretical density gives the ceramic the highest strength. The effect of porosity in the increase of the strength is debateable: pores can act both as crack stoppers or stress concentrators if they are large [Zimmermann and Rodel, 1999]. Hence, limiting the size of discontinuities in the ceramics like large pores can be beneficial for the increase in the material’s strength.

Features such as the uniformity in grain dimension and shape and small residual porosity positioned on the grain boundaries are known to be advantageous for the ceramic strength.

From the considerations just made, directives were given to improve the resistance to stress through the modification of the ceramic microstructure. In detail:

- To achieve an increase of the green density. The higher, the better.
- To obtain a reduction of grain size. The smaller, the better.
- To improve the microstructural homogeneity by
 - o positioning of residual porosity at the triple points
 - o achieving a more uniform grain size.

The cause-effect diagram shown in Fig. 68 summarises the main factors known to be influential on the ceramic sintered microstructure [Rahaman, 1995]. Principally, they can be grouped into two categories:

- The sintering conditions
- The green ceramic characteristics

The category “sintering conditions” comprises two sub-groups of factors: the sintering profile and the lead oxide atmosphere. As noted in the results section, during this work, the effects of the variation of the sintering atmosphere could not be evaluated due to technical limitations in measuring the lead oxide concentration in the sintering crucible. However, the three factors characterising the sintering profile, i.e. the sintering temperature, the sintering temperature dwell time and the heating rate, were investigated separately.

7.1.2.1 Sintering atmosphere

The PZT processed powder contained a small percentage, 1% weight., of lead oxide as a sintering aid. This was thought to provide:

- firstly, an internal source of lead oxide to avoid losses during sintering;
- secondly, a small percentage of liquid phase to achieve a better microstructure at lower temperatures [Corker et al., 2000, Megriche and Troccaz, 1998].

The expected result if PbO was lost during sintering was a change in the samples composition, leading to a variation in the electrical properties. In the case under study, the electrical characteristics (not reported in this thesis) of the ceramic were satisfactory as compared with the ones expected for the material [Stringfellow et al., 2002].

As a consequence of this observation, it was assumed that the lead oxide atmosphere during sintering was appropriate and fit for purpose to avoid excessive lead oxide losses and to obtain stoichiometric PZT.

7.1.2.2 Sintering temperature and the dwell time

The effects of the sintering temperature and the dwell time were studied with a combination of two experiments. In all the experiments the sintering conditions set in the original process were taken as the maximum and were progressively reduced. This experimental trend was decided as the microstructural features could be associated with the ones of an over-sintered material. The data here discussed are reported in the Results section 6.3.1 at page 119.

Fig. 123 describes the sintering profiles used for one experiment where the dwell time was reduced for two sintering temperatures: 1270 and 1250 °C. In the following discussion, it was considered that the sintering process was happening just during the heating ramp and the dwell time at the maximum temperature (i.e. the sintering temperature). This assumption was made in consideration of the fast (10°C/min) cooling rate which reduced the time for any effect to happen at a specific temperature.

The characteristics of the samples obtained with the four sintering profiles were compared two by two, in order to consider the variation of one factor per time, i.e. either the sintering temperature or the dwell time. However, since the heating rate was kept constant both for the heating and the cooling ramps, by decreasing the sintering temperature by 20°C and keeping constant the dwell time, the total sintering time was also reduced by approximately 7 minutes (compare the sintering profiles of samples 1 and 3 in Fig. 123). The following discussion considers also this factor.

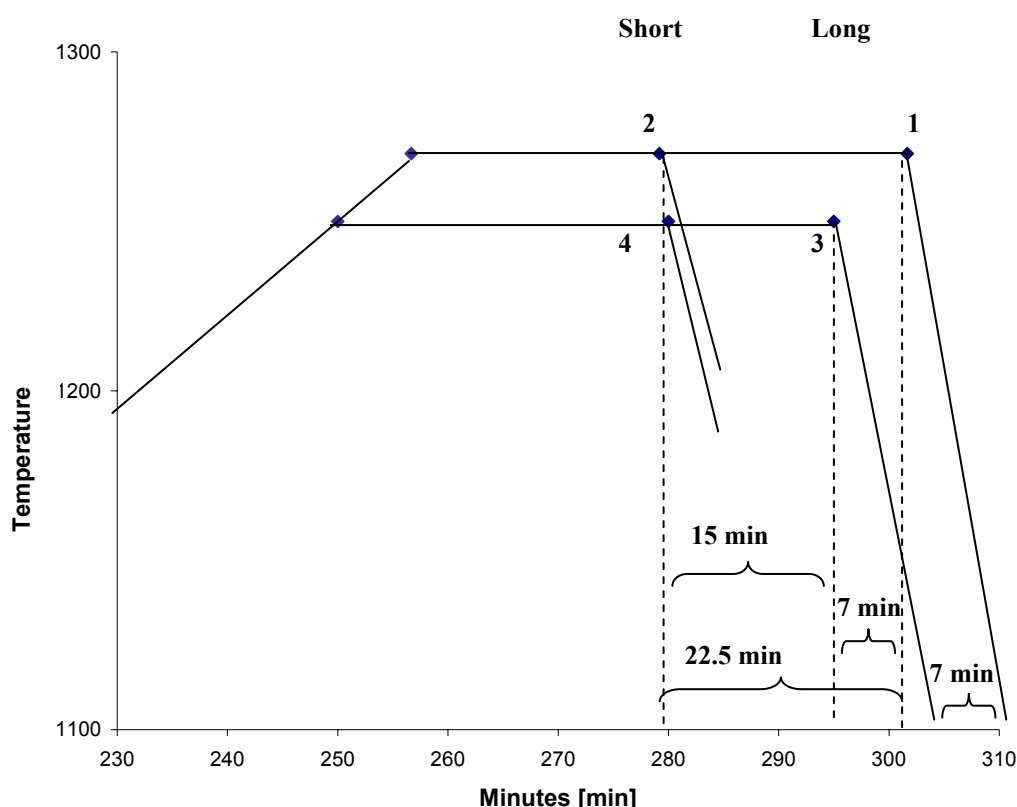


Fig. 123: Visualization of sintering profile variation with the reduction on the dwell time in experiment 1

7.1.2.2.1 Effects of the variation in dwell time

The comparison of samples 1 with samples 2 and of samples 3 with samples 4 in Table 17 and Fig. 70 provided information on the variation of the dwell time on the sample microstructure at 1270 and 1250 °C respectively. As expected, in both cases the sintered density increased with an increasing of sintering time. The sintered density increased by 8.8% of the theoretical for double the dwell time at 1270°C and by 3% of the theoretical for a 33% increase at 1250°C. This testified that the increase in the densification rate was promoted by an increase in sintering temperature. At both temperatures, the increase in dwell time resulted in a reduction of the grain size. This is true both for the value of the calculated average grain size and the difference between the highest and the lowest grain dimension.

From these evidences a mechanism was proposed which inferred that at such temperatures, during the last part of the sintering dwell time, the “third stage” of the sintering process happened. As the samples were characterised by abnormal grain growth it was deduced that when the sintering time was short, just some grains started growing irregularly, while others remained small. This was testified by the great difference in the maximum and minimum grains’ dimension for the samples obtained with a short dwell. This effect was emphasised in the case of the highest sintering temperature (1270°C).

A scenario which would be consistent with the data is that because of the fast boundary motion induced by the discontinuous grain growth, most of the porosity remained trapped inside the grains. When the sintering time was increased, porosity was reduced by the diffusion mechanism. However, the mechanism of porosity reduction favoured the porosity positioned at the triple point. As a consequence the green density was increased, but some of the pores remained trapped within the grains.

Also, when the dwell time was increased, the grains' size became more homogeneous. In fact, it has been recognised that a limited amount of grain growth can have the capability to homogenise a microstructure [Lin et al., 1987].

7.1.2.2.2 Effect of the sintering temperature variation

Samples 2 and 4 were processed for the same total time, but sample 2 was sintered at an higher temperature. Consequently, while the sintering temperature dwell lasted for 22.5 minutes in the case of sample 2, it was 30 minutes for sample 4. For the purpose of this experiment, it was assumed that the only appreciable difference in the two profiles was the 20°C variation in the sintering temperature. In this way it was consciously neglected the potential influence of the temperature rising ramp for sample 2.

The data relative to sample 2 and 4 revealed that 20°C temperature variation inducted little variation in the ceramic characteristic. For sample 4, the sintered density increased by just 1%, from 87.6 to 88.6% and the calculated average grain size by approximately 1.5 µm, from 7.3 to 8.9. The only appreciable difference was in the maximum grain size and in the difference between the largest and the smallest grain size observed. A 20°C increase almost doubled the difference between the largest and the smallest grain size observed, from 13.1 to 24.6 µm. It was consequently deduced that the influence of the variation in the sintering temperature was the exaggeration of the features of the abnormal grain growth.

From the first experiment it was concluded that:

- At these temperatures, the sintering mechanism favoured a abnormal grain growth.
- The abnormal grain growth was increased at the highest temperature (1270°C).
- A long dwell time improved the sintered density and the homogeneity in grain size.
- At these temperatures, during the dwell time, the third stage of the sintering happened which increased the sintering density by reducing the closed porosity. This mechanism favoured the porosity at the triple points.
- The higher temperature resulted in an increase of the sintered density and of the densification rate.

7.1.2.2.3 Combined effects of total sintering times and sintering temperature

The combined effects of the variation in sintering temperature and total sintering time were studied by comparing profiles 1 and 3 of the experiment in Fig. 123. In addition, a second experiment was conducted where the sintering profile was varied as illustrated by Fig. 124. The results of this experiment are reported in section 6.3.1.2.1. In this experiment, the sintering temperature was progressively reduced from 1270°C to 1170°C, while the sintering temperature dwell was kept constant at 45 minutes. For the reasons explained above, as a result, the total sintering time was also reduced. The total, maximum decrease was 33 min.

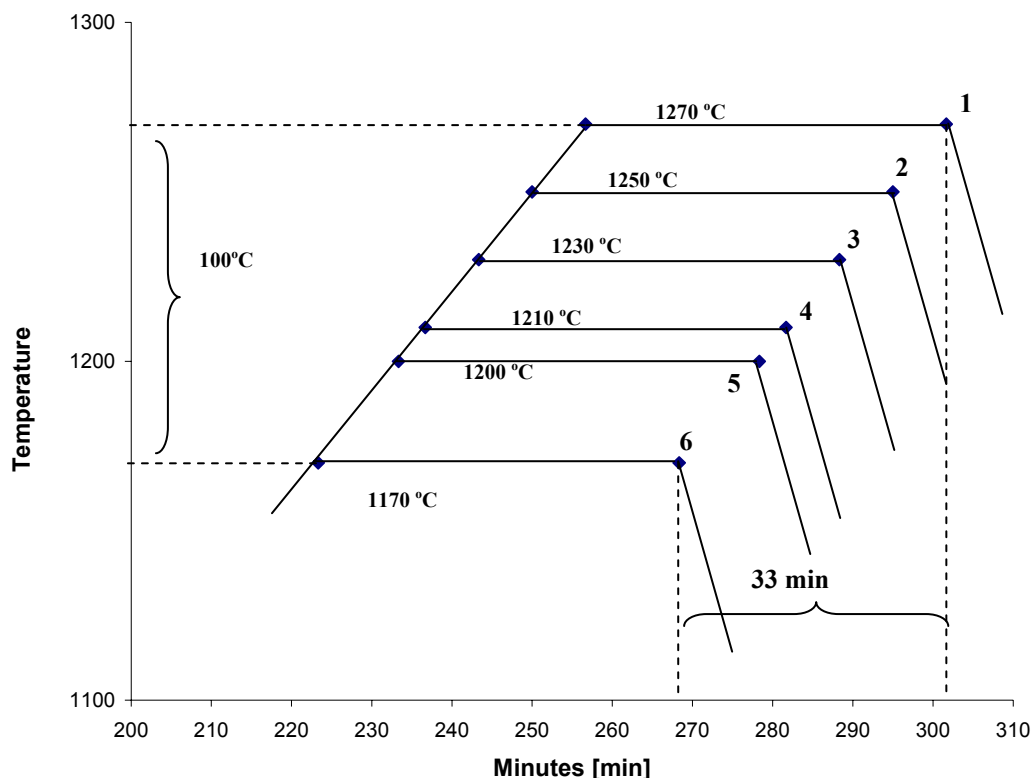


Fig. 124: Visualization of sintering profile variation with the reduction on the sintering temperature and the total sintering time in experiment 2

The sintering profiles 1 and 3 in Fig. 123 differed for 20°C in the sintering temperature. As a result, the total sintering time was reduced by 7 minutes. In this case the data of calculated average grain size, and maximum and minimum grain size observed were very close for the two samples. In addition, both the profiles resulted in samples similarly characterised by abnormal grain growth.

On the other hand, the sintered density of the sample obtained at 1270°C was higher by 4.8% of the theoretical compared to the one obtained at 1250°C. The microstructures of the two samples differed mainly in the shape of the grains. When the sintering temperature was 1250 °C, the shape of the gains was more curved and irregular. The microstructure obtained at 1270°C overall appeared at a more advanced sintering stage. The grains' shape seemed more regular.

From the analysis of the experiment in Fig. 124 data, it was evident that the decreasing of the sintering temperature by approximately 8%, i.e. 100°C, reduced the sintered density by approximately 10%, from 94.2 to 84.6% of the theoretical.

Similarly, the reduction of the sintering temperature induced a reduction of the calculated average grain size. The trends in sintered density and calculated average grain size in the second experiment are shown in Fig. 71. It was noted that both the sintered density and the calculated average grain size showed a steeper increase between 1170 and 1230°C. Between 1230 and 1270°C, while the sintered density increased less rapidly, the grain size increased

A cross evaluation of these results with the micrographs in Fig. 72 suggested that at the lowest sintering temperatures, 1170 and 1200°C, a 45 minutes dwell time wasn't sufficient for a complete removal of the open porosity of the ceramic. However at these sintering temperatures the micrographs showed a normally sintered microstructure, without evidence of irregular grain growth. According to the images, the discontinuous grain growth started between 1210 and 1230°C. The 1230°C microstructure showed an almost complete elimination of the open porosity. Further increases in sintering temperature, and consequently of the total sintering times, resulted in coarsening of the grains and also in an increase in the densification.

From this initial study some preliminary considerations were made on how to improve the microstructure, according to the directives stated above. In particular:

- The sintering temperature had to be reduced below 1210°C, in order to avoid the creation of abnormal grains.
- An increase total sintering time was thought to be beneficial for the improvement of the final ceramic density.

7.1.2.3 The effects of the green body characteristics on the sintered microstructure

The beneficial influence of highly packed green bodies on the sintered microstructure it is well known. Defect free green bodies with de-agglomerated particles are consequently the aim of any forming process.

Green tape produced by the original process, described in the experimental section (page 78), was characterised. The results are presented at page 128.

The average green density of the tapes was 3.17 g.cm^{-3} , about 38.7% of the theoretical density. The process was considered stable as the difference between the maximum and the minimum green density achieved was 0.43 g.cm^{-3} , approximately 5.3% of the theoretical.

The maximum theoretical green density value achievable would be 7.61 g.cm^{-3} , approximately 93% of the theoretical. This figure would correspond to an ideal condition where all the interstices among the particles would be filled by the binder system. However, no real processing technique allows such result. A more realistic aim for the green density of tape cast material would be in the range of 50% of the theoretical [Mistler and Twiname, 2000].

The green tapes were also inhomogeneous. As shown by the micrographs in Fig. 73(1) and (2), the concentration of the organic phase appeared higher on the

surface in contact with the carrier, surface B, than in the rest of the microstructure. This was observed also in the cross section of the tapes in Fig. 75. This effect could be attributed to a percolation of the organics through the particle network during drying.

Heterogeneity was also detected in the way that particles and porosity were distributed. Particles were organised in clusters the packing of which created the tape's structure. The clusters were usually several microns in diameter, large compared to the primary particle size (see Fig. 74). Areas more densely packed were alternated with loosely packed ones. In addition the porosity was found irregular and also sometimes as large as 10 μm .

An investigation was conducted to understand the implications of the green density values on the sintered microstructure and the relative importance of the green density factor and the sintering temperature on the final sintered material characteristics. In order to produce higher green densities, a warm pressing technique was used. The pressing conditions were optimised with a study reported in section 6.3.2.3.1, discussed in section 7.1.2.3.1.

As observable in Fig. 81, there was a strong correlation between high green density and high sintered density. However, a 40 $^{\circ}\text{C}$ variation in sintering temperature had little effect on the sintered density. At 1210 $^{\circ}\text{C}$ a 27.6% increase, from 37% to 65%, of the green density gave an improvement in the sintered density of 11%, while at 1170 $^{\circ}\text{C}$ it gave an increase of 13.6%. In contrast, the increasing of sintering temperature from 1170 $^{\circ}\text{C}$ to 1210 $^{\circ}\text{C}$, for a constant green density, produced a negligible increase in the final sintered density, of about 1%, for the 37% green density. For 65% green density the sintered density actually diminished by 1.6%. On the other hand, the average grain size appeared to be increasing both with the increase in the firing temperature and in green density. (see Fig. 80)

In general, varying the sintering profile from 1210 $^{\circ}\text{C}$ to 1170 $^{\circ}\text{C}$ produced the following effects:

- The grain size was reduced.
- The average grain size showed a smaller decrease.

It was evident from the micrographs of the sintered tapes at the lowest (Fig. 79: A1 and A2) and intermediate (Fig. 79: B1 and B2) green density that, by starting from a low density ceramic the grain coarsening effect was dominant in comparison to an increase of the ceramic density. While for the lowest green density the sintering temperature was insufficient for complete removal of the open porosity, the intermediate density achieved a state of apparent over-sintering, where the grain size was large and the remained porosity was trapped within the grains. However, the material produced from green density of about 65% produced microstructures (Fig. 79: C1 and C2), which showed a different correlation between densification and grain growth, exhibited smaller grains and higher density.

It is arguable that while for the green densities of 37 and 59% of the theoretical density the distance among some particles and/or agglomerates was large and,

hence, the particle/agglomerates number coordinated by a pore was high. For high green densities of 65% most of the pores had dimensions comparable with the grain size. Consequently, it had a lower particle coordination number.

A mechanism for the sintering of highly porous bodies has been suggested by Greskovich and Lay [1972] and Edelson and Glaser [1988]. The mechanism is sketched in Fig. 125 Fig. 125 (1). When particles of slightly different size are in contact, the neck grows mainly by surface diffusion, migrating from the contact plane, and consuming the smaller grain. This mechanism extended to a cluster of particles generates a large granule as in (2). Both neck growth and the boundary relocation in the less porous areas drive the coarsening of the grains. If the grain-boundary migration is rapid, it can, for a certain green density, trap the pores in the cores of the grains. As new contacts between growing grains occur, less faceted grains are created.

If the ceramic had an intermediate and a not uniform green density, it is imaginable that it alternated areas that, as sintering progresses, will evolve differently both in density and morphology as shown in Fig. 79, B1 and B2. More dense green ceramics, as the one with about 65% theoretical density, instead typically present a more uniform microstructure. This might be due to slower grain-boundary motion which can allow the pores to remain at the boundary. Ordinary grain growth and densification rates are known to happen in these circumstances.

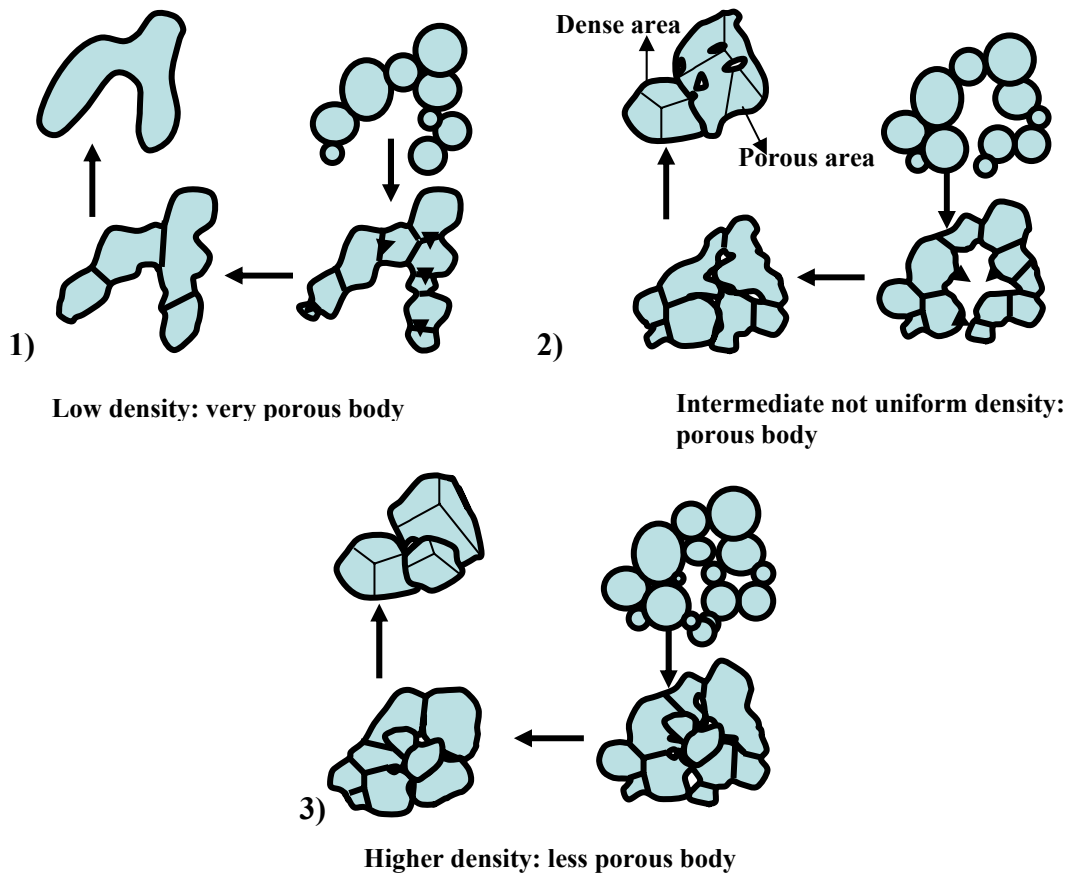


Fig. 125: Proposed mechanism: 1) low green density; 2) porous; 3) less porous.

With regards to green density effects on the final microstructure, it was concluded that:

- the green density had a strong influence on the final ceramic microstructure
- the green density influence was stronger than the effects of the variation of 40°C in sintering temperature
- the increasing of the green density was beneficial for achieving a better sintered microstructures in respect of the targets listed above. An increase in green density was thought to modify the sintering mechanism, so that an almost fully sintered material could be achieved at 1170°C.
- the irregular growth of the grains seemed correlated with a low-dense green body. It was argued that when tapes had intermediate green density and they presented not uniformly packed particles, areas of higher density alternated with less dense areas. In these conditions it was thought that the sintering could develop following different mechanisms across the same sample, according to the area green density. As a result, the sintered microstructure could have presented abnormal alternated with normal grains.
- The pressing of the material seemed overall beneficial, not just for the increase in green density, but also for the achievement of a more homogeneous microstructure.

7.1.2.3.1 The warm pressing technique: optimisation of pressing parameters

The warm pressing technique was studied as it was considered a technique suitable to increase the ceramic green density. This section discusses the results reported at page 131.

Firstly, with a preliminary study, the capability of the warm pressing technique to achieve consistent green density values was assessed. By pressing samples from the same tape with the same processing conditions, i.e. applying 65 MPa for 15 minutes at 20°C, the tapes' green densities increased by an average of 15.17%. The difference between the maximum and the minimum green density was 0.66 g.cm⁻³. The variation was approx 8.1% of the theoretical density. This result encouraged further investigation, especially considering the typical variation of the green density values of approximately 6%.

The second part of the study aimed to optimise the processing parameters, in order to obtain the highest green density possible and the greater area of material processed per pressing.

It was shown that applying an increasing pressure on the samples increased progressively the green density up to a maximum of 55% of the theoretical density obtained for 160 MPa pressure, the highest applied. The green density was most influenced by increases in pressure between 65 and 90 MPa. This could be explained considering that the rearrangement of the particles in the microstructure

becomes progressively more difficult as the green density increases and approaches the maximum packing factor.

As shown by Fig. 83, increasing the pressing temperature at constant pressure increased the green density. The highest increments in the green density were obtained for pressing temperatures above 40°C. The glass transition temperature (T_g) of the polymeric phase was 39°C. It is well known that above the T_g polymers behave in a viscous way. Consequently, the resistance of the binder to the particles motion appeared to have been reduced with increments in temperature above the T_g .

It was also likely that the defects in the microstructure were reduced in size and/or quantity by using temperatures higher than the T_g . In fact, the improvement in the green density in a rigidly structured sample, i.e. a sample below the T_g of the polymeric phase, is likely to be due to sudden yielding (collapse) of the structure under the pressure. The collapses of the structure could cause imperfections which could lead to defects during sintering. On the other hand, the green density increase in a viscous material, i.e. a sample above the T_g , would be deriving from a rearrangement of particles driven by the pressure.

As illustrated by Fig. 84, increasing the pressing time increased the green density. This was true in particular with dwells between 10 and 20 minutes. Further increases in the dwell time resulted in minor improvements in the green density. It is known that microscopically, inside a compressed granular packing, stresses are transferred by the contact of particles. Under gradual loading conditions the particles get slightly displaced changing their contacts and the local load supported by them [Liu et al., 1995]. In a compressed granular system the stresses are transmitted along the direction of the external load by force chains which can branch at the grains and form a complex network. Under pressure the particles move until the system reaches a saturated state when all the particles hold typically the same load and the system behaves as a bulk material. The time dwell effect on the green density might be explainable considering that close to the maximum packing higher energy would be needed to overcome the activation energy that promotes the rearrangement. The same energy applied for longer times would not induce any yielding, but would be elastically stored.

Finally, for processing reasons, it was necessary to investigate a method to increase the area to be pressed at a time. Two configurations of samples under the press were compared: the side-by-side and the stack configuration. Both gave similar results in terms of average green density achieved. However, in the case of the side-by-side, the variation in green density across the samples was higher. This was thought to be due to the variation of the thickness across the samples. As illustrated in Fig. 126, samples with slightly different thicknesses could result in relatively different final green densities. This meant that the side-by-side configuration was more sensitive to the lack of homogeneity in thickness, than the stacked one. In addition, for the same processed area, to achieve the same pressing conditions in the side-by-side configuration as in the stack configuration, a higher load was needed. Consequently the capability of the side-by-side configuration was more constrained than the stack configuration by the maximum load

capability of the machine. Furthermore, the maximum processing area per pressing was limited in the side-by-side configuration by the platens' surface.

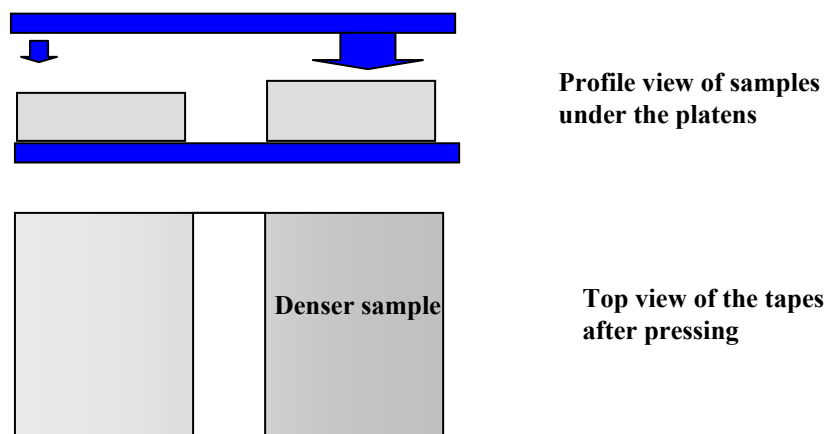


Fig. 126: Representation of pressing of unevenly thickened samples. The pressing results in a gradient of density. Thicker areas would be more influenced by the pressure.

As a conclusion of this study, the optimal pressing conditions were set as:

- Pressure 65 MPa,
- Temperature 50°C
- Time 20 min
- Configuration: stacked samples

With these parameters, samples with approximately 65% of the theoretical density could be achieved.

A more in depth investigation of the causes of the variation in the warm pressing process was required to assess the suitability of warm pressing as ceramic production process. This investigation will be treated in section 7.3.

7.1.2.4 Effects of the sintering heating rate on the ceramic characteristics

The analysis of the microstructures of pressed samples sintered with 3, 6 and 10 °C/min heating rates, found that faster heating rates could improve the ceramic microstructure by reducing the grain size (See Fig. 86).

However, the samples achieved with the three profiles didn't present any relevant variation in the final sintered density, which remained in the range of 97.8% - 98.4%. From this it could be concluded that, in agreement with what suggested in literature [Rahaman, 1995], increasing the heating rate was influencing the mechanism of grain growth. As increased heating rates shortened the time spent at each temperature below the sintering temperature and it is likely that the viscous flow that happened at a given temperature was reduced.

The increase of the heating rate generated also the secondary positive effect of shortening the sintering time. To reach 1170°C from 500°C, 223 minutes were required with the 3°C/min ramp, while 111 and 67 min respectively were sufficient in the cases of 6 and 10 °C/min ramps.

However, adopting a heating rate of 10°C/min was considered to be a high risk strategy. This because higher heating rates could increase the stresses in the material increasing the chances of developing cracks and imperfections. Secondly, as the sintering was performed in an alumina crucible to be re-utilised, higher repeated thermal shocks were considered a potential threat for the crucible integrity.

The 6°C/min heating ramp was chosen to compromise on these factors.

7.1.3 Conclusions of the sintering studies

Table 45 below summarises how the variation of the parameters studied influenced the sintered density and the grain size in the studies reported. To have a higher sintered density, a smaller and more homogeneous grain size were the targets set originally.

Parameter	Variation	Calculate average grain size	Sintered density	Homogeneity (reduction in the difference between max. and min. grain)
Sintering temperature	↑	↑	↑	↓
Dwell time	↑	↑	↑	↑
Green Density	↑	↓	↑	↑
Heating rate	↑	↓	-	-

Table 45 : Summary of the effects on the sintered density and the average grain size, induced by different parameters The ↑ symbol represents an increase. The ↓ symbol represents a decrease.

The increase in the green density appeared to positively influence all microstructural characteristics.

The warm pressing technique was considered a suitable method to increase the green density. Pressed ceramic with up to 65% of the theoretical density was obtained with the optimised pressing setting. However, this green density was very rarely achieved when multiple experiments were run.

An experiment was needed to assess the capability of the warm pressing technique to perform in a consistent way. For this experiment a target green density was set as 5 g.cm^{-3} , approximately 61.2% of the theoretical density.

In consequence of the study highlighted in Table 45, the other sintering parameters were also varied. The sintering temperature was set at 1170°C with a 45 minutes dwell. It was reached with a heating rate of 6°C/min . Fig. 127 shows how the new profile reduced the total sintering time.

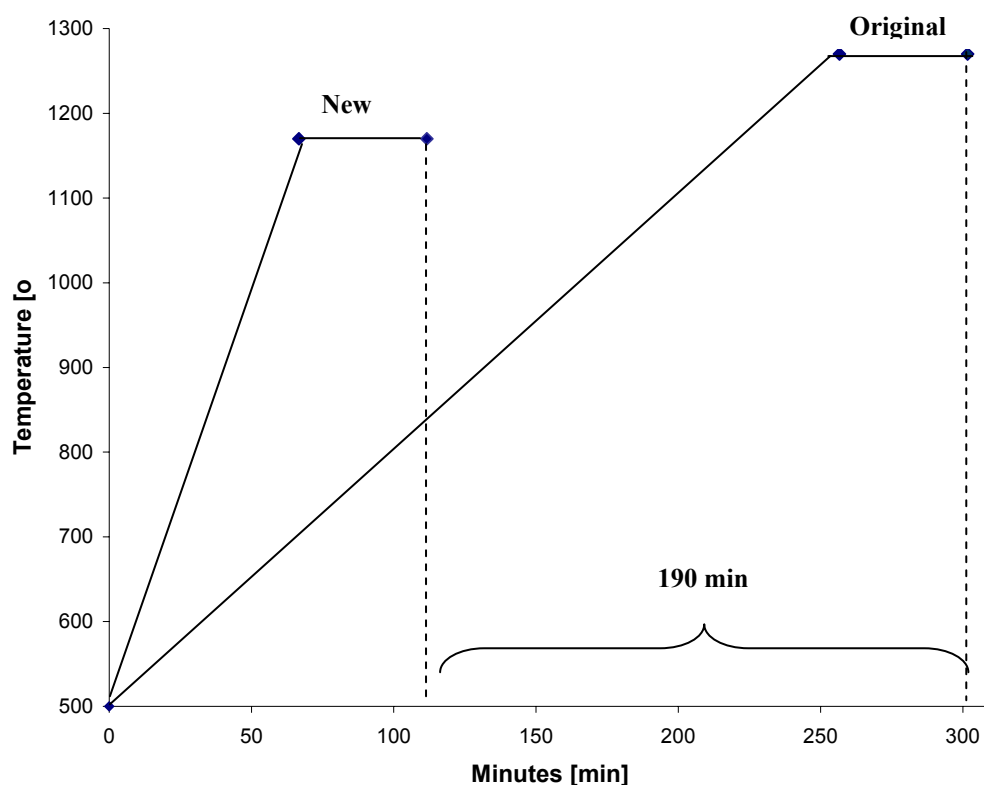


Fig. 127: Comparison of original sintering profile with the newly designed one.

7.1.4 Characteristics of the pressed wafers

The wafers obtained with the newly designed process, encompassing the warm pressing step, possessed characteristics not dissimilar the ones delivered by the original process except for the modification in the microstructure and the increase in the rate of survival of the samples to the poling and dicing stages. As highlighted in the process focused study in section 5.3.1 at page 108, 75% of the warm pressed wafers tested resisted the poling and dicing operations and could be mounted on silicon chips. This signified that the insertion of the warm pressing step improved the strength of the material substantially, as the yield passed from 5% to 75% of survival rate.

The microstructure comparison is shown in Fig. 87. It is possible to appreciate how the new microstructure had a more homogeneous morphology, with smaller grains and small porosity at the triple point. The characteristics of the grains in the

new-process microstructure were those usually associated with a normal grain growth.

Thanks to the warm pressing step, the roughness of the samples faces, side A and B, became similar as shown in Table 13. The warm pressing allowed samples with overall improved average roughness by 100 nm to be produced. However, it had little, if not negligible, effect on their flatness (see Table 13). The failure of the ceramic during the poling and dicing could be improved by improving the flatness.

The reduction of the porosity in the ceramic microstructure didn't compromise the material electrical properties. The samples could be successfully used in application, as shown in Fig. 90.

A summary of the electrical characteristics of the ceramic as by Navarro, before and after the study, are reported in Table 27. The specifications were originally set around the properties of Navarro's material. Observing the table, it can be observed that the data in row 3 in, reporting the electrical properties of the material achieved with the original process, were consistent with Navarro's data. However, it could be noted that the resistivity (ρ) value as well as the F_D figure of merit of the material improved in comparison with Navarro's. On the other hand, the dielectric constant, and consequently the p/ϵ , and the loss ($\tan \delta$) ratio were slightly inferior.

The same considerations could be made for the data in line 5 in the same table, for the warm pressed material. The reduction of the porosity didn't compromise the electrical properties, as it could have been forecasted [Navarro et al., 2004b, Zhang et al., 2005]. Instead, a slight improvement could be noted in the resistivity value contrasted by a small decrease of the p/ϵ and a worsening of the loss. However, the figures of merit, remained constant.

7.2 The Definitive Design Phase I: the Statistical Process Control technique to assess the causes of variation

The Statistical Process Control technique was used to assess the warm pressing technique proposed by the conceptual design as a possible solution to increase the green density of the tape cast.

Very little literature has been found about the use of SPC in ceramic processing [Fang et al., 1999, Mittendorfer and Zwanziger, 2000]. In this thesis, the SPC technique has been employed as a design tool.

In detail, the use of the SPC in this work allowed to:

- Assess the capability of the warm pressing to meet the specification requirements. The specifications were set making use of the concept of the “internal customer” which considered the following operation in the process as if it were the final customer. For this experiment a target green density was set as 5 g.cm^{-3} , approximately 61.2% of the theoretical density. This value was considered a realistic estimation of the capabilities of the process in consideration of the pressing parameters optimisation study where the maximum value of approximately 65% of the theoretical density was rarely achieved.
- Assess the extent of the variation in the green density values achieved with the warm pressing.
- Understand the causes of variation that affected the warm pressing operation.

The individual observation chart in Fig. 92 page 152 plotted the individual data of green density achieved (Table 28). It gave the first indication about the level of process control. The individual observation chart is not, however, as accurate as an instrument as the mean and range charts are to perceive small variations in the mean. The chart reported the individual observations of sample density together with the upper and lower control (at 3σ from the mean line) and warning limit lines (at 2σ from the mean line). The pressed green density of a single tape varied between 4.4 and 5.0 g.cm^{-3} . The average (mean) was 4.7 g.cm^{-3} while the standard deviation (σ) was 0.15. The individual observation chart indicated that no values were out of the lower control limit (LCL) to the upper control limit (UCL) range. However, in some circumstances densities were found outside of the 2σ warning lines. Moreover, rows of points (greater than 8 in succession) were located on the same side of the mean. These observations were the first indicators of an ‘uncontrolled’ process.

A more accurate analysis was made with the use of the Mean and Range charts reported in Fig. 93 page 152. Table 29 reports the values of the main figures used for the analysis. The UCL and LCL lines were placed respectively at $3\sigma (n)^{-1/2}$ above and below the average values of the mean of the means ($\bar{\bar{X}}$) and the mean

of the range (\bar{R}). The mean density and range showed scatter outside of the UCL to LCL range. Five or six points in succession were observed with either consecutive increasing or decreasing trends. It can be noted that the specification value of green density, 5.00 g.cm^{-3} , was rarely achieved. In fact, this value was the highest density attained at all. These data confirmed that the process wasn't in control.

Useful indexes to compare the process results with the specifications are Cpk defined in the literature review section.

For the studied process Cpk was 1.02 and CpkI as -0.51. Both of the values were far below 1, which indicated that the process was not capable at any time to achieve the requirements. An easy to obtain measure of the process 'capability' was Cp. This index compared the variability of the process (the interval 6σ) with the tolerance of the specifications. For the process analysed in this work, Cp was 0.254, so the variability of the process is greater than the specifications tolerance interval.

These remarks lead to the conclusions that the process,:

- was not in control
- did not meet the specification required (i.e. it was not centred on the specification value)
- had variations greater than the tolerance interval. Fig. 128 shows the schematisation of these results. The purple curve represents the distribution of the warm pressing process data. The process exceeds the upper and lower control limits (i.e. the process is not in control and not precise). The blue curve represents the distribution described by the specification and tolerance value. The process is also not accurate as the mean value of the process data (4.7 g.cm^{-3}) doesn't coincide with the 5.0 g.cm^{-3} required by the specification.

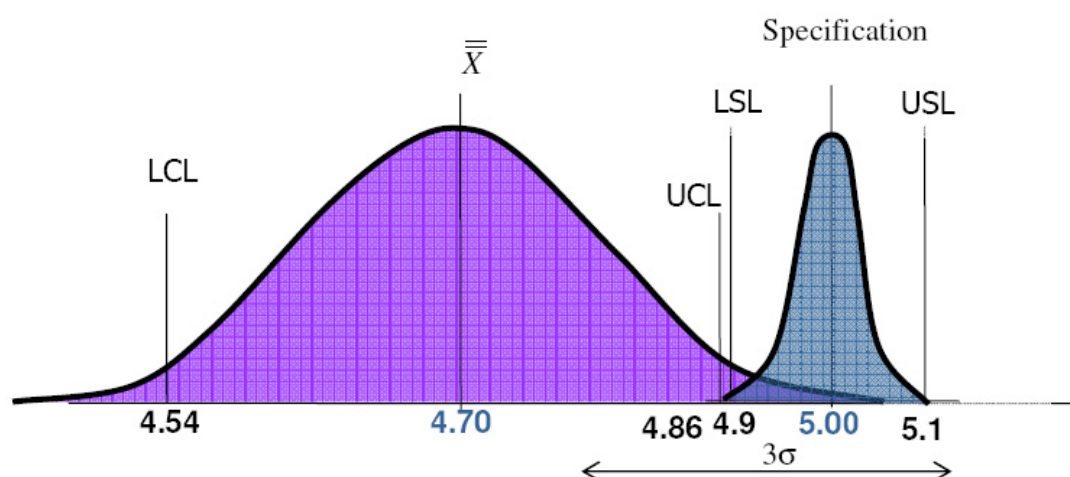


Fig. 128: Representation of the SPC study results.

The capability gave mathematically the same verdict.

C_p which compares the tolerance spread with the 6 σ spread, hence the process “hope” with the “reality”. In this case, C_p was 0.25, indicating that the process spread was approximately four times the tolerance interval.

The C_{pk} value was approximately 1, indicating that the mean was lower than the upper specification limit.

The C_{pk} value obtained was the lowest. It was -0.52, indicating that the mean value was lower also than the lower specification limit, and it was outside the tolerance.

The ‘not-in-control’ situation was not unexpected, since the process was at the early stages of its development. However, the analysis conducted highlighted the importance of a further study in order to define the conditions for an optimal design.

Furthermore, without such an analysis, variability in final sintered density may have been assumed to be associated with variability of the sintering process, rather than control of laminate green density.

On the basis of the above data, a ‘cause-effect’ analysis was conducted to elicit all contributing factors to a variation in the pressed density. The results are shown in Fig. 129. Each of the listed factors noted was ranked:

- The material used was obtained from the same cast tape for all the samples. Therefore it was unlikely to be the dominant factor in the density variability.
- The exposure of the samples to external conditions was negligible as samples were kept in sealed envelopes until the moment of pressing; hence the environmental contribution was taken as minimal.
- The measurement techniques were assessed. Two different techniques were compared for the evaluation of the sample areas (geometrical and digital), the thickness (two micrometers) and the mass (two balances). A maximum error in density of 0.6% was detected. Therefore, the influence of the measurement technique was insignificant compared to the process variations.
- The configuration of the samples in the press was checked. Some samples shifted position on mounting into the press, introducing a taper to the pressed samples. If the density data of those samples was eliminated from the chart analysis as assignable causes no improvement in process control was found. It was therefore concluded that this factor was not the main cause of the variability.
- The equipment pressure setting was considered the most important variation factor, since the applied load was reconfigured each day. In fact, the equipment in use had an analogical gauge to measure the applied load. The scale of the instrument had a minimum of 10 ton. It was consequently imaginable that small variations in the setting resulted in fact in relatively large differences in the applied load.

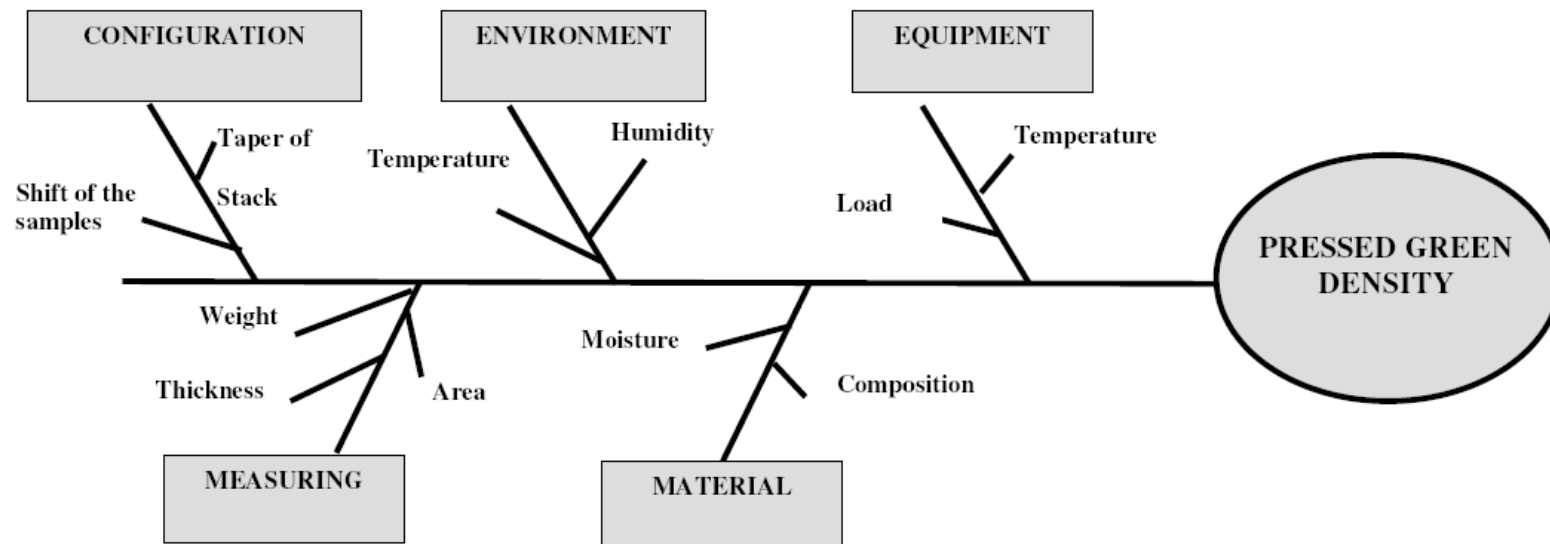
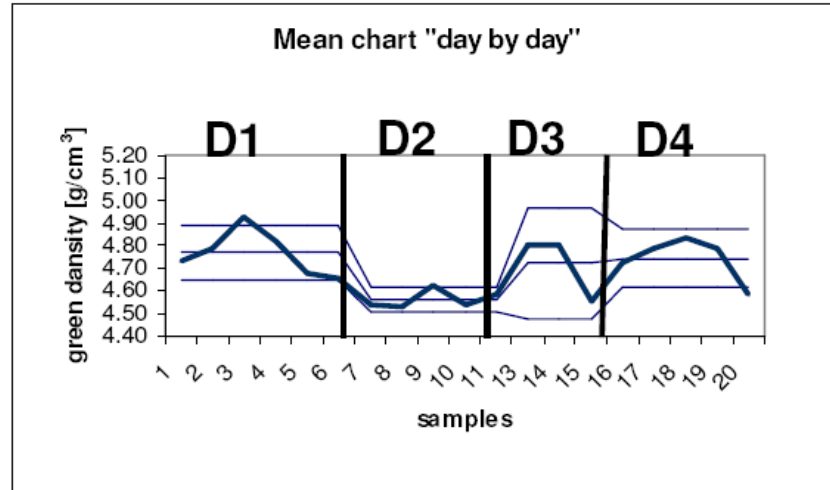


Fig. 129: Fishbone analysis: contribution factors to pressed green density

As a result of the above analysis, control charts plotting day by day control limits were drawn showing the variation with pressure re-setting, i.e. the variability each day. These are presented in Fig. 130. In the new charts the mean line was usually contained within the band of the control limits. This was an indication of a day by day more 'controlled' state. Hence the variability in the setting of the load on the equipment was evaluated to be the assignable cause of density variation. It is likely that redesigned load controls could bring the process back within acceptable tolerances. Secondly, the analysis suggested that the pressing conditions of 50 MPa were an underestimate, since the required final density was rarely obtained. An increase in pressure is therefore suggested. However, the density value required (5.0 g.cm^{-3} , 61% of the theoretical density) is close to the achievable maximum, in consideration of the maximum packing fraction.

1)



2)

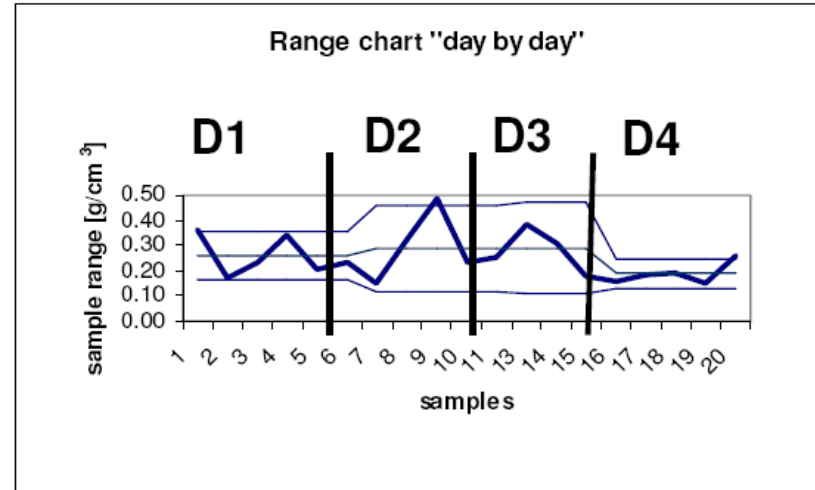


Fig. 130: Mean and range charts reproduced with the day-by-day upper and lower control limit lines.

7.2.1 Conclusions of the statistical process control experiment

The warm pressing process was found incapable of meeting the requirements of green density set-up a specification for the sintering stage. The warm pressing experiment highlighted an ‘uncontrolled regime’.

The problem solving analysis yielded the conclusion that the most significant factor for the lack of process control lay in the control of pressure on the equipment. Moreover, the designed conditions for the process were judged insufficient for the achievement of the targeted specifications. Suggestions for further development of the process were given.

Although the statistical process control technique is commonly used for providing control over processes in a regime state, it demonstrated to be a very flexible tool for the analysis of the process in its design phases.

Despite the specific results of the laboratory scale process just discussed, the warm pressing technique was judged a viable route to achieve constant green density values, providing that the equipment in use was appropriately designed. However, for economical reasons, the implementation of an additional process stage to the original process layout might have signified an increased risk and cost for the scale-up.

It was consequently decided to approach the problem of the low green density from another perspective, trying to understand the reasons underpinning. In the following section, the results of this investigation will be discussed.

7.3 The Conceptual Design Phase II: The influence of the ingredients and the drying conditions on the green tape

At the end of the first phase of the conceptual design, a high green density was found as the most relevant factor for the achievement of a sintered microstructure able to stand the stressful operations required for producing infrared devices. The warm pressing technique was suggested as a method to increase the green density of the tape cast material.

The definitive design study performed on the warm pressing process suggested that the specific equipment used and the setting adopted were inadequate to the scope. The green densities achieved by warm pressing were on the average 57.5% of the theoretical density, lower than the desired 61.2%. The warm pressing was overall judged a suitable technique to achieve high green density cast tape suitable for sintering. However, further investigations were needed to find the appropriate settings and apparatus.

On the other hand, this solution proposed the insertion of an additional processing step into the original process layout. This would have implied the increase of the scale-up risks and costs.

As an alternative, a second approach to the problem of the low green density was adopted, investigating the reasons lying behind it to propose processing modifications.

It has widely been discussed how the attainment of a well stabilised suspensions is an indispensable requisite for high packing behaviour in the green body [Pugh and Bergström, 1994]. Exceptionally, green densities up to 55% -70% of the theoretical can be achieved with a good stabilisation of the particles in the suspension by means of tape casting [Mistler and Twinaime, 2000]. However, 55% of the theoretical density can be considered the average target for an optimised process. Often, the achievement of a low green density in the green body is the result of a not perfectly stabilised suspension which in return is the consequence of an unbalanced mixture of the slurry ingredients.

In this section, a review of the effects of the single ingredients on the slurry and the green tape are discussed in the pursuit of the reasons underpinning the low green density obtained with the original process. The data here discussed can be found in the results section 6.5.

7.3.1 The effects of the ingredients on the green tapes

7.3.1.1 The dispersant and the binder

The optimal dispersant amount is associated with the one that provides monolayer coverage of the particle surfaces [Tadros, 1992a]. This condition is related with a perfectly dispersed suspension, where the inter-particle attractive forces are counterbalanced and counteracted by the repulsive effect of the dispersant. A

general practice for identifying the optimal dispersant/powder ratio is to compare the viscosity of binderless slurries containing different dispersant concentration. The lowest viscosity value in the series is commonly associated with the optimal dispersant concentrations (see literature review section). This is because both lower and higher quantities of dispersant than the optimal would induce flocculation and consequently increase the viscosity. Lower amounts are not sufficient to counteract the inter-particle attractive forces while higher concentrations promote the particles flocculation by acting as free electrolytes [Rahaman, 1995].

In conjunction with standard practice, in this thesis, the effects of the dispersant amount in the slurry were studied by means of rheology tests. However, as the rheology behaviour of suspensions depends on many factors such as the particle size, the particle concentration and the inter-particle forces, a combination of two experiments was needed in order to discriminate among these effects.

- The results data in section 6.5.2.1 refer to samples prepared according to the original slurry procedure (Route 1). In this case, the powder was milled in presence of different dispersant amounts. As a result, the dispersant was believed to have a double influence on the slurry: a suspension and a cominution effect.
- Section 6.5.2.2 at page 176 reports the data relative to the slurries prepared according to Route 2, where different amounts of dispersant have been added to a pre-milled powder suspension in isolation. The study of these samples provided the information of the dispersant effects on the suspension. In addition, the Route 2 experiment was also designed to explore the effects of different powder loadings to the slurry suspension. The maximum powder loading possible with this production method was 21% in volume in the slurries containing all the ingredients. Greater concentrations were difficult to manage because of the very high viscosity of the slurry after the centrifugation.

In order to understand the nature of the interactions between the binder system and the suspended particles in water, the rheology assessments were extended to the suspensions after the addition of the binder system for both the production methodologies.

From the analysis of the rheological behaviour of the samples produced with Route 2, information on the dispersant effects was obtained in isolation. The trends observed in Route 2 samples were used as a reference and used as a comparison with the Route 1 results, for understanding the effects of the dispersant as suspension aid.

7.3.1.2 *Effects of the dispersant on the comminution and comparison of the two preparation routes*

The evaluation of the brown tapes in Route 1 (see results section 6.5.2.1.5) showed that the particles size was varying across the series. The size of the maximum particle observed on the tapes surfaces decreased with dispersant until it reached a minimum for 0.0238 dispersant ratio. Additions above 0.0238 ratio didn't result in any further significant reduction of the particle size. On the opposite, the result was a slight increase of the maximum particle size observed.

The sample with 0.0046 dispersant amount showed the biggest particle size with apparently uniform particle distribution at the top and bottom of the tape. When the dispersant increased in quantity the particle size decreased. For 0.0122 dispersant amount the particles sizes at the two tapes surfaces was different. Largest particles appeared selectively on the surface in contact with the carrier, while the free to air surface showed significantly smaller particle. At 0.0238 and 0.0335 dispersant amount the particles size was again homogeneous on the two sides of the tape.

Considering the evidences collected it was argued that the dispersant added during the milling had effects on the comminution, which reflected in a diversified particles size and distribution across the samples.

This phenomenon is known in literature. The rate of grinding in mills is believed to depend on the number of the contact points between the powder and the media. Hence, the grinding efficiency of wet ball mills depends from a quantity of different factors, such as solid volume content, rate of grinding, grinding media size, shape, density and hardness, or the characteristics of the powder. These factors also hugely influence the viscosity. In fact, as long as the comminution proceeds, the dispersant is absorbed onto the freshly created particles surfaces, keeping the viscosity low. When the particles reach a limiting particle size, they do not break anymore, leaving the excess of dispersant free in the medium [Funk and Dinger, 1994].

Frances et al. [Frances and Laguerie, 1998], who studied the grinding behaviour of an alumina system, showed that the effects of the grinding are mainly related to the fluidity of the slurry. Increasing viscosities lower the grinding performance.

The slurries here considered had a uniform solid loading of about 18% in volume and were produced following the same procedure. Hence any alteration in the grinding performance hereafter was imputable just on the variation in the dispersant amount.

As after 0.0238 dispersant ratio the particles size remained similar, as seen in Table 38, it was argued that the milling process employed reached the best efficiency for 0.0238.

From the observation of the particles size in the brown tapes and the distribution of the binder system in the green tapes it was noted that the PVA was adsorbed to a greater extent in the samples with the smallest particles size. This was

predictable as the adsorption of polymers onto the particles surface is known to depend on their free surface area [Tadros, 2003b] and that the surface area increases with the decrease of particles size.

The sample produced with 0.0238 dispersant ratio had approximately ten times the surface area of the sample achieved with 0.0046 dispersant ratio. This evaluation was made by using the largest particle diameter observed as representative of the whole suspension, and considering the particles spherical. However, the data in Fig. 106 on the amount of PVA adsorbed, suggested instead that the surface area in the sample produced with 0.0238 dispersant ratio was approximately the double than the sample prepared with 0.0046 dispersant amount.

The sample prepared with 0.0335 dispersant absorbed just 44% of PVA, the second lowest amount. This seemed to indicate that the excess of dispersant above 0.0238 created the conditions for a reduced surface area. However, the SEM images in Fig. 103 indicated that the particles dimension in the samples with 0.0238 and 0.0335 dispersant ratio were comparable. A possible scenario in accordance with these data was that, in contrast with the sample with 0.0238 dispersant ratio, the particles in the suspension prepared with 0.0335 dispersant amount were agglomerated. As a result, in the latter case, the apparent surface area free for the binder to graft on was lower than in the sample prepared with 0.0238 surface area.

In the case of the sample prepared with 0.0122 dispersant amount, the largest particles were segregated on the carrier side of the tape. It was inferred that this could have been an indication of particles sedimentation during the drying. If sedimentation occurred also during the rheological tests on the generating slurry, the results could have been biased by this phenomenon.

It was concluded that for Route 1 the dispersant acted as a comminution aid.

All the slurries, regardless the preparation route, showed shear thinning behaviour that could be fitted with the Casson model. Fig. 131 lists qualitatively the trends of the main characteristics observed with dispersant variation, obtained for the two preparation routes. The trends of Route 1 were generally similar to Route 2's.

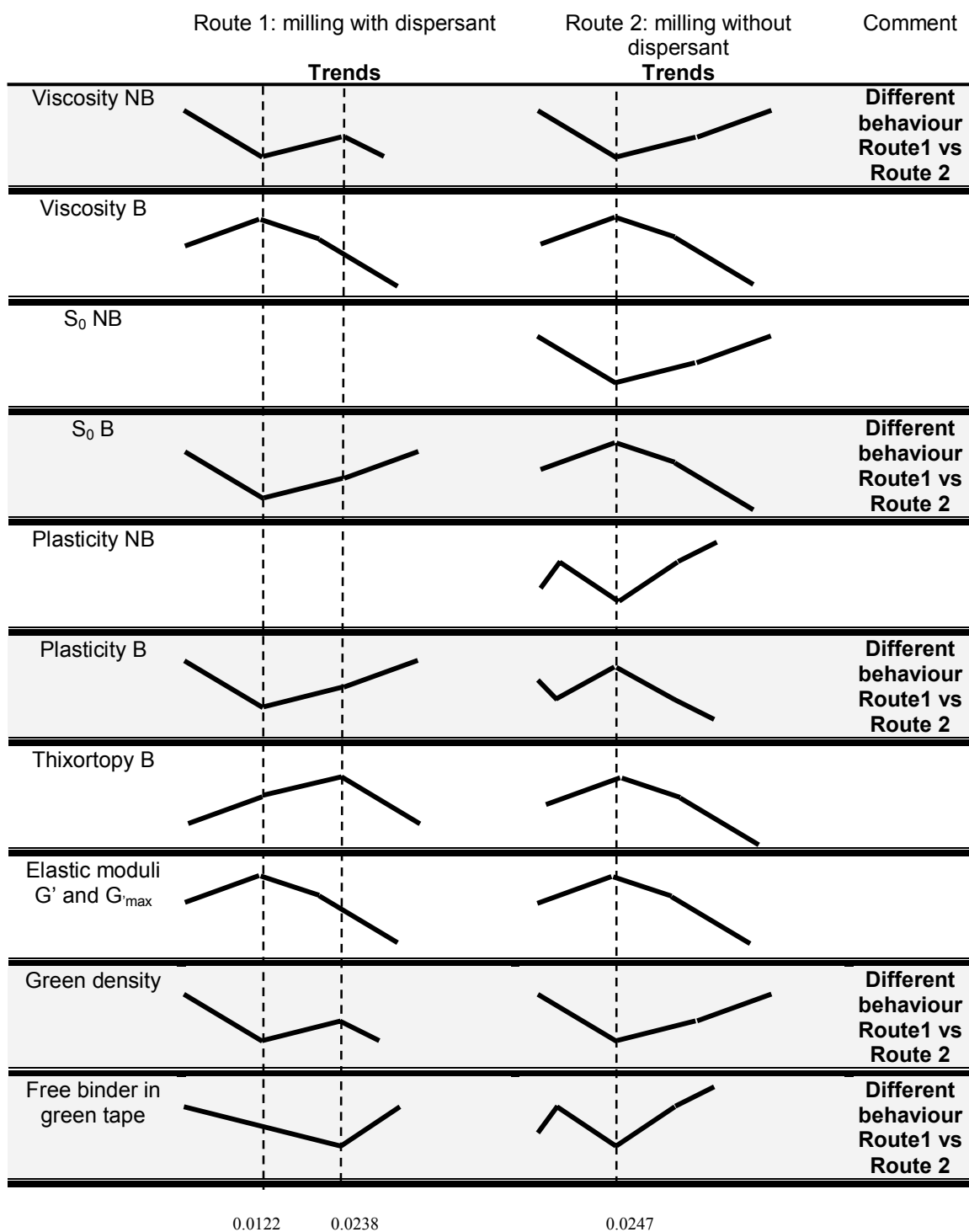


Fig. 131: Summary of the trends for Route 1 and Route 2 (with 68% in weight of powder) as in the results section 6.5.2

The main points of discontinuity in the trends were, in almost all the cases, coinciding within the individual routes with the same amount of dispersant. They were in correspondence of 0.0122 dispersant amount for the slurries milled in presence of the dispersant in Route 1 and 64% in weight of powder and 0.0247 in

the Route 2 series which had the dispersant added after the milling and 68% of powder content .

In both preparation routes, the trends of viscosity obtained without binder was inverted when the binder was added. In addition, for both the preparation methodologies, the trend of the elastic moduli G' and G'_{max} for the slurries with binder were coherent with their viscosity trends.

In the case of Route 2 the inversion of trends occurred also for the plasticity and the Casson yield stress which showed minima for binderless slurries and maxima when the binder was added.

For both preparation Routes, the green density values followed similar trends than the viscosities in absence of the binder system.

However, even if the similarities were many, there were a series of exceptions, listed below.

- The viscosity profile in absence of binder system had a minimum for both preparations routes. However, the trend in case of Route 2 was monotonically increasing after the minimum, while in case of Route 1 it peaked and then decreased again.
- The trend of the Casson yield stress (s_0) was opposite for the two routes (compare Fig. 97 and Fig. 108). The yield stress had a decrease/increase trend for Route 1, while the trend was increase/decrease for Route 2.
- Route 1's plasticity for the samples with binder had a minimum, Route 2 had a maximum, as major discontinuity points. In addition, Route 2 had a second discontinuity point, before the minimum (compare Fig. 98 and Fig. 110).
- The thixotropy followed a similar trend between the two preparation methods. However, Route 1 maximum was obtained for 0.0238 dispersant, not coincident with the other discontinuity points. (see Fig. 102 and Fig. 118)
- For Route 1 the amount of free binder visible in the SEM micrographs (see Fig. 104) had a minimum for 0.0238. The variation with dispersant amount of free PVA in the suspensions before casting was obtained experimentally (See Fig. 106). The trend of free binder for each suspension, coincided with the visual evaluation of the green tapes. However, the minimum was found for 0.0238 dispersant amount, corresponding with the maximum in the thixotropy trend. On the other hand, for Route 2, the trend of free polymer visible from the SEM pictures was similar to the plasticity trend (See Fig. 119).

- While the trends of viscosity were qualitatively similar for the two routes, the order of magnitude of the variation was very different. This can be noted in Fig. 132 which plots a direct comparison of the viscosity profiles for Route 1 and Route 2 at 68% in weight of powder. When the powder was milled with the dispersant, i.e. in Route 1, the viscosities variation was of the order of 1 to 3 Pa.s. When the dispersant was added after the milling the difference in viscosity reached a maximum of approximately 20 Pa.s in correspondence of the discontinuity points.

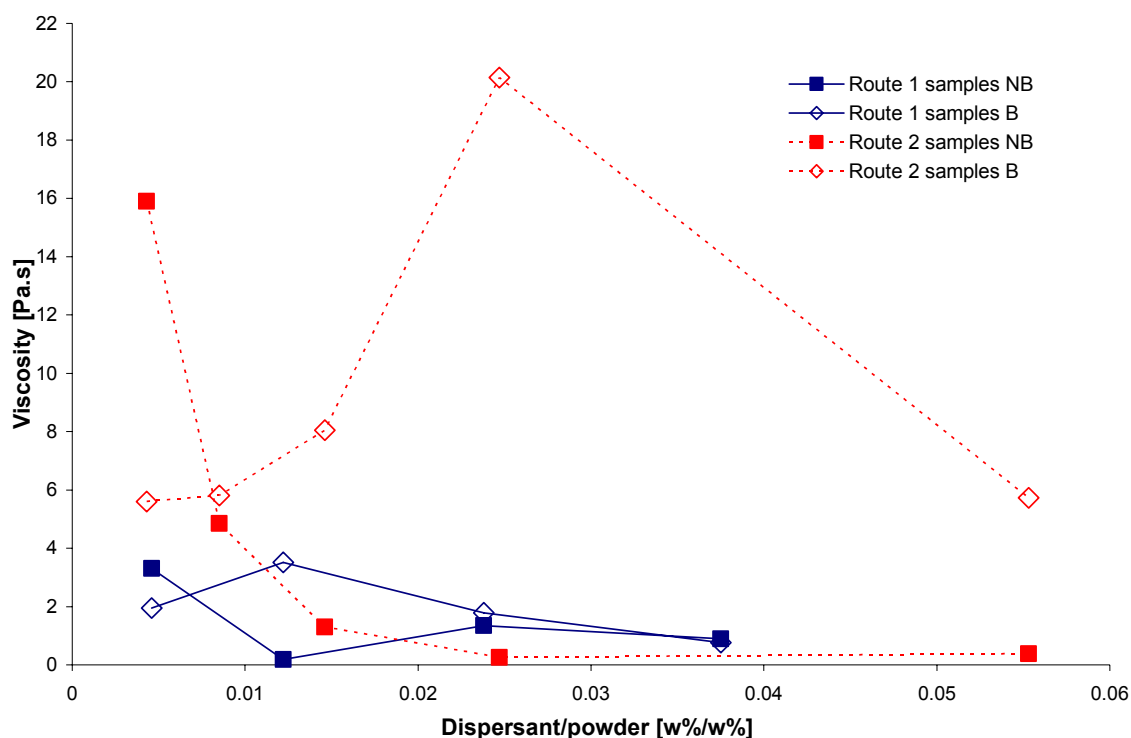


Fig. 132: Comparison of viscosity trends for Route 1 and Route 2 (at 68% in weight of powder)

As the dispersant added before the milling showed to influence the comminution efficiency and considering in addition that the rheological behaviour is known to depend both on the particles size and their distribution as well as on the particles stabilization, it was concluded that it was impossible to discriminate between these effects by means of the rheology tests.

However, in the case of Route 2, when the dispersant was added after the milling, it was argued that the dispersant influence on the comminution was eliminated. It was also reasonable to assume that the particles size across the Route 2 series was constant as the samples were obtained from the same milling batch. In this case, rheological trends could be interpreted as indications of the effects of the dispersant on the stabilization of the particles, in isolation.

7.3.1.3 *The effects of dispersant and binder on the suspension stabilisation*

For the reason just given, the evaluation of the effects of dispersant and binder on the suspension and the green body were obtained from the data of the samples produced according Route 2.

The behaviour of the slurries prepared according Route 2 were compared with the models proposed by the literature.

The trend of viscosity for the binderless samples followed the behaviour described in literature for both the powder concentrations tried of ceramic suspensions when a dispersant is added and a stabilisation occurs. However, when the binder was added, the trends in the rheological figures didn't follow the same patterns.

The commonly acknowledged mechanism associated with polyelectrolyte-type dispersant variations and their consequences on the slurry suspension and rheological characteristics [Rahaman, 1995] was explained in the literature section 2.6.4, and is shown in Fig. 133.

At zero dispersant amount, the particles are attracted one to the other by the Van der Waals forces. In this condition they generate flocs which trap part of the suspending solvent.

When the dispersant is added, but not in a sufficient quantity to provide a complete monolayer coverage of the particles surface, the effect of the Van der Waals forces is partly counteracted. In this case, the dispersion is very weakly flocculated.

The optimal dispersant concentration is represented by the amount which provides a complete deflocculation of the particles by providing monolayer coverage on the particles surface. At quantities above the optimal amount, the excess of dispersant is not absorbed onto the particles surfaces but remains free in the medium. The free dispersant, which is also an electrolyte, completely dissociates in the medium and promotes the flocculation by reducing the thickness of the particles double layer. The flocs are strongly tightened together, trapping little solvent.

These scenarios translate in a V-shape trend in viscosity which has a minimum for the amount of dispersant that better approximates the 'optimal' dispersant amount, i.e. the monolayer coverage of the particles surface.

This trend would be expected also for other rheological figures such as the yield stress and the elastic modulus.

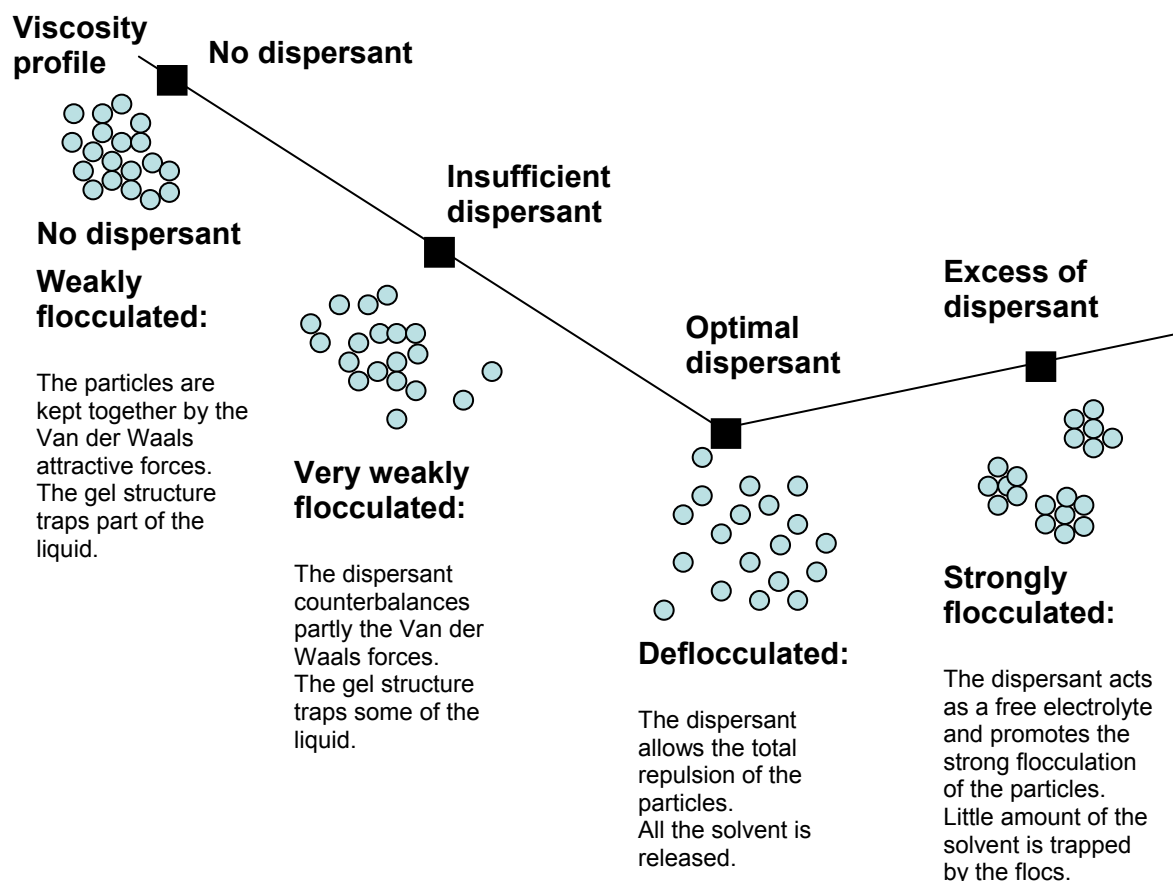


Fig. 133: A model for the effects of the dispersant amount in absence of binder (Samples NB)

This model could be used to interpret the results obtained for the binderless slurries prepared according Route 2. By using the model it could be inferred that the dispersant improved the stability of the suspensions up to the point in which the viscosity trends had a minimum. For further additions, the dispersant induced flocculation, by acting as a free electrolyte.

It was noted that the amount of dispersant to gave the minimum viscosity, i.e. the best stabilisation of the series, varied according to the powder concentration.

As reported in

Table 40, the minimum viscosity at 20 s^{-1} shear rate for the samples without binder system was reached for 0.0146 and 0.0247 dispersant ratios for the suspension with 73 and 82.5% powder content respectively. These minima were coherent with the trends in yield stress and plasticity which also showed minima for the same dispersant concentrations (See section 6.5.2.2.1 and 6.5.2.2.2).

A similar effect (i.e. a shift in viscosity minima for different powder concentrations) was noted by Davies [2000], who however didn't explain the reasons for the minima shift at higher dispersant concentrations.

An interpretation of this phenomenon could be given considering that for lower powder concentration the particles' separation is fairly large. Consequently,

according to the DLVO theory, as the Van der Waals attractive forces are relatively weak, lower concentrations of dispersants are needed to obtain a full dispersion. This explanation was supported also if considering the one order of magnitude difference in the decrease in viscosity when the optimal dispersant concentration was reached. It was 1.91 Pa.s for the 73% in weight suspension and 15.65 Pa.s when the particle concentration was 82.5% in weight. These data could testify the difference in intensity of the attractive forces among the particles for the two suspensions.

The same considerations made for the viscosity trends, could be made for the trend of the calculated yield stress (s_0) obtained by fitting the viscosity curves with the Casson's model, in Fig. 108. Also in this case, the trend for the binderless samples produced following Route 2 were coherent with the literature model.

As highlighted before (see Fig. 132), the addition of the binder to the slurries inverted the trends. This happened for both powder concentrations. In the following discussion, the data of the samples with the highest powder concentrations, i.e. 68% in weight, were used as an example.

In summary the following observations were made:

- The viscosity, and the other major rheological figures (i.e. yield stress, plasticity and elastic modulus), presented maxima for the same dispersant amounts which corresponded to minima in the binderless slurries profiles, i.e. 0.0247 dispersant ratio.
- In addition, the slurries corresponding to 0.0247 were the ones which showed the strongest time dependent characteristics.

The green density figures achieved are reported in

- Table 40 while the microstructures are reported in Fig. 119. As the forming method used was different than the tape casting and the samples couldn't be de-aired before casting, the absolute value of green density and the evaluation of the packing were taken purely as indicative. More attention was paid to the trends of green density, packing, porosity and binder distribution across the series.
As shown in Fig. 132, the trend of green density was inverse than the viscosity of the generating slurry. For 0.0247 dispersant ratio, the lowest green density of the series was obtained. This was also consistent with the sample appearance which showed the greatest pores dimension of the series, especially on the lower side of the sample.
- The amount of free polymeric phase, visible with the SEM analysis varied with dispersant amount. Also in this case, like for the green density, the trend showed a minimum for 0.0247 dispersant amount. The samples with 0.0085, 0.0146 and 0.0553 dispersant ratio showed the highest amount of free binder, more concentrated on the carrier side of the samples.

- A special situation was observed for the sample with the 0.0043 amount of dispersant. Its appearance was very similar to the one obtained with 0.0247 dispersant amount in terms of the polymer distribution. This sample's green density was also the highest in the series. This was in accordance with the SEM pictures which showed a relatively homogeneous distribution of the binder across the samples structure. The viscosity of the slurry which generated this sample was 5.60 Pa.s, the lowest in the series.

With the study on the slurries prepared according to Route 1 reported in Fig. 106, it was observed how the percentage of free polyvinyl alcohol (PVA) in the complete slurry was less than the quantity added originally. As a consequence, it was deduced that the PVA adsorbed onto the PZT particles surface.

The increase of the apparent viscosity, yield stress and elastic modulus are usually associable with the creation of particles network and the consequent reduction of the amount of free medium. In addition, the thixotropic behaviour is usually associated with the destruction of a structure with shearing that tends to rebuild when the shear is removed. This is usually a sign of weak flocculation, typical of a secondary minimum in the DLVO theory [Tadros, 1992b].

It is known that PVA can compete for the adsorption on particles with the polyelectrolyte [Bonekamp et al., 1989]. It is also known that long chain adsorbing polymers can act as stabilisers by the steric mechanism [Pugh and Bergström, 1994] or as enhancers of flocculation through bridging across several particles [Rahaman].

A model was generated from the empirical observations and this literature information. It is shown in Fig. 134.

The reverse trends of the rheological properties with dispersant amount suggested that the binder system interacted with the suspensions. Possibly, as the binder addition influenced all the parameters such as viscosity, elastic modulus and yield stress, to increase, that was the sign that the binder induced the flocculation of the particles. As the PVA was shown to have adsorbed onto the particles surfaces, the flocculation could have happened by bridging mechanism, if the PVA molecules grafted contemporaneously on several particles.

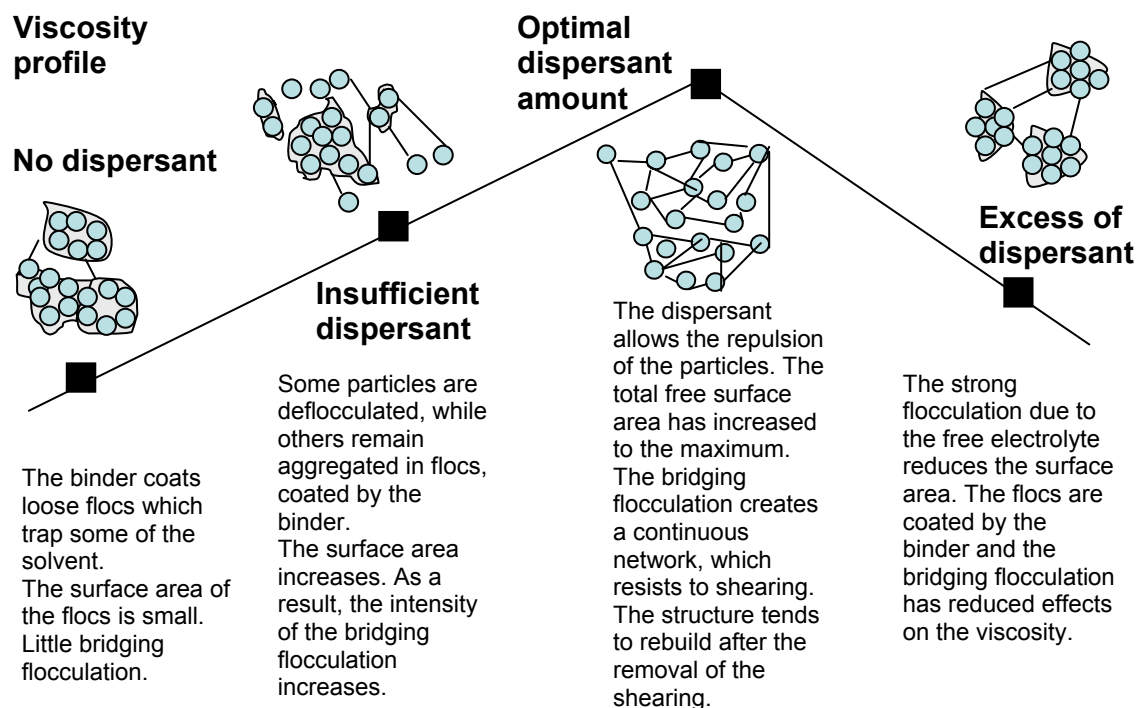


Fig. 134: A model for the effects of the dispersant on the suspension, when the binder system was added

As the absorption of polymers is known to increase with the free particles surface area, and considering the model illustrated in Fig. 133, the free surface area available for the PVA to be absorbed would have been different, depending to the state of aggregation of the particles in the binderless samples. It was argued that, if the particles were agglomerated, they would have presented a reduced surface area free to adsorb the polymer.

In theory, when in the binderless slurries the dispersant was calibrated to provide the best stabilisation effect, the particles' surface area free for access by the polymer was higher than in the case of a not well dispersed suspension. This might have resulted in an increased probability of polymer bridges among the particles to be created, or in other terms, in a reinforced bridging structure. As a result, the structure might have increased the resistance to shearing of the slurries, translating in higher viscosities and, perhaps, time dependent characteristics.

In a not stabilised suspension, i.e with insufficient dispersant to reach a complete stabilisation or with an excess of dispersant, the binder would instead have met the flocs of particles rather than the single particles. It would consequently be adsorbed onto the flocs rather than the particles individually. This scenario is coherent with the Zipper bag theory [Mistler and Twinaime, 2000].

As the apparent average surface area of the particles in flocs would be smaller compared to the one of the disperse particles, the amount of binder adsorbed would have been less.

Hence, in this case, the shown viscosity would have been lower because the surface area where the polymer could bridge was reduced. Also, amount of free

polymer visible with SEM would have increased in these circumstances and perhaps would have been collected preferentially on the carrier side of the tape because of percolation.

This scenario could explain the low green density figures consistently achieved for any dispersant amount across the Route 2 series. In fact, considering the model, any suspension obtained, for any amount of dispersant, was not stabilised while the suspension stabilisation is known to be a fundamental requirement for the achievement of the best packing of the particles in green bodies [Rahaman, 1995]. Potentially, the little difference among the samples green density could be explained by considering that the de-airing was probably less efficient in case of higher viscosity slurries. It was speculated that if the viscosity was high, like in the sample with 0.0247 dispersant ratio, the natural de-airing of the slurry while drying was reduced as the movement of the air bubbles towards the upper surface was hindered by the viscosity. This might have ended in a greater amount of voids remaining in the green body.

This argument could be used as well in the case a de-airing system was used: its efficiency would be reduced at higher viscosities as the air bubbles would have had increased difficulty to move.

A special situation was observed for the sample with 0.0046 amount of dispersant. From the analysis of this sample it could be possible to argue that the PVA and the dispersant somehow interacted. In fact, while the homogeneity of the binder distribution was very similar to the sample obtained with 0.0247 dispersant ratio, the slurry had a lower viscosity. As an explanation for the unexpected relative uniformity and packing observed in the sample with the 0.0046 amount of dispersant, it was inferred that in absence, or for very low amounts, of dispersant, the binder was freely adsorbed onto the particles surface, providing initially steric stabilisation. In these circumstances the PVA mostly didn't have to displace the dispersant to be adsorbed. The binder distribution in the foils can be discussed comparing the data with the results found by Van der Beek et al. [1995] for barium titanate tape cast containing PVA. They observed that the earlier the PVA grafting takes place, the more homogeneous is the resulting binder distribution.

Using this model and the data on comminution to describe the tapes produced with Route 1, it was concluded that potentially the 0.0238 (the amount in the original process) dispersant ratio was sufficient to guarantee an efficient comminution. This amount of dispersant was also seemingly in the range on the 'optimal' dispersant amount as the increase of the dispersant induced a decrease of the comminution efficiency, probably due to an increase in viscosity because of an excess of dispersant.

However, it was suggested that the addition of the binder system induced flocculation probably because of the bridging of the polymer molecules among the particles. The resulting tapes showed consequently low green density, as they derived from a flocculated suspension and because the high viscosity induced by the flocculation partly limited the efficiency of the de-airing system.

It was concluded that the binder employed, was probably inappropriate for the tape casting of this type of PZT powder.

7.3.1.4 *The effects of the binder and plasticizer ratio on the green tape*

Fig. 120 reports the micrographs of green tapes obtained varying the amount of plasticizer (PPG) in comparison to the original process (see section 4.1). The images of the samples with an increased plasticizer amount (in substitution of water) are reported in the right column.

Fig. 121 in the right column reports the brown tape microstructure of the tapes, after the elimination of the organics by burnout.

The values of green density obtained for the cast tapes are reported in Table 43. The relative green density variation obtained with these modifications was 0.32 g.cm^{-3} . This variation was almost negligible, being just approximately 4% of the theoretical density.

The micrographs in Fig. 120 highlighted differences in the binder distribution. As it could be expected, the samples richer in plasticizer showed an increase in the binder amount. This was understandable as the PPG is not volatile and was added in substitution of water. The increased plasticizer content was expected to improve the de-airing of the slurry by increasing the plasticity of the binder. However the green density achieved was 3.08 g.cm^{-3} , lower than 3.17 g.cm^{-3} , the average green density obtained with the original recipe. However this value was higher than the 2.90 g.cm^{-3} obtained with the original process but with the same batch of powder, represented by sample 1 in the micrographs. The comparison of sample 1 and 4 microstructure with their relative brown tape morphology in Fig. 121, led to conclude that there wasn't any significant improvement in packing accountable to the increase of the plasticizer ratio in the composition. The little advantage in green density for sample 4 could be attributed to experimental errors as well as the little improvement in de-airing.

7.3.1.5 *Effects of the powder content on the green tapes*

The powder amount was increased to 72.22% in weight, from 64% of the original process. This amount corresponded to approximately 24% in volume of powder and it was the maximum possible to allow handling and casting.

Typically the suspensions for tape casting use should be prepared with 50-60% of powder volume [Mistler and Twiname, 2000]. However, the solid loading couldn't be increased further because the grade of PVA employed required a great deal of water to be dissolved and handled. Also Chartier et al. [1993] suggested that the use of PVA limited the total solid loadings in a suspension.

Very little differences were noted when the powder content was increased.

The brown tape microstructures showed an apparent increase in the pores dimension for the tapes at higher powder content. This indicated a potentially inefficient de-airing, possibly because of the increased thickness of the slurry with the increase of powder loading. In addition, the particles size appeared slightly increased than in case of the lower powder loaded slurries, probably depending on

the effects of an increased viscosity. The green densities of the tapes were very similar to the ones obtained at lower powder content.

7.3.2 The effects of the drying conditions

The drying conditions were varied as reported in Table 44, together with the values of green density obtained. As for the cast sample in Route 2, the absolute value of green density weren't considered meaningful as the casting was made in plastic moulds without de-airing. However, the trends of green density were taken into account.

The maximum green density achieved in the series was 3.19 g.cm^{-3} , and the minimum was 2.95 g.cm^{-3} . Also in this case, the values of green density remained far from the envisaged 55% of the theoretical density. The maximum variation among the samples green density was 0.28 g.cm^{-3} , just 3.4% of the theoretical density.

By the observation of the trends plotted in Fig. 122, there wasn't any evident correlation or consistent link between the drying time and the final CD of the samples.

It appeared from the analysis of the graph in Fig. 122(B) that, in the range between 17 and 20 °C, the increase in the drying temperature led to a progressive reduction of the green density. However, the variation associated with a 4 °C increase in the drying temperature was less than 0.2 g.cm^{-3} , approximately 2.4% of the theoretical density.

The order of magnitude of such variation could also suggest that experimental errors were instead the primary responsible for the decrease of green density.

8 Conclusions and further work

This study proposed a methodology for developing scale-ups of ceramic processes which builds on the concepts of process design. It was performed in response to a perceived need to provide a support for the development of scale-up of ceramic processes. The methodology has been adopted in a real-life case-study of a tape casting process scale-up to demonstrate its applicability. The alternation of Conceptual and Definitive design phase tools, such as problem solving and statistical process control, allowed the tape casting process to be analysed and improved and to demonstrate its potential to be transferred to an industrial scale. A twofold approach, with product and process focus, has been adopted as the basis of the methodology to perform the process scale-up. The combination of these, run in parallel, provided a comprehensive view on the process issues during the scale-up, in agreement with the concurrent engineering philosophy of design.

During the study, the microstructural characteristics of the ceramic wafers produced by the original process were improved mainly by increasing the green density of the tapes before sintering, via warm pressing. An increase in green density, from approximately 37 to approximately 64% of the theoretical density, favoured the achievement of higher sintered density at equal sintering conditions. It also allowed the reduction of the grain size and was beneficial for an improvement in the uniformity of the ceramic characteristics throughout the microstructure.

As a result, the process yield passed from 5 to 75% thanks to the modifications proposed by the study. In addition, a newly designed sintering profile reduced the total sintering time by approximately 190 minutes.

The variability and capability of the warm pressing step were tested with the help of the statistical process control technique (SPC). $5 \pm 0.2 \text{ g.cm}^{-3}$ were the specification and tolerance interval for this study. The study highlighted that SPC was a suitable and very flexible tool for the analysis of the process in its design phase, although the technique is commonly used to provide control over running processes.

A second approach was taken, in alternative to the warm pressing, to increase the tapes green density. This was to improve the relevant properties of the tape cast slurry. The ingredients interactions in the suspension were investigated. The study yielded the conclusion that the binder PVA was not apt to tape cast the particular PZT powder used. This was because the PVA was shown to adsorb onto the particles, promoting bridging flocculation and not allowing the achievement of high green density tapes. None of the tested variations in the drying conditions or in the dispersant or plasticizer amount, resulted in any appreciable effect on the green density.

It was concluded that the low packing of the particles in the tape cast resulted from a not stabilised suspension, for any dispersant concentration. Hence, to find a suitable substitute for the PVA binder would be required for the improvement of the green density.

In addition, as part of this work, it was shown that since the dispersant acted as a comminution as well as stabilisation aid, rheological tests on samples milled in presence of the dispersant can not be used in isolation to optimise the dispersant amount. In fact, the rheological parameters for the slurries milled in presence of the dispersant depended both on the stabilisation of the particles and on their size distribution. To fully understand the influence of the dispersant on the rheological characteristics, a method was suggested that encompasses the combination of two slurry preparation routes. In one route, the dispersant is added during milling, in the other, after the comminution.

8.1 Future work

For the improvement of the green density of the tapes it would be advisable to find a substitute binder system for the poly vinyl alcohol. According to the results of this research, a potential alternative binder would have to be non adsorbent onto the PZT particles surface. A potential candidate would be the latex polymer as it is non water-soluble and is provided as an emulsion of polymer in water.

The study presented in this thesis concerned one grade of PVA. Further evidence on the interaction of the PVA and the PZT powder could be obtained investigating the effects on the tape of lower molecular weights or fully hydrolysed grades.

Further investigation would be needed to validate of the model proposed for the interaction between PZT and powder. Additional data could be obtained via the measurement of the particle size and of the agglomerates in suspension, for example with light scattering equipments.

Additional studies would be required to investigate a method to improve the sample's flatness. In particular, further attention would be dedicated to the assessment of the PbO atmosphere impact on the sintering.

Finally, the methodology proposed for the scale-up of ceramic processes needs further testing to understand its strengths and weaknesses.

9 References

- Barnes, H. A., Hutton, J. F. & Walters, K. (1989) *Introduction to rheology*, Elsevier.
- Bicheno, J. (2002) *Quality 75*, PICSIE Books.
- Bitterlich, B. & Heinrich, J. G. (2002) Aqueous tape casting of silicon nitride. *Journal of the European Ceramic Society*, 22, 2427-2434.
- Bonekamp, B. C., Van 't Veen, W. H., Schoute, M. J. & Veringa, H. J. (1989) Deflocculation of aqueous alpha- Al_2O_3 suspensions in the presence of adsorbing polymer and polyelectrolyte. *Euroceramic*, 1, 145-149.
- Briscoe, B. J., Lo Biundo, G. & Ozkan, N. (1998) Drying kinetics of water-based ceramic suspensions for tape casting. *Ceramics International*, 24, 347-357.
- Brue, G. (2002) *Six Sigma for Managers*, New York, Mc Graw Hill.
- Butcher, S. J. & Daghlis, M. (1993) The use of magnesium carbonate hydroxide pentahydrate in the production of perovskite lead magnesium niobate. IN DURAN, P. & FERNANDEZ, J. F. (Eds.) *Third Euro-Ceramics*. Faenza Editrice Iberica S.L.
- Cesarano Iii, J. & Aksay, I. A. (1988) Processing of highly concentrated aqueous α -alumina suspensions stabilised with polyelectrolytes. *Journal of American Ceramic Society*, 71, 1062-67.
- Chartier, T. & Bruneau, A. (1993) Aqueous Tape Casting of Alumina Substrates. *Journal of American Ceramic Society*, 12, 243-47.
- Corker, D. L., Whatmore, R. W., Ringgaard, E. & Wolny, W. W. (2000) Liquid-phase sintering of PZT ceramics. *Journal of the European Ceramic Society*, 20, 2039.
- Creveling, C. M., Slutsky, J. L. & Antis, D., Jr. (2003) *Design for six sigma*, New Jersey, PH PTR.
- Cui, X. M., Ouyang, S., Yu, Z. Y., Wang, C. G. & Huang, Y. (2003) A study on green tapes for LOM with water-based tape casting processing. *Materials Letters*, 57, 1300-1304.

- Das, N. & Maiti, H. S. (1999) Effect of size distribution of the starting powder on the pore size and its distribution of tape cast alumina microporous membranes. *Journal Of The European Ceramic Society*, 19, 341-345.
- Davies, J. & Binner, J. G. P. (2000) The role of ammonium polyacrylate in dispersing concentrated alumina suspensions. *Journal of the European Ceramic Society*, 20, 1539.
- Doreau, F., Tari, G., Pagnoux, C., Chartier, T. & Ferreira, J. M. F. (1998) Processing of aqueous tape-casting of alumina with acrylic emulsion binders. *Journal of the European Ceramic Society*, 18, 311-321.
- Edelson, L. H. & Glaeser, A. M. (1988) Role Of Particle Substructure In The Sintering Of Monosized Titania. *Journal Of The American Ceramic Society*, 71, 225-235.
- Edwards, K. L. (2002) Towards more strategic product design for manufacture and assembly: priorities for concurrent engineering. *Materials & Design*, 23, 651-656.
- Fang, T., Jafari, M. A., Safari, A. & Danforth, S. C. (1999) Statistical feedback control architecture for layered manufacturing. *Journal Of Materials Processing & Manufacturing Science*, 7, 391-404.
- Feng, J. H., Ferguson, L. G. & Dogan, F. (2001) Processing of buffer sheets for sintering PLZT tapes. *Material processing Technology*, 110, 47-52.
- Finch, C. A. (1973) *Polyvinyl Alcohol, Properties and Applications*, New York, Wiley.
- Finley, J. H. (1961) Spectrophotometric determination of Polyvinyl Alcohol in paper coatings. *Analytical Chemistry*, 33, 1925-27.
- Fox, J. (1993) *Quality through design: the key to successful product delivery*, New York, McGraw Hill.
- Frances, C. & Laguerie, C. (1998) Fine wet grinding of an alumina hydrate in a ball mill. *Powder technology*, 99, 147-153.
- Funk, J. E. & Dinger, D. R. (1994) *Predictive process control of crowded particulate suspensions*, Kluwer Academic Publisher.
- Greskovich, C. & Lay, K. W. (1972) Grain-Growth In Very Porous Al₂O₃ Compacts. *Journal Of The American Ceramic Society*, 55, 142-&.

- Gutierrez, C. A. & Moreno, R. (2000) Tape casting of non-aqueous silicon nitride slips. *Journal of the European Ceramic Society*, 20, 1527-1537.
- Harper, C. A. (1990) *Materials and Processes in Microelectronic systems*, Westerville, OH, American Ceramic Society.
- Herbst, J. A. & Fuerstenau, D. W. (1972) Influence on the parameters of the batch grinding equations. *Transactions AIME*, 252, 169-176.
- Herder, P. M. & Weijnen, M. P. C. (2000) A concurrent engineering approach to chemical process design. *International Journal Of Production Economics*, 64, 311-318.
- Hozta, D. & Greil, P. (1995) Review: aqueous tape casting of ceramic powders. *Materials Science and Engineering, A*, 202, 206-217.
- Institute, A.-A. N. S., 2005, <http://www.ansi.org/>
- Jantunen, H., Hu, T., Uusimäki, A. & Leppävuori, S. (2004) Tape casting of ferroelectric, dielectric, piezoelectric and ferromagnetic materials. *Journal of the European Ceramic Society*, 24, 1077-1081.
- Kahdilkar, C. S. & Sacks, M. D. (1988) Effect of polyvinyl alcohol on the properties of model silica suspensions. *Ceramics Transactions: Ceramic powder science II A*, 1, 397-409.
- Kapur, P. C., Healy, T. W., Scales, P. J., Boger, D. & Wilson, D. (1996) Role of dispersants in kinetics and energetics of stirred ball mill. *International Journal of Mineral Processing*, 47, 141-152.
- Kehoe, D. F. (1996) *The fundamentals of Quality Management*, UK, Chapman & Hall.
- Khan, A. U., Briscoe, B. J. & Luckham, P. F. (2000) Interaction of binders with dispersant stabilised alumina suspensions. *Colloids and Surfaces A: Physicochemical and Engineering Aspects*, 161, 243.
- Kingery, W. D. (1978) Firing-The Proof Test for Ceramic Processing. *Ceramic processing before firing*. New York, Wiley.
- Kington, A. I. & Clark, J. B. (1983) Sintering Of Pzt Ceramics.1. Atmosphere Control. *Journal Of The American Ceramic Society*, 66, 253-256.

- Kington, A. I., Terblanche, P. J. & Clark, J. B. (1985) The Control Of Composition, Microstructure And Properties Of Pb(Zr, Ti)O₃ Ceramics. *Materials Science And Engineering*, 71, 391-397.
- Koch, P. N., Yang, R. J. & Gu, L. (2004) Design for six sigma through robust optimization. *Structural And Multidisciplinary Optimization*, 26, 235-248.
- Kristoffersson, A., Lapasin, R. & Galassi, C. (1998a) Study of interactions between polyelectrolyte dispersants, alumina and latex binders by rheological characterisation. *Journal of the European Ceramic Society*, 18, 2133-2140.
- Kristoffersson, A., Roncari, E. & Galassi, C. (1998b) Comparison of different binders for water-based tape casting of alumina. *Journal of the European Ceramic Society*, 18, 2123.
- Kwan, Y. B. P. & Alcock, J. R. (2002) The impact of water impregnation method on the accuracy of open porosity measurements. *Journal Of Materials Science*, 37, 2557-2561.
- Lin, M., Rahaman, M. N. & Jonghe, L. C. (1987) Creep-Sintering and Microstructure Development of Heterogeneous MgO Compacts. *Journal of the American Ceramic Society*, 70, 360-366.
- Liu, C. H., Nagel, S. R., Schechter, D. A., Coppersmith, S. N., Majumdar, S., Narayan, O. & Witten, T. A. (1995) Force Fluctuations In Bead Packs. *Science*, 269, 513-515.
- Maiti, A. K. & Rajender, B. (2002) Terpeneol as a dispersant for tape casting yttria stabilized zirconia powder. *Materials Science and Engineering*, 333, 35-40.
- Markarian, J. (2004) What is Six Sigma? *Reinforced Plastics*, 48, 46-49.
- Megriche, A. & Troccaz, M. (1998) Effects of Excess PbO Addition on the Properties of Ferroelectric Doped PZT Ceramics. *Materials Research Bulletin*, 33, 569.
- Mistler, R. E. & Twinn, E. (2000) *Tape Casting Theory and Practice*, The American Ceramic Society.
- Mittendorfer, J. & Zwanziger, P. (2000) Application of statistical methods (SPC) for an optimized control of the irradiation process of high-power semiconductors. *Radiation Physics And Chemistry*, 57, 629-634.

References

- Nahass, P., Rhine, W. E., Pober, R. L., Bowen, H. K. & Robbins, W. L. (1990) A comparison of aqueous and non-aqueous slurries for tape casting. *Ceramic Transactions*, 15, 355-64.
- Navarro, A., (2001), Cranfield University, Fabricaton of lead zirconate titanate ceramics for pyroelectric applications, PhD.
- Navarro, A., Alcock, J. R. & Whatmore, R. W. (2004a) Aqueous colloidal processing and green sheet properties of lead zirconate titanate (PZT) ceramics made by tape casting. *Journal of the European Ceramic Society*, 24, 1073-1076.
- Navarro, A., Whatmore, R. W. & Alcock, J. R. (2004b) Preparation of functionally graded PZT ceramics using tape casting. *Journal Of Electroceramics*, 13, 413-415.
- Northorp, D. A. (1967) Vaporisation of Zirconate-Lead Titanate materials. *Journal Of The American Ceramic Society*, 50, 441-445.
- Oakland, J. S. (1989) *Total Quality Management*, New York, Nichols Publishing Company.
- Oakland, J. S. (1999) *Statistical Process Control*, Oxford, Butterworth Heineman.
- Occhionero, M. A. & Halloran, J. W. (1984) The Influence of Green Density Upon Sintering. *Sintering and Heterogeneous Catalysis*. New York, Plenum Press.
- Pugh, R. J. & Bergström, L. (1994) *Surface and colloid chemistry in advanced ceramic processing*, Marcel Dekker, Inc.
- Rachas, I., Tadros, T. F. & Taylor, P. (2000) The displacement of adsorbed polymer from silica surfaces by the addition of a nonionic surfactant. *Colloids And Surfaces A-Physicochemical And Engineering Aspects*, 161, 307-319.
- Rahaman, M. N. (1995) *Ceramic processing and sintering*, New York, Marcel Dekker, Inc.
- Reed, J. S. (1988) *Introduction to the principles of ceramic processing*, New York, John Wiley & sons.
- Revelle, J. B. (2002) *Manufacturing handbook of Best practices*, CRC Press.

- Richerson, D. W. (1992) *Modern Ceramic Engineering*, New York, Marcel Dekker.
- Roncari, E., Galassi, C., Craciun, F., Capiani, C. & Piancastelli, A. (2001) A microstructural study of porous piezoelectric ceramics obtained by different methods. *Journal of the European Ceramic Society*, 21, 409-417.
- Roosen, A. & Bowen, H. K. (1988a) Influence Of Various Consolidation Techniques On The Green Microstructure And Sintering Behavior Of Alumina Powders. *Journal Of The American Ceramic Society*, 71, 970-977.
- Roosen, A. & Bowen, H. K. (1988b) Influence of various consolidation techniques on the green microstructure and sintering behaviour of alumina powders. *Journal of American Ceramic Society*, 71, 970-977.
- Rosenthal, S. (1992) *Effective product design and development*, Irwin.
- Roth, G. I. (2005) Capability Indexes: Mystery Solved. *Six sigma forum magazine*, 17-22.
- Sacks, M. D. & Tseng, T. Y. (1984) Preparation Of SiO_2 Glass From Model Powder Compacts.2. Sintering. *Journal Of The American Ceramic Society*, 67, 532-537.
- Scherer, G. W. (1990) Theory Of Drying. *Journal Of The American Ceramic Society*, 73, 3-14.
- Schwarzer, S. & Roosen, A. (1999) Tape casting of piezo ceramic/polymer composites. *Journal of the European Ceramic Society*, 19, 1007.
- She, J. H. & Ohji, T. (2002) Rapid densification of alumina ceramics with fine grains and high strength. *Journal Of Materials Science Letters*, 21, 1405-1406.
- Shi, F. N. & Napier-Munn, T. J. (2002) Effects of slurry rheology on industrial grinding performance. *International Journal of Mineral Processing*, 65, 125-140.
- Snijkers, F., De Wilde, A., Mullens, S. & Luyten, J. (2004) Aqueous tape casting of yttria stabilised zirconia using natural product binder. *Journal of the European Ceramic Society*, 24, 1107-1110.
- Snow, G. S. (1974) Elimination Of Porosity In $\text{Pb}(\text{Zr,Ti})\text{O}_3$ Ceramics By Liquid-Phase Sintering. *Journal Of The American Ceramic Society*, 57, 272-272.

- Song, J.-K., Um, W.-S., Lee, H.-S., Kang, M.-S., Chung, K.-W. & Park, J.-H. (2000) Effect of polymer molecular weight variations on PZT slip for tape casting. *Journal of the European Ceramic Society*, 20, 685.
- Stringfellow, S. B., Gupta, S., Shaw, C., Alcock, J. R. & Whatmore, R. W. (2002) Electrical conductivity control in uranium-doped PbZrO₃-PbTiO₃-Pb(Mg_{1/3}Nb_{2/3})O₃ pyroelectric ceramics. *Journal of the European Ceramic Society*, 22, 573.
- Sumita, S., Rhine, W. E. & Bowen, H. K. (1991) Effects of organic dispersants on the dispersion, packing, and sintering of Alumina. *Journal of American Ceramic Society*, 74, 2189-96.
- Tadros, T. (2003a) Interaction forces between particles containing grafted or adsorbed polymer layers. *Advances in Colloid and Interface Science*, 104, 191.
- Tadros, T. D. (1992a) Control of stability/flocculation and rheology of concentrated suspensions. *Pure & Applied Chemistry*, 64, 1715-1720.
- Tadros, T. D. (1992b) Control of stability/flocculation and rheology of concentrated suspensions. *Pure & Applied Chemistry*, 64, 1715-1720.
- Tadros, T. D. (1996) Correlation of viscoelastic properties of stable and flocculated suspensions with their particles interactions. *Advances in Colloid and Interface Science*, 68, 140-167.
- Tadros, T. D. (2003b) Interaction forces between particles containing grafted or adsorbed polymer layers. *Advances in Colloid and Interface Science*, 104, 191.
- Tadros, T. F. (1990) Use of viscoelastic measurements in studying interactions in concentrated suspensions. *Langmuir*, 6, 28-35.
- Ueyama, T. & Kaneko, N. (1987) Effect of agglomerated particles on properties of ceramic green sheets. *High Tech Ceramics*. Elsevier.
- Van Der Beek, G. P., Gontermann-Gehl, U. & Krafczyk, E. (1995) Binder distribution in green ceramic foils. *Journal of the European Ceramic Society*, 15, 741.
- Webster, A. H., Weston, T. B. & Bright, N. F. H. (1967) Effect of PbO deficiency on the piezoelectric properties of Lead Zirconate-Titanate ceramics. *Journal Of The American Ceramic Society*, 50, 490-491.

References

- Wu, B. (1994) *Manufacturing systems design and analysis*, London, Chapman & Hall.
- Yan, M. F. (1981) Microstructural Control In The Processing Of Electronic Ceramics. *Materials Science And Engineering*, 48, 53-72.
- Yeh, T. S. & Sacks, M. D. (1988) Low-Temperature Sintering Of Aluminum-Oxide. *Journal Of The American Ceramic Society*, 71, 841-844.
- Zhang, Q., Corkovic, S., Shaw, C. P., Huang, Z. & Whatmore, R. W. (2005) Effect of porosity on the ferroelectric properties of sol-gel prepared lead zirconate titanate thin films. *Thin Solid Films*, 488, 258-264.
- Zheng, J. & Reed, J. S. (1989) Effects of Particle Packing Characteristics on Solid-State Sintering. *Journal Of The American Ceramic Society*, 72, 810-817.
- Zimmermann, A. & Rodel, J. (1999) Fracture statistics based on pore/grain-size interaction. *Journal Of The American Ceramic Society*, 82, 2279-2281.

Appendix A: New process flow chart steps description

SLIP PREPARATION			
OPERATION NUMBER	OPERATION DESCRIPTION	TIME (hours)	CONDITIONS
1	Ball milling	8	Pots: 250mL 120 yttrium stabilized Zirconia cylindrical media Speed: 80 RPM
2	Ball milling	18	As n ^o 1
3	Solid content assessment	0.5	Temperature 100°C
3'	Ball milling	1	As n ^o 1 Speed: minimum
4	Slip control	1	Solid contents assessment Viscosity Control
5	Transfer to deairing & filtering equipment	0.2	200 µm
6	Deairing	1-2	Pressure: 1 atm Gentle stirring
BINDER PREPARATION			
2'	Binder preparation: polymer solution	5	Temperature: ambient to 100°C Stirring to avoid agglomeration
2''	Solid content assessment	2	Temperature 100°C
TAPE CASTING			
6'	Transfer to the tape caster reservoir	Few minutes	Quick initial flux then constant flux to maintain the reservoir height uniform
6''	Tape Casting	Few minutes	Carrier speed: Reservoir height: 1 cm Gap heights: front blade 700 µm Rear blade 1400 µm
7	Wet thickness assessment	-	Comb in three tape positions
8	Drying	24	Air flow:

Appendixes

			Air temperature: 50 °C Time: 1h Then at room conditions for 23 hours
9	Cut & shaping	2	Squares 8 cm x 8 cm
10	Storage of dry shaped tape	-	Plastic sealed envelopes
10'	Dry tape measurement	3	Green density (area, thickness, weight)
WARM PRESSING			
11	Transfer to the warm press	-	
12	Stacking of tapes in the		Stack of 5 tapes
13	Warm pressing	30 min/5 tapes	Temperature: 50 °C Time: 20 min Pressure: 60 MPa
14	After pressing measurement	3	Green density (thickness)
14'	Cutting & Shaping	1	Reshape the squares 7cm x 7 cm
BURNOUT & SINTERING			
15	Transfer to firing configuration	0.5	Lead oxide spacer pots
16	Burnout & Sintering	24	Profile: 2°/min up to 260 °C hold 120 min 1°/min up to 500 °C hold 0.1 min 6°/min up to 1170 °C hold 45 min 3°/min up to 0 °C End
17	Wafers shape assessment	0.5	Thickness, visual
18	Poling	2	Temperature: 120 °C (oil bath) Voltage: 3 kV/mm Time: until bath is at 50 °C
POWDER RECYCLING			
4'	Drying of slip	24	Oven temperature 70-100 °C
4''	Grinding	1	Coarse crush of formed ceramic
4'''	Transfer to crucible	-	Wide mouth crucible/ no lid
4^{iv}	Burnout of organics	24	Profile:

Appendixes

			3°C/min up to 600 °C hold for 6 hours 3°C/min to 0°C End
4^v	Mash & Sieve	0.5	Sieve mash: 250 µm
4^{vi}	Burnout assessment	24	Weight loss measurement IR scan for organic bands
DECISION POINTS			
D1	Binder solid content assessment		
D2	Slip viscosity and solid content assessment		
D3	Thickness assessment		
D4	Thickness assessment		
D5	Sintered Wafer assessment		
D6	Organics content assessment		

Appendix B: Papers